Università Iuav
di Venezia

Doctoral Programme in Architecture, City and Design

Curriculum: Innovation for Building and Cultural Heritage

Cycle XXXII

Numerical modelling strategies and design methods for timber structures

Supervisor: Prof. **Anna Saetta**
Co-supervisor: Dr. Eng. **Luca Pozza**

Ph.D. candidate: Eng. **Luca Franco**

April 2020

Foreword

Over the last years timber constructions are gaining back a primary role in the building industry after decades in which they were almost abandoned in favor of concrete and steel structures. A sign of this change is the appearance in the last years in many Italian universities of courses dedicated to the design of timber structures. One of the main reasons behind this success must be sought in the development of new engineered timber materials, such as glued-laminated and cross-lam timber, that allowed to wooden structures to reach structural potentialities that until some decades ago were prerogative of concrete or steel building materials. Tests recently carried out on full-scale buildings have also proven the excellent capabilities of these new timber technologies in providing reliable and highly-performant multi-storey building able to withstand high seismic intensities.

Since the employment of timber to build multi-storey buildings in seismic-prone areas is quite recent, many aspects relating the understanding of their structural behavior and their correct design are still to be sought, as demonstrated by the lack of provisions in current building codes and standards and the still ongoing great amount of research activity on seismic behavior of timber structures.

Modern timber technologies also allow to cover very large spans with long glued-laminated timber beams, satisfying the need of large open spaces and architectural flexibility required by modern building design approaches. These bulky big-size elements anyway result quite expensive in production, transportation and installation phases undermining the economic competitiveness of timber structures. To cope with this problem, the prototype of an innovative timber-steel composite beam consisting of sub-elements assembled on-site to create longer members has been ideated at KTH Royal Institute of Technology of Stockholm in Sweden.

One of the objectives of this thesis is therefore to provide an advance in the state of knowledge of timber building technology adopted for seismic-prone areas, focusing in particular on both numerical modelling strategies and design methods for cross-laminated timber buildings, illustrated respectively in the first and second part of the thesis. The other goal is the development of an analytical tool for the enhancement and the investigation of the structural performances of the innovative composite beam ideated at KTH Royal Institute of Technology, and it will be exposed in the third and last part of the thesis.

The topics illustrated in the Parts I and II this work are the results of the study and research activity carried out within a doctoral program from November 2016 to December 2019 at Università IUAV di Venezia in Italy, while the research activity exposed in the Part III has been carried out within a study-exchange program at KTH Royal Institute of Technology from March to June 2019. The writing of the thesis and the research activity has been carried out under the supervision of Prof. Eng. Anna Saetta, PhD Eng. Luca Pozza and PhD Eng. Diego A. Talledo for the first two parts of the thesis, and also with the supervision of Prof. Eng. Roberto Crocetti for the third part. To all them goes my gratitude for their patience and help in realizing this work.

Luca Franco

April 2020
Venice, Italy

Abstract

In this thesis two macro-topics of research on timber engineering have been analyzed. The first is the study of the seismic behaviour of Cross-Laminated Timber (CLT) buildings. The second is the analysis of the structural behaviour of an innovative timber-steel composite beam made-up of sub-elements to be assembled on site through a system of shear keys and steel cables, conceived and developed at KTH Royal Institute of Technology of Stockholm. The study of the seismic behaviour of CLT buildings illustrated in this work covers two key aspects of the design: the modelling strategies to reproduce the dynamic and hysteric behaviour of CLT structures, and the interaction domains-based methods for the design of CLT wall systems subject to horizontal loads, topics respectively reported in Parts I and II of the thesis. The research activity concerning the innovative timber-steel composite beam, reported in the third and last part of the thesis, has been aimed at the development of an analytical model able to describe its mechanical behaviour both in terms of internal forces and deflections providing an useful design tool for practitioners.

In Part I of the thesis, concerning modelling strategies for the analysis of the seismic behaviour of CLT structures, an overview of multi-storey timber building typologies has been illustrated and, given the importance of connections in defining their seismic behaviour, an overview of the main connection systems has been assessed with a focus on the ones usually employed for CLT buildings. The seismic design criteria for timber buildings available in codes and standards have then been analyzed, highlighting shortcomings and critical issues, particularly in the definition of the behavior factor and in the design criteria for connections. After a state-of-the-art of numerical modeling strategies usually employed for CLT buildings, component-level and phenomenological strategies are analyzed in depth adopting both linear and non-linear modelling approaches. The two strategies are investigated carrying out numerical simulations on reference structures, that in the case of linear analyses consist of three CLT multi-storey buildings with respectively 2, 4 and 6 floors while for non-linear analyses cyclic tests on single monolithic CLT platform-frame walls carried out at the CNR-IVALSA Institute as part of the SOFIE Project have been taken as reference. This dataset has been subjected to an in-depth interpretation and critical reworking in order to identify the peculiarities presented by the experimental campaign. In the component-level modelling approach CLT panels have been modelled with linear elements, while connections have been modeled with axial and shear springs with assigned linear or non-linear constitutive laws depending on the modelling approach adopted. In the phenomenological approach connections were not modeled with *ad-hoc* elements, but the CLT wall system has been modelled in its globality and the mechanical properties have been calibrated to faithfully reproduce the global behaviour of the structure when subjected to lateral loads. In particular, equivalent elastic moduli able to provide the same horizontal displacements as the more refined component-level modeling approach have been assigned to plate elements for the phenomenological linear modelling approach. Tables providing values of the equivalent elastic modulus to wall thickness ratios for each floor-level to the vary of the number of storeys of the building and seismic action intensity have been also furnished. Instead, for non-linear phenomenological modelling approach, the multilinear constitutive law has been calibrated in order reproduce the overall behavior of the tested walls in terms of force-displacement behavior and cumulative energy. The results of linear models have been analyzed in terms of forces on connections, principal vibration period inter-storey drifts, while those of non-linear models were investigated in terms of force-displacement behavior and cumulative energy. In addition, for non-linear component-level models, the axial and lateral displacements measured on connections have also been analyzed. Results show that the component-level modelling approach is an excellent tool for the numerical analysis of the seismic behaviour of CLT buildings composed of heterogeneous wall system configurations, provided the behaviour of each component is properly calibrated. Phenomenological modeling approach is instead an easier tool respect to the one for components, but it is characterized by a more limited versatility due to the dependency of its results from the specific loading, geometrical and connections configurations used for its calibration.

In Part II of the thesis, regarding methods for seismic design of CLT structures, an overview has firstly been given on the state-of-the-art of analytical methods for CLT wall systems available in literature, analyzing their assumptions and formulations and highlighting their limits. A promising design method developed in the last years is the one derived from the well-known cross-sectional analysis techniques adopted to create interaction domains of reinforced concrete members subjected to combined axial and bending actions. One of these methods available in the literature, whose assumptions and formulations have been explained in depth, has been used as starting point for the development of a more refined design method to perform axial-shear interaction domains of CLT wall system subjected to lateral loads. Some of the assumptions of the starting-point model have been changed, in particular an elasto-plastic behavior for compressed timber has been assumed in place of an elasto-fragile constitutive law and coupled resistance of connections have been considered in place of an infinite shear resistance. Two different methods (labelled as #1 and #2) to define the elasto-plastic constitutive laws of connections three coupling criteria of their resistance (rectangular, elliptic and an innovative hybrid force-displacement one) have been defined. The elliptic and rectangular coupling criteria have been implemented with two different formulations. The first, simplified, assumes that the achievement of the ultimate condition of the connection coincides with the yielding point. The second formulation, more refined, considers the failure of connections happened only once they reach the ultimate displacement. After a detailed illustration of the characteristics of the model highlighting the novel aspects, the impact of the different assumptions has been investigated by means of a sensitivity analysis in which the results were compared with experimental data of tests on walls with the same mechanical and geometric characteristics. Sensitivity analysis showed that it is essential to consider the coupling effects of connections in order to avoid getting interaction diagrams with a strength greater than the effective one of the wall systems, and that the adoption of an elasto-plastic constitutive law for timber allows to obtain results much more performant than the elasto-fragile case.

In Part III of the thesis, concerning the analysis of an innovative timber-steel composite beam, a state-of-the-art of timber-based composite structures has firstly been illustrated, analyzing their typologies, the connections employed, and the analytical and numerical methods used for their design. An analytical method for the design of an innovative composite beam developed at the KTH Royal Institute of Technology has been illustrated showing its assumptions and formulations. The analytical model is able to predict the structural behaviour both in terms of internal forces and deflections. The model has then been used to perform a parametric analysis to investigate the influence of the geometric properties of the composite beam on the maximum deflection, given the span, the section size of the wooden component, the loads and the constraint conditions. It resulted on one hand that the parameter that most influences the maximum deflection of the composite beam is the diameter of the tensioned cable at the intrados, and that the external shear key connections are characterized by an optimum longitudinal position point along the length of the beam. This simple parametric analysis has also demonstrated the potential of the analytical model in providing a reliable and manageable tool for both the design and the improvement or optimization of the structural behaviour of the novel composite system.

Keywords: Timber; Cross-laminated Timber; multi-storey buildings; seismic analysis; numerical modelling; modelling strategies; component-level modelling; phenomenological modelling; analytical methods; composite structures; design methods; interaction domains; coupling effect.

Sommario

In questa tesi si sono analizzati due macro-argomenti di ricerca sull'ingegneria del legno. Il primo è lo studio del comportamento sismico di edifici in Cross-Laminated Timber (CLT, o X-Lam). Il secondo è l'analisi e il miglioramento del comportamento strutturale di una innovativa trave mista legno-acciaio, ideata e sviluppata all'Istituto Reale di Tecnologia KTH di Stoccolma, composta da sotto-elementi da collegare in sito mediante un sistema di chiavi di taglio e cavi in acciaio. In particolare, lo studio del comportamento sismico di edifici in CLT riportato in questo lavoro ha riguardato due aspetti che risultano ad oggi essere problematici, ovvero la ricerca di opportune strategie di modellazione per riprodurre il comportamento dinamico ed isteretico di strutture in CLT e lo sviluppo di un avanzato metodo di progettazione per pareti in CLT soggette a carico sismico, argomenti rispettivamente riportati nelle Parti I e II della tesi. L'attività di ricerca riguardante la trave mista legno-acciaio, riportata nella terza ed ultima parte della tesi, è stata invece finalizzata allo sviluppo di un modello analitico in grado di descriverne il comportamento meccanico sia in termini di sforzi interni che di deformazioni. Questo modello analitico non solo aiuta a comprendere meglio il comportamento meccanico rispetto ai modelli numerici, ma costituisce anche un utile strumento di progettazione per i professionisti.

Nella Parte I della tesi, riguardante le strategie di modellazione del comportamento sismico di edifici multipiano in CLT, si è dapprima effettuata una panoramica sulle tipologie di edifici multipiano in legno e, data l'importanza delle connessioni nel definirne il comportamento dinamico, si è effettuata una panoramica sui principali sistemi di connessione con un focus su quelli utilizzati per edifici in CLT. Si sono quindi analizzati i criteri di progettazione sismici per edifici in legno, evidenziandone lacune e criticità in particolare nella definizione del fattore di struttura e nella progettazione delle connessioni. Dopo uno stato dell'arte sulle strategie di modellazione, vengono analizzate nel dettaglio quelle *per componenti* e quella *fenomenologica* sia con approcci di modellazione lineari che non lineari. Lo studio delle due strategie viene effettuato simulando numericamente il comportamento di strutture di riferimento, che nel caso delle analisi lineari sono rappresentate da tre edifici multipiano rispettivamente di 2, 4 e 6 piani. Per le analisi non lineari si sono invece assunti come riferimento i test ciclici su singole pareti platform-frame monolitiche in CLT effettuati presso l'istituto CNR-IVALSA nell'ambito del Progetto SOFIE. I risultati di questi test sono stati oggetto di un'approfondita fase di interpretazione e rielaborazione critica necessaria al fine di individuare le peculiarità presentate dal dataset sperimentale. Nella modellazione *per componenti* i pannelli in CLT sono stati modellati con elementi lineari, mentre le connessioni sono state modellate con molle assiali e a taglio a cui sono state assegnate rispettivamente leggi costitutive lineari e non lineari a seconda dell'approccio di modellazione adottato. Nella modellazione *fenomenologica* le connessioni non sono state modellate con elementi *ad-hoc*, ma le proprietà del sistema-parete in CLT, modellato nella sua globalità, sono state calibrate in modo tale da riprodurre fedelmente il comportamento a carichi laterali. In particolare, nel caso di un approccio di modellazione lineare si è assegnato agli elementi piani elastici con cui è stato modellato il sistema-parete un modulo elastico equivalente in grado di fornire i medesimi spostamenti orizzontali del più raffinato modello per componenti. Sono inoltre stati ricavati degli abachi che forniscono il valore del modulo elastico equivalente adimensionalizzato allo spessore della parete per ogni livello dell'edificio al variare del numero di piani della struttura e dell'intensità dell'azione sismica. Per la modellazione fenomenologica non lineare si è invece calibrata la legge costitutiva multilineare in modo da riprodurre il comportamento globale delle pareti testate sia in termini di forza-spostamento che di energia cumulativa. I risultati dei modelli lineari sono stati analizzati in termini di sforzi sulle connessioni, periodo principale di vibrazione e spostamenti interpiano, mentre quelli dei modelli non lineari sono stati indagati in termini di diagramma forza-spostamento e di energia cumulativa. Inoltre, per la modellazione per componenti non lineare si sono analizzati anche gli spostamenti assiali e laterali misurati a livello di connessione. I risultati hanno mostrato che l'approccio di modellazione *per componenti* costituisce un ottimo strumento per lo studio numerico del comportamento sismico di edifici in CLT composti da un'eterogenea configurazione di pareti in CLT, purché il comportamento dei singoli componenti sia propriamente calibrato. La modellazione *fenomenologica* costituisce invece uno strumento di più facile utilizzo rispetto a quella *per componenti*, ma è caratterizzata da una più limitata versatilità data la dipendenza dei risultati dalla specifica configurazione di carico, di geometria e di connessione utilizzata per la sua calibrazione.

Nella Parte II della tesi, riguardante metodi analitici di progettazione sismica di edifici in CLT, si è dapprima fornita una panoramica sullo stato dell'arte dei metodi disponibili in letteratura, analizzandone le caratteristiche ed evidenziandone i limiti. Un promettente metodo di progettazione è quello derivante dal riadattamento del metodo di costruzione dei domini di interazione a presso-flessione di elementi in calcestruzzo armato al caso di pannelli in CLT in configurazione platform-frame soggetti ad azioni orizzontali. Uno di questi metodi presenti in letteratura, la cui formulazione è stata dettagliatamente illustrata, è stato quindi utilizzato come base per lo sviluppo di un metodo di progettazione più raffinato per la costruzione di diagrammi di interazione sforzo assiale – taglio. Alcune delle assunzioni del modello di partenza sono state modificate, in particolare si è assunto un comportamento elasto-plastico del legno soggetto a compressione in luogo di una legge elasto-fragile e si sono assunte delle leggi di resistenza accoppiate delle connessioni invece di considerare una loro infinita resistenza a taglio. Si sono illustrati e adoperati due diversi metodi di definizione delle leggi costitutive elasto-plastiche delle connessioni #1 e #2 e tre criteri di accoppiamento della loro resistenza: uno rettangolare, uno ellittico e uno innovativo basato su una formulazione ibrida forza-spostamento. I criteri di accoppiamento ellittico e rettangolare sono stati implementati con due diverse formulazioni. La prima, semplificata, assume che il raggiungimento della condizione ultima della connessione coincida con il punto di snervamento. La seconda formulazione, più raffinata, considera invece la rottura della connessione avvenuta solo una volta raggiunto lo spostamento ultimo. Dopo una dettagliata illustrazione delle caratteristiche del modello evidenziandone gli aspetti innovativi, si è indagato l'impatto delle diverse assunzioni mediante un'analisi di sensitività in cui si sono comparati i risultati con dati sperimentali di test condotti su pareti con le medesime caratteristiche meccaniche e geometriche. Dall'analisi di sensitività è risultato come sia indispensabile considerare l'effetto dell'accoppiamento delle connessioni onde evitare d'ottenere diagrammi di interazione sovraresistenti rispetto alla effettiva capacità della parete, e che l'adozione di una legge elasto-plastica per il legno consente di ottenere risultati nettamente più performanti rispetto al caso elasto-fragile.

Nella Parte III della tesi, riguardante l'analisi di un'innovativa trave composta legno-acciaio, si è dapprima illustrato lo stato dell'arte delle strutture composte in legno, analizzandone le tipologie, le connessioni utilizzate e le modalità di modellazione analitica e numerica di tali strutture. Si è quindi presentato un metodo analitico per lo studio di un'innovativa trave composta ideata all'Istituto Reale di Tecnologia KTH illustrandone assunzioni e formulazioni. Il modello analitico, validato mediante comparazione con un modello numerico, è in grado di prevedere il comportamento strutturale sia in termini di sollecitazioni che di deformazioni. Il modello è stato quindi utilizzato per compiere un'analisi parametrica per studiare l'influenza delle proprietà geometriche del sistema composto sulla massima deformazione per un fissato valore di luce della trave e di dimensione sezione della componente lignea e per una data configurazione di carico e di vincolo. Dall'analisi è risultato che il parametro che maggiormente influenza la deformazione della trave è il diametro del cavo teso all'intradosso e che le connessioni a taglio esterne sono caratterizzate da un punto di ottimo per il loro posizionamento longitudinale lungo la trave. Questa semplice analisi parametrica ha inoltre dimostrato la potenzialità del modello analitico nel fornire uno strumento affidabile e di facile gestione sia per la progettazione che per il miglioramento e l'ottimizzazione del comportamento strutturale del sistema.

Parole chiave: Legno; edifici multipiano; Cross-Laminated Timber; X-Lam; analisi sismica; modellazione numerica; strategie di modellazione; modellazione per componenti; modellazione fenomenologica; metodi analitici; strutture composte; metodi di progettazione; domini di interazione; effetto accoppiamento.

List of abbreviations

CLT	Cross-Laminated Timber
DCH	High Ductility Class
DCL	Low Ductility Class
DCM	Medium Ductility Class
EC	Eurocode
EC5	Eurocode 5
EC8	Eurocode 8
ELFP	Equivalent Lateral Force Procedure
EoL	End of Life scenario
EPP	Elasto-Perfectly Plastic
ESFP	Equivalent Static Force Procedure
ETA	European Technical Assessments
EWP	Engineered Wood Products
FE	Finite Element
FEM	Finite Element Method
FRP	Fiber-Reinforced-Polymers
GLT	Glued Laminated (or glulam) Timber
IBC	International Building Code
IDA	Incremental Dynamic Analysis
LSA	Linear Static Analysis
PGA	Peak Ground Acceleration
RC	Reinforced Concrete
SFRS	Seismic Force Resisting Systems
ST	Solid Timber
TBCS	Timber-Based Composite Structure
TCCS	Timber-Concrete Composite Structure
TSCS	Timber-Steel Composite Structure
UFP	U-shaped Flexural Plate

Index

Foreword ... **iii**

Abstract ... **i**

Sommario ... **iii**

List of abbreviations ... **v**

Index ... **vii**

Introduction ... **1**

Motivation and scope of the research ... 1

Organization of the thesis ... 3

Bibliography of Introduction ... 5

I Modelling strategies for CLT multi-storey buildings ... **7**

I.1 State-of-the-art of multi-storey timber buildings ... **9**

I.1.1 Chapter contents ... 11

I.1.2 Overview on timber multi-storey buildings ... 11

I.1.2.1 Spread of technology and scientific background ... *11*

I.1.2.2 Multi-storey building typologies ... *14*

I.1.2.2.1 Light timber frame systems ... 14

I.1.2.2.2 Heavy timber frame systems ... 15

I.1.2.2.3 CLT walls systems ... 15

I.1.2.2.4 Mixed CLT walls-heavy frame systems ... 17

I.1.2.2.5 Structural efficiency of the building typologies ... 17

I.1.2.3 Connections with dowel-type mechanical fasteners ... *18*

I.1.2.3.1 Nailed joints ... 19

I.1.2.3.2 Stapled joints ... 20

I.1.2.3.3 Screwed joints ... 20

I.1.2.3.4 Bolted and dowelled connections ... 21

I.1.2.4 Mechanical connections for CLT structures ... *22*

I.1.2.4.1 Common connection systems for CLT assemblies ... 23

I.1.2.4.2 Innovative connection systems for CLT assemblies ... 27

I.1.3 Code design provisions and modelling strategies for CLT buildings 28

I.1.3.1 Regulatory framework for seismic analysis and design of timber buildings 28

I.1.3.1.1 European seismic design regulatory framework 29

I.1.3.1.2 Extra- European seismic design regulatory framework 29

I.1.3.1 Behaviour factor for CLT buildings 30

I.1.3.2 Design of connections for CLT buildings 34

I.1.3.2.1 Ductility 34

I.1.3.2.2 Calculation models 37

I.1.3.2.3 Capacity design of connections 40

I.1.3.2.4 Coupling models 43

I.1.4 Numerical modelling of CLT buildings 43

I.1.4.1 Modelling strategies 43

I.1.4.2 Modelling of CLT panels 45

I.1.4.3 Modelling of connections 45

I.2 Component-level modelling approach 47

I.2.1 Chapter contents 49

I.2.2 Modelling strategy description 49

I.2.3 Linear analysis 51

I.2.3.1 Reference structure description 51

I.2.3.2 Numerical modelling of the multi-storey building 53

I.2.4 Non-linear analysis 57

I.2.4.1 Reference structure description 57

I.2.4.1.1 Description of the experimental setup adopted within the SOFIE project 57

I.2.4.1.2 Data interpretation of cyclic experimental tests and failure mode analysis 59

I.2.4.1.3 CLT shear walls experimental tests: global and local measurements 60

I.2.4.2 Numerical modelling of CLT shear walls 62

I.2.4.2.1 Modelling assumptions 65

I.2.4.2.2 Components calibration 66

I.2.4.2.3 Numerical Results 67

I.2.4.2.4 Sensitivity analyses 69

I.2.4.2.5 Out-of-plane displacement of the walls 75

I.3 Phenomenological modelling approach 79

I.3.1 Chapter contents 81

I.3.2 Modelling strategy description 81

I.3.3 Linear analysis 81
I.3.4 Non-linear analysis 84

I.4 Conclusions on numerical modelling strategies for CLT buildings 87
I.4.1 Chapter contents 89
I.4.2 Comparison between component level, phenomenological and hybrid modelling approaches . 89
I.4.3 Comparison between linear models 90
I.4.4 Comparison between non-linear models 93

Bibliography of Part I 95

II Design methods for CLT wall systems 109

II.1 State-of-the-art of design methods for CLT wall systems 111
II.1.1 Chapter contents 113
II.1.2 Methods for strength assessment of monolithic CLT shear walls 113
II.1.3 Methods for strength assessment of coupled CLT shear walls 120
II.1.4 Main limits of models for monotonic CLT shear walls 120
II.1.5 Coupling models for CLT connections 120

II.2 State-of-the-art of advanced non-linear design methods for CLT wall systems 123
II.2.1 Chapter contents 125
II.2.2 Assumptions and hypotheses 125
II.2.3 Definition of the stress distribution coefficient 126
II.2.4 Sub-domains definition and formulations 127

II.3 Interaction Domains for CLT Shear Walls with Coupled Constitutive Laws of Connections 133
II.3.1 Chapter contents 135
II.3.2 Assumptions 135
II.3.3 Multicriteria ultimate conditions 137
II.3.3.1 Bi-linearization of uniaxial constitutive laws of connections 137
II.3.3.2 Force-based connection strength domain 138
II.3.3.3 Hybrid force-displacement-based connection strength domain 139
II.3.4 Model calibration and validation 143
II.3.4.1 Case study 143
II.3.4.2 Definition of model mechanical parameters 143

II.3.4.2.1 CLT panel 143

II.3.4.2.2 Connections 143

II.3.4.3 Results 145

II.3.4.3.1 Timber constitutive law effect 145

II.3.4.3.2 Coupling criteria effect 146

II.3.4.3.3 Bi-linearization method of connections constitutive laws effect 147

II.3.5 Conclusions 147

Bibliography of Part II 149

III Innovative timber-based composite structures 153

III.1 State-of-the-art of timber-based composite structures 155

III.1.1 Chapter contents 157

III.1.2 Overview on timber-based composite structures 157

III.1.2.1 Timber-based composite structures typologies 157

III.1.2.2 Mechanical behavior 158

III.1.3 Timber-steel composite structures 160

III.1.4 Connections 164

III.1.4.1 Dowel-type fasteners 165

III.1.4.2 Notched shear key connections 167

III.1.4.3 Glued connections 167

III.1.4.4 Other innovative connections types 167

III.1.5 Analytical modelling of timber-based composite structures 169

III.1.6 Numerical modelling of timber-based composite structures 169

III.2 A mechanics-based analytical model for an innovative timber-steel composite beam 171

III.2.1 Chapter contents 173

III.2.2 Overview 173

III.2.2.1 Description of the novel structural system 173

III.2.2.2 Advantages and drawbacks of the novel technology 174

III.2.3 Analytical model description 176

III.2.3.1 Basic assumptions 179

III.2.3.2 Composite beam internal forces 179

III.2.3.2.1 Tensile force on the cable 179

III.2.3.2.2 Shear force on connections 181

III.2.3.2.3 Bending moment on timber beam 187

III.2.3.3 Composite beam short-term deflections 188

III.2.3.3.1 Rigid contribution 188

III.2.3.3.2 Elastic contribution 190

III.2.4 Results and comparison with numerical analyses 191

III.2.4.1.1 Numerical model description 192

III.2.4.1.2 Comparison of results between analytical and numerical models 193

III.2.4.1.3 Parameters affecting the structural performance of the system 193

III.2.5 Parametric analysis for structural performance enhancement 196

III.2.6 Conclusions and future developments 198

Bibliography of Part III 199

Conclusions and future developments 203

List of figures 207

List of tables 215

List of publications and conferences 217

Introduction

Motivation and scope of the research

Modern urbanization in seismic-prone areas requires the construction of multi-storey buildings that are safe, cost-effective and that can quickly be constructed. Cross-Laminated Timber (CLT) is a relatively new extremely versatile building technology that satisfies all of these requirements [1], making it suitable for multi-storey buildings for rapidly expanding cities [2]. Actually, the high prefabrication level of these buildings allows on one hand to reduce the construction time [3] and on the other hand to reduce the possibility of on-site human errors [4]. Another aspect that make this building technology attractive is its sustainability, thanks to its capacity to store carbon dioxide (CO_2) [5, 6], and it is one of the most economical and environmental beneficial building technology if the end-of-life (EoL) scenario is considered [7, 8]. In add, the high seismic performance of CLT multi-storey buildings [9] led to a high interest in the use of this technology in seismic-prone areas over the past two decades [10]. Actually, the high strength-to-weight ratio, high in-plane stiffness and ductility of both traditional [11, 12] and innovative connections [13] guarantee both resistance and energy dissipation capacity against seismic actions. Another reason behind the success of this kind of structures is its good fire performance [14], contrary to what could be believed at a first glance thinking to timber as a combustible material. There are anyway some issues relating multi-storey timber buildings that still need to be addressed in order to make this building technology reliable and competitive with traditional ones. Firstly, there is a lack of knowledge on the dynamic behavior of CLT buildings when subjected to wind [15] or seismic actions [16]. Many aspects on the seismic behavior of these structures have been investigated by the scientific community in the last years, to name a few the determination of the behavior factor [17], the lack of analytical models for connections that take into account the peculiarities of CLT material [18], the correct way to consider coupling effects of connections [19], the distribution of acceleration response along the height of the building [20] and reliable ways to numerically model the seismic behavior of these structures [21, 22]. Scope of the Part I of this thesis is to gain a deeper insight in two numerical modelling approaches used to predict the seismic behavior of CLT buildings, namely component-level and phenomenological models. Strategies and ploys necessary to guarantee the reliability of results will be investigated in depth, both in case a linear or non-linear model is adopted, also analyzing advantages and drawbacks of the two approaches.

Other aspects relating the seismic behavior of CLT buildings constitute an open problem, for example the shortage of adequate design criteria. Current versions of codes and standards lack in provisions for the structural design of CLT buildings [23], both for static and seismic design as it can be observed respectively in Eurocode 5 [24] and Eurocode 8 [25], and the main reference is to date constituted by European Technical Assessments (ETAs) of building products. Many authors in recent years have furnished analytical design approaches for seismic design of CLT wall systems [26] in order to address the lack of design criteria. However, these models are more suitable for the pre-design phase rather than for the final design since they are based on simplified assumptions that do not allow an efficient exploitation of the mechanical properties of the structure. For example, most of them consider the rocking failure happening because of balanced tensile failure of connections and compressed timber, without considering other failure mechanisms. A promising design method recently developed is the one derived from the well-known cross-sectional analysis techniques adopted to create interaction domains of reinforced concrete members subjected to combined axial and bending actions and adopted to axial-shear interaction domains of CLT wall system subjected to lateral loads [27]. Scope of the Part II of the thesis is the development of an enhanced method to perform axial-shear interaction domains of CLT wall system subjected to lateral loads starting from the model presented in [27]. New hypotheses and assumptions have been considered, allowing to obtain predictions of the structural behavior of CLT wall systems subjected to lateral loads both more performant and more on the safe-side.

Timber is also a versatile material that can be used in conjunction with concrete [28], steel [29] or different types and grades of timber [30] to create composite structures characterized by excellent performances both at serviceability and ultimate limit states. Timber-based composite structures represent a building technique that has been successfully used for many years both to new buildings [31] and bridges [32, 33], as well as for restoration purposes like the strengthening of existing timber floors [34]. Many are the reasons of its success, among them structural advantages like good seismic performance thanks to high strength-to-weight ratio [35] and better performances to serviceability limit state thanks respect to traditional timber floors thanks to higher damping and stiffness [36]. Composite timber-based structures present anyway some issues that need investigation, like their mechanical characterization since the composite action is influenced by many parameters, primarily the efficiency of connections [37]. On the other hand, relatively new engineered timber products like glued-laminated timber allowed to create long-span structural elements that can cover very large spans furnishing a very high architectural flexibility. These long elements have anyway many drawbacks: they are difficult to transport from factory to site, their installation is complicated requiring big lifting machinery, they are difficult to produce and, as a consequence, they increase the construction cost of the building. In order to find a solution to these problems, an innovative timber-steel composite beam has been ideated at KTH Royal Institute of Technology of Stockholm [38]. This structural member is composed of separated timber joists then joint together on site through a steel system composed of notched shear-keys and tensioned cables. Thus, longer structural elements can be obtained assembling smaller ones, allowing a considerable decrease of the total construction cost thanks to an increased easiness of transportation and handling on site. This novel technology is still a prototype and has been subjected only to preliminary numerical and experimental investigations [38] that showed on one hand the great potentialities of the structural system, and on the other hand highlighted the necessity of a deeper understanding of the mechanical behavior and the need of improving its structural performance. Scope of the Part III of this thesis is the development of a mechanics-based analytical model able to predict both internal forces and deflections of the composite system. The analytical model not only allows for a better understanding of the mechanical behavior of the novel composite beam respect to numerical models, but it is also a manageable tool that can be used to easily carry out parametric analysis for enhancement and optimization of structural performances.

Organization of the thesis

The thesis is organized in three parts, each subdivided in different chapters with the structuring listed below:

Part I

- ***Chapter I.1*** A state-of-the-art of multi-storey timber technology is given, with a particular focus on CLT structures. After a general overview of the typologies usually adopted for the construction of multi-storey timber buildings, a description of the principal connections used for CLT buildings will be provides since their utmost relevance in defining the seismic behavior of these structures. The current state-of-the-art of codes and standard relating the static and seismic design of CLT structures is analyzed, highlighting in particular lack in the provision given for the determination of the behavior factor and the design criteria of connections. A brief overview of the modelling strategies available in scientific literature and used by practitioners for seismic analysis of CLT buildings is also given.
- ***Chapter I.2*** Component-level numerical modelling approach will be studied both adopting linear and non-linear analyses, analyzing strategies to be adopted to guarantee reliability of results. Analyses are carried out with plane models on references structures, a multi-storey CLT building and single monolithic CLT shear walls respectively for linear and non-linear models. A preliminary phase of interpretation of the experimental results used as reference for non-linear analyses will be presented. Outcomes of linear and non-linear models are analyzed in order to define advantages and limits of the modelling strategy.
- ***Chapter I.3*** Phenomenological numerical modelling approach will be studied both adopting linear and non-linear analyses, highlighting strategies and ploys to be adopted to guarantee reliability of results. Analyses are carried out with plane models on the same reference structures assumed for component-level approach. Outcomes of linear and non-linear models are analyzed in order to define advantages and limits of the modelling strategy.
- ***Chapter I.4*** A summary of the main findings of the first part of the thesis is reported, comparing component-level and phenomenological numerical outcomes in order to highlight advantages and drawbacks of each approach. In add, comparisons between linear and non-linear models are carried out both for component-level and phenomenological approaches.

Part II

- ***Chapter II.1*** A state-of-the-art of analytical design methods for seismic design of CLT structures is given. Different methods available on scientific literature to derive shear strength of CLT shear walls are compared in order to highlight advantages, drawbacks and the main limits of the current available methods.
- ***Chapter II.2*** An advanced method to create axial-shear N-V interaction domains of CLT wall systems subjected to lateral loads is presented. Its assumptions and formulations are described in depth, highlighting the main limits of the methods that will be enhanced in a new model described in the next chapter.
- ***Chapter II.3*** An improvement of the N-V interaction domain method for CLT structures presented in the previous chapter is presented. New enhanced assumptions were considered, like a ductile behavior of timber in compression and failure mechanism of connections accounting for coupling phenomena. Basic assumptions and novelty aspects of the improved N-V interaction domain method are presented and discussed. Finally, the N-V domain for a case study CLT shear-wall is presented and the impact of the different basic assumptions on the results are discussed.

Part III

- ***Chapter III.1*** A state-of-the-art of timber-based composite structures is reported. After describing the different types of timber-based constructions highlighting the advantages of the system, hints of their mechanical behavior are furnished. A description of the available types of connections, their modelling and their behavior is then be provided, comparing advantages and drawbacks of each one. Finally, analytical and numerical modellings of these structures are also discussed.

- ***Chapter III.2*** A mechanics-based analytical model able to predict both internal forces and displacements of a novel composite timber-steel structure ideated at KTH Royal Institute of Technology is presented. After a description of the assumptions used to develop the analytical model, its formulation will be analyzed in depth. The model is then compared with a numerical model. Finally, a simple parametric analysis is carried out to investigate the performance of the system to the vary of the main mechanical and geometrical properties of the beam.

Chapters ***Introduction*** and ***Conclusions and future works*** are also present respectively at the beginning and at the end of the structuring listed above, the former reporting motivations and scope of the research, the latter synthetizing the main findings of the three Parts of this Thesis.

At the end of each Part, the correspondent ***Bibliography*** is reported with a sequential numbering independent for each.

Bibliography of Introduction

[1] S. Pei, J. Berman, D. Dolan, J. Van De Lindt, J. Ricles, R. Sause, H. Blomgren, M. Popovski, D. Rammer, Progress on the development of seismic resilient tall buildings in the Pacific Northwest, in: World Conf. Timber Eng. 2014, 2014.

[2] J.W.G.V. De Kuilen, A. Ceccotti, Z. Xia, M. He, Very Tall Wooden Buildings with Cross Laminated Timber, Procedia Eng. 14 (2011) 1621–1628. doi:10.1016/j.proeng.2011.07.204.

[3] R. Brandner, Production and Technology of Cross Laminated Timber (CLT): A state-of-the-art Report, in: R. Harris, A. Ringhofer, G. Schickhofer (Eds.), Focus Solid Timber Solut. Conf. Cross Laminated Timber, The University of Bath, Bath, 2013.

[4] N. Doyle, R. Emberley, J.L. Torero, Fire Behavior of Cross-Laminated Timber (CLT) Slabs: Two-Way Action, in: Fire Sci. Technol. 2015, Springer Singapore, Singapore, 2017: pp. 281–288. doi:10.1007/978-981-10-0376-9_28.

[5] S. Lehmann, Sustainable Construction for Urban Infill Development Using Engineered Massive Wood Panel Systems, Sustainability. 4 (2012) 2707–2742. doi:10.3390/su4102707.

[6] H.J. Darby, A.A. Elmualim, F. Kelly, A case study to investigate the life cycle carbon emissions and carbon storage capacity of a cross laminated timber, multi-storey residential building, in: Sustain. Build. Conf. SB13, Munich, Germany, 2013.

[7] A. Takano, M. Hughes, S. Winter, A multidisciplinary approach to sustainable building material selection: A case study in a Finnish context, Build. Environ. 82 (2014) 526–535. doi:10.1016/j.buildenv.2014.09.026.

[8] A. Dodoo, L. Gustavsson, R. Sathre, Lifecycle primary energy analysis of low-energy timber building systems for multi-storey residential buildings, Energy Build. 81 (2014) 84–97. doi:10.1016/j.enbuild.2014.06.003.

[9] A. Ceccotti, C. Sandhaas, M. Okabe, M. Yasumura, C. Minowa, N. Kawai, SOFIE project - 3D shaking table test on a seven-storey full-scale cross-laminated timber building, Earthq. Eng. Struct. Dyn. 42 (2013) 2003–2021. doi:10.1002/eqe.2309.

[10] L. Pozza, D. Trutalli, A. Polastri, A. Ceccotti, Seismic design of CLT buildings: Definition of the suitable q-factor by numerical and experimental procedures, in: P.J.S. Cruz (Ed.), Struct. Archit. Concepts, Appl. Challenges - Proc. 2nd Int. Conf. Struct. Archit. ICSA 2013, Taylor & Francis Group, London, Boca Raton, FL, 2013.

[11] I. Gavric, M. Fragiacomo, A. Ceccotti, Cyclic behaviour of typical metal connectors for cross-laminated (CLT) structures, Mater. Struct. 48 (2015) 1841–1857. doi:10.1617/s11527-014-0278-7.

[12] R. Tomasi, I. Smith, Experimental Characterization of Monotonic and Cyclic Loading Responses of CLT Panel-To-Foundation Angle Bracket Connections, J. Mater. Civ. Eng. 27 (2015) 04014189. doi:10.1061/(ASCE)MT.1943-5533.0001144.

[13] R. Scotta, L. Marchi, D. Trutalli, L. Pozza, A Dissipative Connector for CLT Buildings: Concept, Design and Testing, Materials (Basel). 9 (2016) 139. doi:10.3390/ma9030139.

[14] M. Fragiacomo, A. Menis, I. Clemente, G. Bochicchio, A. Ceccotti, Fire Resistance of Cross-Laminated Timber Panels Loaded Out of Plane, J. Struct. Eng. 139 (2013) 04013018. doi:10.1061/(ASCE)ST.1943-541X.0000787.

[15] T. Reynolds, R. Harris, W.-S. Chang, J. Bregulla, J. Bawcombe, Ambient vibration tests of a cross-laminated timber building, Proc. Inst. Civ. Eng. - Constr. Mater. 168 (2015) 121–131. doi:10.1680/coma.14.00047.

[16] S. Pei, J.W. van de Lindt, M. Popovski, J.W. Berman, J.D. Dolan, J. Ricles, R. Sause, H. Blomgren, D.R. Rammer, Cross-Laminated Timber for Seismic Regions: Progress and Challenges for Research and Implementation, J. Struct. Eng. 142 (2016). doi:10.1061/(ASCE)ST.1943-541X.0001192.

[17] L. Pozza, D. Trutalli, An analytical formulation of q-factor for mid-rise CLT buildings based on parametric numerical analyses, Bull. Earthq. Eng. 15 (2017) 2015–2033. doi:10.1007/s10518-016-0047-9.

[18] T. Uibel, H.J. Blaß, Load carrying capacity of joints with dowel type fasteners in solid wood panels, in: Int. Counc. Res. Innov. Build. Constr. - Work. Comm. W18 - Timber Struct. - Meet. Thirty-Nine, Florence, Italy, 2006.

[19] L. Pozza, A. Saetta, M. Savoia, D. Talledo, Coupled axial-shear numerical model for CLT connections,

Constr. Build. Mater. 150 (2017) 568–582. doi:10.1016/j.conbuildmat.2017.05.141.

[20] C. Demirci, C. Málaga-Chuquitaype, L. Macorini, Seismic shear and acceleration demands in multi-storey cross-laminated timber buildings, Eng. Struct. 198 (2019) 109467. doi:10.1016/j.engstruct.2019.109467.

[21] M. Izzi, A. Polastri, M. Fragiacomo, Investigating the Hysteretic Behavior of Cross-Laminated Timber Wall Systems due to Connections, J. Struct. Eng. 144 (2018) 04018035. doi:10.1061/(ASCE)ST.1943-541X.0002022.

[22] B. Dujic, K. Strus, R. Zarnic, A. Ceccotti, Prediction of Dynamic Response of a 7-storey Massive XLam Wooden Building Tested on a Shaking Table, in: 11th World Conf. Timber Eng. 2010, WCTE 2010, Riva del Garda, Italy, 2010: pp. 3450–3457.

[23] M. Popovski, S. Pei, J.W. Lindt, E. Karacabeyli, Force Modification Factors for CLT Structures for NBCC, in: Mater. Joints Timber Struct., Springer Netherlands, Dordrecht, 2014: pp. 543–553. doi:10.1007/978-94-007-7811-5_50.

[24] European Committee for Standardisation, EN 1995-1-1 - Eurocode 5: Design of timber structures - Part 1-1: General - Common rules and rules for buildings, 2004.

[25] European Committiee for Standardization, ed., EN 1998-1: Eurocode 8: Design of structures for earthquake resistance—Part 1: general rules, seismic actions and rules for buildings., 2004.

[26] I. Lukacs, A. Björnfot, R. Tomasi, Strength and stiffness of cross-laminated timber (CLT) shear walls: State-of-the-art of analytical approaches, Eng. Struct. 178 (2019) 136–147. doi:10.1016/j.engstruct.2018.05.126.

[27] G. Tamagnone, G. Rinaldin, M. Fragiacomo, A novel method for non-linear design of CLT wall systems, Eng. Struct. 167 (2018) 760–771. doi:10.1016/j.engstruct.2017.09.010.

[28] A. Ceccotti, Timber-concrete composite structures, in: Timber Eng. STEP 2, Centrum Hout, Netherlands, 1995.

[29] A. Hassanieh, H.R. Valipour, M.A. Bradford, Experimental and numerical investigation of short-term behaviour of CLT-steel composite beams, Eng. Struct. 144 (2017) 43–57. doi:10.1016/j.engstruct.2017.04.052.

[30] C. Leyder, F. Wanninger, A. Frangi, E. Chatzi, Dynamic response of an innovative hybrid structure in hardwood, Proc. Inst. Civ. Eng. - Constr. Mater. 168 (2015) 132–143. doi:10.1680/coma.14.00043.

[31] A. Fadai, W. Winter, M. Gruber, Wood based construction for multi-storey buildings. The potential of cement bonded wood composites as structural sandwich panels, in: World Conf. Timber Eng. 2012, Auckland, New Zealand, 2012.

[32] Z. Lyu, C. Málaga-Chuquitaype, A.M. Ruiz-Teran, Design of timber-concrete composite (TCC) bridges with under-deck stay cables, Eng. Struct. 189 (2019) 589–604. doi:10.1016/j.engstruct.2019.03.059.

[33] J.P. Wacker, A. Dias, T.K. Hosteng, Investigation of Early Timber-Concrete Composite Bridges in the United States, in: 3rd Int. Conf. Timber Bridg. (ICTB 2017), Skelleftea, Sweden, 2017.

[34] M.A. Parisi, M. Piazza, Restoration and Strengthening of Timber Structures: Principles, Criteria, and Examples, Pract. Period. Struct. Des. Constr. 12 (2007) 177–185. doi:10.1061/(ASCE)1084-0680(2007)12:4(177).

[35] T. Herzog, J. Natterer, R. Schweitzer, M. Volz, W. Winter, Timber construction manual, Birkhauser Verlag AG, 2004.

[36] K. Quang Mai, A. Park, K.T. Nguyen, K. Lee, Full-scale static and dynamic experiments of hybrid CLT–concrete composite floor, Constr. Build. Mater. 170 (2018) 55–65. doi:10.1016/j.conbuildmat.2018.03.042.

[37] B.L. Deam, M. Fragiacomo, A.H. Buchanan, Connections for composite concrete slab and LVL flooring systems, Mater. Struct. 41 (2008) 495–507. doi:10.1617/s11527-007-9261-x.

[38] T. Wang, Y. Wang, Hybrid structures with shear-key connections, KTH - Royal Istitute of Technology, 2019.

I

Modelling strategies for CLT multi-storey buildings

I.1 State-of-the-art of multi-storey timber buildings

Abstract

The request of a new generation of buildings that is more sustainable, seismically safe and of rapid execution is answered by multi-storey timber building technology. New engineered timber materials and recent removal of building codes limitations to the maximum height allowed for multi-storey timber buildings to rapidly spread in recent years even in seismic-prone areas. A key-factor in the success of this new building technology is its excellent seismic performances as proved by many research projects conducted in the last decades on multi-story timber building realized with different construction technologies. Successful applications of this new building technology can be found in many multi-storey timber buildings already built all over the world, also in seismic-prone areas, especially in Europe, North America and Australasia, like the Dalston Lane in London (U.K.), the Wälludden building in Växjö (Sweden) and the Mjøstårnet in Brumunddal (Norway) respectively presenting a CLT, a light-framed and a heavy-framed load-bearing structure.

In this Section an overview of the structural typologies adopted to build up multi-storey timber buildings will be given. The behavior of these structures is strictly correlated to connections characteristics, especially when they are subjected to high-amplitude lateral loads. Hence, an overview on the most widespread types of connections used in these structures will also be provided. One of the most promising multi-storey timber buildings technologies for seismic-prone areas is the CLT one. Since it is a relatively new material, many aspects on its structural behavior still need to be investigated further and it suffers lack of adequate code provisions for its design. For this reason, an overview of provisions given by existing and upcoming codes and standards for the design of CLT structures will be provided, focusing in particular on the behavior factor and design criteria of connections. Finally, an overview of different modelling strategies available in literature and used to study the seismic behavior of CLT multi-storey structures will be given, aspect will then be analyzed in depth in the following Sections I.2 and I.3 of this thesis.

I.1.1 Chapter contents

In this Chapter a state-of-the-art of multi-storey timber building technology will be given. In Section I.1.2 an overview on multi-storey buildings will be furnished, illustrating their main typologies and the connections usually employed. In Section I.1.3 an overview on design provisions for CLT systems furnished by codes and standards will be given, mainly focusing on issues relating the seismic design of these structures like the behaviour factor and the design of connections. Finally, a state-of-the-art of numerical modelling strategies for CLT buildings will be given in Section I.1.4.

I.1.2 Overview on timber multi-storey buildings

I.1.2.1 Spread of technology and scientific background

Modern urbanization requires the construction of sustainable multi-storey buildings that are safe, cost-effective and that can quickly be constructed [1]. Especially for areas in the world where wood availability is high, timber multi-storey buildings are gaining high interest as a reliable way to build multi storey buildings for townhouse, commercial and tertiary designated use. Actually, timber presents many advantages: it's a natural and sustainable, thanks to a low carbon footprint and CO_2 storage and its low weight gives advantages for static loads (e.g. fewer resistant foundations are needed) and seismic actions, since they are directly proportional to the mass of the building. In add, timber has an excellent structural efficiency in the direction parallel to grain: actually, given ρ the mass density and f the strength of timber, it's possible to observe (Table I.1-1) that strength on mass density ratio f/ρ is similar to the steel one, and about 6 times the one of concrete. Another aspect that makes timber an excellent building material is its durability that, contrary to what could be believed at a first glance, is very good if correct design principles are followed, and Japanese Pagodas are an evidence of both durability and high seismic performance of multi-storey timber structures [2].

Table I.1-1 – Structural efficiency of timber and other traditional building materials (adapted from [3]).

Material	*f/ρ [m²/s²]*	*E/f [m²/s²]*
Timber (Glulam GL24)	~ 63000	~ 480
Concrete (R_{ck} 30 MPa)	~ 10400	~ 1200
Steel (S275)	~ 55000	~ 480

Anyway, timber construction industry has to face a path dependency over the past century, that has been characterized mainly by concrete usage, slowing down the growth and spread of timber multi storey buildings [4]. A turnaround is possible through government policies and funding that could lead to industry's interest on this new technology and a greater involvement of research community on timber topics.

The main stumbling block to the spread of this technology in last century may be sought in limitations of the maximum height of timber buildings present in Codes of many States that have been repealed only in recent years, e.g. the Ministerial Decree of 9th January 1996 (DM 96) in Italy valid until 2008 with the introduction of the new Italian Building Code NTC 2008 [5], which limited the maximum height of timber buildings to 7 or 10 storeys as a function of the area seismic grading [6]. Other countries that removed height restrictions of timber buildings are Sweden [4] and New Zealand [7], while in others height limitations are still present, like Canada [8] where 6 storeys are allowed, and U.S.A. where the International Building Code [9] make it difficult to exceed 5 storeys. It's worth noting that these limitations primarily reflect the lack of knowledge of the dynamic response of taller wood buildings to lateral actions (seismic and wind loads), as well as fire safety considerations [10]. Therefore, research activity by scientific community on the dynamic and fire performances of timber structures is still necessary in order to have a deeper insight and spread knowledge on these aspects.

After the removal of these limitations and despite their persistence in some States, timber multi-storey industry has seen a rapid growth, with the construction of many multi-storey timber buildings, e.g. the Dalston Lane in London [11] and the Forte building in Australia [12], both 10-storey buildings with a bearing structure made of Cross Laminated Timber (CLT) and the former being the tallest and largest building in the world with this structural typology [11] (Figure I.1-1). CLT multi storey building is a structural typology that is spreading quite quickly during the last decade thanks to its great potentialities [13], with examples recently built in Sweden, United Kingdom, Germany, Italy and Australia [14].

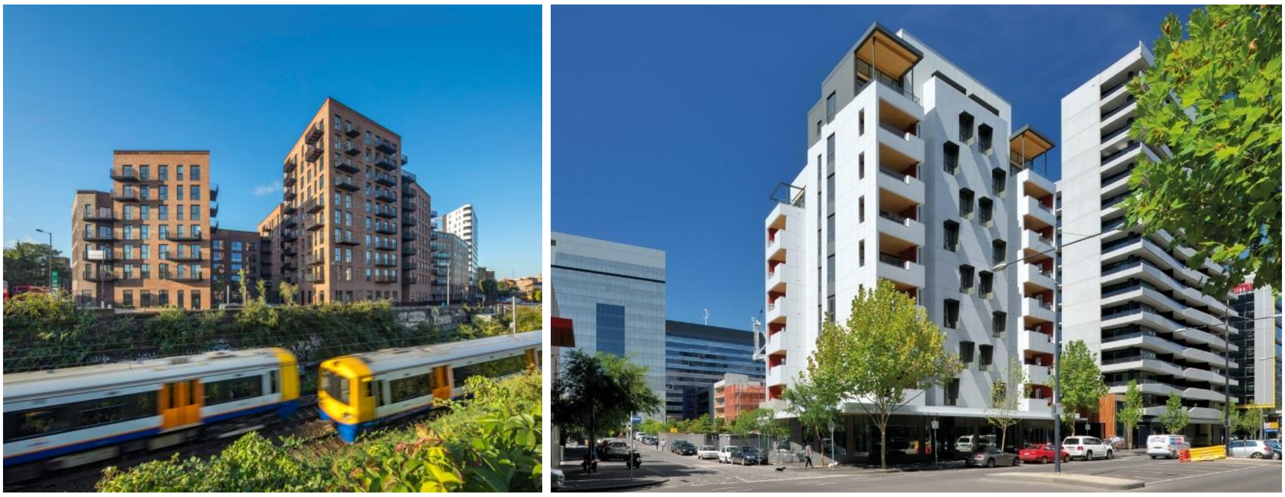

(*a*) (*b*)

Figure I.1-1 – CLT multi-storey timber buildings: (*a*) Dalston Lane building in London (United Kingdom) and (*b*) Forte building in Melbourne (Australia) (*image credits*: (*a*) Waugh Thistleton Architects website [15] and (b) The Possible website [16]).

Another example that proof the high structural capabilities of timber to build high-rise buildings is the Mjøstårnet, completed in Norway on March 2019 and that with his 81m is the highest timber building in the world. The 18-storey structure is composed of a heavy glulam timber (GLT) post-and-beam frame, with inclined joists on facade walls in order to create a truss system that both works for vertical loads and provide lateral stability and stiffness [17]. In add, a CLT wall structural system, that doesn't contribute to lateral stability, is adopted for staircases and elevators. Another multi storey timber building that has proven timber capabilities in multi-storey building industry is the Treet in Bergen (Norway) [18]. It is a 14 storey residential building completed in 2015 whose structure is similar to the Mjøstårnet, with the main structure made of glulam post and beams and CLT walls used for elevator shaft and that do not contribute to the main load bearing system. From the dynamic studies conducted on this building, it's possible to observe that the main structural issue for timber multi-storey buildings is the limitation of accelerations at upper levels, and this is mainly due to timber low modulus of elasticity-strength ratio E/f (Table I.1-1), therefore a deeper knowledge of dynamic behaviour and damping properties of these structures is necessary [19]. The main differences between Mjøstårnet and Treet buildings is that the former is 30 m taller and that this latter does not use a modular scheme differently from Treet.

Modular multi-storey buildings are gaining interest thanks to many advantages, among which it is possible to cite faster and safer manufacturing, a better quality thanks both to quality checks carried out on production sites and the reduced risk of errors on site, a better predictability to completion time and excellent structural performances [20]. A common and economically advantageous solution for multi-storey modular buildings is the usage of timber in combination with other materials [20], e.g. steel [21], creating composite structures whose overview will be provided in Section III.1.

Under a structural point of view, two are the main key-factors that lead to success of multi-storey timber buildings, namely the engineered wood products (EWP) to obtain more performant timber structural members and assemblies (e.g. Cross-Laminated Timber and glulam), and hybridization of timber with other materials (see Section III.1) [22]. One of the engineered timber materials that mostly contributed to the development of high-rise timber buildings is Cross-Laminated Timber (CLT) [13]. CLT is a plate-like EWP, introduced at the end of the last century in Germany and Austria [23, 24], formed by gluing an uneven number of timber layers (generally from three to seven) with 90° crosswise grain direction between adjacent layers (Figure I.1-5.a). It is designed for structural purposes and it can withstand loads both in-plane and out-of-plane. Each layer is composed of finger-jointed lamellas having the same grain direction placed side by side, with a width ranging between 40 and 300 mm and a thickness that span from 12 to 45 mm, glued on the major faces to the adjacent layers, while the narrow face can be or not glued to the coplanar adjacent lamella [25]. This internal structure, characterized by grains at a right angle between adjacent layers, allows both to optimize its structural behaviour in the in-plane and out-of-plane directions, and to add dimensional stability reducing swelling and shrinkage effects due to moisture variations [23]. CLT has also allowed the usage of low-grade and low-density wooden species for structural applications. An extensive overview on manufacturing process and mechanical characteristics of this material has been presented by Brandner *et al.* [23].

CLT is a relatively new type of material, but it has already gained popularity in North America, Australasia and Europe. Actually, the research activity on this material technology is still quickly ongoing. As a proof of this, some authors are proposing novel CLT panel solutions [26], and the research activity on its mechanical behavior is still flourishing [27, 28]. CLT allows for architectonic freedom thanks to the possibility to think in planes and volumes rather than lines. In add, installation of additional layers (e.g. insulation) is eased by the presence of a continuous planar support. One of the main issues of this novel structural typology is represented by the lack of knowledge about modelling strategies: this first part of the thesis will mainly rely on this aspect, focusing particularly on analyzing advantaged and advantages of different numerical strategies for seismic design of CLT structures. Seismic behavior of timber buildings with seismic protection technologies (e.g. supplemental damping and base isolation) is out of the scope of this Thesis, and the reader is referred to [29] for a broad state-of-the-art on this topic.

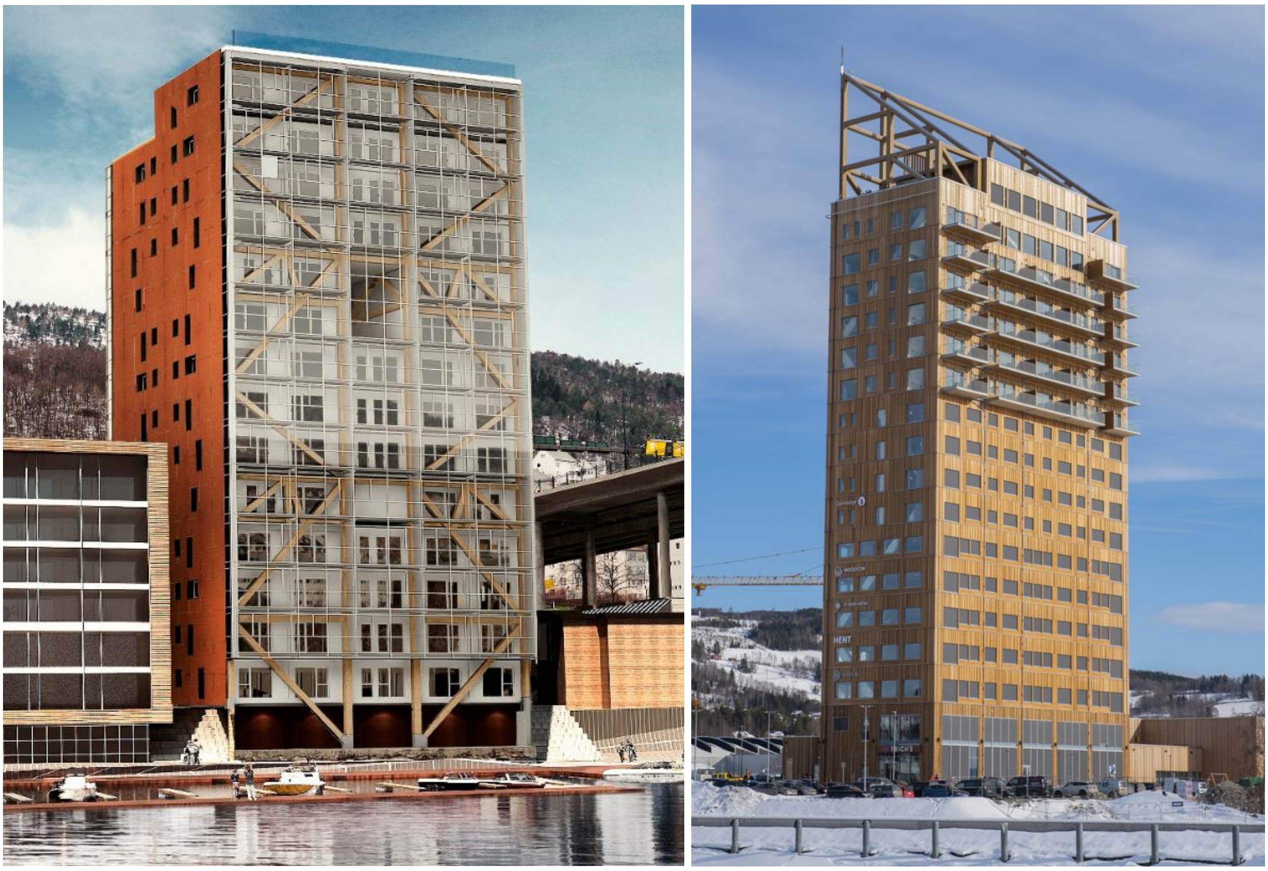

(*a*) (*b*)

Figure I.1-2 – High timber buildings in Norway: (*a*) Treet and (*b*) Mjøstårnet (*image credits*: (*a*) Abrahamsen & Malo [18] and (*b*) Moelven website [30]).

I.1.2.2 Multi-storey building typologies

It is possible to distinguish different types of multi-storey building as a function of the technology used for horizontal and vertical load-bearing structures.

I.1.2.2.1 Light timber frame systems

Light timer frame system is a nail-assembled combination of lumber, I-joists, trusses, oriented strand board decking and sheathing suitable to build multi-storey buildings up to 4-6 floors [1]. This timber building technology has been used for many years, and it's very efficient to build prefabricated structures, since fully scale insulated panels (Figure I.1-3.a) can be assembled in factory, transported on construction site and there rapidly lifted and mounted. Two sub-types of light-frame timber buildings are present:

1. *platform frame*, where individual floors framed separately (Figure I.1-3.b);
2. *balloon frame*, for which the vertical elements extend for more than one storey (usually two) (Figure I.1-3.c).

They present good seismic performances thanks to a highly-dissipative behavior mainly governed by sheathing-to-framing joints [31]. Several dynamic shaking table tests on full-scale structures investigated the seismic performance of this type of structures, like the ones carried out within the NEESWood project [32, 33] and the SERIES project [34]. These tests showed excellent seismic performances both in terms of inter-storey drifts and peak measured accelerations at upper floors. In add, they usually can withstand even strong seismic actions without significant damage to the structural parts of the buildings [35].

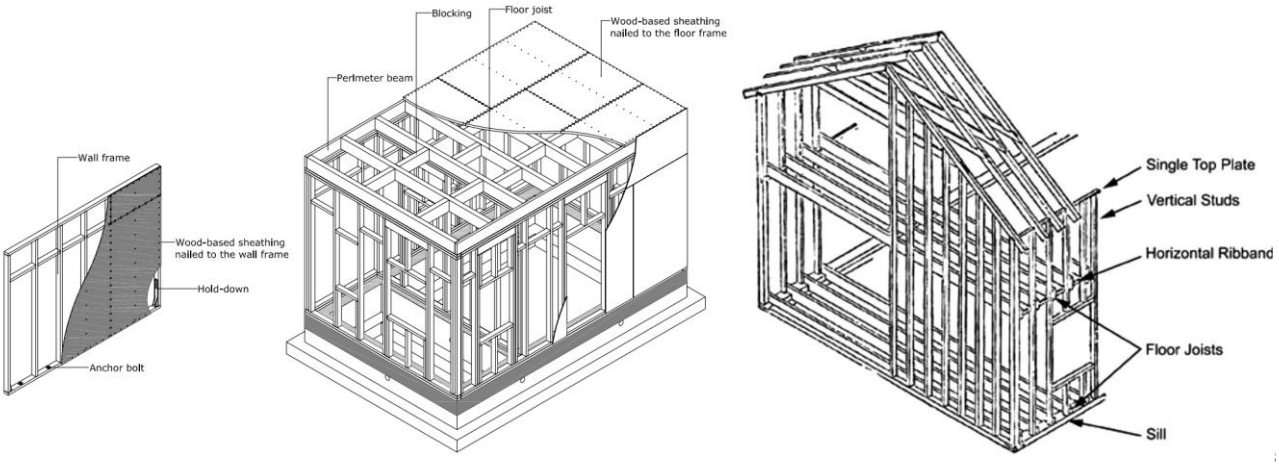
Wall frame
Wood-based sheathing nailed to the wall frame
Hold-down
Anchor bolt
Blocking
Floor joist
Wood-based sheathing nailed to the floor frame
Perimeter beam
Single Top Plate
Vertical Studs
Horizontal Ribband
Floor Joists
Sill

(*a*) (*b*) (*c*)

Figure I.1-3 – Light timber frame system: (*a*) wall components, (*b*) platform frame structure and (*c*) balloon frame structure (*image credits*: (*a-b*) Follesa *et al.* [36] and (*c*) Acar [37]).

I.1.2.2.2 Heavy timber frame systems

Heavy timber frame buildings are systems whose vertical and lateral load bearing structure is composed by post-and-beams assemblies usually made of glulam or LVL (Figure I.1-4.a). These engineered materials indeed allowed larger cross-sections of members and consequently larger span lengths. Treet and Mjøstårnet buildings [17, 18] are two examples of the great potentialities of this structural typology. Researchers at University of Canterbury have been studying seismic behaviour of these structures for years, developing an innovative post-tensioned LVL timber framed system with excellent seismic performances [7] (Figure I.1-4.b).

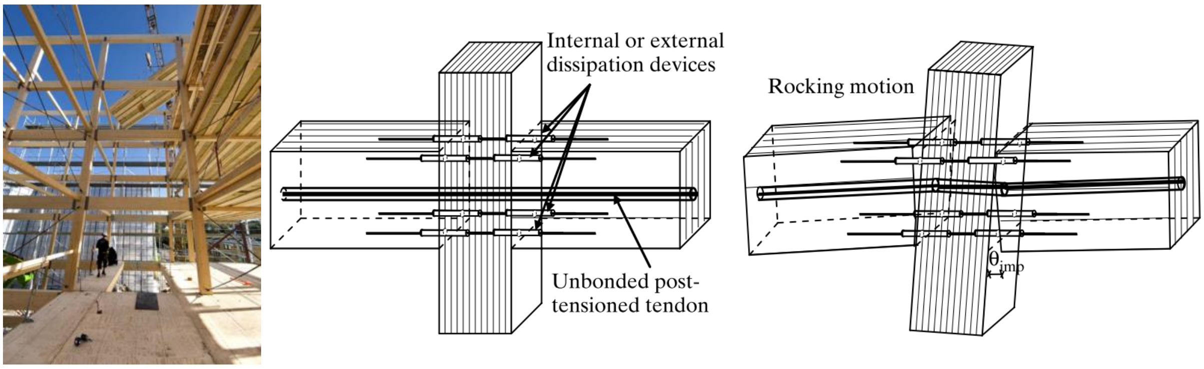
Internal or external dissipation devices
Unbonded post-tensioned tendon
Rocking motion
θ_{imp}

(*a*) (*b*)

Figure I.1-4 – Heavy timber frame system: (*a*) example of building [38] and (*b*) detail of a post-tensioned joint [7] (*image credits*: (*a*) Swedish Wood [38], (*b*) Buchanan *et al.* [7]).

I.1.2.2.3 CLT walls systems

CLT walls systems are structures up to 10 storeys (e.g. Dalston Lane in London) where both vertical and lateral load bearing structure is represented by CLT wall panels (Figure I.1-5.b). CLT panels width spans from 0.5 to 3 m (also 5 m wide panels are produced, but they are less common), and height up to 18 m are available [39]. In order to reach higher width and heights, panels are jointed together though connections (Figure I.1-5.c), in non-seismic zones usually arranged as evenly spaced angle brackets (Figure I.1-15.a) that connect perpendicular panels at vertical intersections between walls and at horizontal wall-floor intersections. In seismic prone areas, a different connection configuration is usually provided (Figure I.1-5.c), with hold-downs

(Figure I.1-15.a) at either end corners of the panel with the main function to resist uplift (viz. their shear resistance is usually disregarded in common design practice, see Section II.1.2), while angle brackets are commonly assumed to resist only shear loads (Section II.1.2). The latter configuration of connectors has been the focus of research activity for many authors in the last decade, with many scientific publications investigating the response to horizontal actions of CLT wall systems (e.g. [40–48]). Either the first and second part of this thesis will focus on aspects within this framework, relying on numerical modelling strategies and design methods for CLT wall systems.

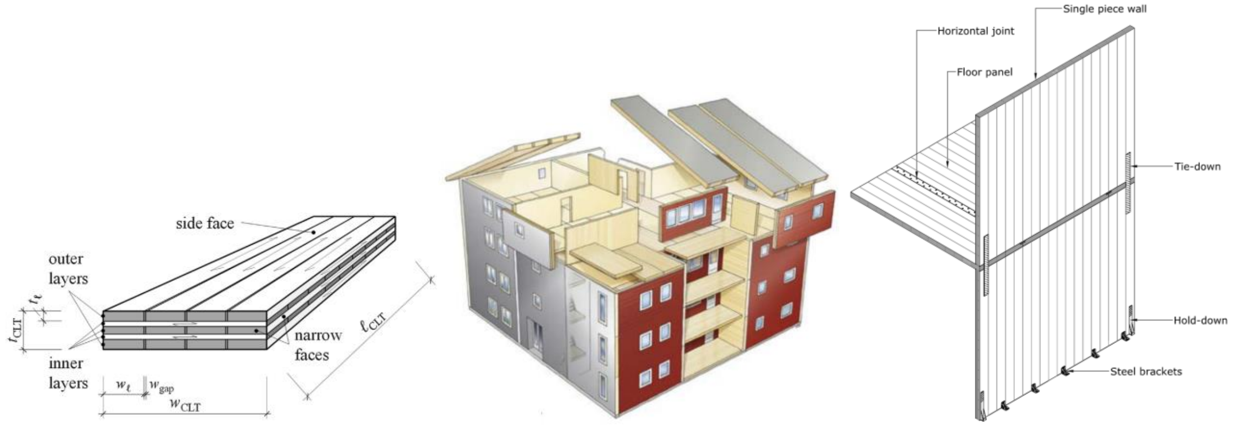

(*a*) (*b*) (*c*)

Figure I.1-5 – CLT wall system: (*a*) internal crosswise layered structure, (*b*) structural system representation and (*c*) typical connection assemblies (*image credits*: (*a*) Martínez-Martínez [49], (*b*) Swedish Wood [38] and (*c*) Follesa *et al.* [36]).

Similarly to the distinction made for light frame timber buildings (Section I.1.2.2.1), for CLT wall system is possible to define two sub-categories [39]:

- *Platform construction* (Figure I.1-6.a), where CLT floor panels lay on top edge of walls that form a platform for the subsequent floor. It is the most common solution for multi-storey timber buildings, and it’s the typical solution for CLT structures erected in North America and Europe. It has many advantages, like a well-defined load path, simple connections and easiness in erect upper storeys.
- *Balloon construction* (Figure I.1-6.b), where intermediate floors are attached to wall panels that span over the height of a single storey. This is a less common solution mainly adopted for low- and medium-rise commercial and industrial constructions with mezzanines between the main floors.

Platform frame CLT buildings are usually employed for residential, office and school buildings up to 3 storeys. For heavier (e.g. industrial and commercial buildings) or higher (e.g. multi-storey CLT buildings higher than 5 storeys) buildings, balloon frame typology is usually adopted. They both can also be used in combination with concrete cores for lift-shafts and stairwells [50] (eventually in combination with outriggers [13]) in order to reach higher heights thanks to the significant increase of the structural lateral stiffness, that usually is the main limit in height extension of timber buildings.

CLT structures usually have a higher in-plane stiffness and a greater load-carrying capacity respect to light-frame buildings, thanks both to the usage of stiffer panels and to hold-downs and angle brackets stronger and stiffer than the one employed for light-frame buildings.

Seismic characterization of CLT multi-storey buildings is still a topic of study for many researchers, as it is witnessed by huge amount of research activity (e.g. [51, 52]), and this first part of the thesis will relate to it. Seismic behaviour of CLT buildings is strongly affected by connections [53] (Section I.1.2.4), therefore their correct characterization and design is fundamental to guarantee reliability of these structures to high-amplitude lateral loads like strong winds and earthquakes. CLT buildings can exploit different level of energy dissipation depending on whether large monolithic CLT panels or slender panels vertically connected with screws are employed. In the first case, the energy dissipation is low, while medium-to-high values can be reached if connections are properly designed [54].

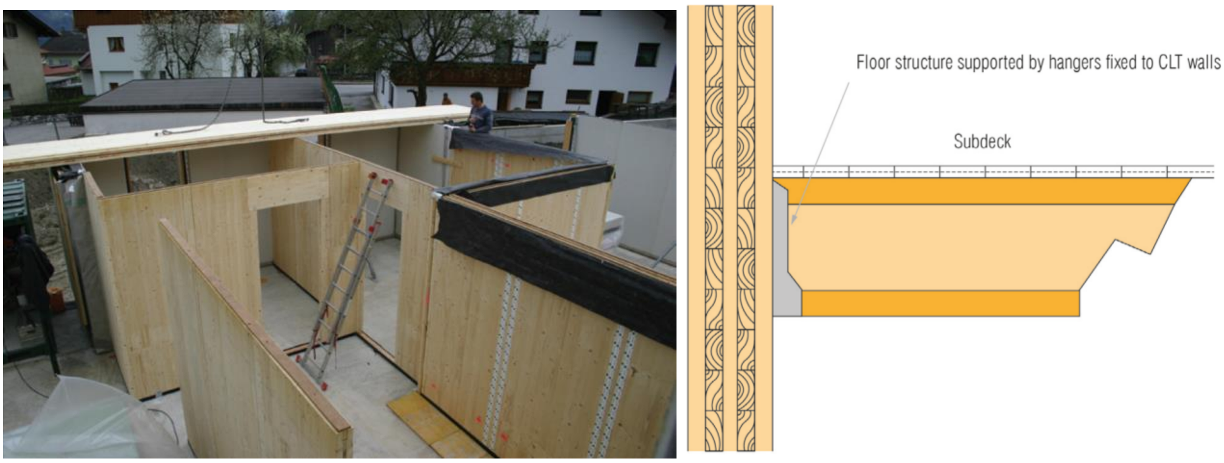

(*a*) (*b*)

Figure I.1-6 – CLT wall system sub-types: (*a*) platform construction and (*b*) balloon construction (*image credits*: (*a*) CLT Handbook [39] and (*b*) Structural Timber Association [55]).

I.1.2.2.4 Mixed CLT walls-heavy frame systems

Mixed CLT walls-heavy frame systems (or *glulam megaframe with CLT*) are structural solution where the vertical load bearing system is constituted by a heavy timber frame, while horizontal stability is given by CLT walls (Figure I.1-7.b). They both have excellent seismic performances and they allow to create large open interior spaces [56]. This building solution is therefore suitable for offices or commercial buildings. An example of this structural typology is the NMIT Arts and Media Building in New Zealand, that applies Pres-Lam technology to bracing post-tensioned shear walls that, thanks to post-tensioning and U-shaped steel dissipators, allow both resilience and dissipation to seismic actions (Figure I.1-7.a).

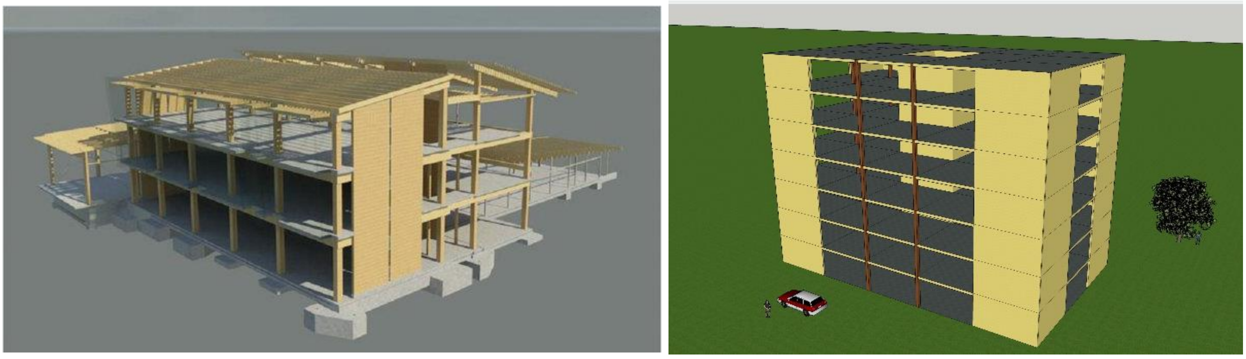

(*a*) (*b*)

Figure I.1-7 – Mixed CLT walls-heavy frame system: (*a*) 3D view of the NMIT Arts and Media Building Structure and (*b*) example of a 7-storey multi-storey mixed CLT walls-heavy frame system (*image credits*: (*a*) Devereux *et al.* [57]).

I.1.2.2.5 Structural efficiency of the building typologies

The efficiency of a building technology can be defined as the amount of building material necessary to build a structure given a geometry (vis. number of storeys and spans to be covered). The efficiency of the abovementioned multi-storey timber building types (Section I.1.2.2.1 to I.1.2.2.4) can therefore be described by the density of structural timber used to achieve a given height of building. Ramage *et al.* [58] showed that light timber frames are the most suitable buildings up to six storeys, from six to eight storeys an hybrid solution CLT-light frame is the most efficient, from eight to ten storeys the best solution is given by CLT buildings, while for buildings higher than ten storeys only the mixed CLT walls-heavy timber frame system is efficient (Figure I.1-8).

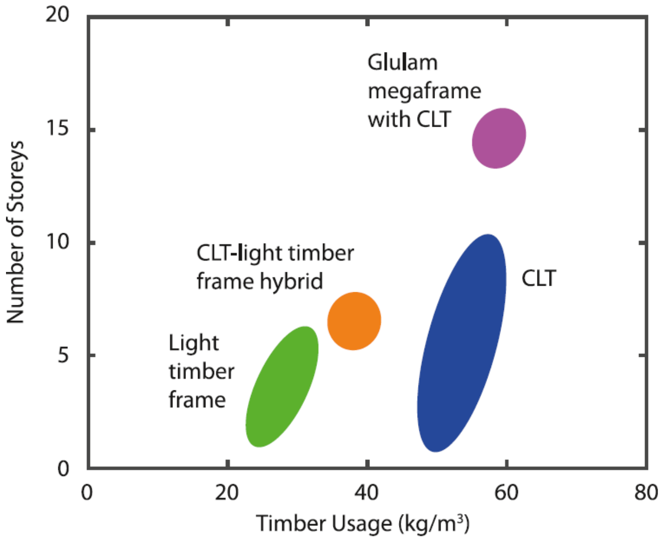

Figure I.1-8 – Density of structural timber used vs. number of storeys for different multi-storey timber building typologies (*image credits*: Ramage *et al.* [58]).

I.1.2.3 Connections with dowel-type mechanical fasteners

Connections play an important role in defining the overall behavior of timber structures both at Serviceability Limit State (SLS) and Ultimate Limit State (ULS), since they usually are the weakest part of these structures [59] and they highly influence stiffness of structural members. It is worth noting that this last aspect impacts both on the overall stiffness of the structure – with implications for deflection and vibration performances – and on the load bearing capacity of members subjected to buckling phenomena, since effectiveness of bracing systems can be highly influenced [60].

Connections are usually distinguished into two main categories [3]:

- *carpentry joint* (Figure I.1-10.a), connections traditionally used in timber constructions realized through shaping of contact surfaces of timber structural elements, and where loads are transferred through to the connected elements by means of compression areas;
- *mechanical joint* in which forces transmission is realized through steel devices or glue, therefore they can be distinguished into the following three sub-categories based on the type of connector employed:
  - *dowel-type connector* (Figure I.1-10.b): nails (Section I.1.2.3.1), staples (Section I.1.2.3.2), screws (Section I.1.2.3.3), bolts and dowels (Section I.1.2.3.4);
  - *surface connector* (Figure I.1-10.c): split rings, toothed plates and punched steel plate fastener;
  - *glued connector* (Figure I.1-10.d): high-performance adhesive, usually in combination with a steel rod (*glued-in steel rod*).

The efficiency of connections can be defined as the ratio of the strength of the connection to the strength of the member it connects, and in Figure I.1-9 the efficiency of different type of connections is shown. It can be observed that glued connections have the maximum efficiency, carpentry joints have the minimum one, while dowel-type ones reach intermediate values of efficiency.

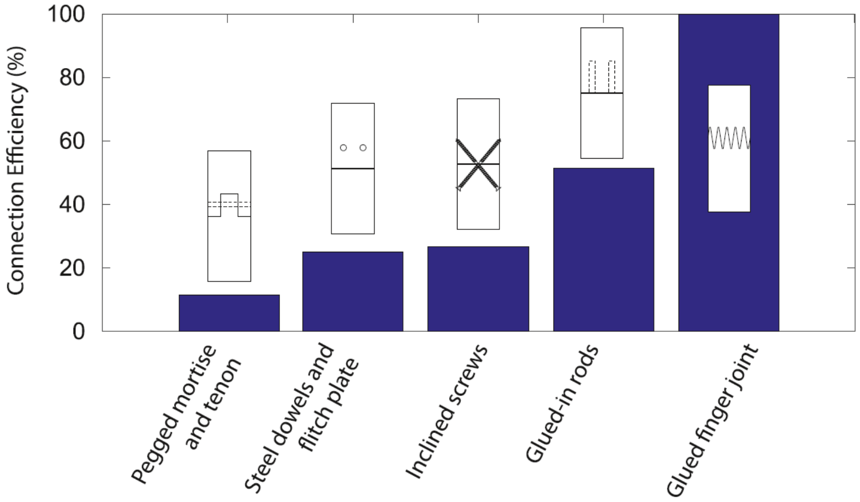

Figure I.1-9 – Efficiency of different types of connections (*image credits*: Ramage *et al.* [58]).

For multi-storey timber buildings erected in seismic-prone areas, connections with dowel-type mechanical fasteners are the most used. Connections with glued bars are also used in post-tensioned resilient multi-storey timber buildings [7], but it is an argument out of the scope of this thesis, while carpenter joints and surface connectors are usually employed for secondary connections that do not significantly impact on the seismic behavior of the building. In the following Section therefore the behavior of connections with dowel-type mechanical fasteners will be addressed, mainly focusing on their seismic behavior.

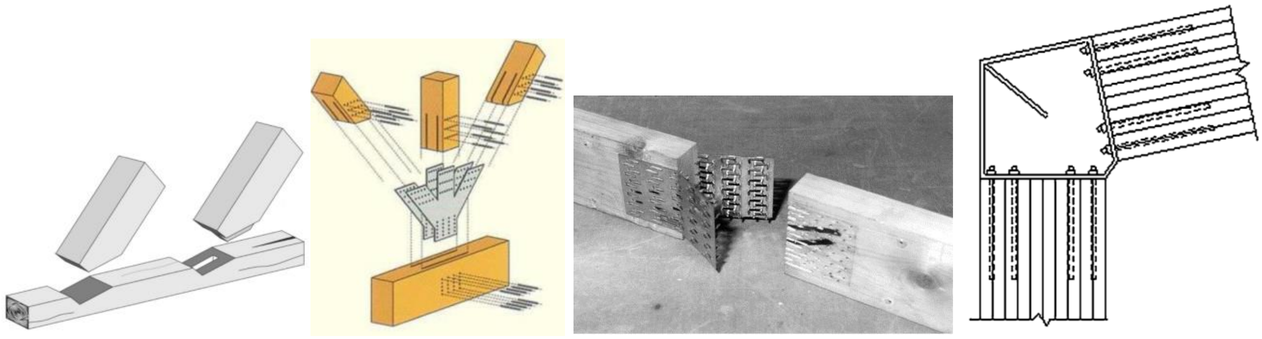
(*a*) (*b*) (*c*) (*d*)

Figure I.1-10 – Connection typologies for timber structures, examples: (*a*) carpentry joint (skewed tenon), (*b*) connections with dowel-type mechanical fasteners (truss lattice joint), (*c*) surface connector (punched steel plate fastener) and (*d*) glued-in steel rods. (*images credits*: (*a*) Branco et al. [61], (*b*) Ballerini [62], (*c*) Karadelis & Brown [63], (*d*) Tlustochowicz *et al.* [64]).

Connections with dowel-type mechanical fasteners are very popular, they are the most frequently employed in timber construction and come in wide-ranging sizes and shapes. In the following a brief overview will be provided.

I.1.2.3.1 Nailed joints

Nailed joints are the frequently employed in timber construction and they tend to be used in single-shear joints (Figure I.1-11.e). They have many advantages: they are cheap, they are made with performant steel (cold-formed), they are easy to use, and they tend to weaken the timber element less than dowel-type fasteners with bigger diameter. The main drawback is represented by their limited resistance if compared to other mechanical fasteners, that could lead to the usage of a high number of connectors sometimes not acceptable for merely aesthetic reasons.

Nails come in different shank (smooth or annual-ringed) shapes (circular or squared), and they have a round head with a diameter usually two times the shank one (Figure I.1-11.a-d). Annual-ringed nails are experiencing a high success in the last decade and they also are employed for CLT connections (Section I.1.2.4), since they combine advantages of nails with a higher withdrawal strength, making it possible to adopt lower lengths. Sizes range from 2.75 to 8 mm in diameter and 40 to 200 mm in length. Predrilling of nail holes, usually with a diameter equal or less than 80% of the shank of the connector, may be necessary to prevent timber splitting or facilitate the penetration of the steel connector into timber even if it is important to observe that predrilling can cause a weakening of the timber structural element [3].

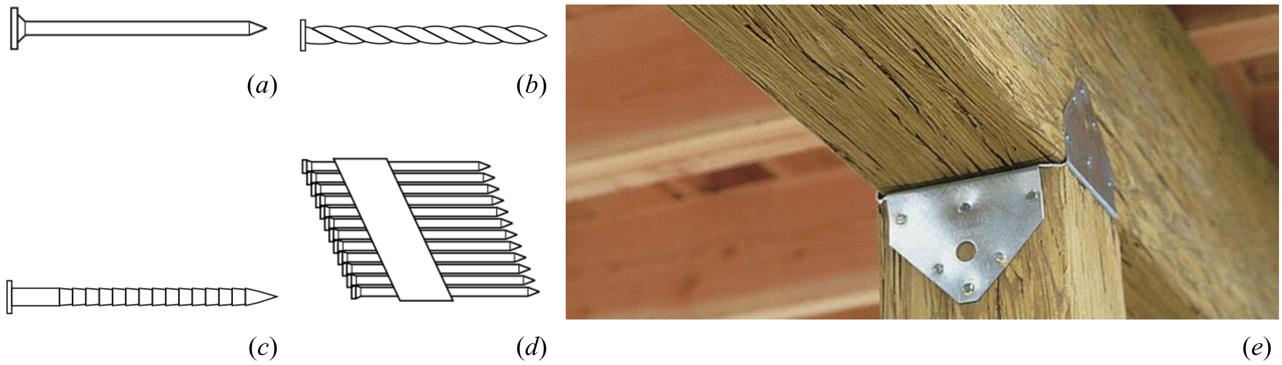

Figure I.1-11 – Nailed mechanical connections: (*a*) Round smooth shank nail, (*b*) spiral nail, (*c*) ringed shank nail, (*d*) machine driven nails and (*e*) example of nailed connection (*images credits*: (*a-d*) Blaß & Sandhaas [59] and (*e*) Weyerhaeuser website [65]).

I.1.2.3.2 Stapled joints

Stapled joints are a spread solution in timber light-frame buildings thanks to rapidity of execution (Figure I.1-12.b). *Staples* are made with ductile high-strength because of the production process that imposed a 90° shaping, obviously requiring the connector to remain undamaged (Figure I.1-12.a).

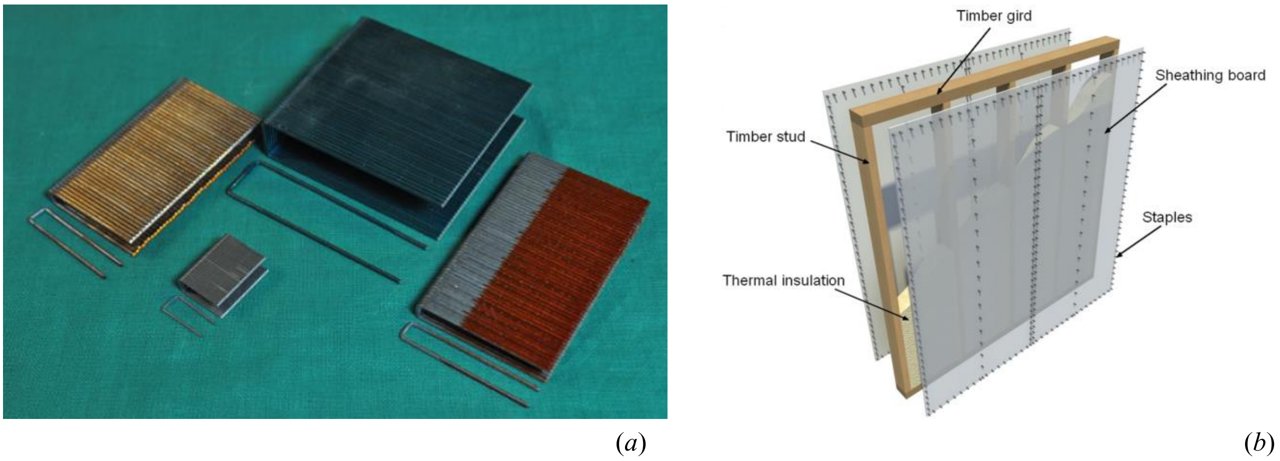

Figure I.1-12 – Stapled joints: (*a*) staples and (*b*) example of stapled connection (*images credits*: (*a*) Blaß & Sandhaas [59] and (*b*) Pintarič *et al.* [66]).

I.1.2.3.3 Screwed joints

Screws are connectors formed by a shank subdivided into threaded and smooth parts (usually equal to 40% of the total length of the shank), with a slotted head and a pointed-shape end (Figure I.1-13.a). The diameter of the threaded part (core diameter) is usually 70% the diameter of the smooth part (nominal diameter). Their nominal diameter ranges between 4 and 10 mm for screws with round and plane head, while it ranges between 8 and 20 mm for hexagonal ones. They must be inserted in predrilled holes if the nominal diameter in more than 5 mm, in order to avoid cracking in the timber, and the shank direction should never be parallel to the grain direction. A correct mounting of screwed connections has to be carried out through screwdrivers (manual or electrical), and they should never be placed by hammering, otherwise their withdrawal strength and overall mechanical performance could be heavily compromised (Figure I.1-13.b). Screwed connections are usually employed to connect steel plates to timber members, and they represent an easy and reliable solution for joints where both shear and withdrawal strength must be guaranteed.

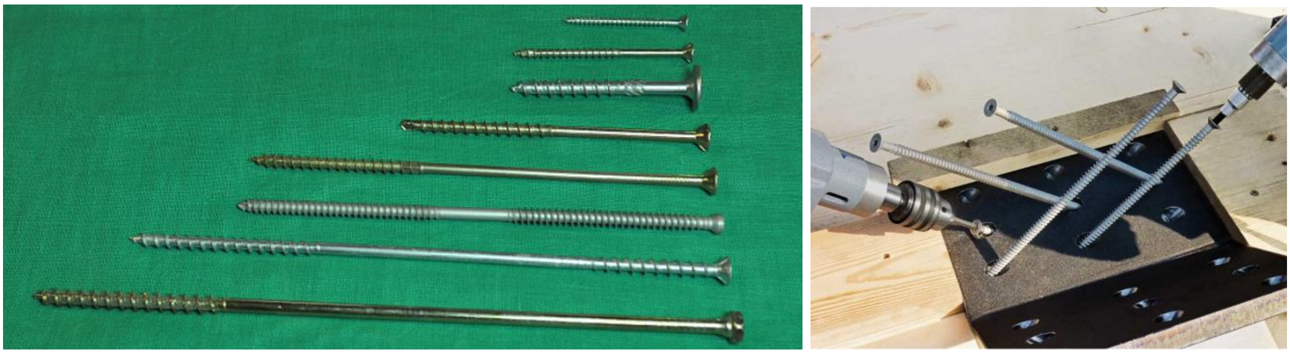
(*a*) (*b*)

Figure I.1-13 – Screwed joints: (*a*) self-tapping screws and (*b*) example of screwed connection (*images credits*: (*a*) Blaß & Sandhaas [59] and (*b*) Fastfix website [67]).

I.1.2.3.4 Bolted and dowelled connections

Bolts (Figure I.1-14.a) and dowels (Figure I.1-14.b) are steel cylindrical connectors inserted in predrilled holes that mainly resist to shear forces (except for secondary effects, e.g. the rope one), with shank diameter usually comprised between 8 and 30 mm.

Dowels have a smooth shank, sometimes tapered on one side in order to ease the insertion into the predrilled hole (that usually have the connector diameter) in the timber element, therefore they must be hammered manually or by a machinery. If steel plates are used in the connection, it should be predrilled with a diameter slightly larger than the shank one (usually 1 mm of tolerance is adopted). In these connections with steel plates, dowels should be placed into holes a little time after their drilling, since the dimensional variation due to hygroscopicity of timber could misalign the holes. In order to avoid this drawback, self-drilling dowels are available on the market. Thanks to a steel blade at one extremity, they are able to pierce both timber and steel plates up to a maximum number of 3 and a thickness of 5 mm.

Bolts are inserted into holes slightly larger than their nominal diameter (usually 1 mm of tolerance), and their shank is threaded only on the side where the nut must be placed. It's therefore straightforward that bolted connections will be less rigid than dowelled ones because of the tolerance. These connections may need re-tightening after some period to ensure contact between elements even after their dimensional variation due to hygroscopic equilibrium with the environment.

It is also possible to use *threaded rods*: in this case, the design is the same adopted for bolts, considering the external thread diameter as the nominal one.

Bolted (Figure I.1-14.c) and dowelled (Figure I.1-14.d) connections are very versatile and resistant, and they are usually employed when high shear resistance is required. Particularly, multiple shear connectors with slotted-in steel plates are structurally highly performant, and they behave optimally under fire, therefore they have been used in recent years to build high multi-storey timber buildings [68].

It is a good practice to use at least four bolts placed on the corners of dowelled connections in order to avoid their opening. In this case, bolts contribution to both resistance and stiffness of connection is neglected, since most of the shear force is taken from dowels (since it is obviously proportional to their shear stiffness).

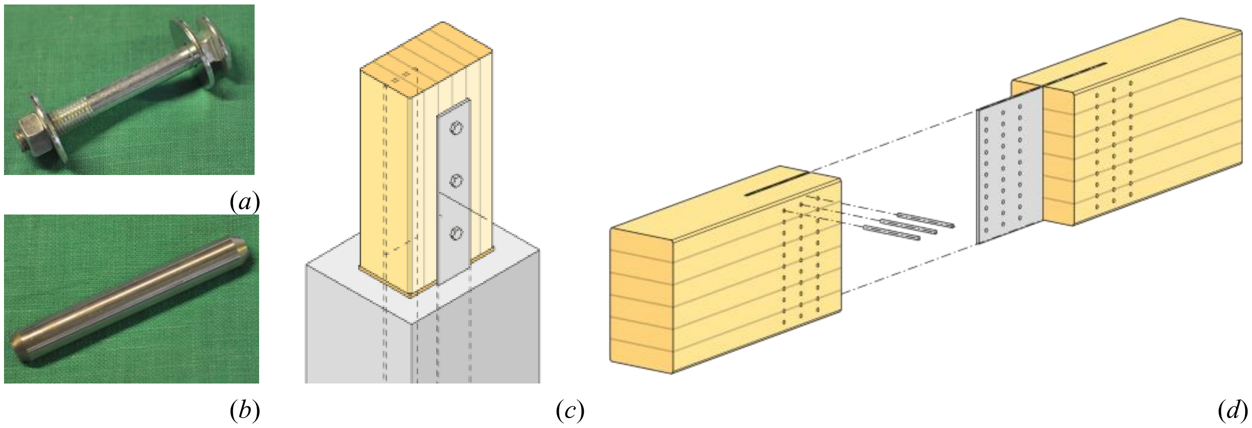
(*a*)

(*b*) (*c*) (*d*)

Figure I.1-14 – Bolted and dowelled connections: (*a*) dowel connector, (*b*) bolt connector, (*c*) example of bolted connection and (*d*) example of dowelled connection (*images credits*: (*a-b*) Blaß & Sandhaas [59], (*c-d*) Setra Group webpage [69]).

I.1.2.4 Mechanical connections for CLT structures

Connections play a key-role in defining structural strength, stiffness, stability and global ductility. Indeed, connections guarantee the energy dissipation necessary to reduce the induced seismic action of multi-storey timber buildings [70], since CLT panels behave elastically while connections’ steel yielding is the prevalent cause of energy dissipation, unless dissipators are employed [71]. Connections are important in defining the seismic behavior of CLT multi-storey buildings as their behavior influence both the efficiency of floors to act as diaphragms and vertical panels to act as lateral resisting walls. Their mechanical characterization is therefore fundamental to determine how CLT multi-storey buildings behave to high-amplitude cyclic forces like earthquakes, and, in general, practitioners must deal carefully to connections design, since post-collapse surveys evidenced how inadequately designed or improperly fabricated connection were the main cause of building failure. Because of the contrast between stiff timber panels and relatively flexible connections usually employed for CLT multi-storey buildings, stiffness of connections may be key-factor in defining the behaviour of this structural typology to wind actions [72]. For sake of completeness, it must be remarked that for low-amplitude cyclic vibrations, like normal winds, the structural behavior could be not related to connections stiffness, since forces may be mainly transferred through friction and normal edge forces, since connections would require higher displacements to activate their resistance [50, 73].

Current building codes lack in giving guidelines in calculation methods for CLT connections and little research on the topic has been carried out since now. The most extensive study on this aspect has been carried out by Uibel and Blaß [74, 75] and a state-of-the-art of research and standard provisions on the design of connections in CLT structures is reposted in Section I.1.3.2. The lack of studied and standard design criteria for connections is evenly more marked for CLT panels with hybrid layups constituted of inner core layers with a lumber grade lower than face layers. Actually, Mahdavifar *et al.* [76] showed that if the failure of dowel-type connectors (i.e. yielding of the fastener or damage to the embedding timber) occur in the core layers, the mechanical behavior of connections can be statistically different respect to CLT panels composed of homogeneous lumber grades.

In the following Section I.1.2.4.1, an overview on connection types employed in CLT structures will be provided, and a focus on the state-of-the-art of the research activity on their seismic behaviour will be given.

I.1.2.4.1 Common connection systems for CLT assemblies

Unless self-tapping screws are the type of connector usually recommended by CLT producers, all the traditional types of dowel-type connectors (Section I.1.2.3) can be successfully used to connect CLT panels (Figure I.1-15.a).

In the following, a rapid overview (for more details, please refer to [39]) of the most common connections for CLT assemblies will be given as a function of their location into multi-storey buildings (Figure I.1-15.b).

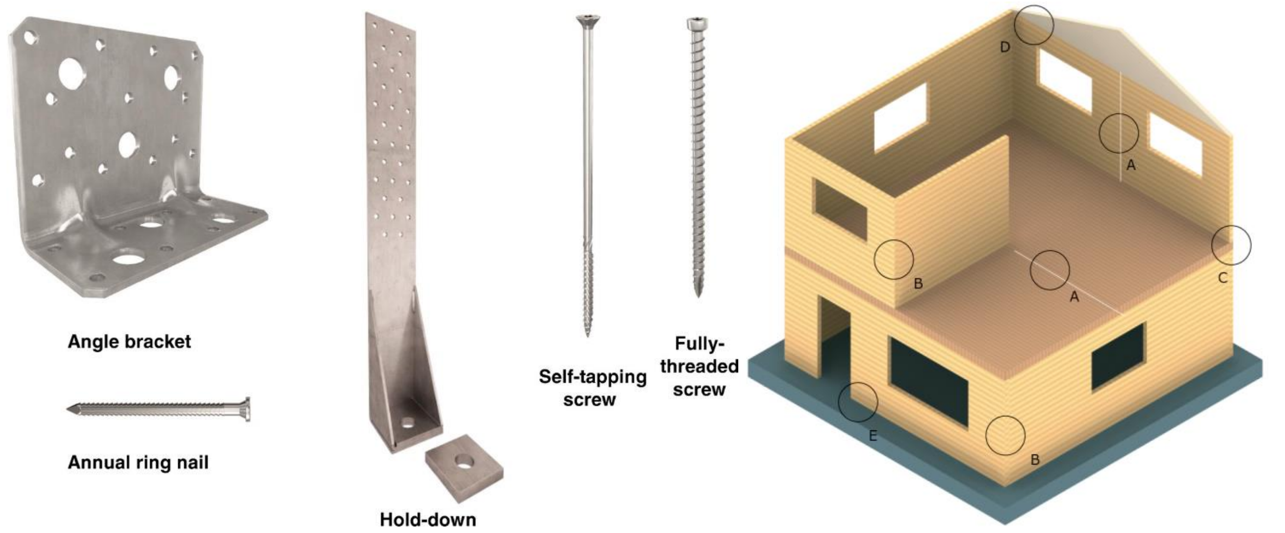

(*a*) (*b*)

Figure I.1-15 – Connection system for CLT assemblies: (*a*) example of connectors used with angle bracket and hold-down connections and (*b*) location of connections in multi-storey CLT buildings and their detail ID henceforth adopted. (*images credits*: (*a*) Gavric *et al.* [77] and (*b*) CLT Handbook [39]).

I.1.2.4.1.1 Panel-to-panel connections (Detail A)

Panel-to-panel connections are necessary to create larger structural elements such as walls and floors assembling on site panels whose dimensions are restricted by production necessities and transport limitations. An extensive experimental campaign on these types of connections is presented in [78]. The more common panel-to-panel connections are briefly illustrated below.

- *Internal splines* (Figure I.1-16.a) are connections composed of one spline inserted into profiled hollows, shaped at CLT panel edges to be jointed assuring accurate profiling (e.g. through CNC machining). The main advantage of this connection typology is the fact that is a double-shear connection.
- *Single surface splines* (Figure I.1-16.b) are obtained by shaping the edge of CLT panels on one side in order to accommodate a spline that will be screwed to panels on site. The main advantage is only the easiness of execution, since it has relatively low stiffness because of a single shear section.
- *Double surface splines* (Figure I.1-16.c) is similar to the single surface one, with the only difference that spline is present on both sides of the panel. The advantage is therefore a higher stiffness, while the drawback is the higher cost due to more machining and more time needed for assembly.
- *Half-lapped joints* (Figure I.1-16.d) is formed by machining a half-lapped joint and joining the panels with screws. It is a very simple connection type, but it cannot be considered resistant to bending moments.
- *Butt joint* (Figure I.1-16.e) is the simplest panel-to-panel connection, since it does not require machining on CLT panel edges because the panels are joined by simply placing their edges together without any shaping. An extensive experimental survey on their mechanical characterization is presented in [79].

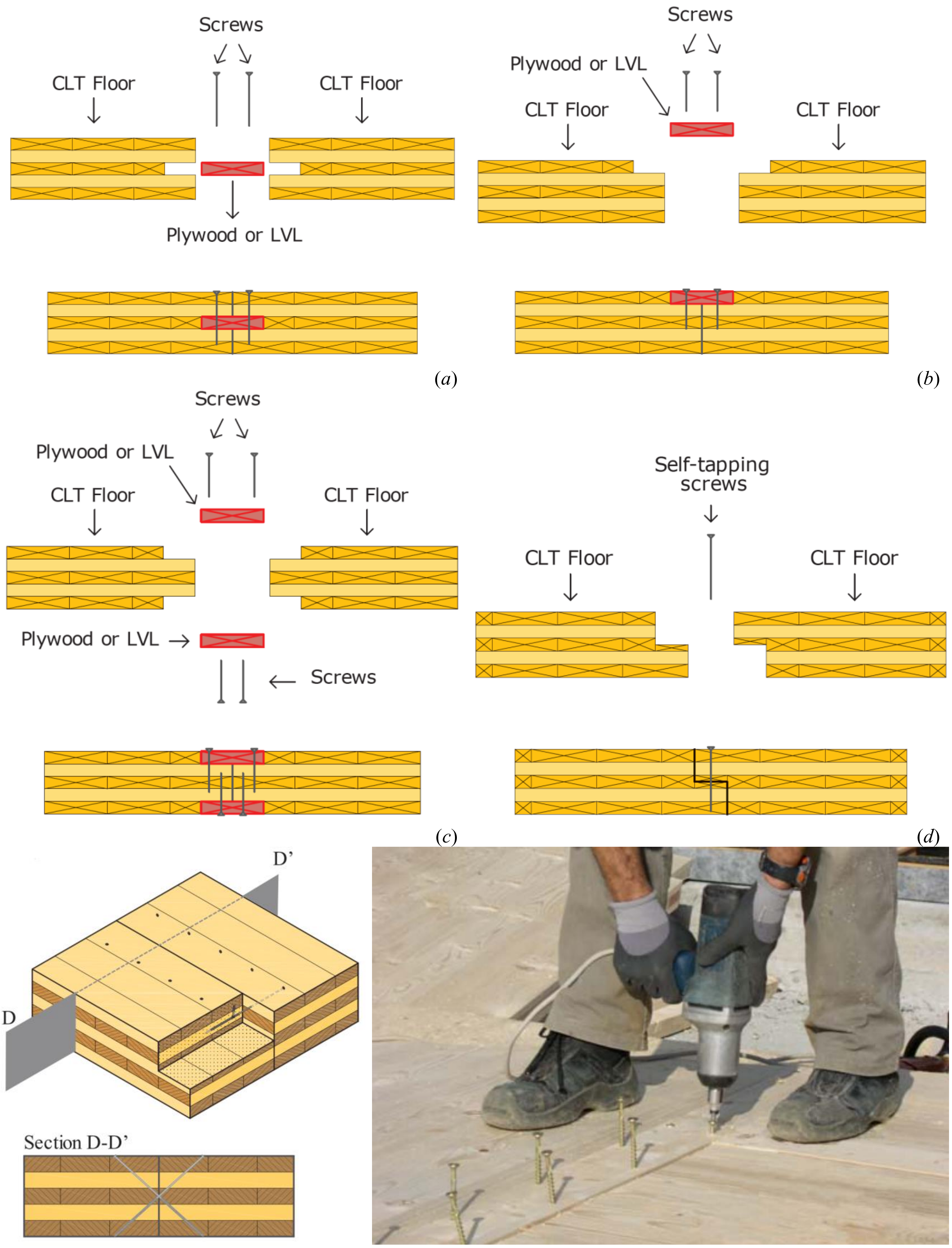
Screws
CLT Floor
CLT Floor
Plywood or LVL
(a)
Screws
Plywood or LVL
CLT Floor
CLT Floor
(b)
Screws
Plywood or LVL
CLT Floor
CLT Floor
Plywood or LVL
Screws
(c)
Self-tapping screws
CLT Floor
CLT Floor
(d)
D'
D
Section D-D'
(e)
(f)

Figure I.1-16 – Panel-to-panel connections: (*a*) internal spline, (*b*) single surface spline, (*c*) double surface spline, (*d*) half-lapped joint, (*e*) butt joint and (*f*) example of screwing of a screwed panel-to-panel joint. (*images credits*: (*a-d*) CLT Handbook [39], (*e*) Loss *et al.* [79] and (*f*) Follesa *et al.* [80]).

I.1.2.4.1.2 Wall-to-wall connection (Detail B)

Wall-to-wall connections are used to connect wall to other walls positioned at a right angle, both for exterior ones and internal partitions. The more common wall-to-wall connections are briefly illustrated below.

- *Self-tapping screws* (Figure I.1-17.a) are the simplest wall-to-wall connection solution. Some concern is represented when screws are installed in the end grain of cross layers for wall panels subjected to high lateral loads like strong winds and earthquakes. For this reason, screws can also be driven at an inclined angle to optimize the performance of these connections (*toe screwing*).
- *Wooden profile wall-to-wall connections* (Figure I.1-17.b) are a performant solution.
- *Metal brackets* (Figure I.1-17.c) are one of the simplest and easiest solution for wall-to-wall connections, but they usually have low fire performance. A ploy to outflank the issue is profiling the panel to insert the plates in a cavity and covering them with finishing materials or a wooden cap.

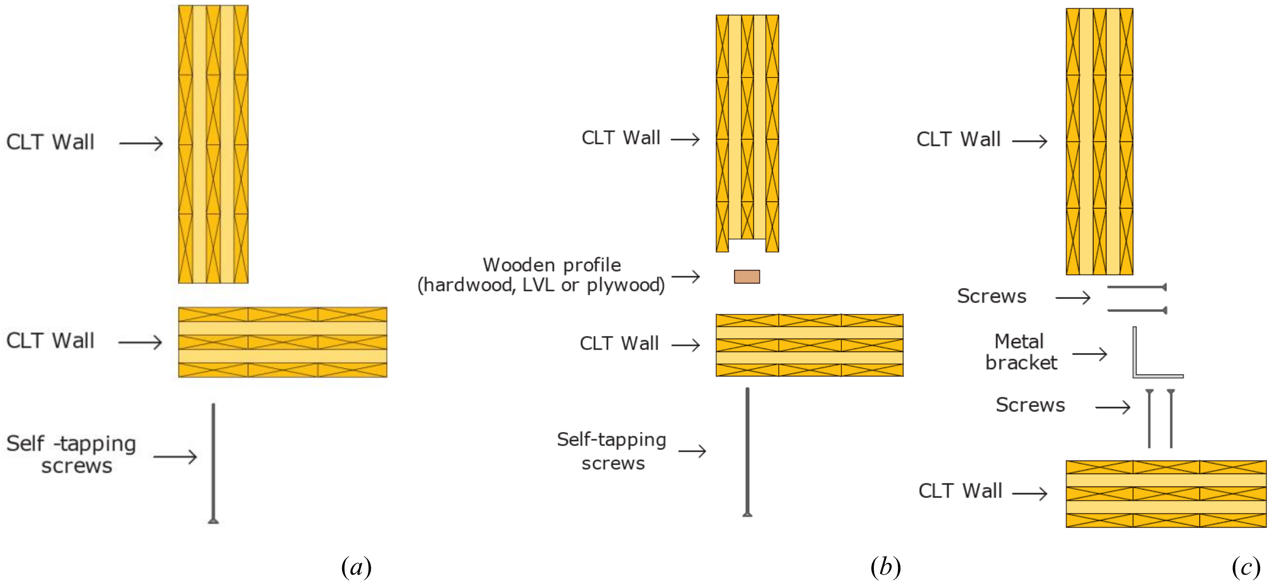

Figure I.1-17 – Wall-to-wall connections: (*a*) self-tapping screws, (*b*) wooden profiles and (*c*) metal brackets (*images credits*: CLT Handbook [39]).

I.1.2.4.1.3 Wall-to-floor connection (Detail C)

In the following the main solutions of wall-to-floor connection for platform and balloon frame constructions (Section I.1.2.2.3) will be given.

For *platform constructions* three wall-to-floor connection solutions are the most common, namely connections with self-tapping-screws, with metal brackets and with concealed metal plates:

- *Self-tapping screws* are driven from the CLT floor directly into the narrow side of the wall edge (Figure I.1-18.a). Screws could also be driven at an angle, even to connect upper walls to lower floor.
- *Concealed metal plates* are good when high fire performance is required, even if they require CNC machining of CLT panel edge (Figure I.1-18.b).
- *Metal brackets* (Figure I.1-18.c) are one of the easiest, performant and most employed solution for wall-to-floor connections in CLT multi-storey buildings. They are made by connecting steel elements and CLT panels with dowel-type fasteners (Section I.1.2.3) which are loaded either axially, laterally or with a combined action. Two metal brackets are the most commonly used in CLT buildings, namely hold-down connections (Figure I.1-18.d) used to transmit uplift forces, and angle brackets (Figure I.1-18.e) used to transmit shear loads. They can easily be mounted on site and they are easily available on the market.

The main drawbacks are represented by low fire performances and the fact that they are sensitive to a correct design procedure in order to guarantee a good seismic ductile behavior to the whole building [53]. Since they strongly affect the seismic performance of CLT buildings, their behavior has been studied by many authors [81–83].

In *balloon constructions*, mezzanine floors usually lay on a wood ledger (Figure I.1-19.a) or metal plates (Figure I.1-19.b).

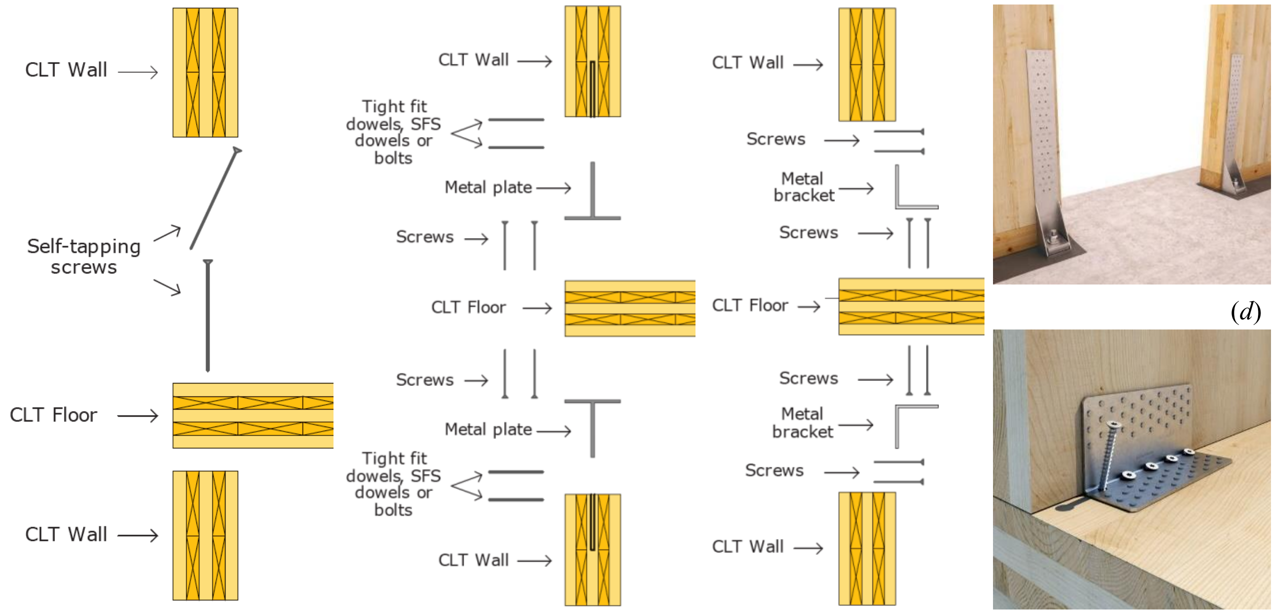
CLT Wall
Self-tapping screws
CLT Floor
CLT Wall
CLT Wall
Tight fit dowels, SFS dowels or bolts
Metal plate
Screws
CLT Floor
Screws
Metal plate
Tight fit dowels, SFS dowels or bolts
CLT Wall
CLT Wall
Screws
Metal bracket
Screws
CLT Floor
Screws
Metal bracket
Screws
CLT Wall
(d)

(*a*) (*b*) (*c*) (*e*)

Figure I.1-18 – Wall-to-floor connections for platform CLT constructions: (*a*) self-tapping screws, (*b*) concealed metal plates, (*c*) metal brackets, (*d*) hold-down and (*e*) angle bracket (*images credits*: (*a-c*) CLT Handbook [39], (*d*) Progetto Energia Zero [84] and (*e*) Timber-Online [85]).

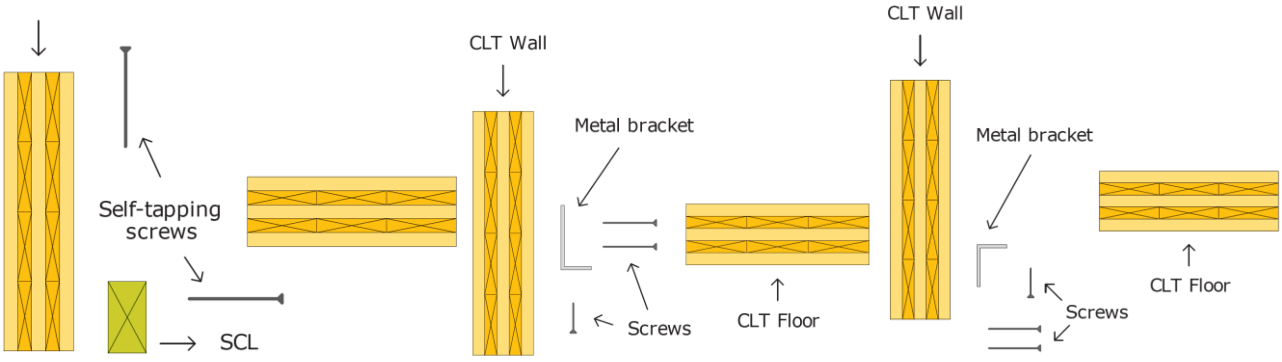
Self-tapping screws
SCL
CLT Wall
Metal bracket
Screws
CLT Floor
CLT Wall
Metal bracket
Screws
CLT Floor

(*a*) (*b*) (*c*)

Figure I.1-19 – Wall-to-floor connections for balloon CLT constructions: (*a*) wooden bearing support [39] and (*b-c*) metal bracket (*images credits*: CLT Handbook [39]).

I.1.2.4.1.4 Wall-to-roof connection (Detail D)

The same details of wall-to-floor connections for CLT platform constructions are used (Section I.1.2.4.1.3).

I.1.2.4.1.5 Wall-to-foundation connection (Detail E)

The main solutions used to connect CLT walls to concrete foundation will be shown in the following.

- Exterior metal plates and brackets are commonly used to realize wall-to-foundation connections. When connections are installed from outside, *metal plates* (Figure I.1-20.a) are commonly used, while when a concrete slab exists, *hold-downs* (Figure I.1-18.d) and *angle brackets* (Figure I.1-18.e) are installed in the internal side of the building.

- *Concealed hardware* (Figure I.1-20.b) is used when better fire or aesthetic performances are required.
- Metal shafts (Figure I.1-20.c) are inserted into holes on the lower edge of CLT panel and fixed to it through dowels or bolts. Threaded anchor bolts casted in the concrete are connected to the shaft through a nut tightened accessing it through an access hole then covered with a wooden cap.

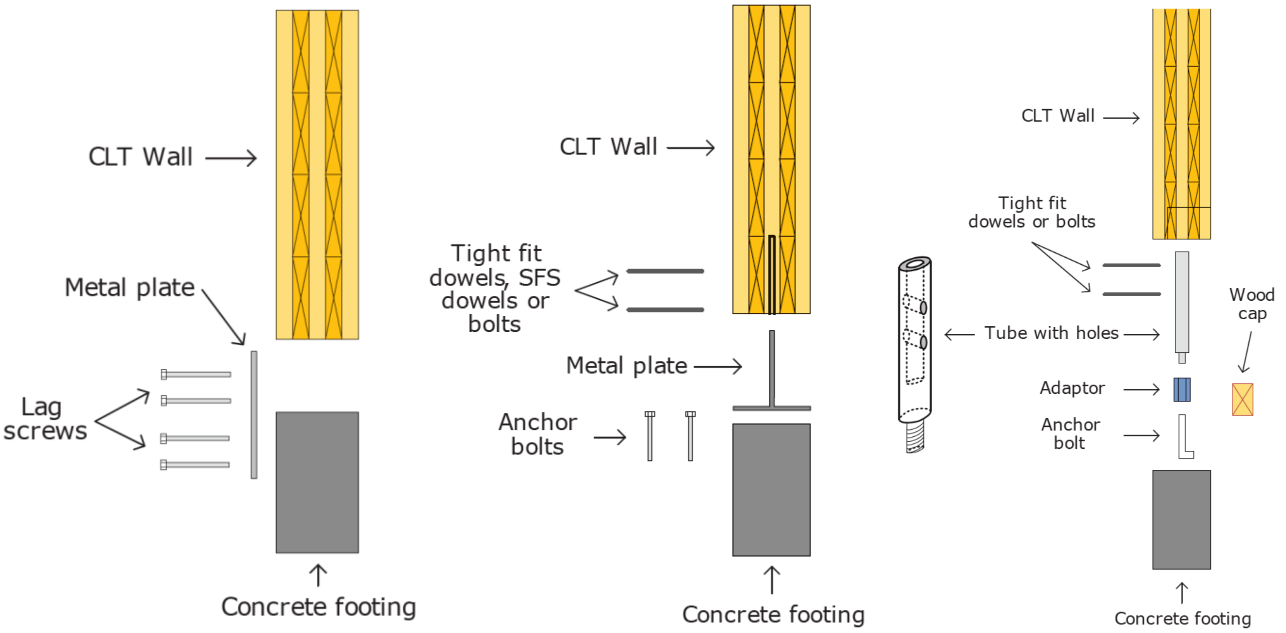
CLT Wall
Metal plate
Lag screws
Concrete footing
CLT Wall
Tight fit dowels, SFS dowels or bolts
Metal plate
Anchor bolts
Concrete footing
CLT Wall
Tight fit dowels or bolts
Tube with holes
Wood cap
Adaptor
Anchor bolt
Concrete footing

(*a*) (*b*) (*c*)

Figure I.1-20 – Wall-to-foundation connections: (*a*) visible plates, (*b*) concealed hardware and (*c*) metal shaft (*images credits*: CLT Handbook [39]).

I.1.2.4.2 Innovative connection systems for CLT assemblies

Traditional connections used for CLT in seismic-prone areas hold-down and angle brackets (Section I.1.2.4.1.3 and I.1.2.4.1.5) are able to withstand high loads given by seismic actions and can dissipate a significant amount of energy thanks to their high ductility [86]. However, they are susceptible of brittle failures, mainly because strength of its ductile components (i.e. dowel-type connectors) is usually underestimated, requiring higher strength demands to brittle components (e.g. steel plates) [87]. For this reason, innovative types of connections that guarantee higher ductility and energy dissipation have been proposed by researchers in recent years, like the X-bracket [88] the X-RAD [89], the SHERPA [90] and the XL-stub [91] connection systems. Finally, a connection system composed of shear steel plates placed between adjacent CLT panels to be connected has been proposed by Schmidt & Blaß [92] (Figure I.1-21.a and b). The plates are bonded into notches and the gap between panels t_{gap} can be adjusted so that they develop plastic hinges without embedment of wood, allowing therefore for hysteretic energy dissipation without strength and stiffness impairments due to pinching behaviour of traditional dowelled connections (Figure I.1-21.c).

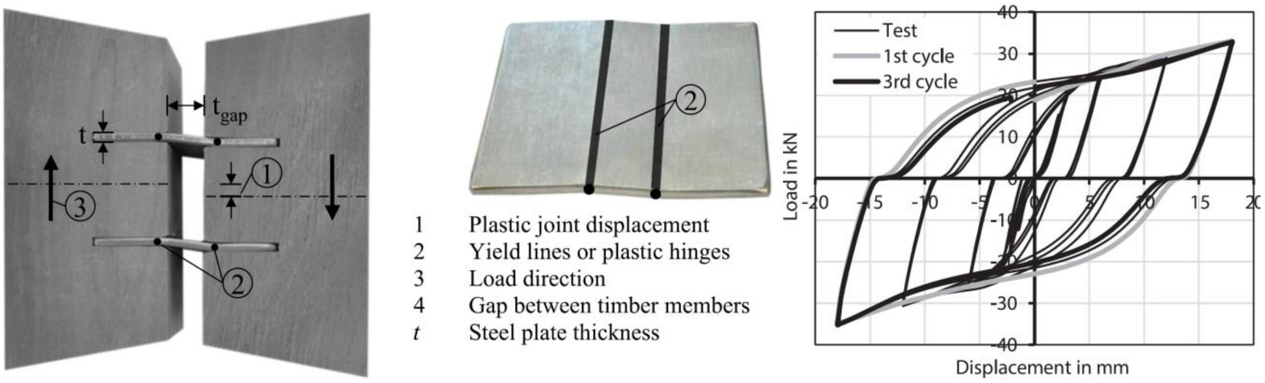

(*a*) (*b*) (*c*)

Figure I.1-21 – Dissipative connector proposed by Schmidt & Blaß [92]: (*a*) representation, (*b*) steel plate and (*c*) hysteretic behavior with a gap opening t_{gap}=50 mm (*images credits*: Schmidt & Blaß [92]).

I.1.3 Code design provisions and modelling strategies for CLT buildings

CLT multi-storey buildings are spreading very rapidly thanks to many advantages, like the high prefabrication level and the rapidity of execution. Furthermore, thanks to their excellent seismic performances - as proved by several research projects – they have been used also in seismic-prone areas in the last decades, as witnessed by the CLT 5-storey and the 6-storey buildings erected near L'Aquila (Italy) in a high seismicity area [93] and the 7-storey hotel in Pesaro (Italy) in a medium seismicity area [94]. CLT buildings response under earthquake actions has been widely studied through experimental tests and numerical simulations in last years. One of the most comprehensive research on seismic behaviour of low- and mid-rise CLT buildings has been carried out at CNR–IVALSA in Trento (Italy) within the SOFIE Project [95–97]. Using as reference such research, several experimental campaigns and numerical studies have been conducted in recent years by various research groups. Relevant are the tests conducted at the University of Ljubljana, Slovenia, where the behaviour of 2-D CLT shear walls having various load and boundary conditions was assessed [98]. FPInnovations in Canada has undertaken tests to determine the structural properties and seismic resistance of CLT shear walls [99] and small-scale 3-D structures [45]. Failure mechanisms in large shear wall systems have been characterized in multiple studies [77, 100, 101]. Connection elements suitable for assembling CLT panels together and anchoring them at the bases have been studied, with the aim of developing a capacity-based design approach for CLT structures [46, 102] and to define the tension-shear interaction phenomenon [103]. Several numerical models have been developed and calibrated on the results obtained by the above-mentioned tests with the aim of reproducing the response of single connection elements [104, 105] or more in general of entire CLT shear wall and buildings [41, 105–107].

Anyway, since CLT is a relatively young building technology, studies on their seismic behavior still need to be carried out. Indeed, on one hand codes and standards are still lacking in adequate design provisions, and on the other hand their numerical modelling still needs to be investigated further to detect in the best strategies to guarantee the reliability of the outcomes. Therefore, an overview of the state-of-the-art of Codes design provisions (Section I.1.3.1) and of different modelling strategies available in literature used to study the seismic behavior of CLT multi-story structures (Section I.1.4) will be provided in the following.

I.1.3.1 Regulatory framework for seismic analysis and design of timber buildings

One of the main barrier to the adoption of CLT building technology and timber buildings in general in earthquake-prone areas is the lack of adequate code design procedures and little availability of technical informations about structural performance, especially for connections [108]. Actually, even if design principles for seismic design of timber structures have been studied for more than 20 years [109], technical informations and seismic design methods for timber structures are incomplete and for CLT structures such informations are to-date available only in European Technical Assessments (ETAs). Eurocode 5 [110], Eurocode 8 [111] and new Italian Building Codes NTC 2018 [112] lack of adequate design principles, Austria being the only European country that included general design principles in the national annex [54]. In order to develop Eurocodes design strategies for timber structures and CLT, CEN (European Committee of Standardization) Project Teams have been established, and the final updated version of new Eurocode prescriptions for timber is expected to be released around 2020 [113].

Two are the main deficiencies that limit the employment of CLT building technology into seismic-prone areas, namely (*i*) a reliable way to determine the values of the *q*-behaviour factors and (*ii*) design principles for connections, aspects mutually correlated and analysed in the following Sections I.1.3.1 and I.1.3.2 after an overview of the seismic design regulatory framework for timber buildings in Europe (Section I.1.3.1.1) and in other seismic-prone World regions (Section I.1.3.1.2).

I.1.3.1.1 European seismic design regulatory framework

Chapter 8 of EC8 [111] is the only part of Eurocodes where prescriptions on the seismic design of timber buildings are given, and it represents the main regulatory framework for buildings in Europe. The design criteria there reported are anyway outdated considering the rapid development of timber building technology, especially concerning earthquake design, so they are few, incomplete, sometimes misleading and give no specifications for CLT buildings. For example, instructions on capacity design criterion are only partial, the definition of structural typologies is fuzzy and over-strength factors are not given.

In the following a summary of the force-based design criteria given in Chapter 8 of EC8 is furnished. Buildings are subdivided into three Ductility Classes, namely Low (DCL), Medium (DCM) and High (DCH) depending on the dissipative capacity guaranteed in the dissipative zone as a function of the structural typology. It is worth noting that the Code furnishes a *q*-factor equal to 2 for "Glued wall panels" in Table 8.1, but it cannot be intended as CLT structural systems, since the standard has been published in 2004, therefore prior to the investigation on seismic performances of this building technology [54]. For DCM and DCH it is required that the dissipative zones are located in joints with an appropriate cyclic fatigue behaviour and with devices for carpentry joints able to prevent their brittle failure, while timber elements shall react elastically. To allow a ductile behaviour in the dissipative zones, minimum thickness of timber elements and maximum diameters of dowels and bolts are assigned to ensure the development of plastic hinges in steel connectors and avoid brittle failure of timber. Minimum thickness of CLT panels to guarantee ductile behaviour is not reported by EC8, Fragiacomo [114] suggests a value equal to 90 mm. Bolts and dowels with a diameter exceeding 16 mm should not be used in timber-to-timber and steel-to-timber connections, except if timber connectors are employed. In add, usage of dowels, smooth nails and staples is avoided unless provisions against withdrawal are adopted.

In 2020 a new version of EC8 with new prescriptions and a deep update of existing ones should be published, also containing design criteria for CLT structural systems and capacity design rules both at a connection level and building level assigning an overstrength factor equal to 1.3 [113], in accordance with the results shown in a previous research on CLT ductile design [114]. Other general seismic principles applicable for all the wall-type lateral resisting systems are introduced, like the necessity to avoid interruption of shear walls below a certain floor in elevation in order to avoid soft storey mechanism. In add, it is underlined the importance of ensuring simultaneous plasticization of as many storeys as possible in order to increment global ductility and dissipative capacity.

I.1.3.1.2 Extra- European seismic design regulatory framework

In this Section an overview of the state-of-the-art of seismic design procedures of seismic-prone countries other than European ones is provided. Hints of Standards and Codes for the seismic design of CLT buildings of Canada, U.S.A., Japan, New Zealand, Chile and China will be given in the following.

In *Canada* the standard that contains the principles of structural design is the National Building Code of Canada (NBCC) [8] that adopts an objective-based design criterion. The Canadian Standard Association CSA-086 [115] enacts standards specifically for timber, and it is the first one that introduced CLT building technology in Canada. This standard introduces some of the basic concepts of seismic design of CLT structures, like the rigid behaviour of CLT panels and the necessity to dissipate energy through ductile connections. In add, in order to prevent sliding failure of CLT walls, a height-to-length ratio of the wall comprised between 1:1 and 4:1 should be guaranteed.

In the *U.S.A.* the most widely used Code for design of CLT structures is the American Society of Civil Engineers Standard 7 (ASCE-7) [116]. Since CLT technology is not included yet in the standard, Equivalent Lateral Force Procedure for their seismic design cannot be employed and a more costly and time-consuming alternative performance-based design method [117] is needed, reducing therefore the competitiveness of CLT technology.

In *Japan* the structural design is regulated by BSL [118], a performance-based code that furnishes seismic coefficients maps to derive the base shear of the building then reduced as a function of its ductility. Design of CLT structures have been introduced in 2016 with a guidebook [119] and a design manual [120]. For small-scale buildings with height and total area respectively lower than 13 m and 500 m^2, simplified calculation methods are allowed. Considerations about ductility of CLT structures have been introduced with the seismic action calculated accordingly.

In *New Zealand* the Building Code (NZBC) is the standard used for the seismic design of timber structures, together with the New Zealand Timber Structures Standard NZS 3603 [121]. The latter has anyway been released in 1993, resulting therefore outdated respect to new technologies like CLT. Actually, in New Zealand no design approach for CLT technology is present, and this is mainly due to the fact that this technology has been used in that country for the first time only in 2012. The approach usually adopted for design of CLT buildings is elastic, but ongoing studies at university of Canterbury on connections and failure modes [122] will help in defining more articulated standards.

In *Chile* structural design is regulated by General Law of Urban Planning and Construction (DFL N°458) [123] and by General Urban Planning and Construction Ordinance (OGUC) (DS N°47) [124]. For seismic design of timber structures, the reference standards are the NCh1198 [125] and the NCh433 [126]. No regulation is furnished for the design of CLT structures and R-factors are provided only for light-frame timber buildings.

In *China* the seismic design of buildings is regulated by the Code for Seismic Design of Buildings GB 50011 [127] that adopts a “three-level and two-stage” approach, defining firstly the performance that the building should satisfy for three different seismicity levels and then checking the structure for 2 stages. That standard, together with the GB/T 51226 [128] are the references for the design of CLT structures, with specified requirements for CLT material properties and design methods.

Table I.1-1 reports a comparison of the different seismic design approaches and specifications of the different coded and standards herein introduced.

I.1.3.1 Behaviour factor for CLT buildings

The behaviour q-factor (also named R-response modification factor or R-strength reduction factor in America) is a fundamental parameter in inelastic force-based design of buildings [129]. It allows to implicitly consider the reduction of induced seismic force in the building due to energy dissipation correlated to structural damping and non-linear behaviour of materials when a linear analysis method is adopted for the calculation of the seismic forces [130]. This factor also takes into account for overstrength phenomena [131]. Accordingly to Fajfar [132], the behaviour factor q can actually be described by two contributions, an intrinsic effective dissipative capacity of the structure q_0 and an overstrength factor Ω:

$$q = q_0 \cdot \Omega \qquad (I.1\text{-}1)$$

An extensive overview on q_0 is given in [130], while sources of overstrength are discussed in [133–136]. It is paramount that the strength reduction operated by the behaviour factor is associated to a global structural ductility, that for CLT buildings is given by a correct design of connections that act as dissipative zones (Section I.1.3.2).

The assessment by researchers of the q-factor for CLT buildings has usually been carried out in two ways, namely experimentally and numerically.

The *experimental* methodology usually considers full-scale shaking table tests, in which the q-factor is determined as the ratio of the PGA at which near-collapse state is reached and the PGA used for elastic design of building [97]. Two are the drawbacks of this approach: on one hand shaking table tests on full-scale buildings are expensive, and on the other hand the derived value of the behaviour factor is restricted to the analysed building configuration and the chosen earthquakes. Quasi-static cyclic tests can also be adopted for the determination of the behaviour factor, allowing for less expenses in the experimental campaign [137]. Pozza *et al.* [138] also proposed a mixed analytical-experimental procedure that schematizes the wall as a Single Degree of Freedom (SDOF) system with a capacity curve equal to the force-displacement curve derived by quasi-static test and a mass correspondent to the constant applied vertical load. The capacity curve is then bi-linearizes through the procedure proposed by Munoz [139]. The pushover method is then applied to derive the maximum earthquake spectra compatible with the displacement capacity of the wall and the behaviour factor is finally defined as the ratio between the PGA of the ultimate spectrum and the PGA of the yielding spectrum.

The *numerical* approach [41, 140, 141] can solve all the issues of experimental approach, since the q-factor is derived carrying out numerical analyses of different configurations of structures and earthquakes, allowing therefore for a more generalized result and less costs. Simulations to the vary of ground motion records, geometries, loads and regularity in elevation can be relatively easily carried out. With numerical model approach, the q-factor is evaluated in two ways depending whether a non-linear static or dynamic analysis is considered. In the first case the behaviour factor is derived using the force-displacement curve following Newmark [142] or N2 [143] method. If non-linear dynamic analyses are adopted, the factor can be derived or as the ratio between the PGAs at yielding and ultimate displacement (acceleration-based approach [96, 106]), or as the ratio between shear at yielding and ultimate displacement (base shear approach [141]). It is remarkable that this procedure could give not univocal results, since the definition of yielding point of timber shear walls subjected to quasi-static monotonic and reversal cyclic in-plane loads depends upon the method used to derive it [144].

Pei *et al.* [145] derived the behavior factor for CLT structures assigning a value that allows for a reference building designed with a force-based approach to equal the performances of the same building designed with a PBD approach.

Ceccotti [146] and Pozza [147] proposed a *combined (or hybrid) testing-modelling* approach in which quasi-static cyclic tests on simple wall systems are used to calibrate dynamic non-linear numerical models. The behaviour factor is then derived in the same way as for experimental methodology, hence as the ratio between the PGA at near-collapse state and the one used to elastically design the building. The tested construction scale is coincident with the minimum construction element that is going to be modelled, e.g. it is possible to test single materials if a model that starts from material level is used. A model built in this way is however computationally heavy since many analyses have to be carried out in order to obtain a generalized result for q-factors at the vary of seismic input and building configuration. A wall-level testing and modelling is therefore the best compromise between generalization (only buildings with the tested configuration of loads, connections and geometry used to calibrate the model can be analysed) and time cost.

Because of the way the q-factor is derived from the abovementioned methods, it is implicitly required that the displacement reached by the structure with elastic design is the same of inelastic response, and

Filiatrault [117] underlines how this behavior is inappropriate for short-period timber structures. A more accurate method to derive the behaviour factor for short-period timber structures would be the adoption of the equal energy approximation that computes q through an energy balance between elastic and inelastic response [148].

Table I.1-2 – Comparison between different Codes and Standards for the seismic design of CLT buildings (*table credits*: Tannert *et al.* [149]).

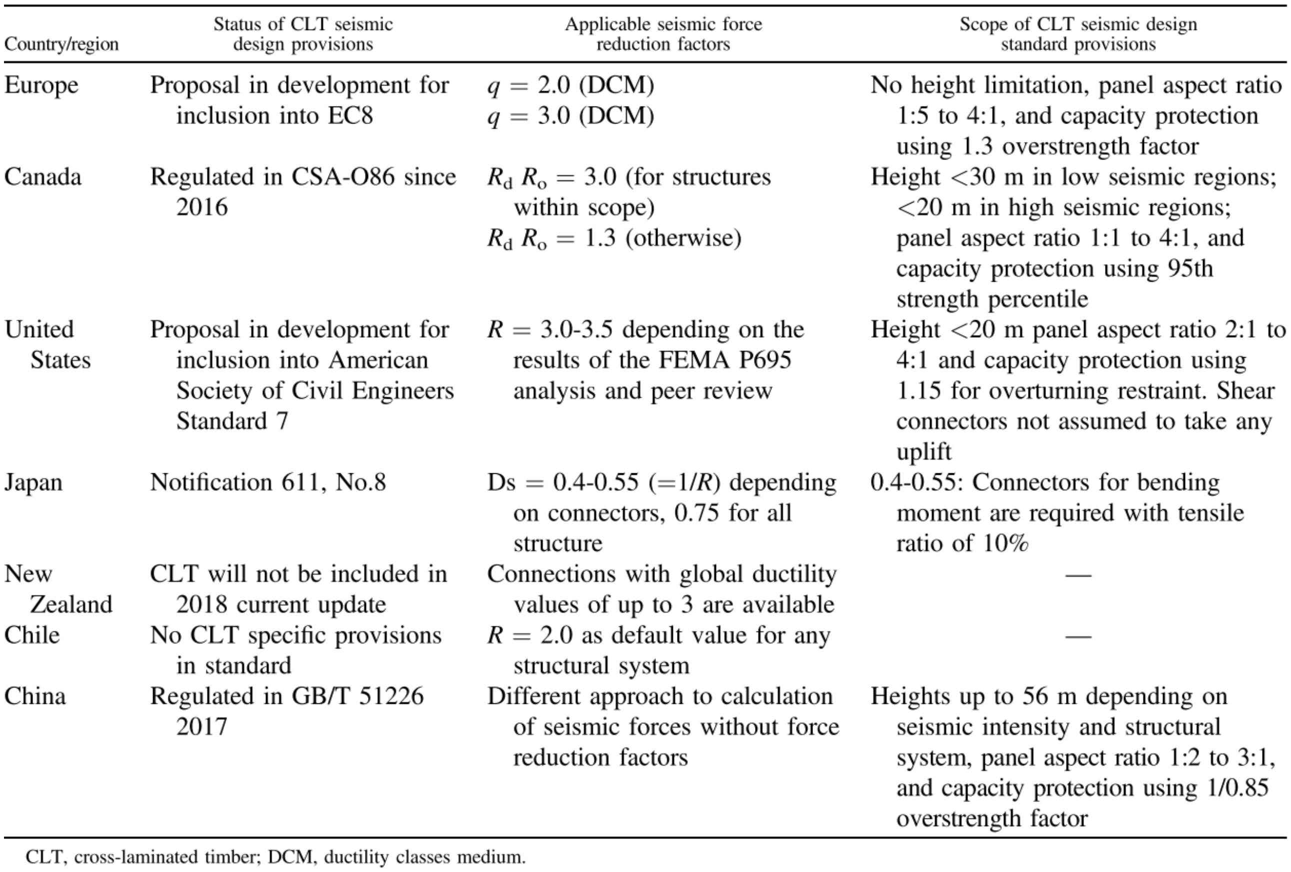

Country/region	Status of CLT seismic design provisions	Applicable seismic force reduction factors	Scope of CLT seismic design standard provisions
Europe	Proposal in development for inclusion into EC8	$q = 2.0$ (DCM) $q = 3.0$ (DCM)	No height limitation, panel aspect ratio 1:5 to 4:1, and capacity protection using 1.3 overstrength factor
Canada	Regulated in CSA-O86 since 2016	$R_d\ R_o = 3.0$ (for structures within scope) $R_d\ R_o = 1.3$ (otherwise)	Height <30 m in low seismic regions; <20 m in high seismic regions; panel aspect ratio 1:1 to 4:1, and capacity protection using 95th strength percentile
United States	Proposal in development for inclusion into American Society of Civil Engineers Standard 7	$R = 3.0$-3.5 depending on the results of the FEMA P695 analysis and peer review	Height <20 m panel aspect ratio 2:1 to 4:1 and capacity protection using 1.15 for overturning restraint. Shear connectors not assumed to take any uplift
Japan	Notification 611, No.8	Ds = 0.4-0.55 (=1/R) depending on connectors, 0.75 for all structure	0.4-0.55: Connectors for bending moment are required with tensile ratio of 10%
New Zealand	CLT will not be included in 2018 current update	Connections with global ductility values of up to 3 are available	—
Chile	No CLT specific provisions in standard	$R = 2.0$ as default value for any structural system	—
China	Regulated in GB/T 51226 2017	Different approach to calculation of seismic forces without force reduction factors	Heights up to 56 m depending on seismic intensity and structural system, panel aspect ratio 1:2 to 3:1, and capacity protection using 1/0.85 overstrength factor

CLT, cross-laminated timber; DCM, ductility classes medium.

As previously stated, EC8 does not furnish a specific q-factor value for CLT buildings, reason why its evaluation has been a topic investigated by many researchers in recent years. The only building technology in EC8 that could be considered similar to the CLT multi storey wall are “glued wall panels with glued diaphragms, connected with nails and bolts”, for which a behaviour factor equal to 2.0 is given. Pozza & Trutalli [140] proposed an analytical formulation to derive the q_0-intrinsic behaviour factor of CLT structures as a function of a joint density parameter factor β and slenderness parameter λ:

$$q_{0(\beta,\lambda)} = \left(q_{0,ref} + \lambda^k\right) \cdot \beta^k \leq 5.0 \qquad (I.1\text{-}2)$$

where k is a parameter calibrated so as to minimize the summation of the square difference between analytical q_0 values and the numerical values obtained from simulations, and $q_{0,ref}$ is the q_0 value for low-ductility buildings according to EC8 [111].

The regularity of elevation play an important role in the definition of the behaviour factor of CLT buildings, and EC8 [111] and Italian Building Code NTC2018 [112] take into account for this aspect by multiplying the q-factor by a value equal to 0.8 if prescriptive geometrical and structural requirements defining the height regularity are not respected. Therefore, for NTC and EC8 the value of the behaviour factor to be considered in case of multi-storey CLT buildings not regular in height is equal to $q = 1.6$, irrespectively of the structural solutions (e.g. monolithic vs. jointed shear-walls) and of the geometry of the building. The adoption of such prescriptive requirements for height regularity to CLT multi-storey buildings results in contradictory design criteria: assuming a constant distribution of the masses for the different floors, it is required that connections have a constant stiffness along the height of the building and at the same a decreasing stiffness from the foundations to the roof. Trutalli and Pozza [150] carried out an extensive study on the effect of height regularity on the behaviour factor analyzing through Incremental Dynamic Analyses (IDAs) [151] different building configurations to the vary of height regularity, number of storeys, building slenderness and construction methodologies for walls (single-panel or multi-panel). It has been found that designing connections with constant stiffness along the height of the building reduces the global ductility of the structure of about 25% respect to buildings with connections dimensioned to withstand without overstrength the design seismic load at each storey. CLT buildings with strength (and stiffness, proportional to strength) constant along the whole height are less performant in energy dissipation and are susceptible of global brittle failures such as soft-floor. Therefore, a revision of the requirements for in-height regularity for the specific case of CLT buildings is necessary. It has also been found that building slenderness does not worsen or improve the behaviour of in-height irregular buildings, while adoption of monolithic walls significantly decreases performances of such structures. The study resulted in a generalization of Equation (I.1-2) in order to take into account also for irregularity in elevation due to storey strength and stiffness, it is therefore not applicable to the case in which in-height irregularity is due to floor-size changes between storeys. An alternative empirical conservative method has also been proposed in order to reduce q_0 derived for regular configurations directly multiplying this behaviour factor for a reduction factor $k_R(\beta)$ function of the density of vertical joints between CLT wall panels (β parameter). This approach, similar to the one proposed by Italian Building Code NTC 2018 [112], lead to a formulation of $k_R(\beta)$ equal to:

$$k_R(\beta) = k_{R,ref} \cdot \beta^z \leq 1.0 \qquad (I.1\text{-}3)$$

where $k_{R,ref} = 0.6$ and $z = 0.222$.

Also results by Polastri [152] obtained through linear dynamic analyses already showed that height regularity influence all the main structural parameters, like vibrational period, forces on connections and drifts. Incidentally, Linear Static Analyses (LSAs) are not allowed for buildings with height irregularity.

Pei *et al.* [41] proposed an approximate higher value of the *R*-factor equal to 4.5, derived from a Performance-Based Seismic Design (PBSD) of a 6-storey building verified through non-linear time-history simulation. This value can be used for building designed following ASCE-7 [116] equivalent lateral force procedure (ELFP).

The new coming-soon version of EC8 will furnish values of the q-behavior factor specific for CLT buildings for medium ($q = 2$) and high ($q = 3$) ductility classes as a function of the fact that the shear walls are constituted respectively by monolithic and vertically-jointed CLT panels, each having a width not smaller than 25% the inter-storey height [113, 149]. Actually, the difference between DCM and DCH CLT structures is in the fact that the vertical half-lap joint between adjacent panels must behave as dissipative zone, adding therefore global ductility to the structure. Indeed, cyclic tests on CLT wall systems [48], comparison between different buildings tested on shaking table [140, 153] and numerical parametric analyses [96, 101] showed that fragmentation of walls into sub-panels connected through vertical half-lap joints can improve their ductility to horizontal in-plane actions.

Alternative ways to increment the q-factor for timber structures is using dissipative devices with no bearing functions that allow for energy dissipation thanks to yielding of mild steel. These devices have been widely investigated in the 70s for steel and concrete structures [154] and have successfully applied to CLT structures in order to obtain resilient structures, like the U-shaped Flexural Plate (UFP) device shown in [71].

Friction between panels also has an important role in defining non-linear behavior of CLT wall systems subjected to cyclic in-plane loads, and its influence on energy dissipation, stiffness and strength of the CLT structures is strong enough to overshadow the contribution of UFPs [155]. Some innovative connections that make use of the hysteretic behavior of friction have also been studied [156, 157]. The easiest and cheapest way to increment energy dissipation in CLT structures is anyway obtainable through a correct design of connections that avoids brittle behavior and allows for high ductility. Code provisions and design strategies to allow for this will be analyzed in Section I.1.3.2.

I.1.3.2 Design of connections for CLT buildings

Because of the crosswise direction of grain in CLT, design criteria of connections usually differ from the ones employed for glulam and solid timber. An overview of design approaches of CLT structures adopted in Europe, Canada, United States and New Zealand is reported in [158]. In the following, considerations about design of connections will be provided, focusing on ductility (Section I.1.3.2.1), calculation models for the design of dowel-type connections (Section I.1.3.2.2), capacity design (Section I.1.3.2.3) and coupling models (Section I.1.3.2.4).

I.1.3.2.1 Ductility

Connections play a fundamental role in defining the overall ductility of CLT structures. CLT is a material characterized by a high in-plane strength and stiffness, and it is characterized by brittle failure modes except for compression, therefore only a correct design of joints as dissipative zones following capacity design criteria is able to guarantee a dissipative behavior for DCM and DCH CLT buildings [159], otherwise the application of q-factors higher than the values proposed for DCL $q = 1.5$ is incorrect. Ensuring ductility of connections in timber structures is a fundamental aspect of good practice in their design, reason why high-performance connections able to develop huge plastic deformations have been developed [160]. It is also fundamental to respect minimum distances between dowelled connectors in order to avoid brittle failure of timber [148]. In order to ensure ductility of connection, with large cyclic deformations and a stable energy dissipation, some failure modes evidenced by past experimental tests of hold-downs and angle brackets subjected to tension force must be avoided. For example, tensile failure of the net cross section of the metal sheet of hold downs (Figure I.1-22.a) should be avoided, as well as pull-through of the anchoring bolt (Figure I.1-22.b) and withdrawal of the nails respectively for wall-to-foundation and wall-to-floor angle brackets (Figure I.1-22.c) may be prevented.

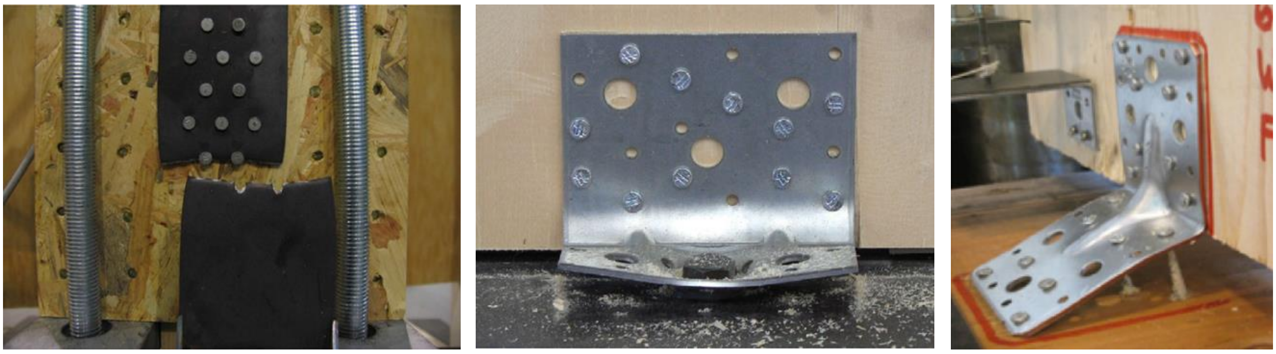

(*a*) (*b*) (*c*)

Figure I.1-22 – Brittle failure mechanisms of typical CLT connections: (*a*) tensile failure of the net cross section of the metal sheet of hold downs, (*b*) pull-through of the anchoring bolt of wall-to-floor angle brackets and (*c*) withdrawal of the nails of wall-to-foundation angle brackets (*image credits*: Follesa *et al.* [113]).

Ductility of connections μ is usually defined on a conventional basis as the ratio between ultimate and yielding displacements v_u and v_y:

$$\mu = \frac{v_u}{v_y} \tag{I.1-4}$$

There is currently no common agreement in the procedure to define the yielding displacement v_y and different methods exist for its determination, like the one proposed in EN 12512 [161], the one by Kobayashi & Yasumura [162] and the method presented in ASTM E2126 [163]. This inhomogeneity in the determination of the yielding point of connections leads as a consequence to misalignment in the definition of ductility parameter for a same connection typology as pointed out by Munoz *et al.* [139].

Ductility capacity of connections is also strongly correlated to the impairment of connection strength Δ_F, that in the European standard EN 12512 [161] is defined as the difference between the strength measured at 1st and 3rd loading cycles for a given displacement amplitude v. An extensive discussion about ductility and force impairment evaluation for hold-down and angle bracket connections has been reported by Gavric *et al.* [102]. A novel method that resembles in some aspect the short procedure of EN 12512 [161] to determine the ductility class of dowel-type connections is the one proposed in the revised version of the standard EN 14592 [164]. The ductility behavior of connections is determined through tests carried out on the fasteners. Three low cycle ductility classes (S1, S2 and S3) are defined as a function of the minimum bending angle α_c (Table I.1-3) that dowel-type connector can reach for three reversed cyclic loadings at constant amplitude (Figure I.1-23.a).

The parameter α is defined as follows:

$$\alpha = \frac{45}{d^{0.7}} \qquad (I.1\text{-}5)$$

where d is the nominal diameter of the shank. In order to comply with a ductility class, the fastener must satisfy the following performances in tests carried out on a standardized test setup (Figure I.1-23.b) without failure:

i. a bending angle $\alpha_c = 20°$ must be reached in monotonic loading conducted prior to cyclic test;
ii. a bending angle at least equal to a value α_c correspondent to a low-cycle ductility class (Table I.1-3) must be reached;
iii. an ultimate bending angle α_u equal to 45° and 30° respectively for shanks with diameter less or greater than 8 mm must be reached;
iv. the residual bending moment M_{res} read at α_u must be greater or equal to 80% of the average yielding moment from monotonic test.

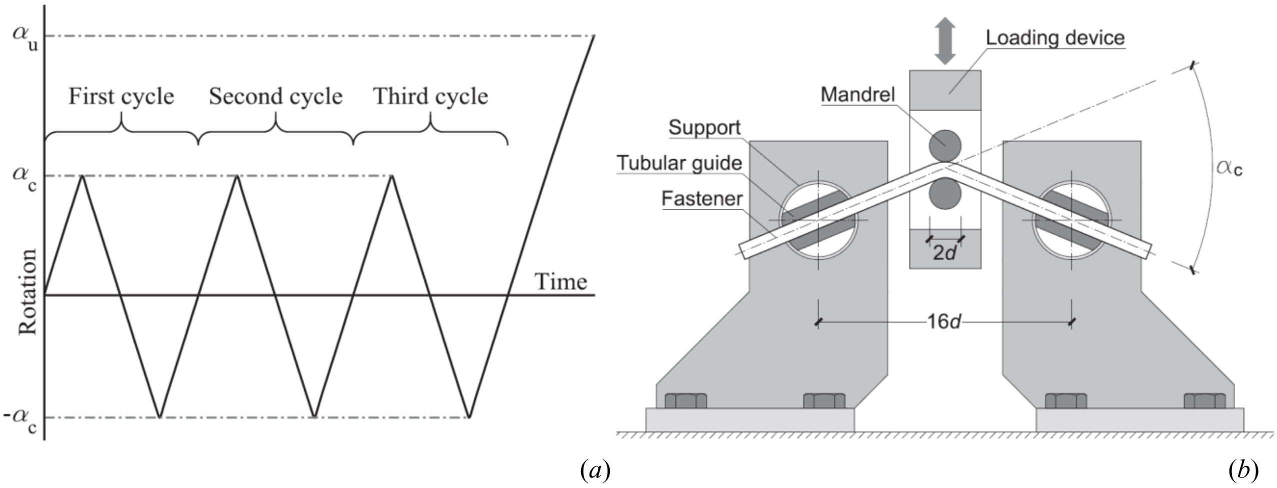

(*a*) (*b*)

Figure I.1-23 – EN 14592 [164]: (*a*) cyclic loading protocol and (*b*) test setup (*image credits*: Izzi *et al.* [165]).

Table I.1-3 – Low cycle ductility classes accordingly to EN 14592 [164].

Low cycle ductility class	α_c
S1	α
S2	$1.5\ \alpha$
S3	$2\ \alpha$

The procedure of revised EN 14592 [164] and EN 12512 [161] differ in the following aspects:

- EN 14592 [164] requires the achievement of either minimum strength and deformation performances at monotonic and cyclic loading conditions, while EN 12512 [161] only requires attainment of minimum strength performances for cyclic conditions;
- EN 12512 [161] has an incremental load history whose amplitude is function of the yielding displacement at monotonic test.

Izzi *et al.* [165] carried out a series of 200 tests on self-tapping screws to evaluate their ductility accordingly to revised EN 14592 [164], founding that low-diameter screws ($d = 6$ mm) belong to class S2, high-diameter screws ($d = 10$ mm) belong to high ductility class S3. Screws with an intermediate diameter $d = 8$ mm have the potential to be assigned to a low cycle ductility class S3, but tests highlighted inappropriate failures on the final monotonic ramp to α_u.

Casagrande *et al.* [166] proposed a new methodology to evaluate the ductility μ of connections taking into account for impairment of strength Δ_F between the 1st and 3rd loading cycles due to cyclic loadings. Accordingly to the current version of Eurocode 8 [111], "*the dissipative zones shall be able to deform plastically for at least three fully reversed cycles at a static ductility ratio of 4 for ductility class Medium (DCM) structures and at a static ductility ratio of 6 for ductility class High structures (DCH), without more than a 20% reduction of their resistance*". This sentence is anyway likely to two different interpretations: (*i*) the impairment of resistance is referred to the loss of resistance of the 1st cycle backbone due to softening behavior, (*ii*) the reduction of resistance is due to strength degradation Δ_F between 1st and 3rd loading cycle (Figure I.1-24.a). Casagrande states that the right interpretation is the latter, therefore he derives a new model to define the interaction between the strength degradation and the ductility capacity. The impairment of strength factor can be defined as

$$\eta_{deg}(v) = \frac{F_3(v)}{F_1(v)} = 1 - \frac{\Delta_F(v)}{F_1(v)} \qquad (I.1\text{-}6)$$

where $F_3(v)$ and $F_1(v)$ are respectively the force of the 3rd cycle and 1st cycle backbone force for a given displacement v. Defined therefore the dimensionless displacement

$$\tilde{v} = \frac{v}{v_y} \qquad (I.1\text{-}7)$$

and the dimensionless ultimate displacement

$$\tilde{v}_u = \frac{v_u}{v_y} \qquad (I.1\text{-}8)$$

it is possible to derive a linear relationship between the impairment factor η_{deg} and the dimensionless displacement $\tilde{v}$ (Figure I.1-24.b):

$$\eta_{deg}(v) = a(\tilde{v} - 1) + \eta_{deg,\tilde{v}=1}, \qquad \tilde{v} \in [0; \widetilde{v_u}] \qquad (I.1\text{-}9)$$

where a is the slope of the linear interpolating curve and represents the influence of the slip amplitude on the impairment of strength. In order to take into account for the impairment of strength between the 1st and 3rd cycle Δ_F, a degradation ultimate displacement $v_{u,deg}$ is introduced:

$$v_{u,deg} = min\left[v_u; v\left(\eta_{deg} = \eta_{deg,lim}\right)\right] \qquad (I.1\text{-}10)$$

where $\eta_{\text{deg,lim}} \in [0; 1]$ is the limit value of the impairment strength factor. The yielding and ultimate displacement v_y and v_u can be derived accordingly to EN 12512 [161], Kobayashi & Yasumura [162] or ASTM E2126 [163]. It is finally checked if the impaired 1st cycle backbone connection has a proper softening behavior requiring the respect of the following condition:

$$\tilde{f}_{deg}\left(v_{u,deg}\right) = \frac{F_1\left(v_{u,deg}\right)}{F_N} \geq f_{deg,lim} \qquad (I.1\text{-}11)$$

where F_N is the nominal strength. In case the inequality is not satisfied, it is necessary to consider a lower value of $v_{u,deg}$ respect to the one resulting by Equation (I.1-10). If it is not possible to satisfy the inequality (I.1-11) even through the reduction of $v_{u,deg}$ the connection should be considered inappropriate for dissipative purposes because of inadequate ductility.

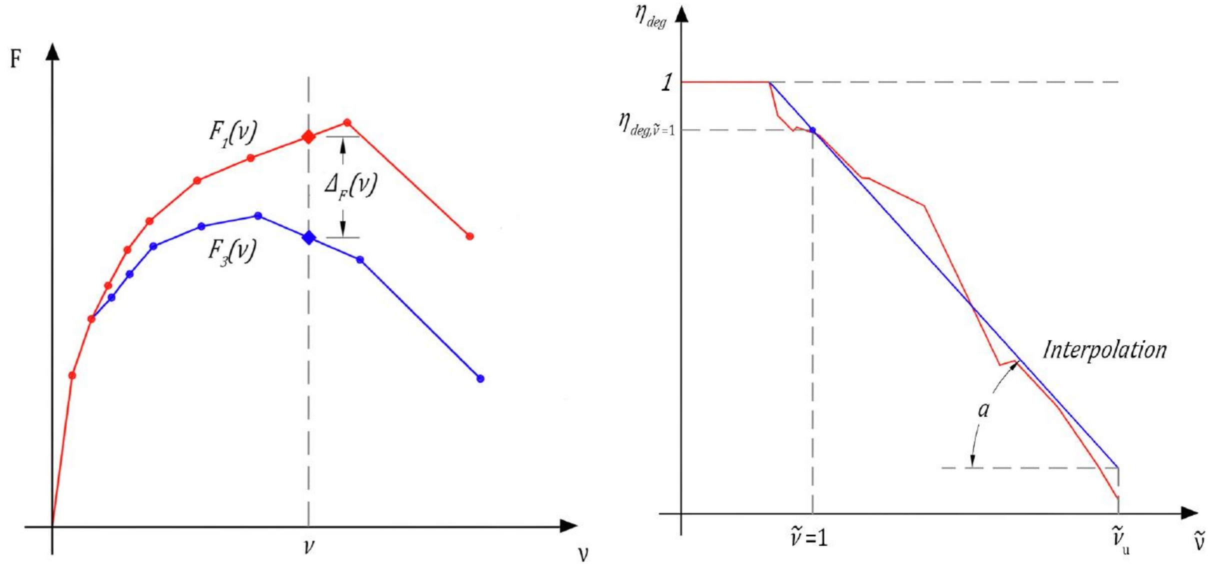

(*a*) (*b*)

Figure I.1-24 – Evaluation of ductility of connections accordingly to Casagrande *et al.* [166]: (*a*) impairment of strength between the 1st (red) and 3rd (blue) backbone curves and (*b*) impairment of strength factor vs. dimensionless slip amplitude (*images credits*: Casagrande *et al.* [166]).

I.1.3.2.2 Calculation models

Current version of Eurocode 5 [110] still lacks in calculation method for dowelled connections for CLT, because of the cross-layered characteristics that make this material behaving quite differently from other wooden materials like solid timber (ST) and glulam (GLT). For this reason, the design methods provided by codes and standards, that to-date are based on Johansen theory [167], need a review and harmonization process to take into account for the peculiar characteristics of CLT due to its internal structure. The only analytical models for design of dowel-type connections in CLT with dowel-type fasteners are given by Blaß [74], that provides a modified formulation for embedment strength of timber and corrective factors to be applied to Johansen's formulas [167]. It should be anyway noticed that some adjustment to this model may be needed, since it has been validated employing CLT panels with layer thickness much lower than the one usually adopted nowadays [168]. Specific rules for dowel-type connections used in CLT structures are necessary since they present two peculiarities respect GLT and ST. Actually, for all laminated timber structures (CLT and GLT), the position of the fastener on the side or narrow face heavily influences the behavior of connections. On the other hand, gaps and stress reliefs in CLT laminations can significantly affect embedment and withdrawal strength.

Both embedment and withdrawal capacity are strongly influenced by timber density of CLT panel ρ_k, that for connections installed on the narrow face can be considered equal to the characteristic value of lamination $\rho_{l,k}$, while for connectors on the side face it can be considered equal to $1.1 \cdot \rho_{l,k}$.

An extensive overview on calculation methods for dowel-type connections in CLT structures is reported by Ringhofer *et al.* [53]. The main aspects are summarized in the following, and the reader is referred to [53] for further informations. Dowel type connections mounted on CLT panels behave differently when mounted on the side and on the narrow face, therefore the mechanical behavior for and laterally- axially-loaded dowel-type connectors will be shown respectively in Section I.1.3.2.2.1 and I.1.3.2.2.2 distinguishing between the two cases. When a connector is placed on the side face, in order to reduce the possibility that the fastener is inserted only on gaps, the fastener should penetrate for at least 3 layers.

I.1.3.2.2.1 Laterally-loaded connections

For *smooth dowels* and *thigh-fitting bolts* on side face a model to derive the characteristic embedment resistance $f_{h,k,CLT}$ has been proposed by Blaß & Uibel [169]:

$$f_{h,k,CLT} = \frac{32(1 - 0.015\,d)}{1.1\,sin^2\,\beta + cos^2\,\beta}\left(\frac{\rho_k}{400}\right)^{1.2} \qquad (I.1\text{-}12)$$

where d is the connector nominal diameter and β is the load-grain angle.

The abovementioned authors also proposed a formulation for axially-loaded *profiled nails* and *self-tapping screws* on side face, even if it must be noted that it is valid for layers thickness $t_l \leq 9$ mm, therefore a revision to current commercial layer thicknesses (20, 30 and 40 mm) is necessary:

$$f_{h,k,CLT} = 60\,d^{-0.5}\left(\frac{\rho_k}{400}\right)^{1.05} \qquad (I.1\text{-}13)$$

The usage of smooth dowels, tight-fitting bolts or profiled nails on the narrow face of CLT panels is not advisable [53]. Anyway, Blaß & Uibel [169] propose a conservative formulation to derive the embedment strength of laterally-loaded *smooth dowels* and *self-tapping screws*:

$$f_{h,k,CLT} = 9\,(1 - 0.017\,d)\left(\frac{\rho_{l,k}}{350}\right)^{0.91} \qquad (I.1\text{-}14)$$

The same authors give a formulation for *profiled nails* and *self-tapping screws*:

$$f_{h,k,CLT} = 20\,d^{-0.5}\left(\frac{\rho_{l,k}}{350}\right)^{0.56} \qquad (I.1\text{-}15)$$

where d is the shank outer diameter.

I.1.3.2.2.2 Axially-loaded connections

When a connector is inserted in the narrow face of CLT panels, there is the possibility that it presents the axis parallel to grain direction or that it is placed on a gap. In add, in a whole connection placed on the narrow face (e.g. corner joints), there is the possibility that each connector can present different conditions of orientation respect to grain direction and insertion in gaps. Dowel-type connectors placed on narrow face can be subjected to in-plane or out-of-plane lateral loading condition, where the last case is more problematic because brittle failure for tension perpendicular to grain can occur. A stochastic-mechanical multivariate model describing the load-displacement behavior of self-tapping screws in the narrow face of CLT to the vary of shank-grain angle α has been derived by Brandner *et al.* [170]. The model, that can also be used to derive stiffness and displacements, has shown a great influence of α on withdrawal performance of self-tapping screws on narrow face of CLT panels.

Different equations can be used to derive the characteristic withdrawal strength $f_{ax,k}$ of axially-loaded *self-tapping screws*, respectively accordingly to Eurocode 5 [110] (Equation (I.1-16)), Blaß & Uibel [169] (Equation (I.1-17)) and Ringhofer *et al.* [171] (Equation (I.1-18)):

$$f_{ax,k} = \frac{18.0\,d^{-0.5} l_{ef}^{-0.1} k_d}{1.2\,cos^2\,\alpha + sin^2\,\alpha}\left(\frac{\rho_k}{350}\right)^{0.80} \qquad (I.1\text{-}16)$$

$$f_{ax,k} = \frac{9.02\,d^{-0.2} l_{ef}^{-0.1}}{1.35\,cos^2\,\varepsilon + sin^2\,\varepsilon}\left(\frac{\rho_k}{350}\right)^{0.80} \qquad (I.1\text{-}17)$$

$$f_{ax,k} = 8.67\,k_{ax,k}\,k_{sys,k}\,d^{-0.33}\left(\frac{\rho_k}{350}\right)^{k_p} \qquad (I.1\text{-}18)$$

where d is the connector nominal diameter, l_{ef} is the effective inserted thread length, α is the thread-grain angle, ε is the primary insertion angle ($\varepsilon = 0°$ for screws inserted in the narrow face and $\varepsilon = 90°$ for screws inserted in the side face) and where:

$$k_d = min\left(\frac{d}{8}; 1\right), d\ in\ [mm] \tag{I.1-19}$$

$$k_{ax,k} = \begin{cases} 1.00, & if\ \alpha \in [45°, 90°] \\ 0.64\ k_{gap,k} + \dfrac{1 - 0.64\ k_{gap,k}}{45}\ \alpha, & if\ \alpha \in [0°, 45°] \end{cases} \tag{I.1-20}$$

$$k_{gap,k} = \begin{cases} 0.90\ CLT\ narrow\ face \\ 1.00\ else \end{cases} \tag{I.1-21}$$

$$k_{sys,k} = \begin{cases} 1.00 & for\ ST \\ 1.00 & for\ CLT, \quad N \geq 3 \\ 1.13 & for\ GLT, \quad N \geq 5 \end{cases} \tag{I.1-22}$$

$$k_p = \begin{cases} 1.10 & if\ \alpha \in [0°, 90°] \\ 1.25 - 0.05\ d & if\ \alpha = 0 \end{cases} \tag{I.1-23}$$

The model by Eurocode 5 [110] (Equation (I.1-16)) - derived for types of timber other than CLT - and the one by Blaß & Uibel [169] result to have a similar approach, while the equation proposed by Ringhofer *et al.* [171] (Equation (I.1-18)) introduces new features, with a density correction factor k_p (Equation (I.1-23)), a system factor k_{sys} (Equation (I.1-22)), a factor that takes into account for gaps and stress reliefs k_{gap} (Equation (I.1-21)) and noticing that l_{ef} is no longer a parameter influencing the withdrawal strength.

For screws placed in the side face, the formulation by Ringhofer *et al.* [171] (Equation (I.1-18)) gives higher values of the withdrawal resistance f_{ax} respect to the other two. On the contrary, the formulation by Ringhofer *et al.* [171] (Equation (I.1-18)) gives more conservative results for connections mounted on the narrow face, therefore its application is advisable in this case.

As long as regards *profiled nails* installed in CLT panels, Blaß & Uibel [169] proposed the following formulation:

$$f_{ax} = \frac{0.16\ d^{-0.4}\ \rho^{0.8}}{3.1\ cos^2\ \varepsilon + sin^2\ \varepsilon} \tag{I.1-24}$$

This approach gives more conservative results respect to the nonlinear empirical formula proposed by Sandhaas & Görlacher [172] for solid timber (ST) structures, given by:

$$f_{ax} = 3.60 \cdot 10^{-3}\ \rho^{1.38} \tag{I.1-25}$$

I.1.3.2.2.3 Effective number and minimum spacings

The models reported in Section I.1.3.2.2.1 and I.1.3.2.2.2 refer to a single connector, therefore, when calculating the resistance of a whole connection, group effects should be considered, for example through the coefficient n_{ef} that gives a fictious effective number of connectors. The resistance reduction is due to brittle failure modes that could rise, see Table I.1-4. In order to prevent such failures, minimum spacings between connectors and edge distances are given in Blaß & Uibel [169] and are summarized in Table I.1-5 and Table I.1-6 respectively for axially- and laterally-loaded connections.

If minimum spacings are fulfilled, it is not necessary to reduce the connection resistance for laterally loaded dowel type connections mounted on the side face, thanks to a high capacity of redistribution given by natural reinforcement given by orthogonal layers of CLT material. On the contrary, when laterally loaded dowel type connectors are mounted on the narrow face, the effective number n_{ef} should be calculated accordingly to EC5 [110].

For axially-loaded self-tapping screws, Brandner *et al.* [23] propose the following equation to calculate the withdrawal resistance of a group of connectors:

$$F_{ax,n} = 0.90 \sum_{i=1}^{R} F_{ax,ref,i} n_i \qquad (I.1\text{-}26)$$

where R is the number of penetrated CLT layers, n_i is the number of screws and $F_{ax,ref,i}$ is the reference withdrawal capacity per layer.

I.1.3.2.3 Capacity design of connections

The correct design of connection is a key-aspect in the application of capacity design to buildings seismically dimensioned with force-based methods. Capacity design criterion, studied since 70s in New Zealand by Park & Paulay for RC structures [173], makes use of overstrength factors, defined as the ratio between the design value of the 95th percentile of the ductile element and the design value of the characteristic strength (5th percentile) of the ductile element valuable by practitioners through analytical models available on literature and codes. In addition, an overdesign factor should be considered, defined as the ratio between the designed strength of ductile element and the design seismic demand on it [114]. Capacity design assumes a fundamental role to guarantee structural ductility of timber structures, since, differently from concrete and steel structures, timber members outside the dissipative zones located in the connections do not have non-linear capacities [148].

Capacity design rules prescribe that design strength of brittle elements $F_{Rd,b}$ must be greater or equal to the design strength of ductile parts $F_{Rd,d}$ multiplied by an overstrength factor γ_{Rd}. In add, accordingly to Follesa [113, 174] and Izzi [168], $F_{Rd,d}$ should be divided by a strength degradation factor β_{Sd} due to cyclic loading, defined as ratio between force obtained at 3rd $F_{max(3rd)}$ and 1st $F_{max(1st)}$ cycle:

$$\beta_{Sd} = \frac{F_{max(3rd)}}{F_{max(1st)}} \qquad (I.1\text{-}27)$$

It is therefore possible to write the general equation for design a connection accordingly to capacity design criterion:

$$\frac{\gamma_{Rd}}{\beta_{Sd}} \cdot F_{Rd,d} \leq F_{Rd,b} \qquad (I.1\text{-}28)$$

However, Trutalli *et al.* [87] underline how the cyclic strength reduction is already considered in the definition of the behavior factor according to EC8 [111], therefore it is not necessary to take into account for the strength degradation factor β_{Sd}.

Current codes, like EC8 [111] and Italian NTC 2018 [112], lack in the definition of overstrength factors to apply capacity design to timber structures, while New Zealand Timber Standard NZS3603:1993 [121] gives a value of 2. More informations about capacity design applied to timber structures and relative overstrength factors must therefore be found in scientific literature.

Accordingly to Izzi *et al.* [168], the overstrength factor γ_{Rd} can be seen as the product between two sub-factors, γ_{an} considering the underestimation of effective bearing capacity of connection due to analytical models given by codes or standards, and γ_{sc} due to the experimental scattering between 5% (characteristic) and 95% percentile resistance:

$$\gamma_{Rd} = \gamma_{sc} \cdot \gamma_{an} \qquad (I.1\text{-}29)$$

Both sub-coefficients usually result to be quite high, on one hand because the statistical variability of traditional connections resistance (described by sub-coefficient γ_{sc}) is usually remarkable, and on the other hand because the actual peak strength of fasteners often exceeds a lot the corresponding analytical value usually derived accordingly to Johansen [167].

Table I.1-4 – Failure types and behavior for axially- and laterally-loaded dowel-type connectors.

Loading condition	*Failure type*	*Behaviour*	*Failing material*
Lateral	Embedment	Ductile (Pinching)	Timber
	Yield in bending	Ductile	Steel
	Block shear, row shear, plug shear	Brittle	Timber
	Tension perpendicular to grain (splitting)	Brittle	Timber
Axial	Withdrawal	Ductile	Timber
	Head-pull-through	Brittle	Timber
	Fastener tension	Ductile	Steel
	Fastener buckling	Limited ductility	Steel and Timber
	Tension perpendicular to grain (splitting)	Brittle	Timber
	Block shear and row shear	Brittle	Timber

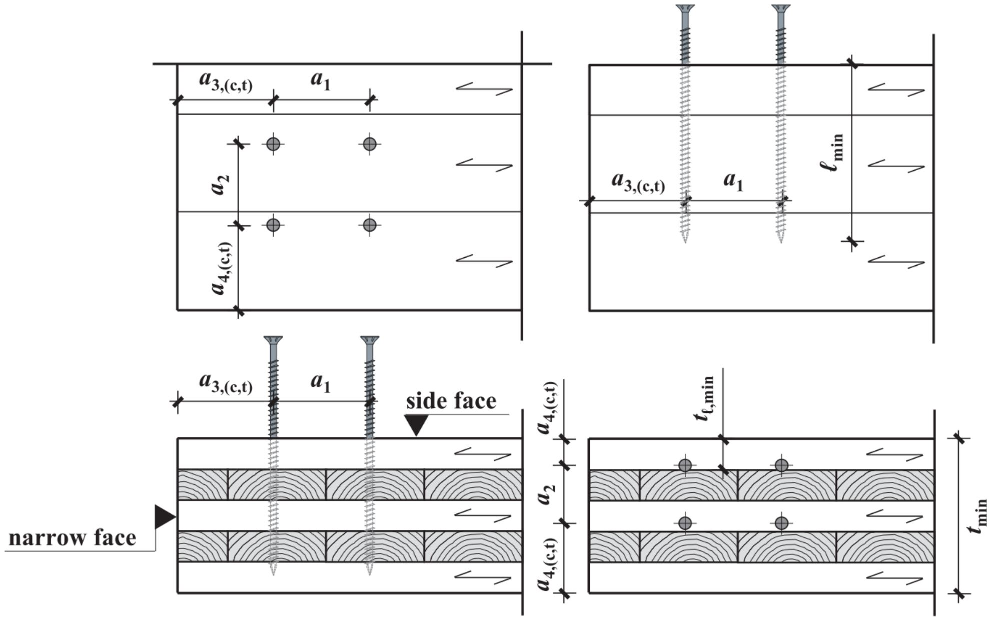

Figure I.1-25 – Minimum spacings and end-distances for self-tapping screws (*image credits:* Ringhofer *et al.* [53]).

Table I.1-5 – Spacings for dowel-type fasteners for laterally loading condition in CLT according to Blaß & Uibel [169].

Fastener	*Face*	a_1	a_2	$a_{3,t}$	$a_{3,c}$	$a_{4,t}$	$a_{4,c}$
Self-tapping screws	*Side*	$4\ d$	$\frac{5}{2}d$	$6\ d$	$6\ d$	$6\ d$	$\frac{5}{2}d$
	Narrow	$10\ d$	$3d$	$12\ d$	$7\ d$		$5d$
Nails[*]	*Side*	$(3+3\cos\beta)d$	$3d$	$(7+3\cos\beta)d$	$6\ d$	$(3+4\sin\beta)d$	$3d$
Dowels	*Side*	$(3+2\cos\beta)d$	$3d$	$5\ d$	$max\{4d\sin\beta\ ;3d\}$	$3\ d$	$3d$
	Narrow	$4\ d$	$3d$	$5\ d$	$3\ d$		$3d$

[*] *Profiled (annual ringed) nails*

Table I.1-6 – Spacings for dowel-type fasteners for axially loading condition in CLT as a function of thread-grain angle α according to Plüss & Brandner [175].

α	a_1	a_2
0°	$2.5\ d$	$5d/2.5d$[a]
45°	$5\ d$	
90°	$7\ d$	
0°|90°	$7\ d$	
45°|45°	$7\ d$	

[a] 5 d if inserted in the same layer, 2.5 d if inserted in different layers

Gavric *et al.* [176] remarked how, during some of the tests on connections [102] and CLT wall systems [77] carried out within the SOFIE project [42], some brittle failures were observed, for example tearing failure of steel plate for hold downs with too many nails or bolt pull-through and nails withdrawal in angle brackets subjected to tension. Starting from the observation of these failure modes, the authors give prescriptions necessary to guarantee ductility for CLT walls that adopt traditional connections with dowel-type fasteners. Prescriptions are given at all scale-levels, from single connection, to wall system until building level. It is remarkable that, when the hold-down is not tested to verify the compliance with capacity design criteria, partial nailing is suggested in order to assure a the occurrence of plastic hinges on connections prior to the tearing failure of steel plate [87]. As a general rule, at least one plastic hinge on dowel connectors must be attained, therefore failure modes *a*, *c*, *f* and *j*/*l* of Figure I.1-26 should be prevented.

Many authors have studied the application of capacity design criteria to timber structures in recent years, to mention a few Ottnehaus [122], Loss [177], Brühl [178] and Dickof [179]. Comprehensive studies of capacity design of typical metal connectors for CLT structures (viz. hold-downs, angle-brackets, self-tapping screws for corner joints and annual-ringed nails) have been carried out by Fragiacomo [114], Sustersic [180], Gavric [102] and Izzi [168], whose results in terms of overstrength factor γ_{Rd} are synthetized in Table I.1-7.

It is possible to observe that the values given by the various authors are not totally in accordance with the provisions of the upcoming revision of EC8 [113], that furnish a unique value $\gamma_{Rd} = 1.3$ for connections in CLT structures.

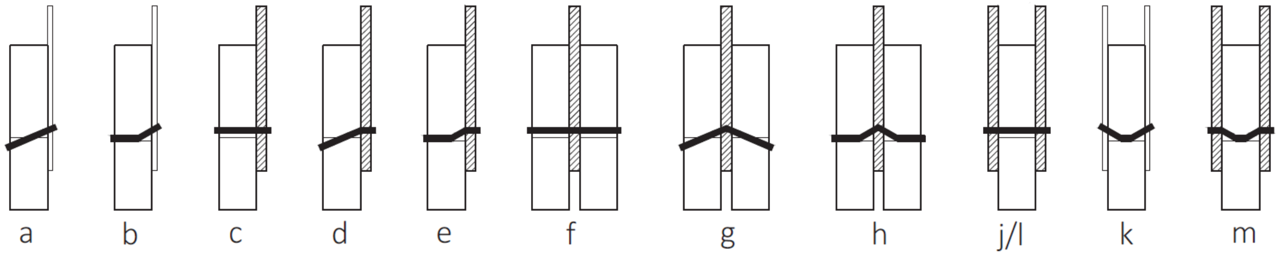

Figure I.1-26 – Failure modes of steel-to-timber dowelled joints (*image credits*: Blaß *et al.* [59]).

Table I.1-7 – Values of overstrength factors γ_{Rd} for different connection types usually employed for CLT buildings for different loading conditions by author.

Connection type	*Load direction*	*Fragiacomo* [114] *and Sustersic* [180]	*Gavric* [102]	*Izzi* [168]
Hold-down	*Axial*		1.3	
	Shear		1.25-1.38(2)	
Angle bracket	*Axial*	1.2-1.9(1)	1.23(3)-1.44(4)	
	Shear	1.3-2.2(1)	1.16(3)-1.40(4)	
Self-Tapping Screws	*Shear between perpendicular CLT panels*	1.6		
Single annual-ringed nails	*Withdrawal*			1.8(5)-2.0(6)
	Shear parallel to face lamination			1.3(5)-1.8(6)
	Shear perpendicular to face lamination			1.5(5)-2.3(6)

[a] Values for a group of nails could be lower, since the values are derived for single nails
[1] Lower values for greater nails diameter
[2] Value that depends on connection configuration
[3] Wall-to-foundation connections
[4] Wall-to-floor connections
[5] Characteristic strength calculated from standards
[6] Characteristic strength calculated from experimental tests

In order to guarantee a global ductile seismic response of the building, capacity design criterion must be adopted not only looking at wall systems behavior, but also at the whole box-like mechanism typical of this type of buildings. For this reason, it is necessary to guarantee an overstrength to panel-to-panel floor connections in order to guarantee their rigidity and allow for dissipation in the dissipative zones localized in lateral-resistant wall systems [114].

Many innovative connections have been proposed in the last years in order to fulfill capacity design requirements (Section I.1.2.4.2), and an adaption of traditional angle brackets to avoid brittle failures has been analyzed by D'Arenzo *et al.* [181].

I.1.3.2.4 Coupling models

So far as strengths both in axial and shear directions are considered in the design of traditional hold-down and angle-bracket connections, it would be recommendable to consider a coupled resistance domain. Actually, mutual interaction between forces in the two directions determine a decrease of the maximum resistance that could be reached by connection if loaded in uniaxial conditions. Moreover, it should be noted that the analytical models provided by codes and standards (e.g. Eurocode 5 [110]) or by academic literature (e.g. formulations by Blaß [74]) apply to uniaxial lateral loading conditions. Similarly, tests on connections, often taken as reference for calibration of numerical models, are usually carried out with uniaxial loading conditions (e.g. [46, 102, 182]). Noticing that CLT walls subjected to horizontal seismic actions determine a combination of axial and lateral forces on connections, models to take into account coupling interaction are necessary. Codes and standards do not consider the phenomenon, and only ETAs (e.g. ETA-06/0106 [183] and ETA-11/0086 [184]) furnish a simple elliptical coupling criterion. Academic research has recently been conducted to have a deeper insight into this topic, both with experimental campaigns, (e.g. Pozza *et. al.* [185] and by Liu and Lam [186, 187]) and advanced parametric numerical simulations by Izzi [188]. Pozza *et al.* also developed a novel hybrid force-displacement based approach to take into account for coupling phenomena of hold-down [83] and angle-bracket [82] connections. This model has been successfully employed to create a new design tool illustrated in Section II.3. The authors also showed the feasibility of this coupling criterion for numerical modelling, adopting a more refined coupling approach respect to elliptic one based on ETAs usually adopted for numerical modelling (e.g. Rinaldin *et al.* [104] and D’Arenzo *et al.* [181]). Further details on coupling methods are also reported in Section II.1.5.

I.1.4 Numerical modelling of CLT buildings

The fast development in recent years of more and more advanced finite element analysis tools has allowed the spread of numerical modelling as a tool for the analysis of structures, both for research and design purposes. An important aspect when dealing with numerical modelling is the adoption of strategies that allow the outcomes of the model to reliably predict the effective structural behavior, and this aspect is even more important for a novel technology like the CLT one. In the following an overview of the state-of-the-art of modelling strategies for CLT structures (Section I.1.4.1) and methodologies usually adopted to model CLT panels (Section I.1.4.2) and mechanical connections (Section I.1.4.3) is given. Since it is out of the scope of this thesis, for a state-of-the-art review of modelling criteria used for panel-to-panel interaction the reader is referred to Izzi *et al.* [54].

I.1.4.1 Modelling strategies

Different modelling strategies have been adopted in the last years for the seismic analysis of CLT buildings, most of them being advanced tools for research purposes (*research oriented* models), while some of them are more simple modelling strategies (*design oriented* models) used by practitioners to design structures with an accuracy level not allowed by current analytical approaches (see Section II.1).

Numerical models to reproduce the behaviour of CLT wall systems can be distinguished in three different approaches (Figure I.1-27): *phenomenological* [83, 104, 140, 189], *component-level* [146, 147, 190] and *hybrid* [96, 146, 147, 150]. All these approaches can be profitably employed for linear and nonlinear analyses of CLT structures depending on whether a design-oriented or research-oriented activity is carried out [191].

Component-level modelling approach [56, 104, 105] is based on the reproduction of the structural response of all the single components of the structural system, i.e. connections and timber panels. This approach is suitable to reproduce the response of a CLT structure with any panel configuration but in order to take into account for second order effects (e.g. out of plane movements) or friction phenomena it requires the adoption of specific strategies that increase difficulty of modelling with this strategy. Since connections play a fundamental role in the definition of the behavior of CLT structures, the accuracy of their numerical modelling is a key-factor to guarantee the reliability of the model, and a list of researches carried out in the last decade on this topic is reported in [192].

Phenomenological modelling approach reproduces the global behavior of the CLT wall system (i.e. force-displacement curve and cumulative energy over time of the entire CLT wall system) disregarding the behaviour of its components (i.e. panels and connections). It is an approach that is relatively easy, since by simply calibrating the global constitutive law of the model it is possible to include secondary effects and friction phenomena. It has anyway a huge drawback constituted by the representativity of the model that is restricted to only the configuration of the panel used to calibrate the model. Therefore, to analyze another geometry of the CLT panel or another configuration of connections the calibration of a new model is necessary.

Hybrid modelling approach corresponds to a component level model where connections are calibrated so that the whole model can reproduce the global response of the CLT wall system. This approach can be considered belonging to the more general category of phenomenological ones. This is a reliable modelling approach [106] that overcomes the problems highlighted for the component-level approach, since it takes onto account for friction phenomenon and second order effects, but it keeps the strong limitation of the phenomenological approach, i.e. the dependency of the calibration on the geometry and arrangement of the wall system. For this reason, since it is more complex than a phenomenological approach and it keeps its limitations, this approach will not be further analyzed in this work, focusing the attention on component (Section I.2) and phenomenological (Section I.3) approaches.

It is in add possible define another type of modelling approach for multi-storey CLT buildings named *distributed connection model*. It has recently been proposed by Christovasilis *et al.* [190] for linear analyses where connections can be modelled with planar finite elements whose mechanical characteristics are calibrated in order to reproduce the stiffness of connections. It is possible to reconduct this modelling approach in the general component-level category, representing *de facto* a design-oriented simplification of the method for practitioners.

These modelling approaches can be performed with linear or non-linear models depending on the desired accuracy of the numerical outcomes and on the scope of the analysis. For example, practitioners usually model linearly the structures (*design-oriented* modelling strategy [56, 152]), unless it is an unusual and complex structure, while researchers are also interested in non-linear models in order to investigate unknown aspects through detailed modelling (*research-oriented* modelling strategy [48, 140]). The former strategy is used to create simple numerical models to design low-and mid-rise CLT buildings, the latter is mainly used by researchers to have a deeper insight into seismic performances and the limits of CLT mid- and high-rise buildings. Non-linear behavior of timber CLT structures subjected to high-amplitude lateral loads is mainly due to friction phenomena and plastic behavior of connections [81] (Section I.1.2.4).

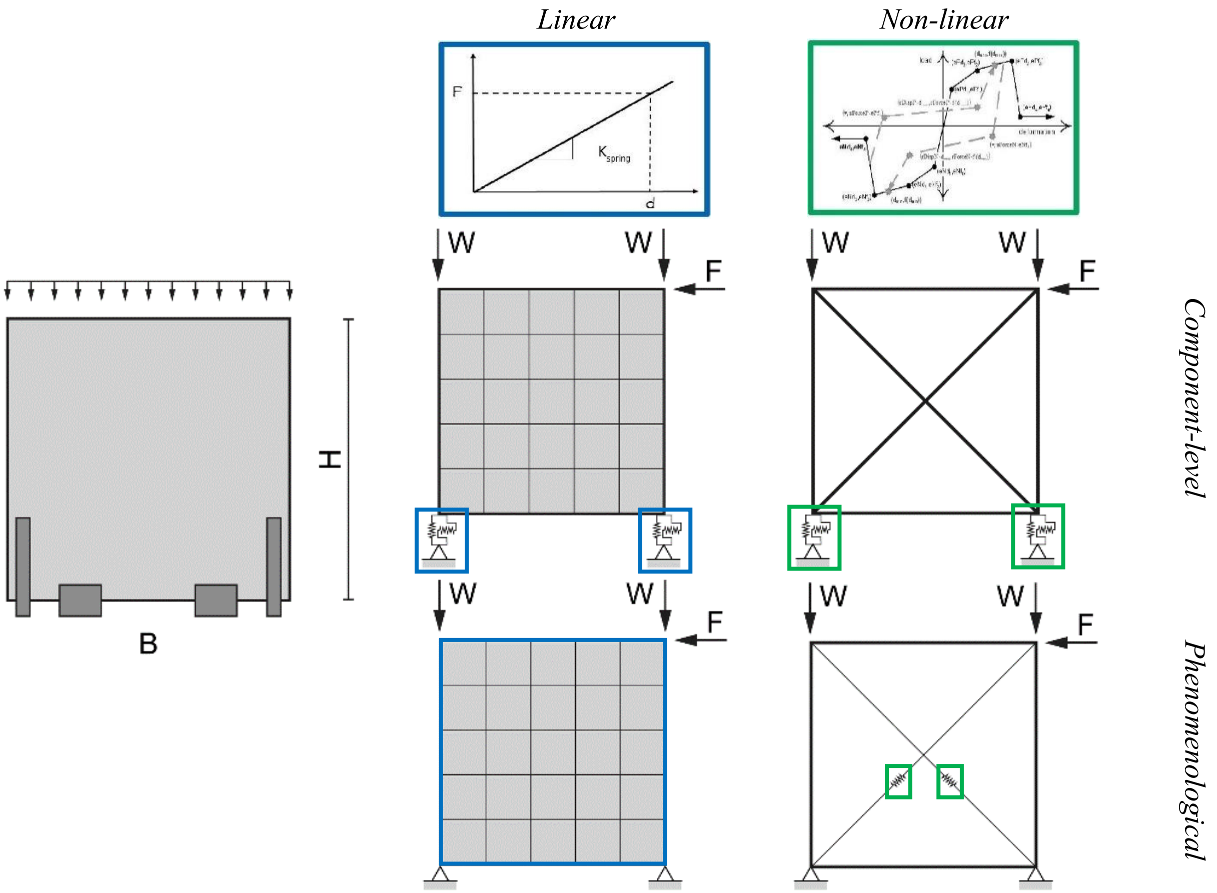

Figure I.1-27 – Schematic representation of modelling techniques for a CLT wall: component-level and phenomenological approaches with linear and non-linear constitutive laws (*image readapted* from Pozza *et al.* [191]).

I.1.4.2 Modelling of CLT panels

CLT wall panels are usually modelled as elastic elements through one of the three following approaches. The first one consists in modelling the panel as a lattice grid (e.g. [96, 140, 147, 191, 193], see also Section I.2.4.2), solution that is the best for computational efficiency and time required for modelling but has the major drawback of not furnishing the stress pattern on the panel. The second approach consists in the employment of shell elements, adopting multi-layer finite elements (e.g. in Section I.2.4.1.3.1) or a homogenization approach (e.g. [14, 104, 194]) based on the theory of Blaß & Fellmoser [195]. In the third approach the CLT panel is modelled using 3D solid elements [153]. The latter is the most suitable method when high accuracy of results on stress distribution of panels is required (for example when the panel presents openings), while the second one is the best compromise between accuracy and computational effort.

I.1.4.3 Modelling of connections

Modelling of connections is a key-factor when numerical analyses of CLT structures and timber structures in general are carried out, since the seismic behaviour of this kind of structures is strongly influenced by the behaviour of mechanical connections. Depending whether a linear or non-linear analysis is required, connections are modelled with springs or links using linear or multi-linear constitutive laws (e.g. Pinching4 and SAWS constitutive laws [196]). While linear modelling can only predict the initial elastic working range of connections, nonlinear modelling is necessary when also the analysis of hysteretic behaviour is required. Their behaviour can be modelled in two ways, namely (*i*) a uniaxial approach where hold-downs work only for tension actions while angle-brackets only for shear actions [153, 191], and (*ii*) a biaxial approach where connections resist both in axial and shear direction (each one with its own constitutive law) [14, 98, 193]. When a biaxial approach is adopted, it is also possible to take into account for coupling effects on resistance of connections due to interaction between forces in the two directions, e.g. analyses carried out by Rinaldin *et al.* [104] and Pozza *et al.* [83]. This aspect will be analysed in further detail in Section II.1.5.

I.2 Component-level modelling approach

Abstract

In this Section component-level numerical modelling approach will be critically analyzed highlighting potentialities and drawbacks. The aim is to gain a deeper insight in the modelling approach illustrating strategies and ploys to guarantee the maximum reliability of results both when linear and non-linear models are adopted. For linear analyses, a parametric spectral analysis on a reference seismically-designed multi-storey CLT building has been carried out. For non-linear analyses, the experimental cyclic tests carried out at CNR-IVALSA within the SOFIE project - after a preliminary phase of interpretation of the experimental dataset, necessary to identify the peculiarities of the test procedures - are used as a comparative basis to assess the quality of the numerical results. In linear analyses connections have been modelled through elastic springs with stiffness derived from both analytical methods of Eurocode 5 and experimental tests, and the main outcomes describing the dynamic behavior of the structures have then been analyzed in terms of principal elastic period, inter-storey drifts and forces acting on connections. For non-linear analyses connections have been modelled with multi-linear hysteretic constitutive laws calibrated on experimental results through an energetic approach, and outcomes are analyzed in terms of both global behavior of the wall system and local response of connections. Results show that the non-linear modelling approach could be a feasible and reliable method to reproduce the seismic behavior of CLT panel provided that the behavior of each individual component is properly calibrated.

Some parts of this section are included in L. Franco, L. Pozza, A. Saetta, M. Savoia, D. Talledo, Strategies for structural modelling of CLT panels under cyclic loading conditions, Eng. Struct. 198 (2019) 109476. doi:10.1016/j.engstruct.2019.109476 and L. Pozza, M. Savoia, L. Franco, A. Saetta, D. Talledo, Effect of different modelling approaches on the prediction of the seismic response of multi-storey CLT buildings, Int. J. Comput. Methods Exp. Meas. 5 (2017) 953–965. doi:10.2495/CMEM-V5-N6-953-965

I.2.1 Chapter contents

The current chapter firstly provides a description of the state-of-the-art of *component-level* modelling strategy for the prediction of the seismic response of multi-storey CLT buildings (Section I.2.2), analyzing peculiarities, advantages and drawbacks. The study has been conducted on references structures shown in Section I.2.3.1 and I.2.4.1 respectively for linear and non-linear analyses. A deep focus on *linear* (Section I.2.3.2) and *non-linear* (Section I.2.4.2) component-level modelling approaches is then given. Their outcomes will then be analyzed and compared in order to define advantages and limits of the modelling strategy.

I.2.2 Modelling strategy description

Multi-storey Cross-Laminated Timber (CLT) buildings have become increasingly common over the last decades thanks to easiness, sustainability, rapidity of execution, as well as high structural static and seismic performances. However, since this innovative material is also used in seismic-prone areas, the assessment of numerical modelling and analysis of CLT buildings under seismic actions and cyclic behaviour of CLT wall systems is still a relevant research topic within the structural engineering field since results available in literature on different modelling approaches are quite heterogeneous. Among the different modelling approaches available to study the seismic behaviour of CLT buildings, the one for components is the most flexible and therefore profitably used by many researchers in recent years to study buildings with CLT wall elements. This Section provides a deep focus on linear (Section I.2.3.2) and non-linear (Section I.2.4.2) *component-level* modelling approaches, usually adopted respectively by practitioners and researchers for the prediction of the seismic response of multi-storey CLT buildings. Their outcomes will then be analyzed and compared in order to define advantages and limits of different modelling strategies. Linear and non-linear modelling approaches have been studied critically analyzing the outcomes of structures taken as reference, that will be described in the following.

Component-level modelling approach [56, 104, 105] is based on the reproduction of the structural response (linear or non-linear) of all the single components of the structural system, i.e. connections and timber panels. In add, friction phenomena between panels or between panel and foundation can be modelled through contact elements. This method requires the calibration of the constitutive law for each component based on the results from experimental test, advanced numerical simulations or on proper analytical assessments. For instance, modelling of CLT panel behavior can be performed from experimental tests [197–201] or can be assessed using suitable analytical and numerical models capable of accounting for the panel layering [27, 28, 202–204]. It is worth noting that when the connection is modelled as the smallest component of the CLT panel-connection system, this means that the whole connection is modeled using a phenomenological approach, without the explicit modelling of fasteners, embedment behavior of timber and cold-formed steel plates. It is also possible to carry out component-level numerical analyses where each of these parts are modelled separately, e.g. [188]. Connections can be implemented with two different approaches in component-level models: (*i*) the *uniaxial* one, where connection resists only in the direction exhibiting the highest strength and stiffness, and (*ii*) the *biaxial* one, where the connection exhibits strength and stiffness both in the strong and the weak directions. The tension-shear interaction in typical hold-down and angle bracket connections has been tested experimentally and modelled numerically in [82, 83, 103, 185]. Since previous studies have shown that uniaxial models give inaccurate results when compared with experimental evidences [153, 191], the present work focuses on biaxial modelling strategies.

Concerning *linear* component-level analyses, the data required for the component-level approach are the CLT panel's elastic mechanical properties (Young and shear moduli) and the elastic stiffness of connections k_{ser}. Elastic mechanical properties of CLT panels are easily available in literature [77, 100]. These walls are usually modelled as an isotropic material, with an equivalent modulus of elasticity [56, 106] given by the weighted mean values of the modulus in the parallel and perpendicular direction to the grain, corresponding to the glued crosswise-alternated layers of the panel. Sometimes an orthotropic material model is adopted, e.g. [107].

As regards the values of elastic stiffness to be assigned to connections, two different approaches can be adopted. The first one refers to the prescriptions of Eurocode 5 [110] concerning the calculation of the sliding modulus (k_{ser}) of a nailed steel-timber connection. The second method is based on the linearization of the force-displacement curve obtained from experimental tests on the single connection elements.

Results available in literature [56] show that stiffness estimations obtained using the formulation proposed by Eurocode 5 [110] overestimate the actual elastic stiffness of the connection defined by the experimental tests. This could be due to the fact they only consider the deformability of dowel-type connectors disregarding that the actual stiffness of the joint is given by the in-series contribution of nailing, metal plate and base anchor [102]. This last aspect represents a strong limitation in the applicability of linear analyses with linear component-level approach, since it requires the validation of the analytical stiffness with experimental tests, which are not always available for all type of connectors.

Concerning *non-linear* component-level analyses, non-linearity in CLT structures is due to the connections behaviour since the timber panel reacts elastically thanks to its relatively high resistance and stiffness. Consequently, component-level non-linear analysis requires the calibration of the constitutive law used to reproduce the non-linear behaviour of connections. It is therefore necessary to define the force-displacement law that characterizes the behaviour of the connection, whose parameters can be obtained from uniaxial experimental tests (monotonic or cyclic) performed on individual devices. Of course, in component-level models for wall assemblies, the mechanical characterization of individual connections is a crucial issue for a reliable calibration. Tests on CLT connections have been carried out by many authors [43, 182, 205–207]. An extensive review of the main outcomes of experimental tests on CLT connection system can be found in [54]. Another significant aspect in the calibration of the connection's behavior is the adoption of a reliable multi-linearization method of the load-displacement curve, e.g. [139], capable of accurately reproduce the elastic and the post-elastic behavior, the load bearing and the displacement capacity. In the case of non-linear analyses under cyclic loadings, it is also necessary to calibrate the hysteretic behavior of the connection (including the pinching effect). As for the frictional phenomena between the wall panels and the foundation, the calibration phase generally involves the definition of the friction coefficient which is however complex, and sometimes requires simplified assumptions [153, 208]. When experimental tests cannot be carried out, connection's response can be studied using advanced numerical models able to simulate the wood-connection interaction [188, 209]. However, these models cannot be used in ordinary design, being generally complex and computationally demanding. Analytical models for connection's characterization [110, 167] can be employed only in the case of linear analyses, which require a limited number of parameters (e.g. elastic stiffness and load bearing capacity). Finally, there exist different approaches from the multi-linearization method, e.g. Flatscher [210] who provides a mathematical model which allows to represent both the pre- and post-peak linear and non-linear behavior of the load-displacement curve with a good approximation.

In summary, the component-level approach is suitable to reproduce the response of a CLT structure with any geometry and panel configuration assembled employing connection elements previously calibrated by means of specific experimental tests. However, results obtained with the component-level approach are reliable only if the displacement field on the connections during full-scale tests of CLT shear wall is similar to that considered in the tests on individual components and used in the calibration phase (e.g., absence of secondary effects due to the local failure mechanism of shear wall connections, as extensively discussed in Section I.2.4.2.5).

The main drawback of component-level modelling approach is that it generally requires a laborious calibration of the elements that reproduce the structural behaviour of connections (both for linear and nonlinear analyses). The advantage is that, once calibration phase is completed, it is possible to simulate the structural behaviour of any structure assembled with the connections that have been calibrated, regardless of the geometrical configuration of the wall and the connections' arrangement.

In summary, the component-level approach is suitable to reproduce the response of a CLT structure with any geometry and panel configuration assembled employing connection elements previously calibrated by means of specific experimental tests. However, results obtained with the component-level approach are reliable only if the displacement field on the connections during full-scale tests of CLT shear wall is similar to that considered in the tests on individual components and used in the calibration phase (e.g., absence of secondary effects due to the local failure mechanism of shear wall connections, as extensively discussed in Section I.2.4.2.5).

Moreover, component-level models for connections can be implemented in numerical models following two different approaches: (*i*) the only uniaxial behavior is considered in the direction exhibiting the highest strength and stiffness, (*ii*) the biaxial behavior, in both strong and weak directions, is considered. The tension-shear interaction in typical hold-down and angle bracket connections has been tested experimentally and modelled numerically in [82, 83, 103, 185].

The analyses carried out in this work to study strategies to reliably employ component-level approach to model the seismic behaviour of CLT multi-storey buildings have been carried out on reference structures described in the following respectively for linear (Section I.2.3.1) and non-linear (Section I.2.4.1) analyses.

I.2.3 Linear analysis

I.2.3.1 Reference structure description

For *linear analyses*, carried out with Straus7 FEA software [211], the behaviour of a bracing shear wall of a mixed CLT wall-heavy frame building (Section I.1.2.2.4) with increasing number of storeys and Peak Ground Acceleration (PGA) will be studied through parametric dynamic analyses (Figure I.2-1).

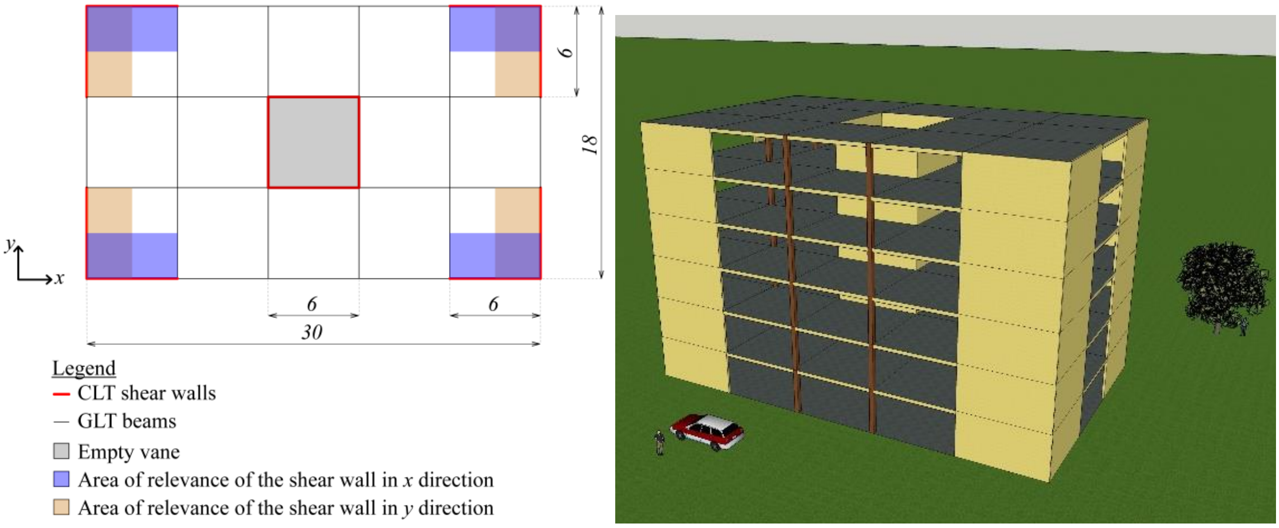
6
18
y
x
6
6
30
Legend
— CLT shear walls
— GLT beams
▨ Empty vane
▨ Area of relevance of the shear wall in x direction
▨ Area of relevance of the shear wall in y direction

(*a*) (*b*)

Figure I.2-1 – Multi-storey building considered as reference structure for linear analyses: (*a*) layout of the building with the areas of relevance for the calculation of vertical loads acting on CLT shear walls in X (blue pattern) and Y (orange pattern) directions (measurements in meters) and (*b*) isometric view of the 6- storey configuration.

2-, 4- and 6-storey mixed CLT-heavy frame timber building configurations were considered as reference structures for the linear analyses carried out both with component-level (Section I.2.3.2) and phenomenological (Section I.3.3) approaches. CLT building configurations have been seismically designed to withstand three increasing levels of PGA=0.15 g-0.25 g-0.35 g characterized by the design ULS spectra according to Italian Building Code NTC2008 [5] (Figure I.2-2).

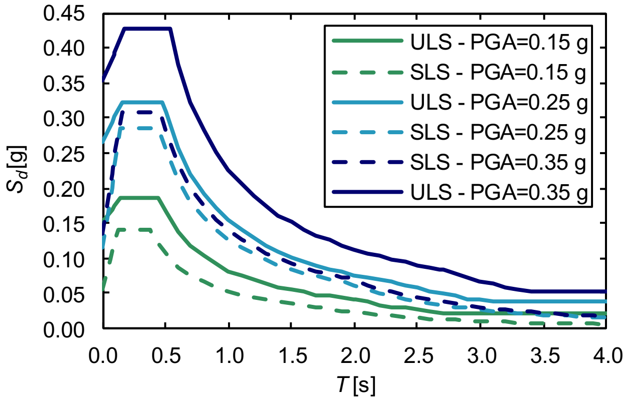

Spectral parameters	
V_R	50 years
Ground	C
Topographic category	T_1
S_T	1
q	2

Figure I.2-2 – Design spectra and spectral parameters for the three seismicity levels considered and for SLS and ULS conditions.

Connections have been designed for each building configuration adopting a linear static analysis (LSA) [111] in conjunction with the iterative procedure proposed by Polastri & Pozza [152]. Since the configuration is regular, a behaviour factor $q = 2$ was adopted (see Section I.1.3.1).

In order to determine the actions necessary to design the connections, the seismic mass and vertical loads of the area of relevance of the shear wall must be evaluated. For each floor a dead load $G = 4.50$ kN/m^2 and a live load $Q = 3.00$ kN/m^2 (except for roof level) have been considered, with combination factors $\psi = 0.0$ for snow action (roof) and $\psi = 0.6$ for live loads acting on floors. Table I.2-1 lists, for each building configuration and storey, the seismic mass M, the corresponding vertical loads W and the thickness of the CLT panels t.

Table I.2-1 – Seismic mass M and vertical load W at each level for building configurations considered for linear analyses.

		2-storey			*4-storey*			*6-storey*	
level	*M* [t]	*W* [kN/m]	*t* [mm]	*M* [t]	*W* [kN/m]	*t* [mm]	*M* [t]	*W* [kN/m]	*t* [mm]
1	28.90	18.90	100	28.90	18.90	160	28.90	18.90	200
2	20.64	13.50	80	28.90	18.90	120	28.90	18.90	200
3				28.90	18.90	100	28.90	18.90	160
4				20.64	13.50	80	28.90	18.90	120
5							28.90	18.90	100
6							20.64	13.50	80

Connections were designed considering their resistance only in the strong direction [96] through equilibrium equations at each storey [48], following a design-oriented approach usually adopted by practitioners to design multi-storey CLT buildings. This assumption can be considered acceptable for safe quick design of these buildings, since stiffness and load-bearing capacity of angle brackets in axial direction is quite lower than hold-downs [48, 102]. In add, shear stiffness and strength of hold-downs are very low [83].

The strength of dowel-type hold-down and angle bracket connections was evaluated according to Johansen theory, as reported in different standards, e.g. Eurocode 5 (EC5) [110], or in the specific product approval certificates. In order to evaluate the stiffness of connections, both the formulation presented in EC5 [110] for estimation of k_{ser} and available experimental tests on the same connections [56] were considered. Table I.2-2 summarizes strength and stiffness values for the connections adopted. It is worth noting that EC5 formulation significantly overestimates the elastic stiffness of the connection [152]. For this reason, the experimental values of stiffness should be adopted for an accurate analysis of a CLT building.

Table I.2-2 – Main mechanical parameters of connections elements.

Connection type	*Analytical Load bearing capacity F_d^**	*Analytical elastic stiffness k_{ser}*	*Experimental elastic stiffness k_{el}*
Hold-down WHT340	42.00 kN	20987.81 N/mm	5704.81 N/mm
Hold-down WHT440	63.40 kN	31481.72 N/mm	6608.75 N/mm
Hold-down WHT620	85.20 kN	54568.31 N/mm	13247.18 N/mm
Angle bracket TCF200	22.20 kN	31481.72 N/mm	8479.13 N/mm
Angle bracket TTF200	35.50 kN	31481.72 N/mm	8211.60 N/mm

* *values obtained assuming* $k_{mod} = 1.1$ *and* $\gamma_M = 1$

The resulting type and number of connections at each level is reported for all the considered configurations in Table I.2-3. It can be observed that the number of connections at the bottom of the CLT panels increases for increasing number of storeys and for increasing level of seismic intensity.

Table I.2-3 – Connection pattern at each level for the considered case studies configurations.

PGA	*level*	*2-storey*		*4-storey*		*6-storey*	
		HD	*AB*	*HD*	*AB*	*HD*	*AB*
0.15 g	*0*	2 WHT340	5 TTF200	4 WHT620	9 TTF200	9 WHT620	13 TTF200
	1	1 WHT340	5 TCF200	3 WHT440	8 TTF200	7 WHT620	13 TTF200
	2			2 WHT340	6 TTF200	5 WHT620	11 TTF200
	3			1 WHT340	5 TCF200	3 WHT620	9 TTF200
	4					2 WHT440	7 TTF200
	5					1 WHT340	5 TCF200
0.25 g	*0*	2 WHT620	9 TTF200	8 WHT620	15 TTF200	18 WHT620	23 TTF200
	1	2 WHT340	8 TCF200	5 WHT620	14 TTF200	14 WHT620	22 TTF200
	2			3 WHT440	10 TTF200	10 WHT620	20 TTF200
	3			2 WHT340	8 TCF200	6 WHT620	16 TTF200
	4					4 WHT440	11 TTF200
	5					2 WHT340	9 TCF200
0.35 g	*0*	3 WHT620	11 TTF200	11 WHT620	20 TTF200	25 WHT620	31 TTF200
	1	2 WHT340	10 TCF200	7 WHT620	18 TTF200	19 WHT620	29 TTF200
	2			5 WHT440	13 TTF200	13 WHT620	26 TTF200
	3			2 WHT340	11 TCF200	8 WHT620	21 TTF200
	4					4 WHT620	15 TTF200
	5					2 WHT440	11 TCF200

I.2.3.2 Numerical modelling of the multi-storey building

In this Section linear component-level modelling approach is analyzed. The elastic plane model (Figure I.2-3) has been built with the purpose of faithfully reproduce the dynamic seismic behavior of a multi-storey CLT wall system through the modelling of single components (i.e. CLT panels and connections). To do this, panels have been modelled using elastic isotropic plate elements, while connections have been modelled as linear springs with stiffness in both axial and shear direction equal to the experimental one. For connections a uniaxial model has been adopted, i.e. only the resistance in their strong direction has been considered. A modulus of elasticity $E = 5685\ MPa$ and a Poisson modulus $v = 0.35$ have been assigned to CLT panels. Two lumped masses calculated from the vertical loads acting on the building (Table I.2-1) are placed at the top of each CLT panel. No inertial mass has been assigned to plate elements.

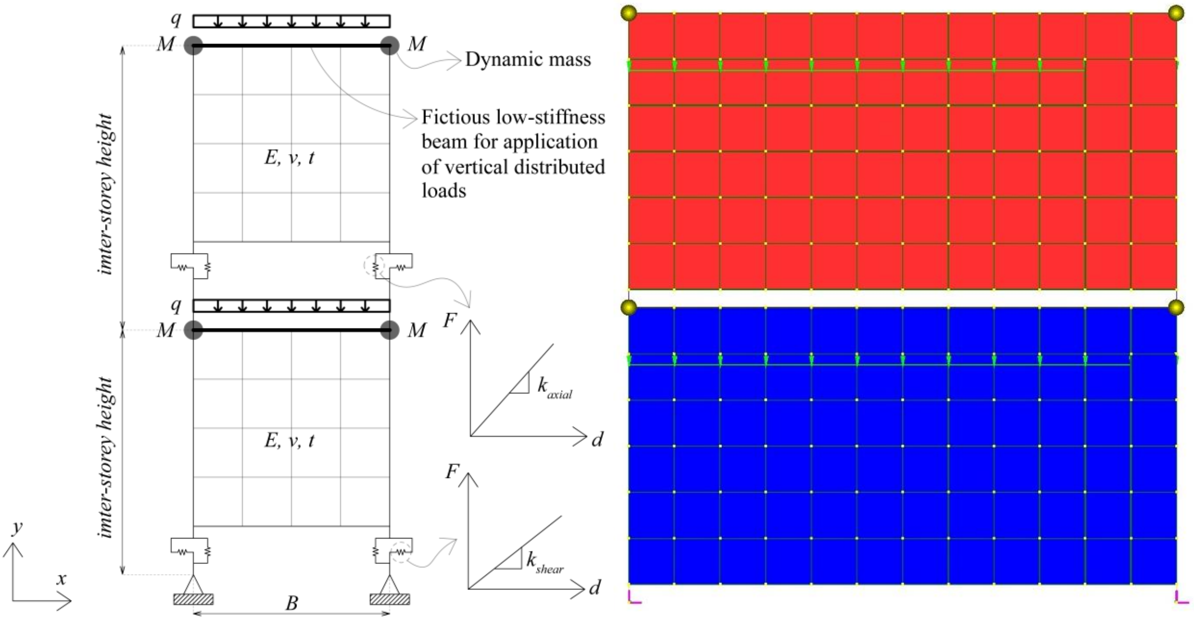

(*a*) (*b*)

Figure I.2-3 – Component-level linear model: (*a*) schematic representation and (*b*) pictures of the finite element model for the 2-storey building configuration.

The elastic constitutive laws assigned in the two main directions of connections are uncoupled (i.e. the strength and stiffness of connection in one direction is not affected by forces acting in the other direction), because coupling models for connections available in literature have been derived for non-linear constitutive laws (e.g. [82, 83]) and are mainly intended for research-oriented modelling approaches. Linear numerical models, on the other hand, are design oriented simplified models that facilitate simplicity for practitioners at slight expense of accuracy of results, it is therefore meaningless complicating this linear model with complex coupling laws. CLT panels were modelled with isoparametric four-node quadrilateral membrane finite elements, with an equivalent isotropic material whose mechanical properties were averaged between the longitudinal and transversal direction.

Spectral analyses were carried out for all the configurations considered in the parametric study, and results in terms principal elastic periods (T_1), forces on connections (v and N) and inter-storey drifts (d_{i-s}) and inter-storey slip displacement (d_{sl}) are shown in the following. Table I.2-4 shows the obtained values of principal elastic periods T_1 together with the estimation proposed by Eurocode 8 (EC8) [111]. It can be observed that for the 4- and 6-storey building configurations the values of elastic period T_1 is much greater than the analytical prediction proposed by EC8 [111]. The difference is due to the fact that the stiffness of the CLT wall is highly influenced by the stiffness of connections, and as previously observed (Table I.2-2) the effective measured stiffness during tests on connections is significantly lower than the one obtainable from analytical formulations of EC5. A further evidence of this aspect is represented by the decreasing gap between T_1 given by numerical analyses and the one evaluated by EC8 [111] for increasing PGA, and it is due to the increasing number of connections that increments the global stiffness of connection system.

Table I.2-4 – First period T_1 for each analyzed building configuration.

T_1	*PGA=0.15 g*		*PGA=0.25 g*		*PGA=0.35 g*	
[s]	*EC8*	*Component-level*	*EC8*	*Component-level*	*EC8*	*Component-level*
2-storey	0.20	0.75	0.20	0.57	0.20	0.53
4-storey	0.34	1.33	0.34	1.06	0.34	0.98
6-storey	0.46	1.83	0.46	1.59	0.46	1.51

As expected, it is possible to observe that both the base shear per unity of length v and uplift forces N increase both incrementing the seismic intensity and the number of storeys (Table I.2-5).

Table I.2-5 – Base shear forces per unit of length *v* and base uplift force *N* for each analyzed building configuration.

Forces at the base	*PGA=0.15 g*		*PGA=0.25 g*		*PGA=0.35 g*	
	v [kN/m]	*N* [kN]	*v* [kN/m]	*N* [kN]	*v* [kN/m]	*N* [kN]
2-storey	14.32	18.11	32.38	90.83	48.22	191.28
4-storey	21.92	25.16	43.98	129.09	62.96	320.02
6-storey	23.96	41.58	51.82	179.47	72.6	438.88

The maximum SLS inter-storey drift along the height of the building $d_{i-s,max}$ (i.e. the difference between the value of the horizontal displacement measured at the floor level and the one measured at the lower storey) and the maximum value of inter-storey slip displacements $d_{sl,max}$ are analyzed. This last parameter is obtained depurating the inter-storey drift d_{i-s} from the displacement contribution d_{rock} due to the uplift rotation $\varphi = \frac{d_{up,l}+d_{up,r}}{B} = \frac{d_{rock}}{H}$ of the CLT panel with dimensions BxH, where $d_{up,l}$ and $d_{up,r}$ are uplift displacements at left and right corner of the wall system (Figure I.2-4). Values of $d_{sl,max}$ are reported as a percentage respect to the inter-storey height (Table I.2-6).

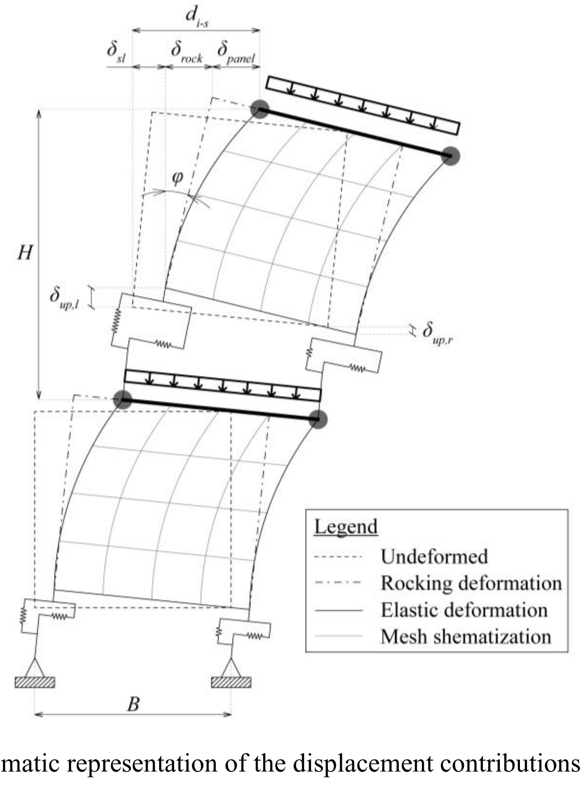

Figure I.2-4 – Schematic representation of the displacement contributions to inter-storey drift d_{i-s}.

It is important to derive also the inter-storey slip d_{sl}, since it gives information on pure shear behaviour of CLT wall systems separating it from the rocking mechanism. Actually, the total shear behavior is equal to:

$$d_{sl} + d_{panel} = d_{i-s} - d_{rock} \qquad (I.2\text{-}1)$$

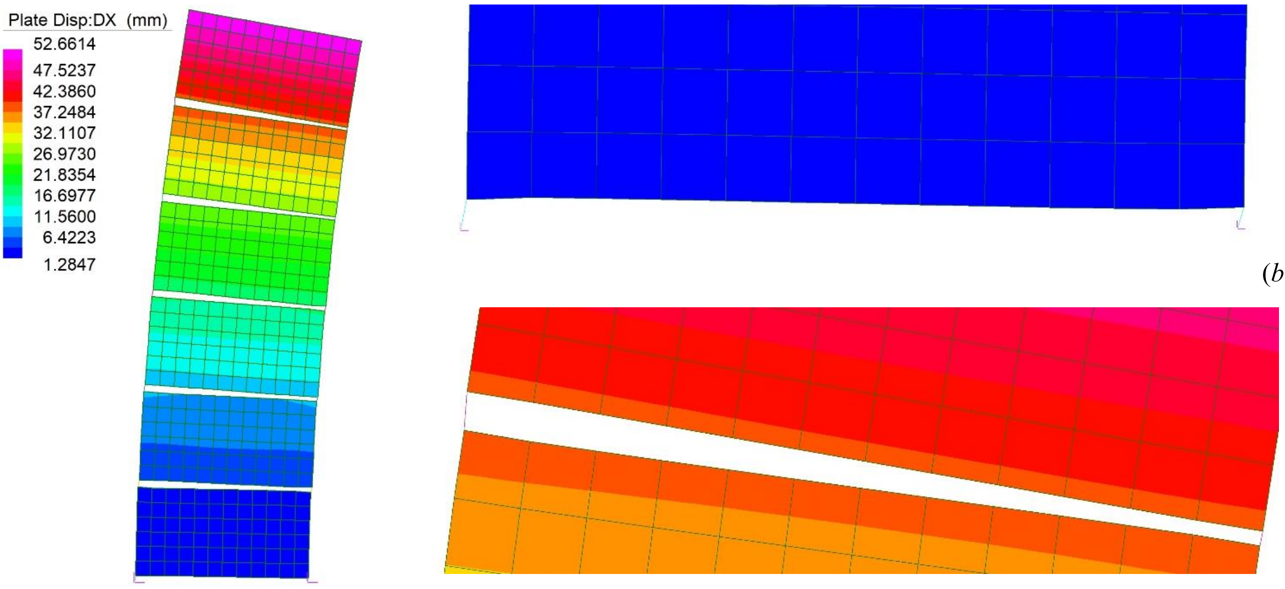

(*b*)

(*a*) (*c*)

Figure I.2-5 – Spectral analysis for 6-storey building configuration and PGA=0.35 g: (*a*) results of in terms of horizontal displacements, with underlined the opposite sliding directions of (*b*) lower and (*c*) upper springs.

Table I.2-6 – Maximum percentage inter-storey drift $d_{i\text{-}s,max}$ and inter-storey sliding displacement $d_{sl,max}$ for each analyzed building configuration.

Maximum inter-storey displacements	*PGA=0.15 g*		*PGA=0.25 g*		*PGA=0.35 g*	
	$d_{i\text{-}s,max}$	$d_{sl,max}$	$d_{i\text{-}s,max}$	$d_{sl,max}$	$d_{i\text{-}s,max}$	$d_{sl,max}$
2-storey	0.17%	0.05%	0.33%	0.09%	0.34%	0.09%
4-storey	0.25%	0.05%	0.47%	0.09%	0.49%	0.08%
6-storey	0.27%	0.05%	0.56%	0.08%	0.58%	0.07%

Table I.2-7 – Inter-storey sliding displacement d_{sl} *of 2-storey building with maximum values underlined.*

	d_{sl} - *2-storey building configuration*		
Floor level	*PGA=0.15 g*	*PGA=0.25 g*	*PGA=0.35 g*
Storey n° 1	**0.05%**	**0.09%**	**0.09%**
Storey n° 2	0.00%	0.03%	0.03%

Table I.2-8 – Inter-storey sliding displacement d_{sl} *of 4-storey building with maximum values underlined.*

	d_{sl} - *4-storey building configuration*		
Floor level	*PGA=0.15 g*	*PGA=0.25 g*	*PGA=0.35 g*
Storey n° 1	**0.05%**	**0.09%**	**0.08%**
Storey n° 2	0.02%	0.05%	0.04%
Storey n° 3	*-0.01%*	0.01%	0.02%
Storey n° 4	*-0.03%*	*-0.03%*	*-0.03%*

Table I.2-9 – Inter-storey sliding displacement d_{sl} *of 6-storey building with maximum values underlined.*

	d_{sl} - *6-storey building configuration*		
Floor level	*PGA=0.15 g*	*PGA=0.25 g*	*PGA=0.35 g*
Storey n° 1	**0.05%**	**0.08%**	**0.07%**
Storey n° 2	0.02%	0.04%	0.03%
Storey n° 3	0.01%	0.02%	0.02%
Storey n° 4	0.00%	0.00%	0.00%
Storey n° 5	*-0.02%*	*-0.03%*	*-0.03%*
Storey n° 6	*-0.04%*	*-0.07%*	*-0.07%*

From the obtained results (Table I.2-6) it is possible to observe that, similarly to base shear per unity of length v and uplift forces N analyzed in the previous paragraph, the maximum inter-storey drift $d_{i-s,max}$ grows with the increment of the seismic intensity and the number of storeys of the building. On the contrary, for the maximum pure sliding inter-storey drift $d_{sl,max}$ it can be observed that it decrements with the increasing number of storeys. To have a deeper insight on the behavior of the sliding contribution between panels, its value d_{sl} is reported for each building configuration and each floor in Table I.2-7-Table I.2-9. It is possible to observe that the lower-floors connections have a sliding deformation d_{sl} in the same direction as the inter-storey drift displacement d_{i-s}, and its value tend to decrement and also reverse its sign for upper storeys, so the sliding direction in the upper CLT shear walls can be opposite to the inter-storey drift $d_{i-s,max}$ (Figure I.2-5). This result is in accordance with the expected reduction of shear forces acting on CLT walls for upper floors. In all cases, the maximum value of the inter-storey slip $d_{sl,max}$ has been measured at the lower floor, while the maximum value of the inter-storey drift $d_{i-s,max}$ has always been observed at the highest storey. Besides, the sliding contribution $d_{sl,max}$ is much lower than the inter-storey drift global value $d_{i-s,max}$, which means that most part of the lateral deformation of CLT shear wall is due to uplift forces rather than to shear forces transmitted between upper and lower panels.

I.2.4 Non-linear analysis

I.2.4.1 Reference structure description

In recent years, several experimental test programs were carried out on individual connections, CLT wall systems, and full-scale buildings. Remarkable results were obtained at University of Ljubljana (Slovenia), where CLT shear walls were tested varying loading and boundary conditions [98]. Similarly, FPInnovations (Canada) performed tests to determine the structural properties and seismic resistance of CLT shear walls and small-scale 3D structures [45]. Failure mechanisms of large shear wall systems were also studied by many authors in the past [77, 100, 101]. In addition, connections between walls, as well as between wall and horizontal elements (floor or foundation) have been studied to develop a capacity-based design approach for CLT structures [46, 102].

In the following, the experimental campaign carried out within the SOFIE Project, e.g. [44, 77, 102, 212], is thoroughly analyzed and then used as the reference for non-linear analyses carried out with component level (Section I.2.4.2) and phenomenological (Section I.3.4) approaches. The main reason for which this experimental campaign is the most proper one for being a reference in a comparative analysis of different numerical modelling strategies, is that most of the experimental measures conducted during the tests are available in the literature. In particular, together with the results at the global level (i.e., the force-displacement curve and the cumulative energy), all the results at the local level (e.g., uplift and slip displacements) are also reported.

In the following, after a description of the experimental setup (Section I.2.4.1.1), a preliminary analysis and interpretation of the experimental results of tests carried out on CLT wall systems at CNR-IVALSA National Research Council - Trees and Timber Institute during the SOFIE project (Italy), extensively illustrated in [77, 212, 213], has been conducted in order to correctly define the component behavior and the consequent global and local responses of the shear walls tested in that project (Section I.2.4.1.2). A significant disagreement between recordings of global and local displacements is underlined, whose causes have been investigated (Section I.2.4.1.3).

I.2.4.1.1 Description of the experimental setup adopted within the SOFIE project

Wall system configurations I.1, I.2 and I.3 tested at CNR-IVALSA within SOFIE project [77] have been considered as reference structure of non-linear analysis. All these wall systems are constituted by a monolithic

CLT panel with height H = 2950 mm, width L = 2950 mm and thickness t=85 mm, and each one is characterized by different vertical load conditions and layouts of connections. Wall I.1 is anchored to a rigid steel profile, representing the wall foundation, with 2 hold-downs and 2 angle brackets, whereas walls I.2 and I.3 are anchored with 2 hold-downs and 4 angle brackets. The vertical load is equal to q=18.5 kN/m for walls I.1 and I.2, and q=9.25 kN/m for wall I.3. The hold-down connections are Simpson HTT22 [214], fastened to the CLT shear wall with 12 annular ring nails with 4 mm diameter each, and anchored to the foundation with one 16 mm diameter bolt. The angle brackets are BMF 90x48x3x116 [183], fastened to the wall with 11 annular ring nails, 4 mm diameter, and anchored to the foundation with one 12 mm diameter bolt.

The experimental setup, described in [77], applies the vertical load to the wall system through four rollers placed on a steel profile used to connect the CLT panel with the horizontal hydraulic actuator anchored to the steel reaction frame (Figure I.2-6). The load was kept constant during the tests, thanks to translational and rotational degrees of freedom of rollers. In addition, horizontal rollers were installed in order to avoid out-of-plane movements of the top of the walls, while none of these devices was installed at the bottom side. Measurement instruments were installed on the wall panels in many positions [77], as depicted in Figure I.2-6 and summarized in Table I.2-10.

Connections similar to those adopted in the wall experimental setup were tested during an extensive experimental campaign conducted at CNR-IVALSA. The angle brackets adopted in the connection [102] and in the full-scale wall tests [77] were identical (BMF90x116x48x3 [183]), whereas two different hold-downs were used in the connection tests (WHT540 type) [102] and in the full-scale wall tests (HTT22 type) [77].

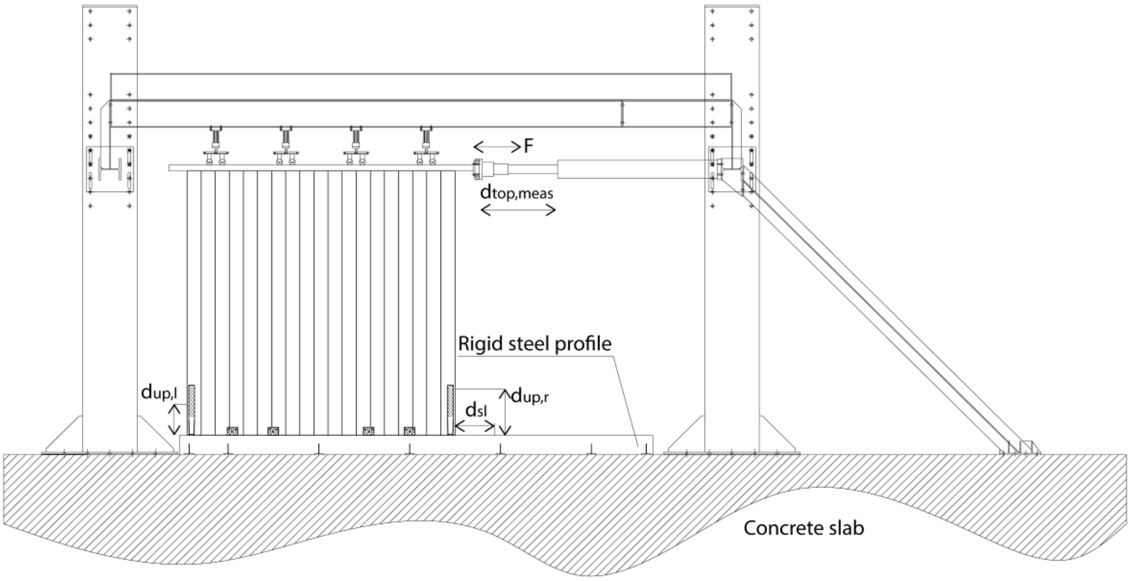

Figure I.2-6 – Shear wall test setup and instrument position [77].

Table I.2-10 – Quantities measured during the tests of the walls.

Tag	*Quantity measured*
F	Load cell
$d_{top,meas}$	Imposed horizontal top displacement
$d_{up,l}$	Bottom-left corner uplift
$d_{up,r}$	Bottom-right corner uplift
d_{sl}	Relative sliding between the lower steel profile and the CLT panel

I.2.4.1.2 Data interpretation of cyclic experimental tests and failure mode analysis

An accurate analysis of the deformation and failure modes of the shear walls showed that secondary deformation effects occurred in angle bracket connections due to out-of-plane displacements of the wall base, reducing strength with respect to the ideal behavior of connections subject to displacements only in the plane of the wall. Therefore, this out-of-plane effect, that at a first glance could seem only secondary in affecting the cyclic behavior of the wall system, has on the contrary a notable impact on the structural response of the tested wall systems that have not been transversally restrained at the base. These phenomena, that however could also occur in real situations (mainly when the connection system is not accurately designed), considerably reduce the angle bracket shear strength with respect to the one obtained from tests on individual connections under controlled (usually uniaxial) loading conditions. Actually, it is worth noting that the experimental setup of tests on connections usually allows for large displacements up to the maximum strength capacity without showing any out-of-plane behavior. Therefore, if connections exhibit an out-of-plane behavior during global wall tests, the connection test cannot be considered effectively representative of the actual behavior that the connection exhibits during the global wall test.

As for the failure modes of the three walls, wall I.1 failed by sliding, due to rupture of angle brackets, while walls I.2 and I.3 exhibited a mixed rocking-sliding failure. More details on the wall behavior at failure can be found in [77].

The deformed configuration at failure evidenced an out-of-plane movement at the base of the walls (see Figure 7 of [77] or Figure 12 of [48]) due to the absence of horizontal restraints at the bottom of the wall and to the adoption of connections along one side of the wall only, with a consequent load eccentricity due to the distance between the bolt of the angle bracket and the plane of the timber panel (Figure I.2-7.a). This eccentricity induces a secondary moment on the connection system between wall and angle bracket. Since only one bolt was used to fix the bottom plate of angle brackets to the foundation, only the withdrawal capacity of the nails can withstand the secondary moment (Figure I.2-7.b).

It is worth noting that this effect is generally inhibited if the panel is equipped with connections on both sides, or in experimental tests on walls with individual connections but if panel out-of-plane displacements are restrained also at the bottom side.

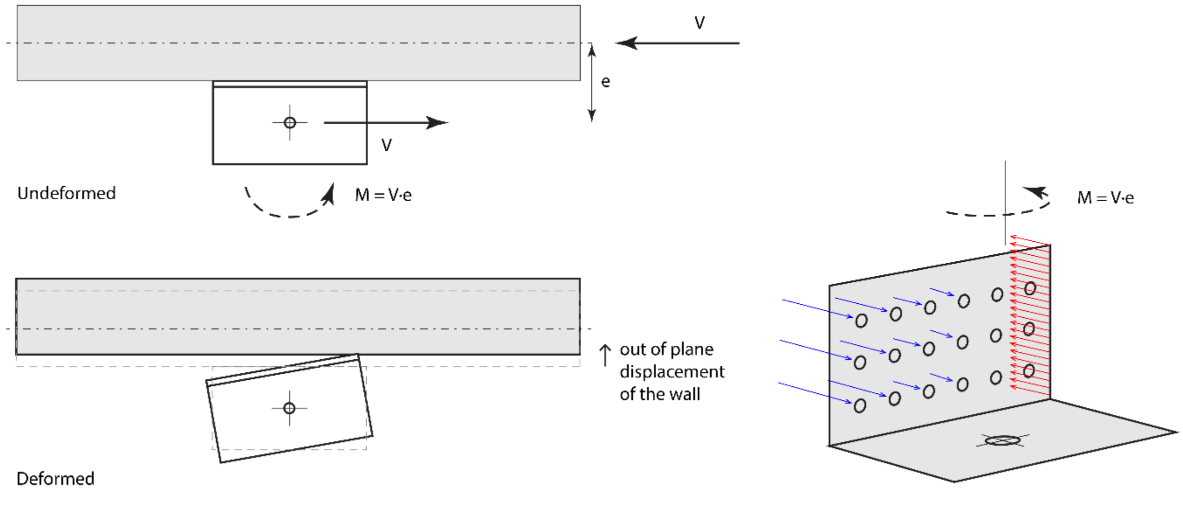

(*a*) (*b*)

Figure I.2-7 – Out-of-plane behavior of angle brackets caused by secondary moment due to eccentricity between wall and connection: (*a*) undeformed and deformed configurations; (*b*) detail of forces on connections.

I.2.4.1.3 CLT shear walls experimental tests: global and local measurements

In this Section, the experimental outcomes of the three tests on CLT shear walls are deeply examined, comparing the data obtained at the global level (i.e. global force-displacement curve of the wall) with those at the local level (i.e. uplift and slip displacements, inducing deformations at the connection level). Only by performing both the comparisons, i.e. at global and local levels, the actual cyclic response of the CLT panel connection systems can be fully understood and profitably used as a reference for the development of accurate and reliable numerical models able to capture all the different features of CLT panel connection system behavior.

The first aspect to be dealt with is the definition of an actual top displacement time history, in the following named d_{top}. Specifically, the wall top displacement can be decomposed in three contributions (see Figure I.2-8, where H and L are respectively the height and the width of the panel):

$$d_{top} = d_{rock} + d_{sl} + d_{panel} \qquad (I.2\text{-}2)$$

where:

- d_{rock} is the top displacement of the wall due to rocking, derived from experimental measurements according to the following equation:

  $$d_{rock} = \left(d_{up,l} - d_{up,r}\right) \cdot \frac{H}{L} \qquad (I.2\text{-}3)$$

  where $d_{up,l}$ and $d_{up,r}$ are the experimental uplifts of the left and right corner of the wall respectively (Figure I.2-8.a);
- d_{sl} is the base sliding displacement of the CLT wall (Figure I.2-8.b);
- d_{panel} is the elastic top displacement due to the shear and the bending deformability of the CLT panel (Figure I.2-8.c). It was not measured during the test but can be estimated by means of analytical and numerical models (see Section I.2.4.1.3.1).

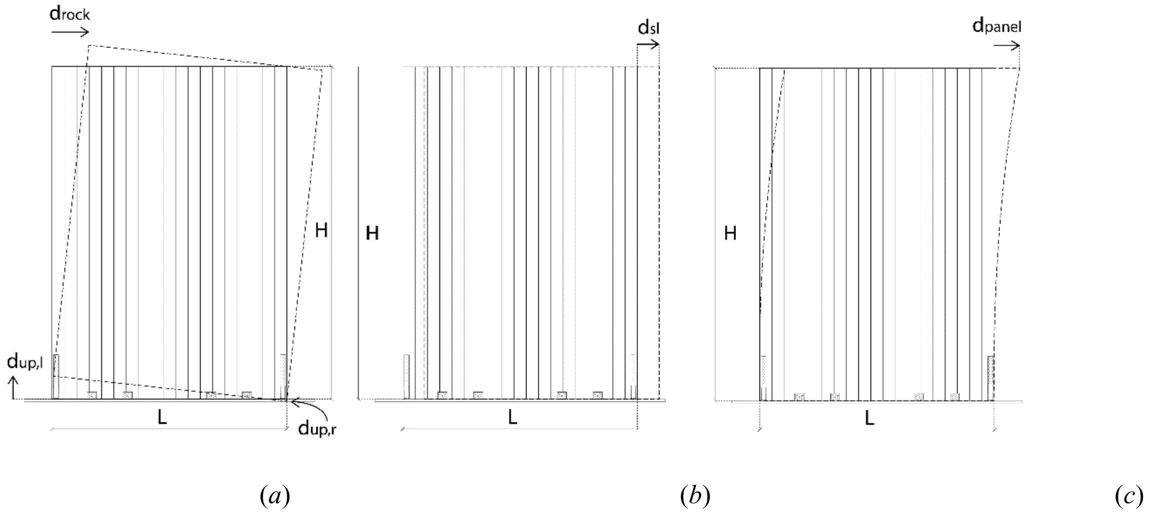

Figure I.2-8 – Horizontal displacement components of the wall system due to: (*a*) rocking; (*b*) sliding; (*c*) panel elastic deformation. Sign convention: horizontal displacement positive towards right direction; vertical displacement positive upward.

The comparison between the displacement $d_{top,meas}$ experimentally measured and d_{top} obtained as the sum of the three displacement contributions d_{rock}, d_{sl} and d_{panel} is reported and critically discussed below.

I.2.4.1.3.1 Elastic top displacement of the panel

In the present Section, some analytical and numerical models with different levels of complexity are presented and compared in order to provide a reliable estimation of the panel deformability, which was not measured during the tests. All the models consider a fixed restraint condition at the base (Figure I.2-8.c); in Finite Element (FE) models, the top applied force has been distributed along the upper nodes of the mesh.

The total horizontal displacement of the panel top is given by a shear term and a bending contribution:

$$d_{panel} = d_{shear} + d_{bending} \tag{I.2-4}$$

As for the shear contribution, the analytical model developed at Graz University of Technology [202, 215, 216] ("Graz model" for simplicity in the following) has been adopted. The shear stiffness is evaluated by considering two different mechanisms: mechanism I takes into account the shear deformation γ_1 of each layer, whereas mechanism II considers the deformation γ_2 due to relative torsional displacement between glued adjacent layers.

Therefore, the overall top displacement of the panel due to shear deformation can be obtained as:

$$d_{shear} = d_{shear,\gamma_1} + d_{shear,\gamma_2} = \frac{F}{t^* \cdot L}\left[\frac{1}{G_{0,mean}} + \frac{6}{G_{0,mean}}\left(\frac{t_{mean}}{a}\right)^2\right]H \tag{I.2-5}$$

where t^* is the ideal thickness of the CLT panel (i.e., the overall thickness of all ideal Representative Volume Sub Elements [202], that is always smaller than or equal to the geometric thickness of the CLT panel), L the panel width, $G_{0,mean}$ the mean shear modulus of the boards, F the horizontal force acting at the top of the panel, a the width of the lamellas and t_{mean} the average thickness of the lamellas. The top displacement of the panel due to bending can be simply calculated adopting the gamma method ([110]), accounting for the layered configuration of the CLT panel, as follows:

$$d_{bending} = F\frac{H^3}{3E_{0,mean}J_{eff}} \tag{I.2-6}$$

where $E_{0,mean}$ is the mean Young's modulus and J_{eff} the effective moment of inertia defined as:

$$J_{eff} = \frac{n_{vl}t_lL^3}{12} \tag{I.2-7}$$

with n_{vl} is the number of layers with vertical grain direction and t_l the thickness of the individual layer.

The mechanical parameters assumed in the analysis, according to [217], are $E_{0,mean} = 11000$ MPa and $G_{0,mean} = 690$ MPa. The resulting elastic stiffness of the panel is:

$$k_{panel-Graz\,model} = F/d_{panel} = 41.27kN/mm \tag{I.2-8}$$

A similar result is obtained by means of a refined Finite Element model, named "orthotropic layered model" in the following, with the layered shell element implemented in SAP2000 [218] and an orthotropic material model.

It is worth noting that, during the experimental campaign, the mechanical properties of the CLT panels were not characterized, therefore in this work the values of the elastic (E, G) and Poisson's (ν) moduli have been selected according to [217]: $E_L = 11000$ MPa, $E_R = E_T = 370$ MPa, $G_{LR} = G_{LT} = 690$ MPa, $G_{RT} = 50$ MPa, $\nu_{LR} = \nu_{LT} = 0.44$ and $\nu_{RT} = 0.64$, where the subscripts L, R, T indicate, respectively, the Longitudinal, Radial and Tangential direction of timber material. The obtained stiffness is equal to 41.60 kN/mm, in good agreement with the outcome of the Graz model. The simplified model adopted in [104], which assumes elastic isotropic plane-stress behavior with averaged mechanical properties ($E = 5685$ MPa and $\nu = 0.35$, with a resulting shear modulus G equal to 2106 MPa), predicts a panel stiffness equal to 67.53 kN/mm, which is about 60% larger than the two previous results.

In the following, a stiffness value consistent with that obtained with Graz model has been adopted, which is in good agreement with the one obtained with the orthotropic layered FE model. With this value of stiffness, it is possible to compute the contribution to the top displacement due to the elastic deformation of the panel.

I.2.4.1.3.2 Evaluation of the actual top displacement history

The value of the top horizontal displacement of the panel at each moment of the load history $d_{top,meas}$ experimentally measured is compared with the three displacement contributions d_{rock}, d_{sl} and d_{panel}.

Figure I.2-9 to Figure I.2-11 show the three displacement components and their percentage with respect to the measured value of top displacement $d_{top,meas}$, for the peak of each half cycle of the cyclic loading test.

Comparing the results for the three walls, it can be noted that the sliding contribution is larger for panel I.1 than for I.2 and I.3, with the latter exhibiting a larger rocking contribution. As expected, for all the configurations, the percentage contribution of the panel deformation to the total displacement decreases with increasing cycle's amplitude, being the plastic deformations localized mainly on the connections. However, the main outcome is that, in all cases, the sum of three displacement contributions d_{rock}, d_{sl} and d_{panel} is significantly smaller than the top displacement of the wall measured during tests, $d_{top,meas}$. Actually, such a significant gap means that there is some additional component of the total displacement which has not been taken into account. A possible hypothesis considers the presence of some spurious and unintentional sliding phenomenon between the base steel profile and the concrete foundation in the setup, labeled as $d_{spurious}$. In this case, at each instant of the load history, the actual top displacement of the wall d_{top} differs from the top displacement $d_{top,meas}$ measured during the test. Such an actual horizontal top displacement d_{top} represents a modified experimental displacement history, Equation (*I.2-9*), which will be assumed as the reference in the following comparison with the numerical simulations.

$$d_{top} = d_{top,meas} - d_{spurious} = d_{rock} + d_{sl} + d_{panel} \qquad (I.2\text{-}9)$$

where all symbols are those previously defined.

Table I.2-11 reports the positive and negative peaks of the actual horizontal top displacement load history d_{top}. In order to interpret the results more easily, in Table I.2-11 the actual top displacement d_{top} history has been graphically divided into three displacement ranges for small, medium and high amplitude cycles, represented in violet, yellow and green colors' area, respectively. This graphical subdivision will be adopted for all the results of non-linear component-level approach.

I.2.4.2 Numerical modelling of CLT shear walls

This Section gives a deep focus on different strategies used to create reliable nonlinear component-level models able to reproduce the CLT-system cyclic behavior both at the local and global level. The experimental tests carried out at CNR-IVALSA within the SOFIE project [77], after a preliminary phase of interpretation of the experimental dataset necessary to identify the peculiarities of the test procedure (Section I.2.4.1), are used to validate the quality of numerical results.

Validations of non-linear component models are generally performed by simulating the experimental tests on CLT shear walls and then comparing the global load-displacement curve and the cumulative or dissipated energy obtained from the numerical simulation with the analogous data obtained from experimental tests [44, 153, 191]. The capability of the model to capture also the local behavior of the individual components is generally omitted. This represents a significant lack in the use of this modelling approach because, if the model is not able to reliably reproduce the local response but only captures the global behavior, the use of component modelling becomes meaningless. Indeed, despite of the expensive calibration of the various components, the coherence with the experimental results is ensured only at the global level, similar to that achieved with a phenomenological or hybrid model.

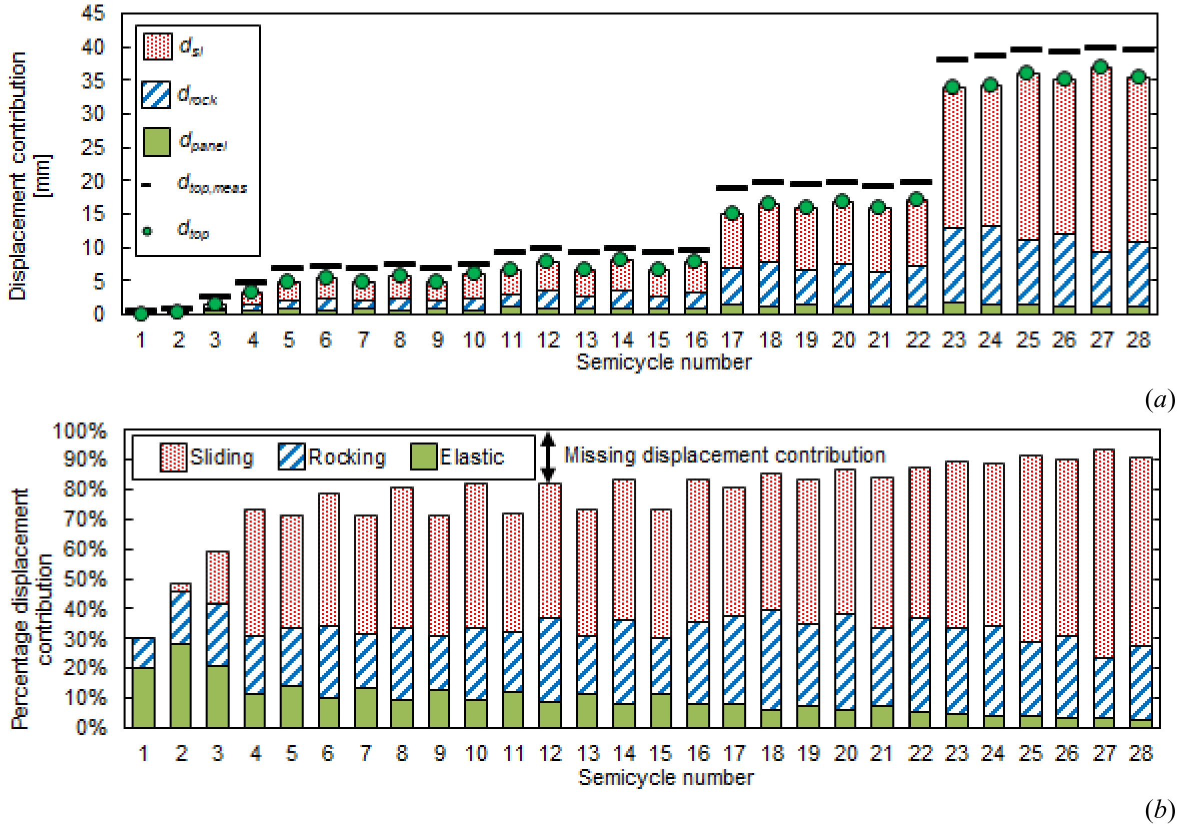

(*a*)

(*b*)

Figure I.2-9 – Wall I.1: displacement contribution to total lateral deflection: (*a*) individual contributions compared with the measured displacement; (*b*) percentage relative to the horizontal top displacement measured in the experimental test $d_{top,meas}$.

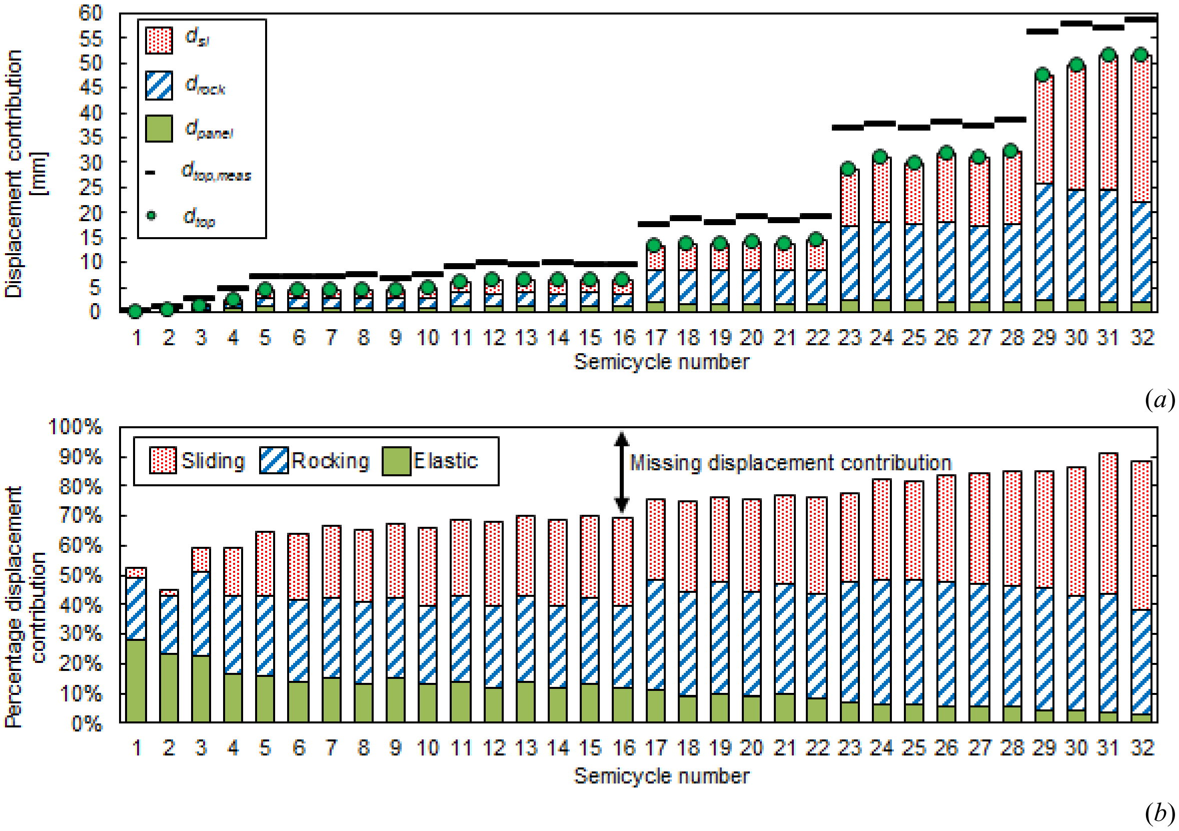

(*a*)

(*b*)

Figure I.2-10 – Wall I.2: displacement contribution to total lateral deflection: (*a*) individual contributions compared with the measured displacement; (*b*) percentage relative to the horizontal top displacement measured in the experimental test $d_{top,meas}$.

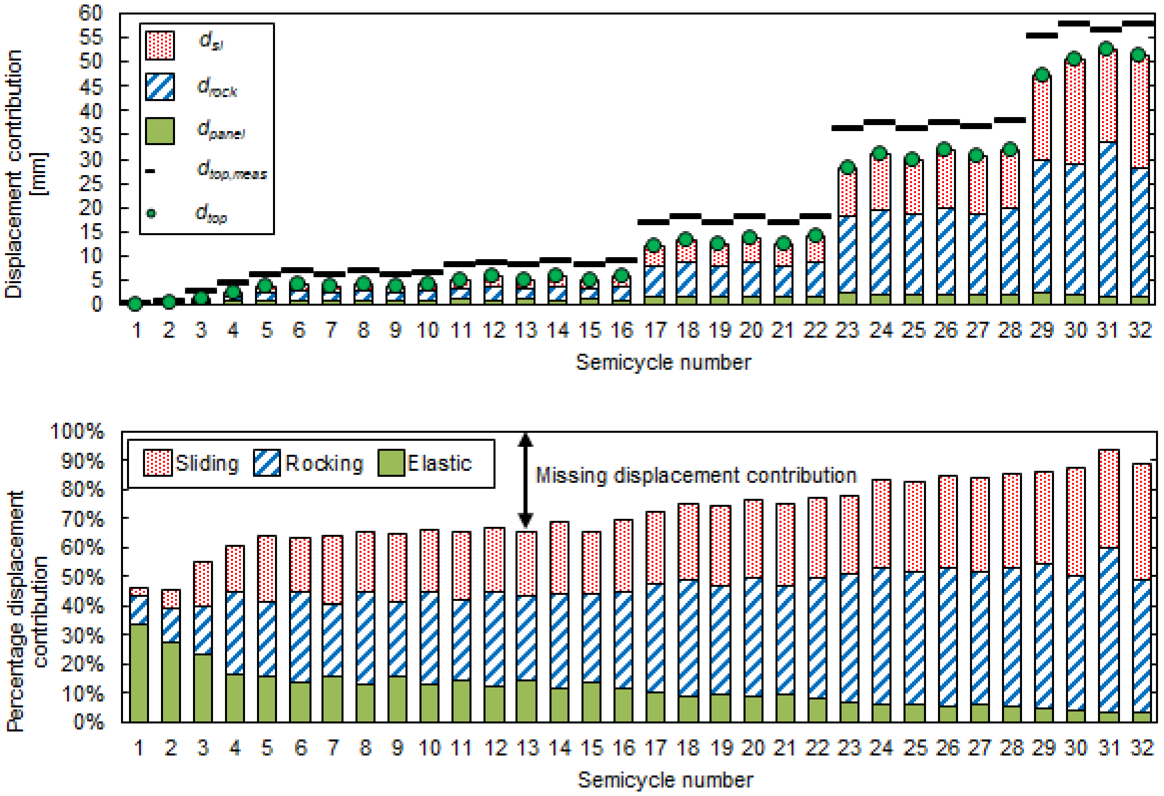

(*a*)

(*b*)

Figure I.2-11 – Wall I.3: displacement contribution to total lateral deflection: (*a*) individual contributions compared with the measured displacement; (*b*) percentage relative to the horizontal top displacement measured in the experimental test $d_{top,meas}$.

The present Section aims to give a further improvement in the knowledge of non-linear component modelling approach, investigating the capability of reproducing both global and local responses of CLT shear walls. In particular, we refer to “global” response as the load-displacement curve and cumulative energy of the wall and “local” response as displacements at the level of individual components (i.e. axial and transversal displacements of hold-downs and angle brackets).

Numerical strategies for model calibration and validation are presented and discussed, and sensitivity analyses have been performed with respect to the most important parameters of the model. Finally, numerical model results are critically compared with the experimental outcomes, showing that the global results of tests on CLT walls and corresponding failure modes can be captured accurately only taking into account the reduction of load bearing capacity of angle brackets due to out-of-plane movements of the CLT wall system.

The obtained outcomes demonstrate that non-linear component-level approach could be a feasible and reliable method to accurately reproduce the cyclic behavior of CLT wall systems, also at a local level, provided that every single component is properly calibrated. It is in add pointed out the necessity of a correspondence in the experimental behavior of tested connections used for calibration and the actual behavior that they will develop in the global wall system subjected to cyclic actions.

This Section focuses on the strategies to be adopted in order to obtain reliable results at both the global and local level with a non-linear component-level modelling approach. It is worth noting that, only by a proper calibration of the component-level model, the actual behavior of the CLT structure and of its components can be profitably assessed.

Table I.2-11 – Positive and negative peaks of load history d_{top} for small (violet), medium (yellow) and high (green) amplitude cycles.

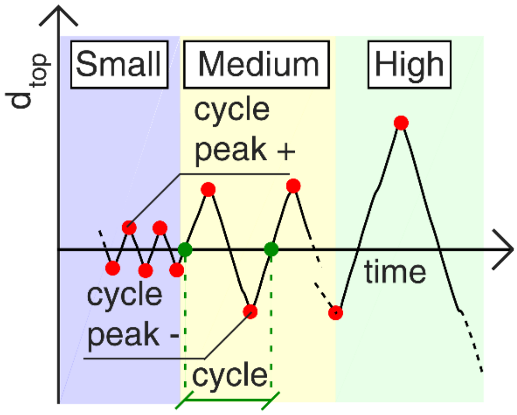	**Wall I.1**		**Wall I.2**		**Wall I.3**	
	Peak +	**Peak –**	**Peak +**	**Peak –**	**Peak +**	**Peak –**
	(mm)	(mm)	(mm)	(mm)	(mm)	(mm)
1st cycle	0.05	-0.32	0.09	-0.30	0.09	-0.30
2nd cycle	1.50	-3.37	1.46	-2.69	1.41	-2.68
3rd cycle	4.83	-5.69	4.38	-4.62	3.92	-4.20
4th cycle	4.82	-5.85	4.50	-4.69	3.86	-4.28
5th cycle	4.82	-5.92	4.59	-4.71	3.87	-4.29
6th cycle	6.67	-7.96	6.33	-6.56	5.23	-5.88
7th cycle	6.78	-8.07	6.45	-6.63	5.22	-6.02
8th cycle	6.81	-8.13	6.50	-6.69	5.17	-6.09
9th cycle	15.62	-16.77	13.51	-14.20	12.18	-13.61
10th cycle	16.00	-17.01	13.73	-14.40	12.45	-13.86
11th cycle	16.16	-17.17	13.94	-14.56	12.56	-13.98
12th cycle	34.69	-34.53	28.56	-31.47	28.27	-31.38
13th cycle	36.18	-35.46	30.02	-31.99	30.08	-31.86
14th cycle	37.03	-35.58	31.09	-32.45	30.66	-32.08
15th cycle	41.66		48.52	-50.24	48.87	-50.53
16th cycle			52.02	-51.81	52.80	-51.45

I.2.4.2.1 *Modelling assumptions*

The numerical model has been created with an approach based on the strategy proposed in [191] within the OpenSees framework [219]. In particular, the wall is first modelled as an elastic truss lattice grid capable of reproducing correctly the panel deformability estimated in accordance with the Graz Model. Moreover, the connections (i.e. both hold-downs and angle brackets) are simulated as zero-length uncoupled multi-spring elements with the OpenSees hysteretic constitutive law named Pinching4 [220]. Their laws were properly calibrated from the experimental tests on the connections carried out at CNR-IVALSA Trees and Timber Institute [102, 212], see Section I.2.4.2.2. It is worth noting that, for well-designed connections with ductile behavior, strength and stiffness degradation at large deformations becomes no longer crucial. On the contrary, the pinching effect on cyclic behavior cannot be neglected, since it significantly affects the energy dissipation capacity [106, 221, 222]. Accordingly, force and stiffness cyclic degradation phenomena are not numerically modelled in this work, since for the examined connection elements their effect is negligible in the typical displacements range of a structure subjected to seismic action [153].

The interaction between the bottom of the wall and the rigid steel profile at the base is modelled using a 2D node-to-segment contact element named SimpleContact2D with the constitutive law "ContactMaterial2D" in the OpenSees framework [219]. The parameters of the constitutive law are the tensile strength f_t, the cohesive intercept c, the friction coefficient μ and the shear modulus G according to a penalty formulation. The assumed values are $f_t = c = 0.0$ MPa, $G = 5.0 \cdot 10^5$ MPa and $\mu = 0.20$, a realistic value for timber-to-smooth-steel interface [223, 224]. In order to assess the influence of the friction coefficient on the response of the wall, sensitivity analyses have been carried out with different values of friction coefficient ranging from 0 to 0.4, see Section I.2.4.2.4.1.

I.2.4.2.2 Components calibration

The individual components of the model were calibrated using the experimental tests carried out on the connections at IVALSA Trees and Timber Institute [102, 212]. Each connection type (i.e., angle brackets and hold-downs) was tested under cyclic loading, both in axial and lateral direction. Six specimens were tested for each configuration. In the following, the load-displacement curves of all tests are dealt with, except for one of the angle brackets loaded in the lateral direction whose results can be considered an outlier.

As far as the backbone curve of the constitutive law is concerned, the six parameters defining the characteristic points (P_{y1}, first yielding, P_{y2}, second yielding, and P_{max}, peak point) were calibrated for each connection (i.e. angle brackets and hold-downs) with the energy-balance criterion proposed in [83]. The slope k_4 of the softening branch was then calculated imposing an energy balance between numerical and experimental curve in the post-peak range of displacements, according to [82]. Finally, the various parameters were averaged to obtain a mean curve for each connection (i.e. angle brackets and hold-downs) and each direction of loading (i.e. lateral and axial).

Regarding the hysteretic behavior of the Pinching4 law (see Figure I.2-12), the slope of branches 1 and 4 is equal to k_{unload}, according to the approach detailed in [83], while the slopes $k_{pin,up}$ and $k_{pin,low}$ of branches 2 and 5 are set in order to fit the experimental mean pattern. The slope k_{reload} of the reloading branches 3 and 6 is determined imposing an energy balance between the numerical and experimental curves, for complete cycles in the typical working displacement range.

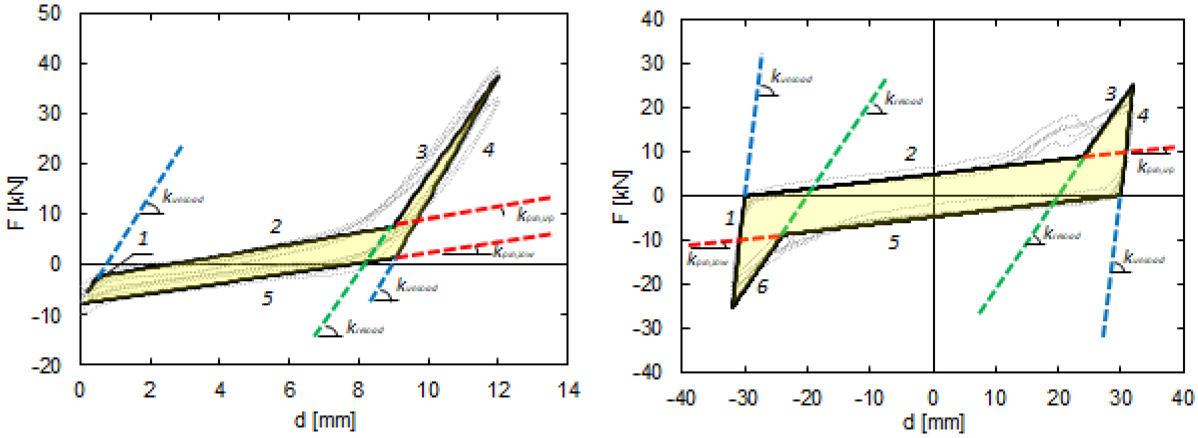

(*a*) (*b*)

Figure I.2-12 – Schematic representation of the parameters defining the hysteretic behavior of the OpenSees Pinching4 law [219], for a general connection (angle bracket or hold-down) under: (*a*) axial; (*b*) shear loading, starting from experimental data.

The results of the abovementioned calibration phase are shown in Figure I.2-13 for all the connections, where the model linearized curves using average data are represented in bold. A significant scattering of experimental data in the force-displacement curves is observed, particularly significant for the hold-down connections loaded in the axial direction.

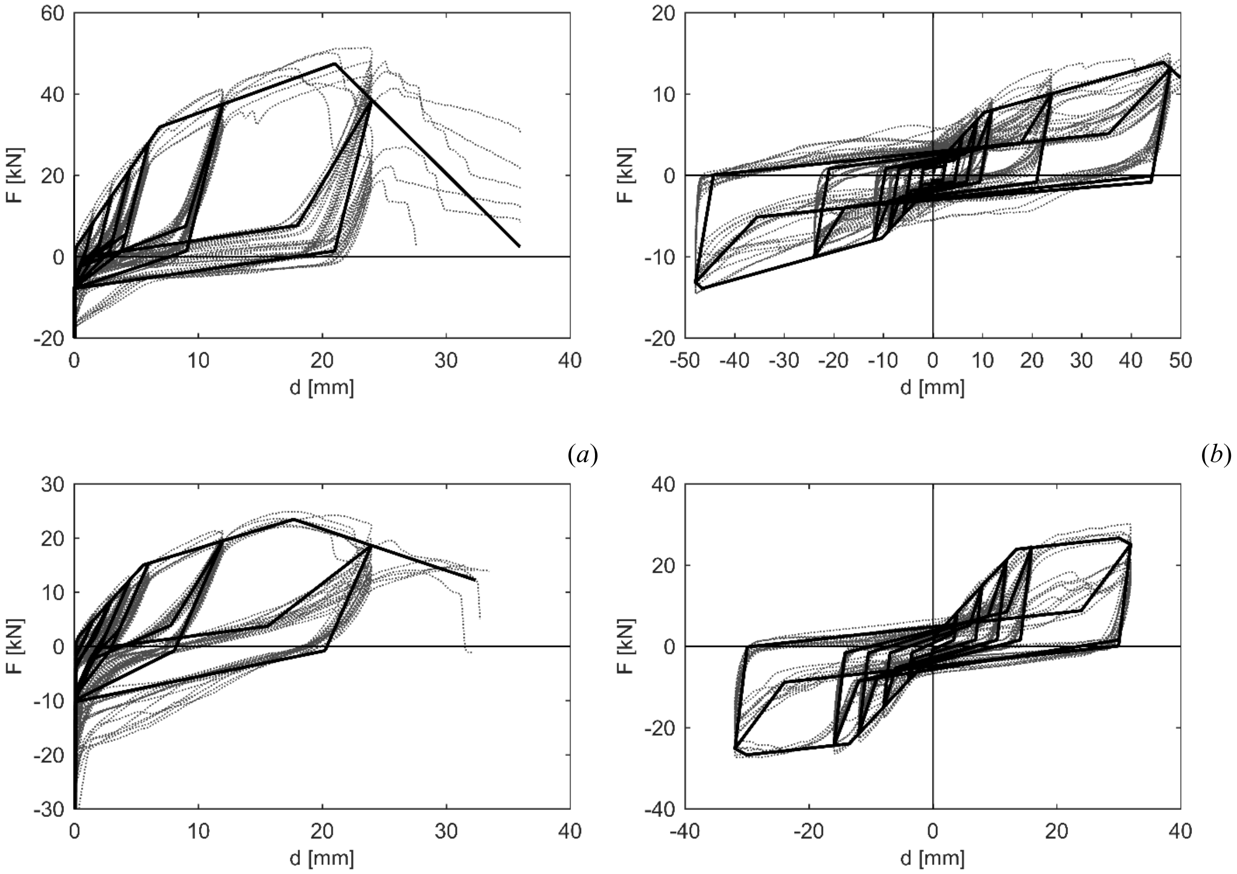

(*a*) (*b*)

(*c*) (*d*)

Figure I.2-13 – Results of the calibration of hysteretic law of connections: (*a*) hold-down loaded in the axial direction; (*b*) hold-down loaded in lateral direction; (*c*) angle bracket loaded in the axial direction; (*d*) angle bracket loaded in lateral direction.

I.2.4.2.3 Numerical Results

The results of numerical simulations for the three walls subjected to experimental tests are presented in the following. In order to have a deeper insight on the reliability of the proposed model, results are compared with the experimental outcomes not only in terms of global response (force-displacement curve), but also investigating the local response of each component (i.e. connection displacements). In all the following graphs, as previously mentioned, the shading colors correspond to the three different working ranges of the connections according to Table I.2-11.

At the global level, Figure I.2-14 shows, for all the walls, a good agreement between experimental and numerical results in terms of force-displacement curves (Figure I.2-14.a) and cumulative energy (Figure I.2-14.b). In detail:

- Wall I.1 – The peak force is overestimated by 17%, while the corresponding peak displacement is well captured;
- Wall I.2 – The peak force and the corresponding peak displacement are well captured, but the experimental and numerical curves show significant differences in the post peak range;
- Wall I.3 – The peak force and the corresponding peak displacement are underestimated by 10% and 22% respectively.

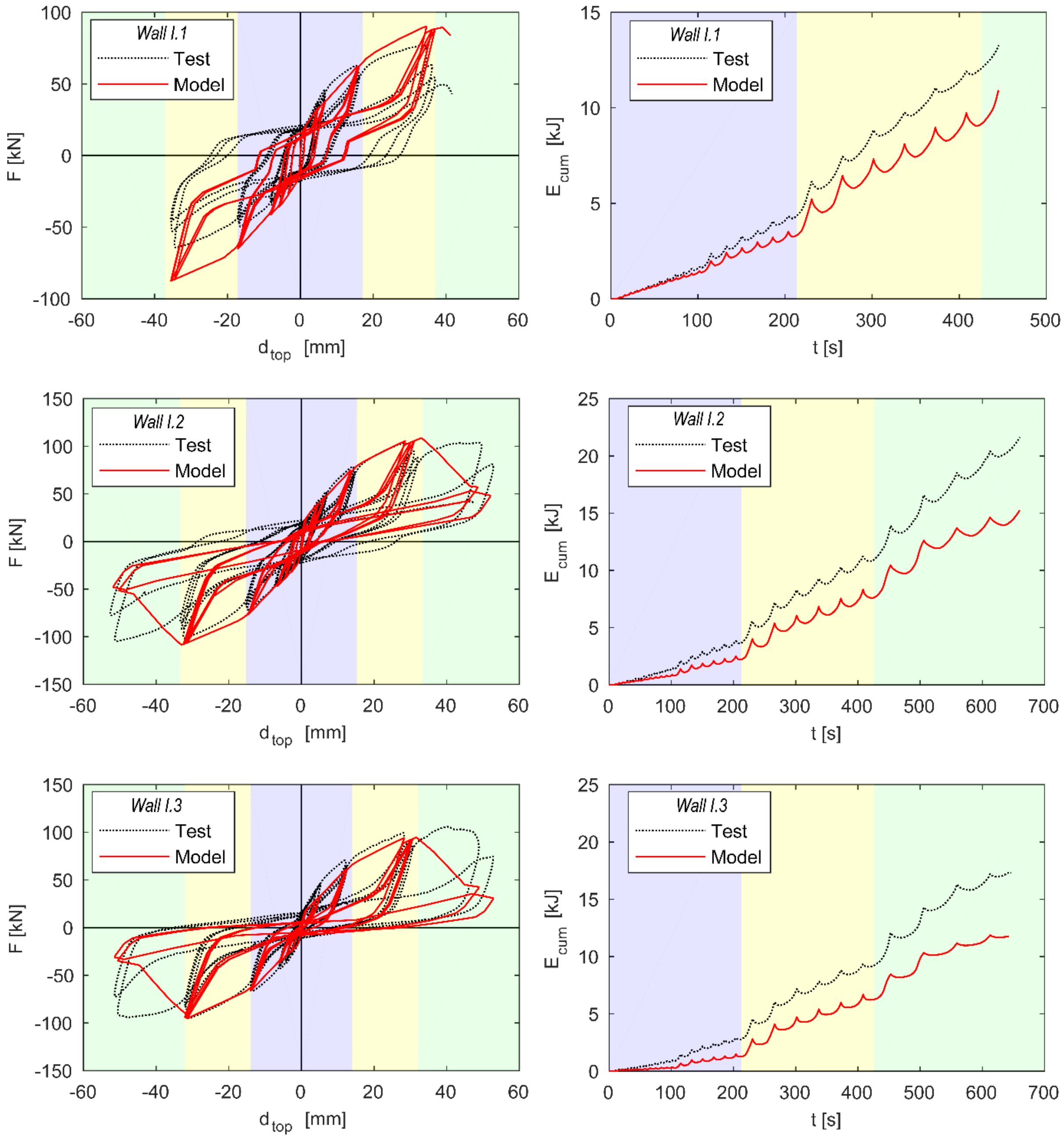

(*a*) (*b*)

Figure I.2-14 – Comparison between numerical simulations and test results, global behavior in terms of: (*a*) force-displacement curve; (*b*) cumulative energy.

As for the cumulative energy, numerical results generally underestimate the experimental value of about 20-30%, similarly to other numerical models adopted to simulate these tests and reported in the literature [153, 208]. This could be ascribed to the adopted constitutive laws, which cannot represent exactly the actual hysteretic behavior (i.e., the dissipative capacity) of the CLT panel-connection system.

At the local level, Figure I.2-15 shows the comparison between experimental and numerical results in terms of uplift (Figure I.2-15.a) and slip (Figure I.2-15.b) displacements of the connections, for all the walls. In all cases, an excellent agreement between numerical and experimental results can be observed in the small amplitude cycles range (i.e. violet region). On the contrary, for medium and especially for high amplitude cycles (i.e. yellow and green regions) the uplift is significantly overestimated and consequently, the slip displacement is underestimated.

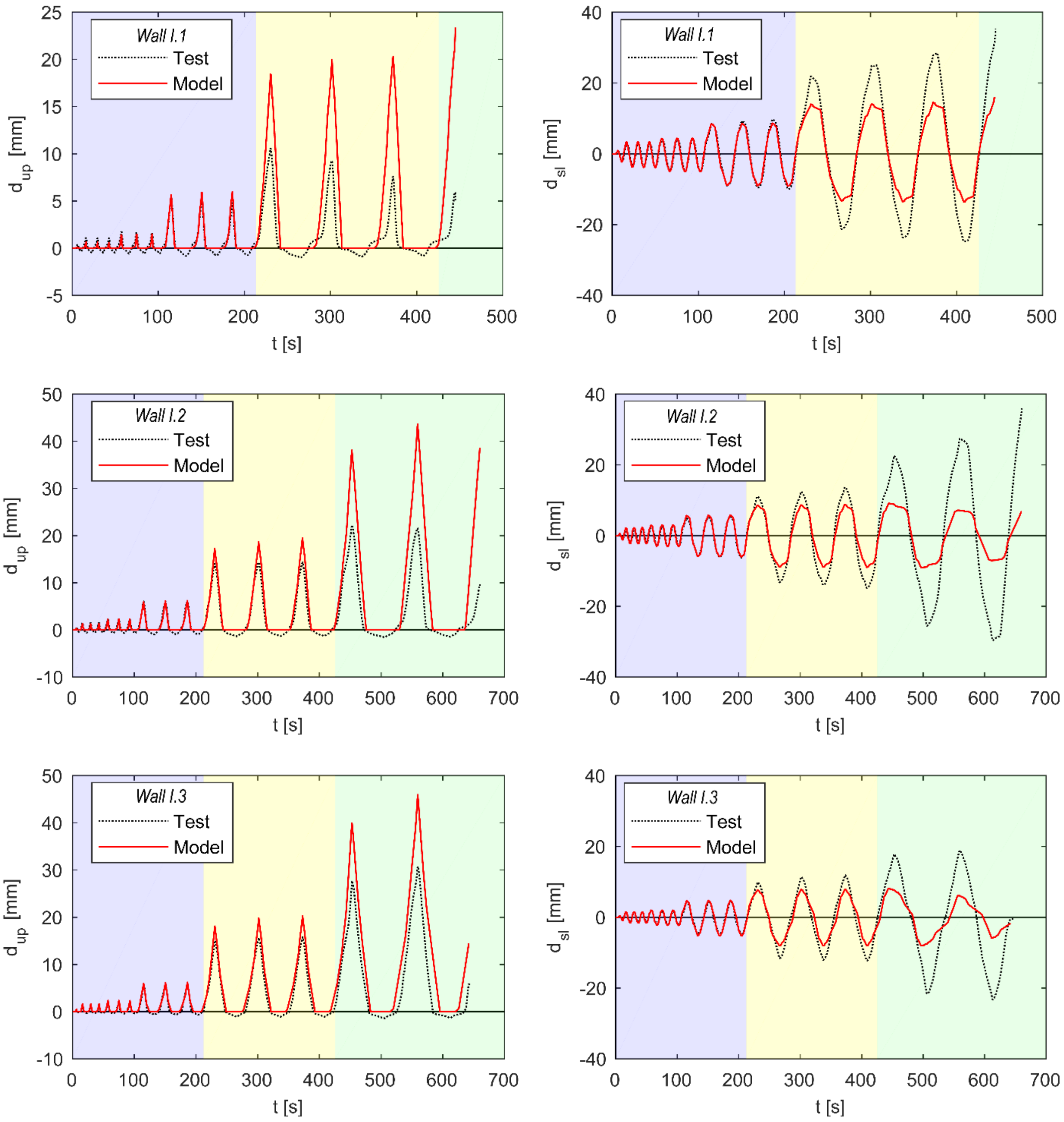

(*a*) (*b*)

Figure I.2-15 – Comparison between numerical simulations and test results, local behavior in terms of: (*a*) uplift displacement; (*b*) slip displacement.

I.2.4.2.4 Sensitivity analyses

In order to motivate the differences between numerical and experimental responses evidenced in Section I.2.4.2.3, some sensitivity analyses were conducted, considering the variability of friction coefficient, connections constitutive law parameters and post peak slope.

In the following, the numerical simulations described in the previous Section I.2.4.2.3 for the three walls are referred to as “Reference model”, labelled with “Ref” tag, and represented with a continuous red line in all the graphs.

I.2.4.2.4.1 Effect of the friction coefficient values

The first parameter that could affect the local and global responses of the wall system is the friction coefficient at the interface between the CLT panel and the base steel profile. Two limit conditions of null and high friction (i.e. $\mu = 0.00$ and $\mu = 0.40$ respectively) are examined and compared with the value adopted in the reference solution (i.e. $\mu = 0.20$). Figure I.2-16 to Figure I.2-18 show, for the three walls, the comparison between the results obtained assuming the different levels of friction in terms of: (*a*) force-displacement curve; (*b*) cumulative energy; (*c*) uplift displacement; (*d*) slip displacement.

Regarding shear wall I.1 (Figure I.2-16), it can be observed that all the results obtained with μ= 0.40 are not significantly different from those with μ = 0.20 (reference). On the contrary, the case with μ = 0.00 fits better the experimental response, apart from the cumulative energy which is remarkably underestimated. Indeed, in this case the small amplitude cycles exhibit a marked pinching, due to the absence of friction.

As for shear walls I.2 and I.3 (Figure I.2-17 and Figure I.2-18), adopting different values of the friction coefficient, the difference is almost negligible. This can be due to the peculiar failure mode for these walls, mainly related to rocking effect. For these walls, adopting a null value of friction coefficient gives slightly better predictions of local displacements. However, in the following, the value of $\mu = 0.20$ is adopted, $\mu = 0.00$ representing a limit condition with no clear physical meaning. Moreover, the results show that the differences are not significant and that the cumulative energy is better predicted with $\mu = 0.20$.

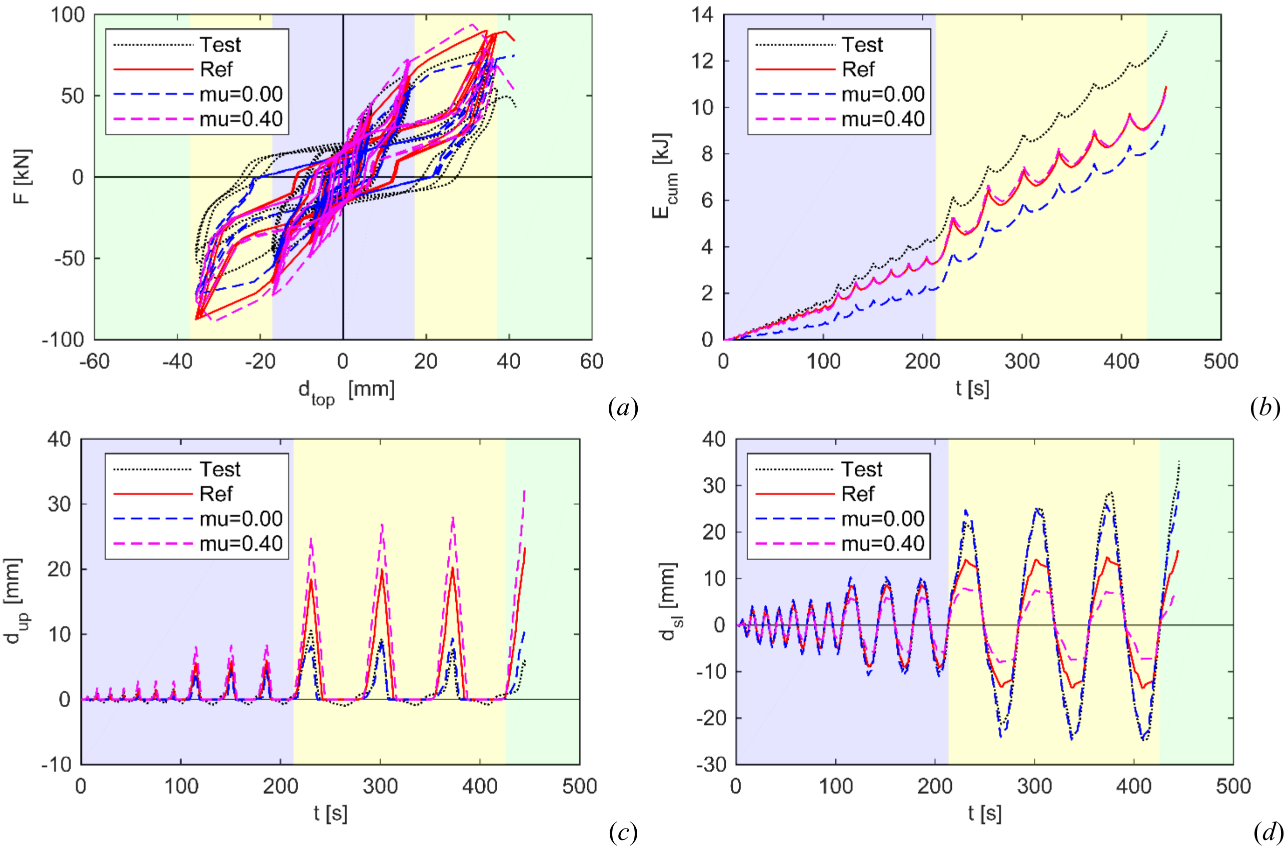

Figure I.2-16 – Sensitivity analyses for Wall I.1. Comparison for different levels of friction coefficient: (*a*) force-displacement curve; (*b*) cumulative energy; (*c*) uplift displacement; (*d*) slip displacement.

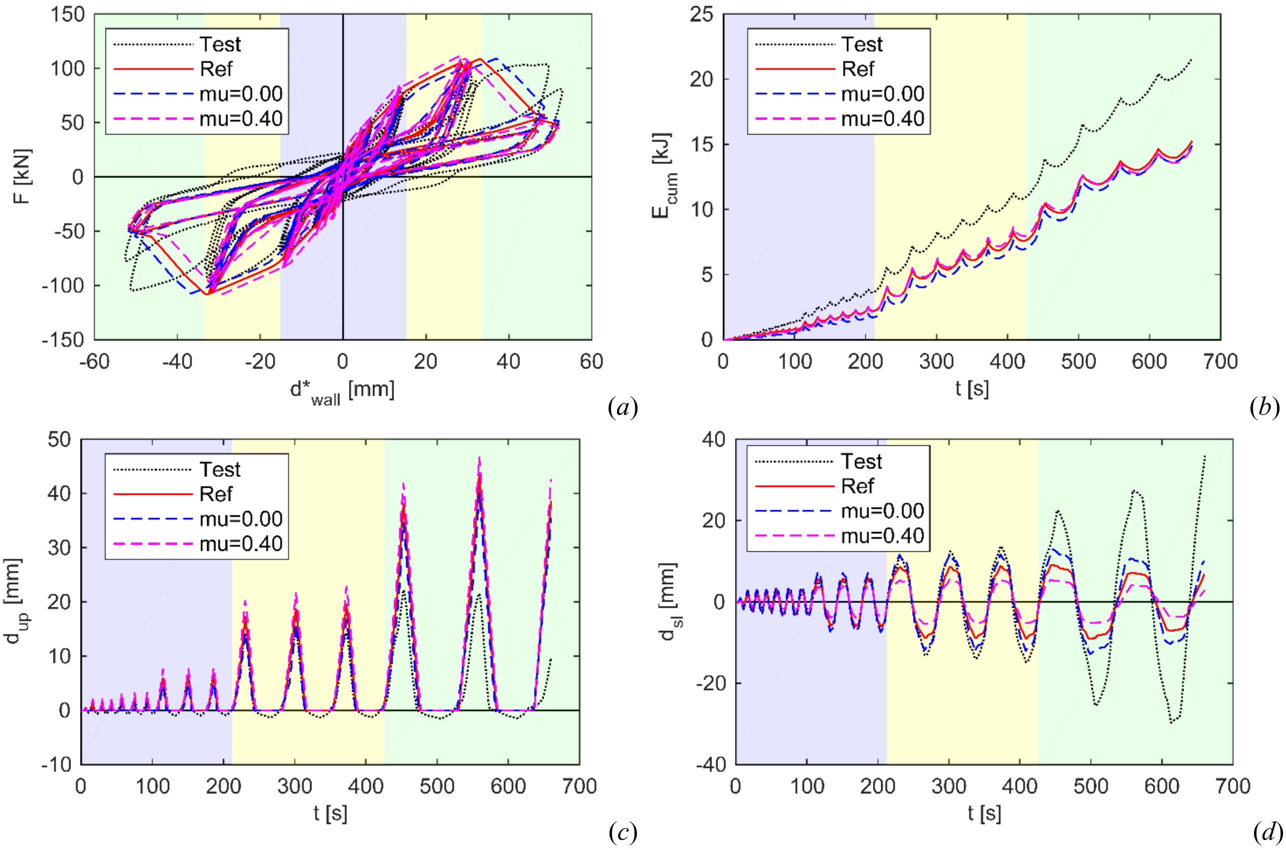

Figure I.2-17 – Sensitivity analyses for Wall I.2. Comparison for different levels of friction coefficient: (*a*) force-displacement curve; (*b*) cumulative energy; (*c*) uplift displacement; (*d*) slip displacement.

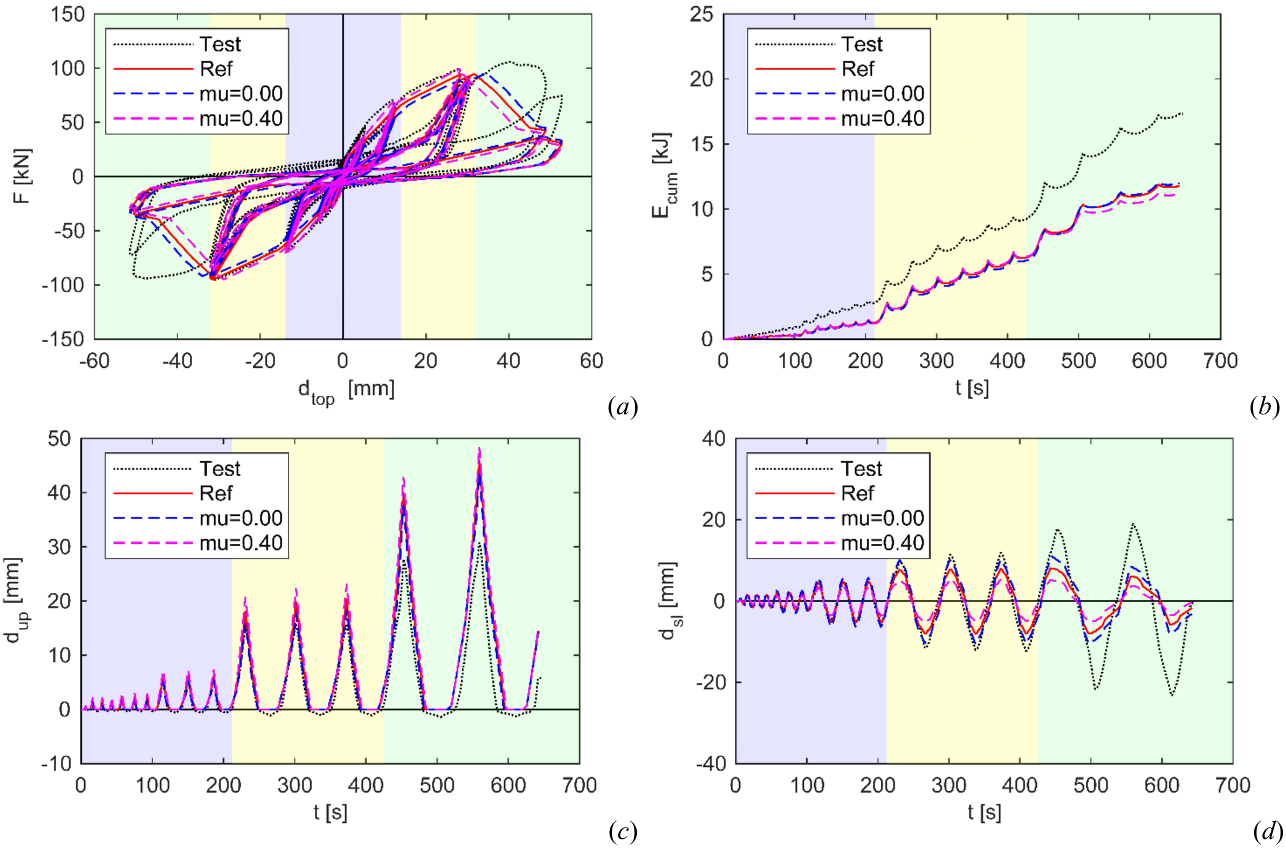

Figure I.2-18 – Sensitivity analyses for Wall I.3. Comparison for different levels of friction coefficient: (*a*) force-displacement curve; (*b*) cumulative energy; (*c*) uplift displacement; (*d*) slip displacement.

I.2.4.2.4.2 Effect of the connections mechanical responses

As mentioned in Section I.2.4.2.2, the reference model is based on the constitutive laws obtained by averaging all the available experimental results. In order to account for the effect of the variations in the mechanical response exhibited experimentally by the various connections, two additional numerical simulations were carried out. The first one considers the strongest connections in the axial direction with the weakest ones in lateral direction (named BW where B stands for Best and W for Worst), selected among all the tested hold-downs and angle brackets. The second numerical model assumes the weakest connections in the axial direction and the strongest ones in the lateral direction (named WB).

Figure I.2-19 to Figure I.2-21 depict the results obtained with the two models at the global (i.e. force-displacement curve and cumulative energy) and local (i.e. uplift and slip displacements) levels, compared with the response of the reference model and the experimental results. Generally, the former model induces a sliding behavior, while the latter induces the rocking behavior of the examined walls.

Similarly to the reference model, both two configurations underestimate the slip displacement and overestimate the uplift. Therefore, the variability of mechanical properties of connections cannot fully explain the offset between numerical and experimental results.

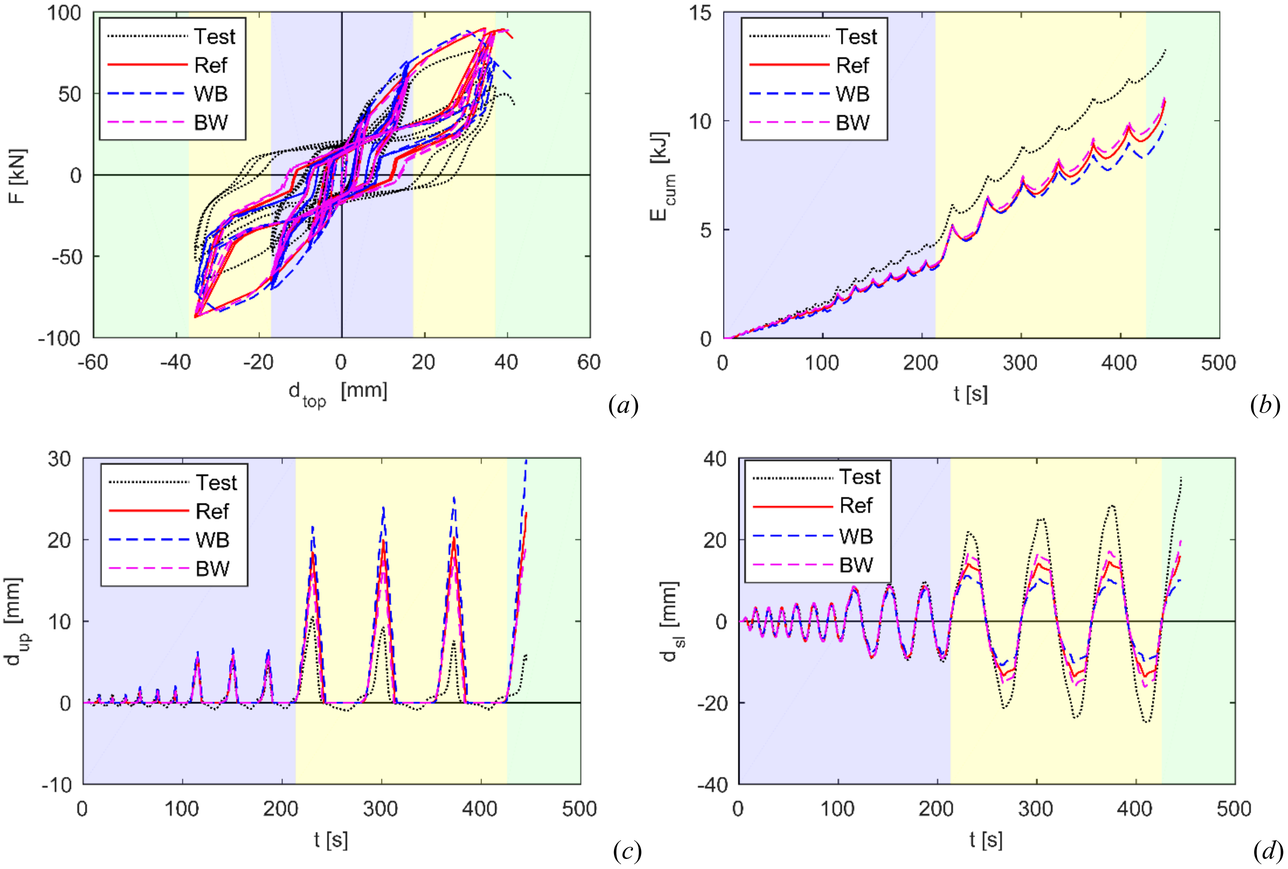

Figure I.2-19 – Sensitivity analyses for Wall I.1. Comparison between results of the numerical models “BW” and “WB”: (*a*) force-displacement curve; (*b*) cumulative energy; (*c*) uplift displacement; (*d*) slip displacement.

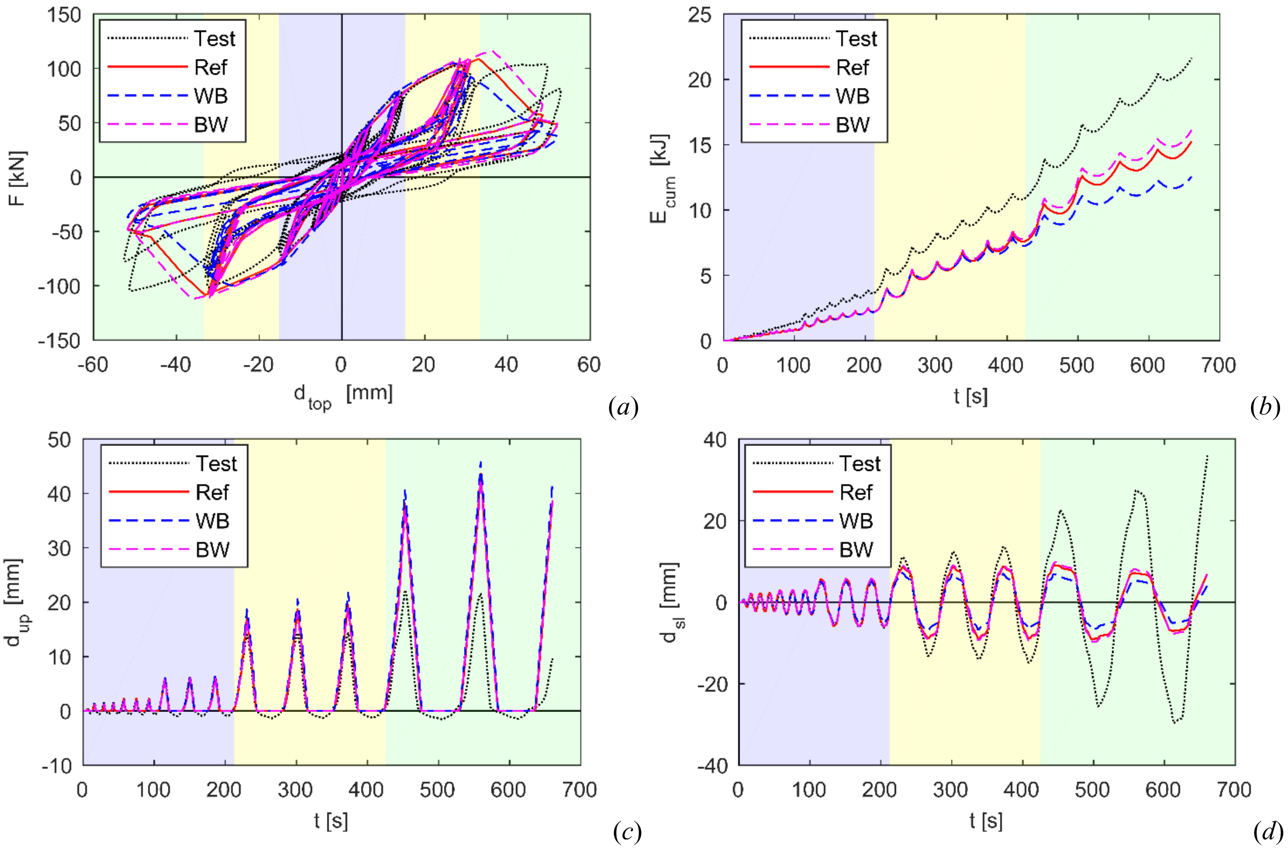

Figure I.2-20 – Sensitivity analyses for Wall I.2. Comparison between results of the numerical models “BW” and “WB”: (*a*) force-displacement curve; (*b*) cumulative energy; (*c*) uplift displacement; (*d*) slip displacement.

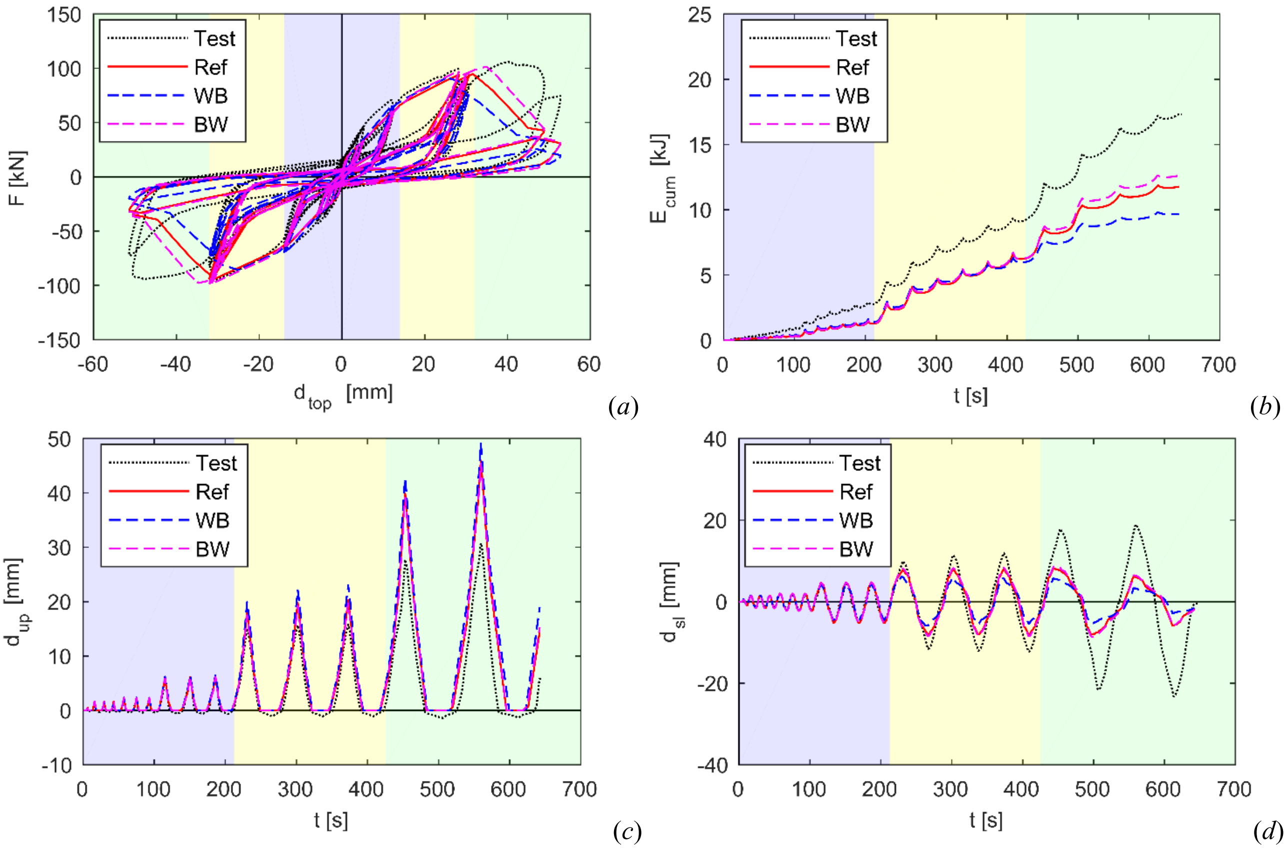

Figure I.2-21 – Sensitivity analyses for Wall I.3. Comparison between results of the numerical models “BW” and “WB”: (*a*) force-displacement curve; (*b*) cumulative energy; (*c*) uplift displacement; (*d*) slip displacement.

I.2.4.2.4.3 Effect of the hold-down axial post-peak slope

The third aspect that may affect the predictive capacity of the numerical model in representing the experimental response of the shear walls is the modelling of the post-peak behavior of the hold-down connections.

Figure I.2-22 and Figure I.2-23 show the effect of assuming two different values of the post-peak slope k_4 of the hold-down loaded in the axial direction, compared with those adopted for the reference model, in terms of global force-displacement curve, cumulative energy, uplift and slip displacement for all the three shear walls. The reference results (continuous red line) refer to a post-peak slope k_4, WHT540=-3.02 kN/mm, obtained by averaging the tests carried out on WHT540 hold-downs (depicted in Figure I.2-13). It is worth noting that this kind of hold-down connection [184] was used for tests on connections [102], while the hold-downs adopted in the global shear wall test [97] were HTT22 type [214]. Even if these two connections exhibit a similar behavior in the pre-peak region [44, 102], the slopes of the softening branches are different [102, 225]. Therefore, the second value assumed in the analyses for the post-peak slope is the one of a typical HTT22 hold-down, [225], i.e. $k_{4,HTT22} \simeq$-1.35 kN/mm (dotted blue line). Finally, a sub-horizontal softening branch ($k_4 = -0.25$ kN/mm) is also considered in order to simulate a limit case often assumed in literature, e.g. [153] (dotted purple line).

The comparative results show that adopting different values of the post-peak slope of the hold-downs loaded in the axial direction provides negligible differences at the local level, i.e. uplift and slip displacements. At the global level, a lower value of stiffness k_4 allows to capture slightly better the experimental evidences in the post peak range (i.e., for high-amplitude cycles) with respect to the reference model, both in terms of global force-displacement and cumulative energy for wall I.2 and I.3, Figure I.2-22 and Figure I.2-23, respectively. Results concerning the wall I.1 are not reported, since in this case the post-peak range is not reached.

It is finally worth noting that, similarly to the previous sensitivity study, differences in the post peak slope cannot fully explain the offset between the numerical and experimental results.

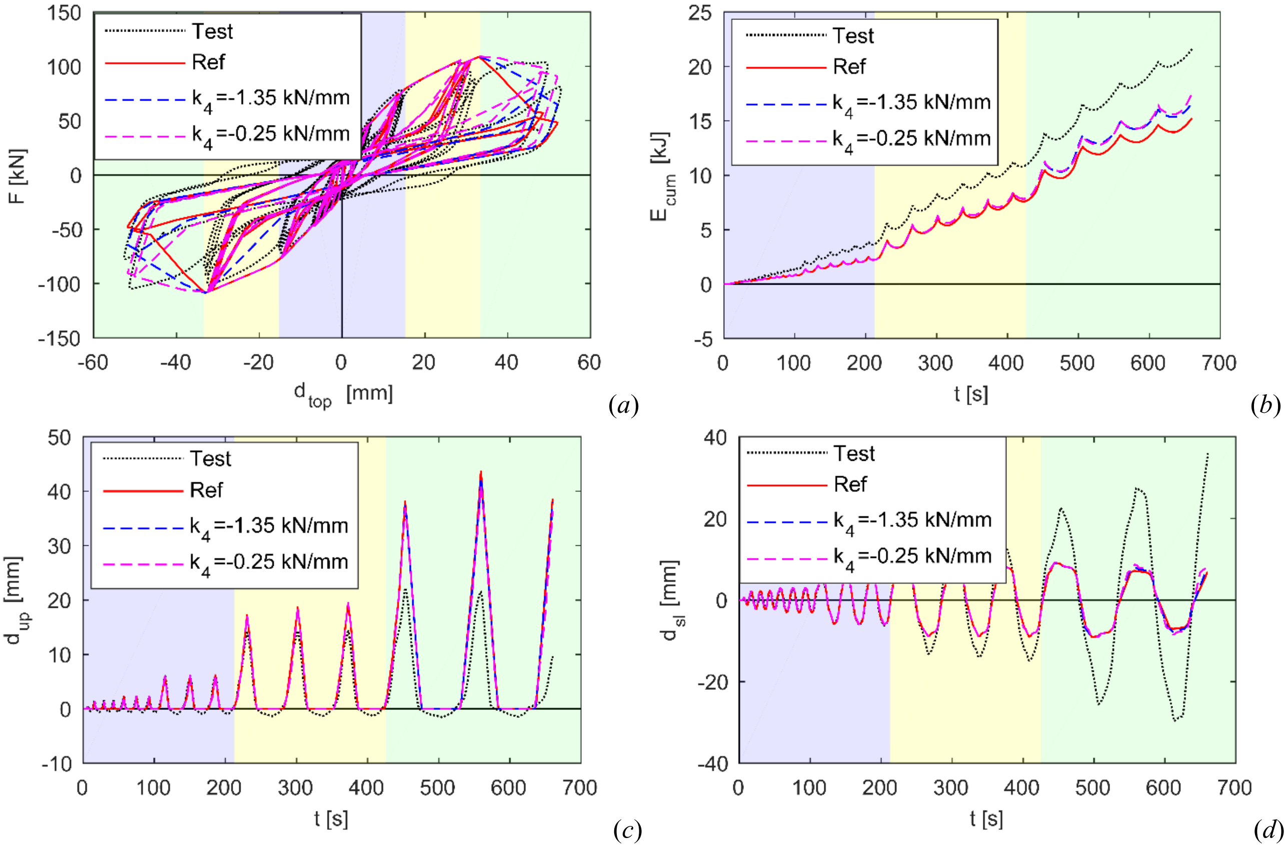

Figure I.2-22 – Sensitivity analyses for Wall I.2. Comparison adopting different post-peak slopes of hold-downs loaded in the axial direction: (*a*) force-displacement; (*b*) cumulative energy; (*c*) uplift displacement; (*d*) slip displacement.

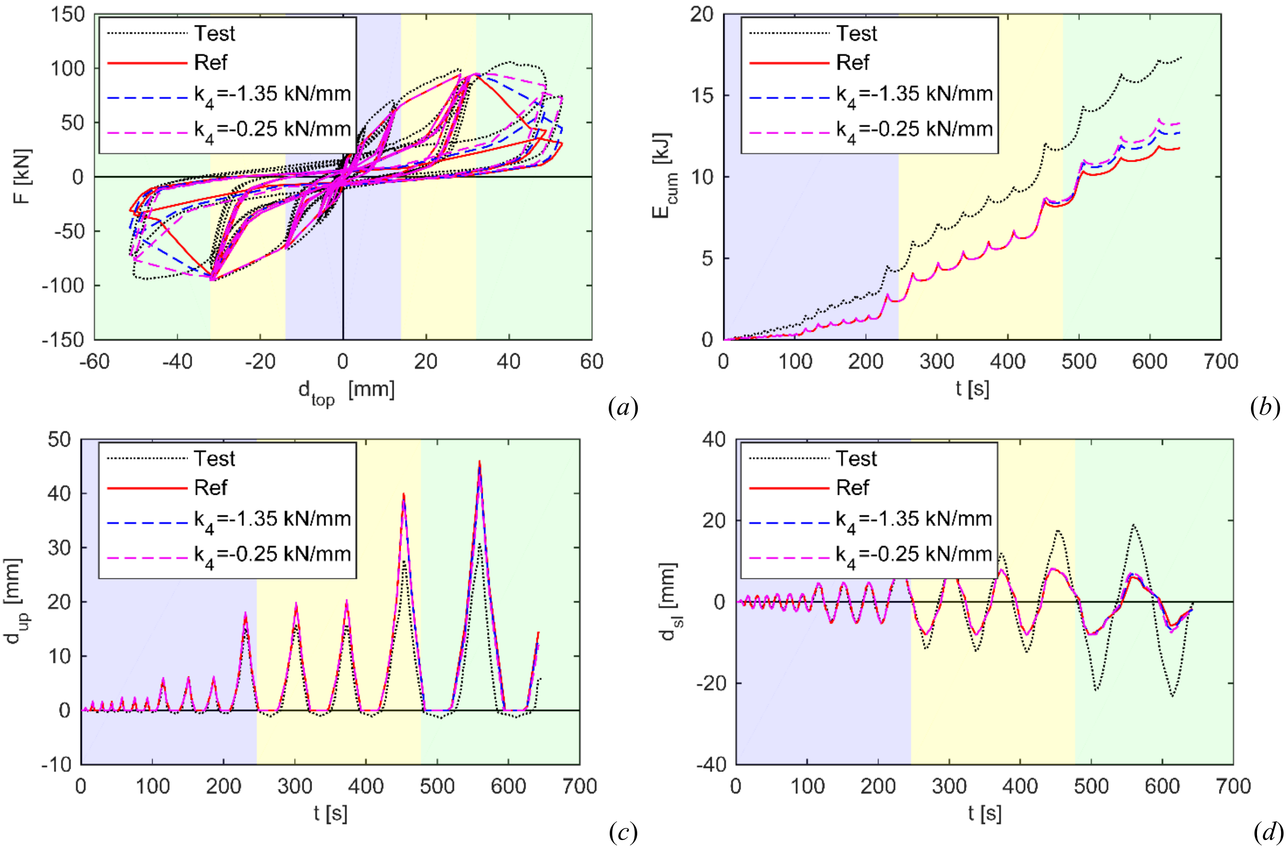

Figure I.2-23 – Sensitivity analyses for Wall I.3. Comparison adopting different post-peak slopes of hold-downs loaded in the axial direction: (*a*) force-displacement; (*b*) cumulative energy; (*c*) uplift displacement; (*d*) slip displacement.

I.2.4.2.5 Out-of-plane displacement of the walls

The significant difference between numerical and experimental results, clearly evidenced by the different relative contributions of rocking and sliding movements to the total displacement at the top of the wall - especially for medium and high amplitude cycles - needs some deeper investigations in order to be justified. By observing the deformed configurations of the three CLT wall systems at the end of the experimental tests (see Figure 7 of [77] or Figure 12 of [48]), it is evident that a significant out-of-plane movement occurred at the wall base due to the absence of an adequate constraint (Figure I.2-7), with a consequent reduction of the shear strength and stiffness of the angle brackets. This experimental evidence was not considered in experimental data interpretation, nor in the numerical models definition by the researches published in the literature [44, 104, 153].

In order to overcome this drawback, the reduction of shear strength of angle brackets due to the out-of-plane movements will be taken into account in the following. To this aim, the shear force acting on the angle bracket inducing the connection failure when subjected to a out-of-plane additional movement must be evaluated first. In the following, a simple analytical model, that assumes the timber panel as rigid, is proposed. According to the failure mechanism schematically depicted in Figure I.2-7, the vertical metal plate rotates almost rigidly around its right corner, and the withdrawal forces in the nails assume a linear distribution along the steel plate (Figure I.2-7.b). The maximum load capacity of the angle bracket is achieved when withdrawal strength of nails, evaluated according to [185], is attained in the nails themselves along the left row. It is then possible to calculate the shear capacity due to this secondary effect as:

$$V_R = \frac{M_R}{e} \tag{I.2-10}$$

where M_R is the resisting moment due to the withdrawal strength of the nail system and e is the eccentricity of the shear force acting on the connection.

The evaluated value, $V_R = 14.24$ kN, is significantly smaller than the strength of the angle bracket in shear obtained from the test on the single connection, i.e. about 26 kN (see Figure I.2-13.d). This difference indicates that the connection strength in the global wall test degrades of 45% respect to the full value.

In order to take the shear strength reduction of angle brackets into account, their constitutive law has been modified by introducing a damage variable d_{OOP} (i.e. "out-of-plane damage variable") and the damaged shear forces $F_{y1}^{(d)}$, $F_{y2}^{(d)}$ and $F_{max}^{(d)}$ corresponding respectively to first yielding point $P_{I,y1}$, to second yielding point P_{y2} and to peak point P_{max} are expressed as function of the relevant undamaged shear forces given by the following equation:

$$F_i^{(d)} = (1 - d_{OOP})F_i \qquad \text{for } i = y1, y2, max \tag{I.2-11}$$

The damage variable d_{OOP}, equal to 0.45, according to the analytical model previously described is assumed constant for all levels of shear forces acting on the connections. Of course, this is an approximation, since the shear strength degradation of the connection should be lower for smaller shear forces, as it influences the value of the withdrawal force. Despite this aspect, the assumed simplification can be considered acceptable, since it affects only small amplitude cycles.

Figure I.2-24 to Figure I.2-26 show the results obtained with the constitutive law including damage, Equation (*I.2-11*) (marked with tag "Dmg"), compared with the experimental tests and the reference model outcomes.

As expected, for small amplitude cycles (i.e. the violet region), the reference model captures better the experimental response both at the global and local level (i.e. force-displacement curve and cumulative energy, as well as uplift and slip displacements), proving that in this region the out-of-plane effect is negligible; the response obtained with Dmg model can however still be considered acceptable. On the contrary, for medium and high amplitude cycles (i.e. yellow and green region), only the results obtained with the damaged constitutive law are in excellent agreement with the experimental ones, both at the local and at the global level, except for the cumulative energy in wall I.3.

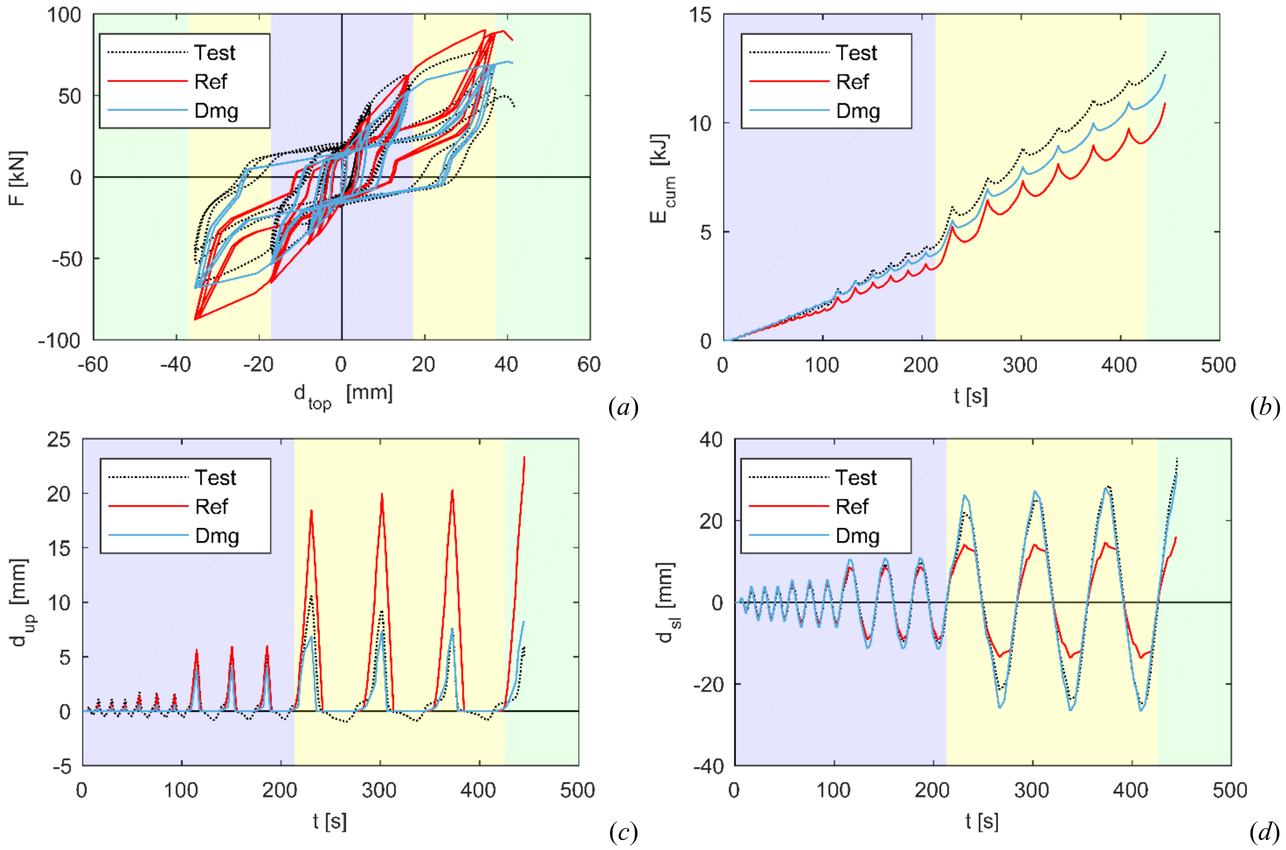

Figure I.2-24– Wall I.1. Results including the damaged law for angle brackets: (*a*) force-displacement curve; (*b*) cumulative energy; (*c*) uplift displacement; (*d*) slip displacement.

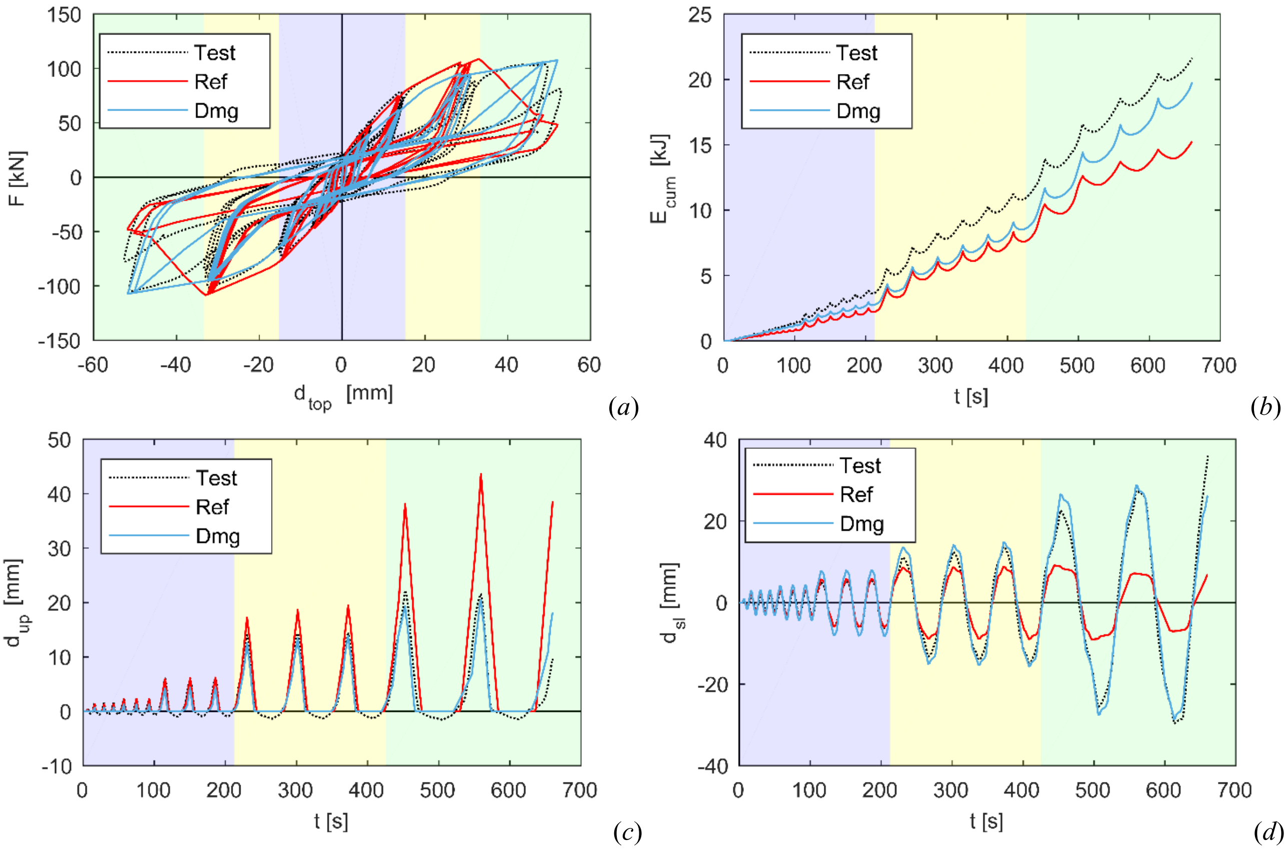

(*a*) (*b*) (*c*) (*d*)

Figure I.2-25 – Wall I.2. Results including the damaged law for angle brackets: (*a*) force-displacement curve; (*b*) cumulative energy; (*c*) uplift displacement; (*d*) slip displacement.

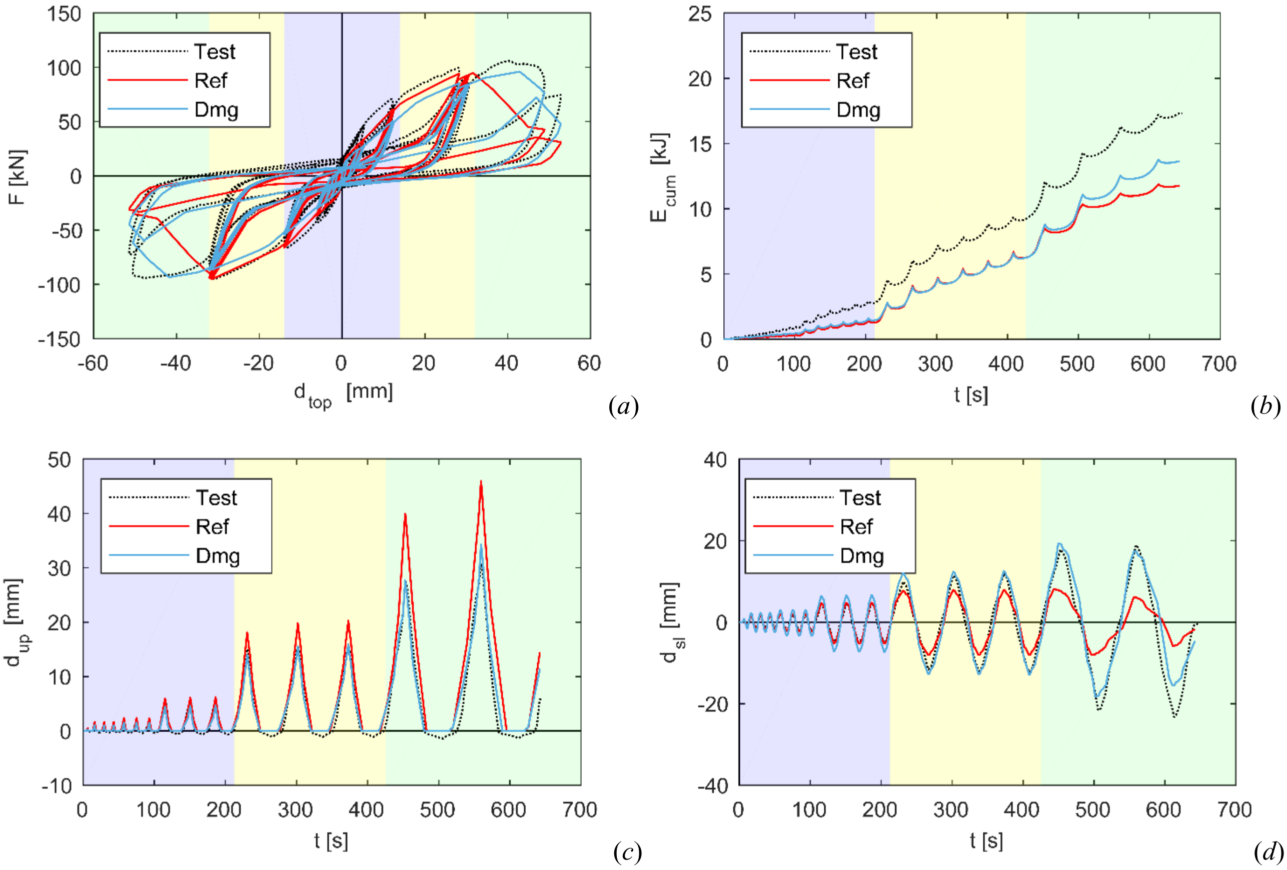

(*a*) (*b*) (*c*) (*d*)

Figure I.2-26 – Wall I.3. Results including the damaged law for angle brackets: (a) force-displacement curve; (b) cumulative energy; (c) uplift displacement; (d) slip displacement.

I.3 Phenomenological modelling approach

Abstract

Between the two modelling approaches mainly used to study the seismic behavior of CLT multi-storey buildings, namely component-level and phenomenological, the latter one is the most promising for practitioners thanks to its easiness. In this Section phenomenological numerical modelling approach will be critically analyzed highlighting its potentialities and drawbacks. The aim is to gain a deeper insight both in the seismic behaviour of CLT superstructures and in modelling strategies to be adopted within this modelling approach in order to guarantee the maximum reliability of results. The study has been conducted adopting both linear and non-linear plane analyses. Strategies and ploys to create both linear and non-linear phenomenological models are described in depth. In the first case, a parametric linear spectral analysis on a reference multi-storey CLT building has been carried out, while for non-linear analyses the cyclic behavior of CLT wall systems tested at CNR-IVALSA within the SOFIE project has been numerically reproduced. For linear analysis equivalent modulus of elasticity able to reproduce the same dynamic behavior of linear component-level models studied in Section I.2.3.2 have been derived, allowing to obtain a modelling approach that is at the same time reliable and easy to use for practitioners. Non-linear phenomenological models have been calibrated in order to fit both force-displacement and cumulative energy over time curves of CLT wall systems taken as reference structures. Results showed that models can predict very well the cyclic behavior of these structures, demonstrating that phenomenological non-linear approach is promising both for practitioners that want to design CLT multi storey buildings with a quite refined model and for researchers.

Some parts of this section are included in L. Pozza, M. Savoia, L. Franco, A. Saetta, D. Talledo, Effect of different modelling approaches on the prediction of the seismic response of multi-storey CLT buildings, Int. J. Comput. Methods Exp. Meas. 5 (2017) 953–965. doi:10.2495/CMEM-V5-N6-953-965

I.3.1 Chapter contents

The current Section firstly provides a description of the state-of-the-art of *phenomenological* modelling strategy for the prediction of the seismic response of multi-storey CLT buildings (Section I.3.2), analyzing peculiarities, advantages and drawbacks. A deep focus on *linear* (Section I.3.3) and *non-linear* (Section I.3.4) phenomenological modelling approaches is then given. Their outcomes will then be analyzed and compared in order to define advantages and limits of the modelling strategy. The study has been conducted on references structures already shown in Section I.2.3.1 and I.2.4.1 respectively for linear and non-linear analyses.

I.3.2 Modelling strategy description

Phenomenological modelling approach reproduces the global behavior of the CLT wall system (i.e. force-displacement curve and cumulative energy over time of the entire CLT wall system) disregarding the behaviour of its components (i.e. panels and connections). It is intended to reproduce the response of the whole wall system or building using the global experimental force-displacement curve to calibrate the model. The advantages of the phenomenological approach mainly concern the simplicity and the possibility of modelling the behavior of the wall by using global parameters, whose calibration will include all the phenomena involved, like friction between the components and at the boundary interface, as well as secondary effects that cannot be evaluated by tests on the individual components. Moreover, global tests on the whole wall are enough to calibrate the numerical model, without the need for testing every individual component, and it is worth noting that tests on timber structures can be easily performed thanks to specimen low weight and loading forces if compared to traditional building materials. The main drawback of the phenomenological approach is the representativeness of the model, that is limited to the wall configuration used to calibrate the model. Therefore, it is not suitable to study structural systems composed of walls with different geometrical configurations or connection arrangements or subject to very different loading conditions. Examples of phenomenological modelling of timber construction systems are given in [83, 104, 140, 189].

Linear phenomenological models, usually adopted by practitioners, are carried out through the definition of an *equivalent modulus of elasticity* to be assigned to walls, so that the displacement obtained from the model equals the ones obtained from experimental tests or advanced analyses.

Non-linear phenomenological models, usually adopted by researchers, require the numerical outcome to fit the force-displacement curve and the hysteretic behaviour of the wall (e.g. global energy dissipation over time curve).

I.3.3 Linear analysis

In this Section the linear phenomenological modelling strategy is analyzed. The elastic plane model (Figure I.3-1) has been created with the purpose of reproducing the dynamic seismic behavior of a multi-storey CLT wall system without modelling the connections. To obtain this, an equivalent modulus of elasticity E_{eq} of the CLT panel has been derived through an optimization procedure that aims at minimizing the difference, in terms of mean square errors, of the ULS horizontal story displacements obtained respectively with the linear component-level (Section I.2.3.2) and phenomenological models. Actually, the latter modelling strategy is more refined than the phenomenological, therefore the results obtained from component-level models can be considered as a reference.

Spectral analyses were carried out for all the configurations considered in the parametric study, and results in terms principal elastic periods (T_1), forces on connections (v and N) and inter-storey drifts (d_{i-s}) and inter-storey slip displacement (d_{sl}) are shown in the following. The resulting values of the equivalent modulus of elasticity times the wall thickness $E_{eq} \cdot t$ are reported in Table I.3-1. The equivalent modules represent a useful reference for practitioners who want to adopt a phenomenological approach taking advantage of its simplicity and computational efficiency. From the obtained values it is possible to observe that the parameter $E_{eq} \cdot t$ increases with the number of storeys of the building and with the seismic intensity, and it is higher for lower floors while it decreases for the upper ones.

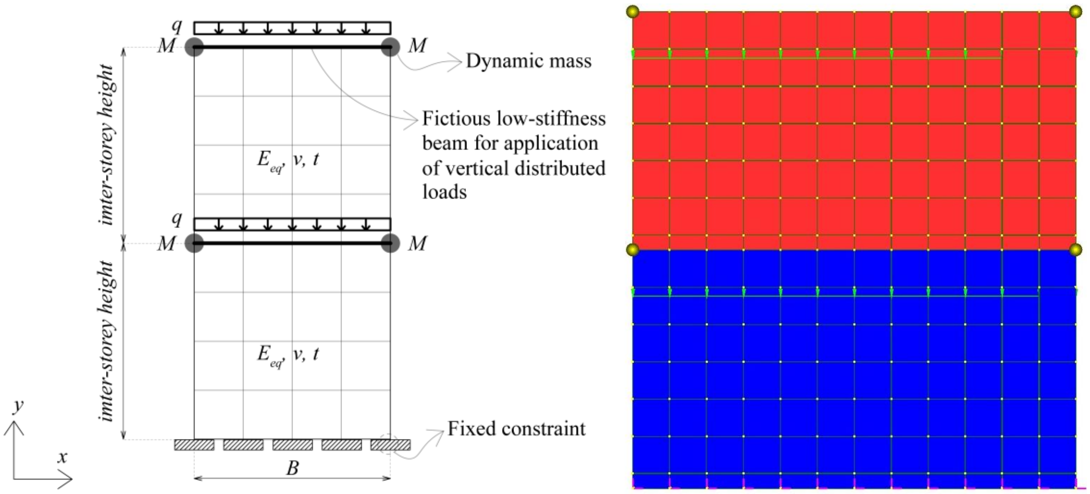

(*a*) (*b*)

Figure I.3-1 – Phenomenological linear model: (*a*) schematic representation and (*b*) pictures of the finite element model for the 2-storey building configuration.

Table I.3-1 – Equivalent modulus of elasticity for walls of phenomenological model for each configuration and increasing level of PGA.

PGA	$E_{eq} \cdot t$ *[N/mm]*	*level 1*	*level 2*	*level 3*	*level 4*	*level 5*	*level 6*
0.15g	*2-storey*	5.00E+04	4.00E+04				
	4-storey	1.15E+05	8.64E+04	7.20E+04	5.76E+04		
	6-storey	1.80E+05	2.40E+05	2.08E+05	1.56E+05	1.30E+05	5.60E+04
0.25g	*2-storey*	7.50E+04	7.60E+04				
	4-storey	1.60E+05	1.44E+05	1.20E+05	1.04E+05		
	6-storey	2.50E+05	3.00E+05	2.56E+05	1.92E+05	1.60E+05	1.04E+05
0.35g	*2-storey*	9.00E+04	8.80E+04				
	4-storey	1.92E+05	1.56E+05	1.40E+05	1.20E+05		
	6-storey	3.00E+05	3.00E+05	2.56E+05	2.04E+05	1.80E+05	1.52E+05

From the analysis of the results of the first vibration period T_1 (Table I.3-2) it is possible to observe that, similarly to what has been observed for linear component-level approach (Section I.2.3.2), the prediction by EC8 underestimates the value of the principal elastic period T_1, that results more than twice bigger in the numerical outcomes, and the gap between numerical and Eurocode values increments for lower seismic intensity of the site and with higher number of storeys of the building. The reasons of this discrepancy are the same seen for linear component-model (Section I.2.3.2).

As expected, it is possible to observe that the base shear per unity of length v and uplift forces N increase both incrementing the seismic intensity and the number of story (Table I.3-3).

Table I.3-2 – First period T_1 for each analyzed building configuration.

T_1		*PGA=0.15 g*		*PGA=0.25 g*		*PGA=0.35 g*
[s]	*EC8*	*Phenomenological*	*EC8*	*Phenomenological*	*EC8*	*Phenomenological*
2-storey	0.20	0.76	0.20	0.59	0.20	0.54
4-storey	0.34	1.30	0.34	1.05	0.34	0.98
6-storey	0.46	1.81	0.46	1.58	0.46	1.50

Table I.3-3 – Base shear forces per unit of length v and base uplift force N for each analyzed building configuration.

Forces at the base	*PGA=0.15 g*		*PGA=0.25 g*		*PGA=0.35 g*	
	v [kN/m]	*N* [kN]	*v* [kN/m]	*N* [kN]	*v* [kN/m]	*N* [kN]
2-storey	15.16	34.03	32.21	170.65	48.08	318.37
4-storey	22.12	64.17	45.36	329.23	66.20	610.03
6-storey	23.61	110.59	49.10	477.38	80.33	863.16

In Table I.3-4 the maximum inter-storey drift $d_{i-s,max}$ and the maximum sliding inter-storey slip displacements $d_{sl,max}$ have been derived and analyzed. The slip displacements d_{sl} have been derived accordingly to Equation (I.2-1) where the uplift rotation of the CLT panel φ has been calculated as the mean rotation value of each node of the plate element of the i-th storey. Similarly to what has been observed for linear component-level modelling strategy (Section I.2.3.2), the maximum inter-storey drift $d_{i-s,max}$ increments with the seismic intensity and the number of storeys of the building and the inter-storey slip displacement $d_{sl,max}$ decrements increasing the number of storeys. To have a deeper insight on the behavior of the sliding contribution between panels, its value d_{sl} is reported for each building configuration and each floor in Table I.3-5 - Table I.3-7. Also in this case it is possible to observe a decrease in the sliding d_{sl} for upper floors, but differently to what has been found for component-level linear model, upper floors tend to a zero value without a reversal of sign. The result is in accordance with the expected reduction of shear forces acting on CLT walls for upper floors. In all cases, the maximum value of the inter-storey slip $d_{sl,max}$ has been measured at the lower floor level, while the maximum value of the inter-storey drift $d_{i-s,max}$ has always been observed at the highest storey. Besides, the sliding contribution $d_{sl,max}$ is much lower than the inter-storey drift global value $d_{i-s,max}$, which means that most part of the lateral deformation of CLT shear wall is due to uplift forces rather than to shear forces transmitted between upper and lower panels, and the rocking contribution increases for upward floors.

Table I.3-4 – Maximum percentage inter-storey drift d_{max} and inter-storey sliding displacement $d_{sl,max}$ for each analyzed building configuration.

Maximum inter-storey displacements	*PGA=0.15 g*		*PGA=0.25 g*		*PGA=0.35 g*	
	$d_{i-s,max}$	$d_{sl,max}$	$d_{i-s,max}$	$d_{sl,max}$	$d_{i-s,max}$	$d_{sl,max}$
2-storey	0.14%	0.09%	0.32%	0.13%	0.33%	0.13%
4-storey	0.23%	0.06%	0.45%	0.09%	0.46%	0.09%
6-storey	0.26%	0.05%	0.53%	0.07%	0.55%	0.07%

Table I.3-5 – Inter-storey sliding displacement d_{sl} *of 2-storey building with maximum values underlined.*

	δ_{sl} - 2-storey building configuration		
Floor level	*PGA=0.15 g*	*PGA=0.25 g*	*PGA=0.35 g*
Storey n° 1	**0.09%**	**0.13%**	**0.13%**
Storey n° 2	-0.04%	0.04%	0.06%

Table I.3-6 – Inter-storey sliding displacement d_{sl} *of 4-storey building with maximum values underlined.*

	δ_{sl} - *4-storey building configuration*		
Floor level	*PGA=0.15 g*	*PGA=0.25 g*	*PGA=0.35 g*
Storey n° 1	**0.06%**	**0.09%**	**0.09%**
Storey n° 2	0.02%	0.04%	0.05%
Storey n° 3	0.01%	0.03%	0.03%
Storey n° 4	0.00%	0.02%	0.03%

Table I.3-7– Inter-storey sliding displacement d_{sl} *of 6-storey building with maximum values underlined.*

	δ_{sl} - *6-storey building configuration*		
Floor level	*PGA=0.15 g*	*PGA=0.25 g*	*PGA=0.35 g*
Storey n° 1	**0.05%**	**0.07%**	**0.07%**
Storey n° 2	0.01%	0.03%	0.03%
Storey n° 3	0.01%	0.02%	0.03%
Storey n° 4	0.01%	0.02%	0.02%
Storey n° 5	0.00%	0.00%	0.00%
Storey n° 6	0.01%	0.00%	0.00%

I.3.4 Non-linear analysis

In this Section non-linear phenomenological modelling strategy is analyzed. The CLT shear-wall, where a hinge- and a slider-type constraint are assigned respectively to the left and the right base node, has been modelled as a plane lattice grid with truss finite elements with non-linear diagonals (Figure I.3-2).

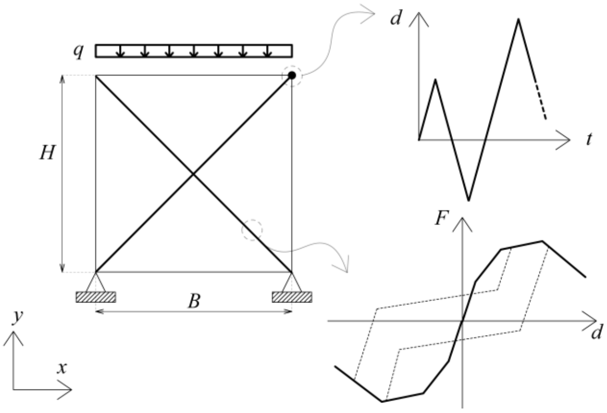

Figure I.3-2 – Schematic representation of non-linear phenomenological model.

The cyclic load history d_{top} derived in Section I.2.4.1.3.2 from the experimental survey carried out at CNR-IVALSA [77] has been assigned to the top right node. The non-linear Pinching4 constitutive model available in OpenSees framework [219] was adopted for non-linear diagonals and has been gauged so that the numerical model can represent with a good approximation the experimental CLT shear wall global behavior, optimizing the shape of the backbone envelope and minimizing the difference between numerical and experimental dissipated energy. It is important noticing that experimental force-displacement charts may present asymmetrical patterns between positive and negative displacement field. Nevertheless, the non-linear diagonals have been modelled with a symmetrical constitutive law since asymmetry in the behavior of CLT walls is attributable to stochastic errors that should not be systematically included into a numerical model.

Results (Figure I.3-3-Figure I.3-5) show a very good matching between numerical and experimental results both for force-displacement curve and cumulative energy over time. It can only be pointed out a slight underestimation (with 7 %) and overestimation (with 15 %) of cumulative energy for respectively little and great loading cycles.

It is worth noting that the phenomenological model is able to take into account for the out-of-plane behavior of the tested panel (Section I.2.4.1.2) without requiring additional expedients like it has been necessary for component-level approach (I.2.4.2.5). Phenomenological model is therefore able to faithfully represent the global response of the wall, also confirming the capability of the Pinching4 constitutive law [219] in representing the CLT shear-walls cyclic response.

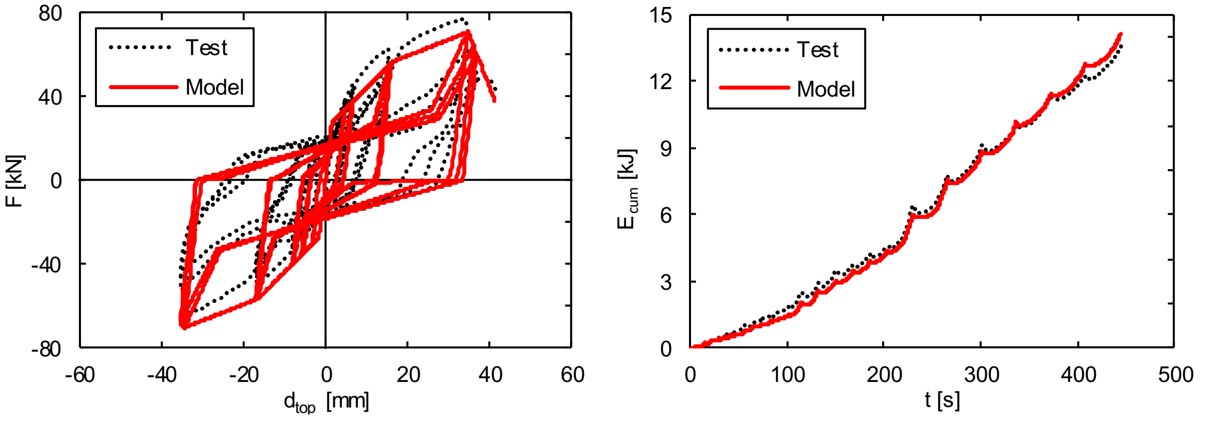

(*a*) (*b*)

Figure I.3-3 – Comparison between numerical and experimental results of phenomenological non-linear model in terms of (*a*) force-displacement and (*b*) cumulative energy curves for wall I.1 tested at CNR-IVALSA [77].

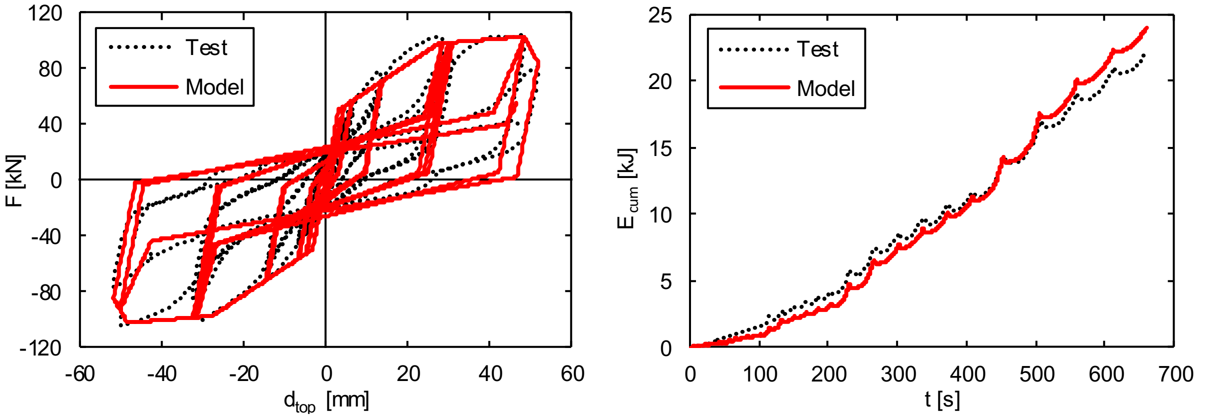

(*a*) (*b*)

Figure I.3-4 – Comparison between numerical and experimental results of phenomenological non-linear model in terms of (*a*) force-displacement and (*b*) cumulative energy curves for wall I.2 tested at CNR-IVALSA [77].

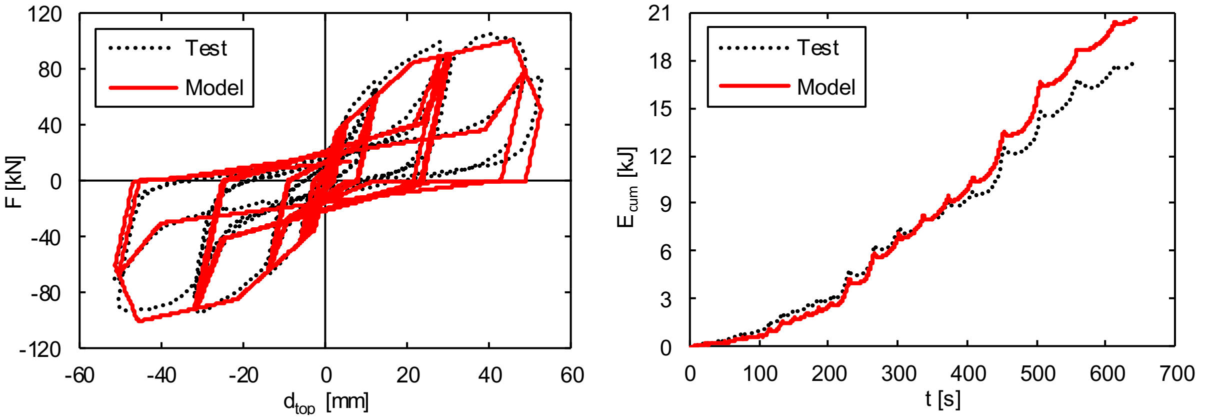

(*a*) (*b*)

Figure I.3-5 – Comparison between numerical and experimental results of phenomenological non-linear model in terms of (*a*) force-displacement and (*b*) cumulative energy curves for wall I.3 tested at CNR-IVALSA [77].

I.4 Conclusions on numerical modelling strategies for CLT buildings

Abstract

This Section reports a summary of the main findings about numerical modelling strategies for CLT buildings discussed in the first Part of the thesis. Advantages and drawbacks on the adoption of component-level or phenomenological modelling approaches have firstly been discussed. The choice whether to use the one or the other approach depends on the scope: while the latter is easier, the former one is preferable for buildings with many different wall configurations. A comparison between component-level and phenomenological linear models has been then carried out, showing that the latter overestimates uplift forces, hence caution must be paid if this modelling strategy is used to design connections of CLT walls subjected to uplift mechanism. The principal period of the analyzed building obtained from linear numerical models has been compared with the value assessed by Eurocode 8, showing a high discrepancy and highlighting therefore the need for a revision of codes provisions for CLT buildings. From linear dynamic simulations it has also been observed that the lateral deformability may be the dimensioning parameter for CLT multi-storey buildings in seismic-prone areas. From a comparison between non-linear models it resulted that phenomenological approach can fit better the cumulative energy but, on the other hand, component-level approach can predict with more accuracy the force-displacement behavior of CLT wall systems. Finally, it has been remarked that component-level approach gives reliable results as long as the tests on single components used for calibration reflect their behavior in the global wall system, otherwise strategies to adapt their constitutive law to their actual behavior must be adopted.

I.4.1 Chapter contents

In this first Part of the Thesis modelling strategies for CLT shear walls have been deeply analyzed. In particular, for the two most common modelling approaches used by researchers and practitioners, namely component-level and phenomenological ones respectively analyzed in Section I.2 and Section I.3, the main aspects relating linear and non-linear modelling have been investigated. This Chapter reports a summary of the main findings and a comparison between the results obtained with the two modelling approaches. Section I.4.2 reports a comparison between component level, phenomenological and hybrid modelling approaches in order to identify advantages and drawbacks. Section I.4.3 compares results between linear models, while in Section I.4.4 a comparison between the results of non-linear models is shown.

I.4.2 Comparison between component level, phenomenological and hybrid modelling approaches

A comparison between component-level (Section I.2) and phenomenological (Section I.3) approaches is carried out in order to highlight advantages and drawbacks of each (Table I.4-1). Also hybrid approach (see Section I.1.4.1) is reported for completeness.

Component-level numerical models are the most complex to create, calibrate and use between the three approaches, but they are the most powerful ones since they allow to analyze every configuration of CLT walls regardless of geometrical configurations, connections arrangements and vertical loads acting on them. They can also take into account for friction forces if the model includes contact elements with frictions laws such as the Coulomb one. They can also include secondary order effects, like out-of-plane movements of the laterally-loaded wall system, if expedients are implemented within the laws that define the behavior of components, for example by scaling the constitutive laws of connections like has been seen in Section I.2.4.2.5.

Phenomenological models are easier to use than component-level ones and they usually are less-time consuming. They anyway suffer of strong limitations respect to component-level modelling, mainly represented by the fact that numerical outcomes are bound to a specific configuration of the wall system used to calibrate the model, therefore this approach is suitable only to analyse CLT buildings with a modular repetition CLT walls with same arrangement of connections and vertical loads. If buildings with heterogeneous panel geometries or connections arrangements have to be numerically analysed, component-level modelling approach is the most suitable for the purpose.

Hybrid modelling approach offer the same potentialities of phenomenological models but with slightly higher difficulty of usage, therefore it has not been dealt with in this work.

Table I.4-1 – Comparison between component-level phenomenological and hybrid modelling approaches in terms of advantages and drawbacks.

Advantages	*Component-level*	*Phenomenological*	*Hybrid*
Independence from geometrical configuration	✓	✗	✗
Independence from connection's arrangement	✓	✗	✗
Independence from vertical load	✓	✗	✗
Inclusion of friction forces	✓	✓	✓
Inclusion of second order effects	✓*	✓	✓
Easiness	✗	✓	✓**

** Strategies to take into account for second order effects are necessary, see Section I.2.4.2.5.*

*** Intermediate easiness between component-level and phenomenological approaches*

I.4.3 Comparison between linear models

A comparison between results of linear analyses carried out with respectively component-level (Section I.2.3.2) and phenomenological (Section I.3.3) modelling approaches is carried out in the following. All the fundamental parameters to describe the dynamic behavior of the analyzed structures have been considered and critically analyzed, namely fundamental period T_1 (Figure I.4-1), inter-storey drift $d_{i-s,max}$ (Figure I.4-2), base shear per unity of length v (Figure I.4-3) and uplift forces N (Figure I.4-4). Comparisons have been performed both (i) to the vary of the number of storeys of the building (2, 4 and 6-storeys) considering the maximum seismic intensity (PGA=0.35 g), and (ii) to the vary of seismic intensity for the 6-storey building configuration. Results to the vary of building configuration for the other two values of PGA and to the vary of PGA for the other two building configurations are herein omitted for sake of brevity since the conclusions that can be drawn are the same.

For all the parameters it is possible to observe a very good agreement between the two modelling approaches, except for uplift forces N. For component-level approach, uplift forces are read from the internal force of the model element that represents the connection. On the other hand, for phenomenological models this value is obtained by integration of tensile stresses at the edge of the wall. Hence, the lever arm between uplift and compression forces at the CLT panel bottom interface is lower in the case of phenomenological approach (a) respect to the component-level one (A), as shown in Figure I.4-5. For this reason, to withstand the same horizontal seismic force, phenomenological approach has to exert a greater uplift force respect to the component-level one to resist rocking mechanism. Caution should therefore be paid in the design of connections when a phenomenological approach is adopted, since uplift forces tend to be overestimated.

Comparison in terms of principal elastic period T_1 (Figure I.4-1) show a very good agreement between the two strategies for all the building configurations and the seismic intensities, confirming the fact that the assumption of an equivalent modulus of elasticity E_{eq} can perfectly assess the dynamic behavior of multi-storey timber structures. Red bars on histograms highlight the big gap between the analytical provision of the principal elastic period given by Eurocode 8 [111] and the actual obtained values. This fact emphasizes on one hand the necessity of a review of the formulation given by Eurocodes to derive T_1 for multi-storey CLT buildings, and on the other hand the need to properly assess the stiffness of connections to correctly derive the values of fundamental vibration period. The percentage gap between T_1 predicted by EC8 and the one assessed through numerical models increase with the number of storeys of CLT buildings, while it decreases with the seismic intensity. For all the building configurations numerically analyzed with a seismic intensity PGA=0.35 g, the fundamental period T_1 falls over the spectral *plateau* ($T_1 > T_C$), with the difference $T_1 - T_C$ that increases with the number of storeys of the building, while Eurocode provisions on the other hand give a dynamic behavior into the constant spectral acceleration branch ($T_B < T_1 < T_C$). This means that high CLT multi-storey buildings benefit from reduced induced seismic action given a seismic intensity of the site (PGA), but their global deformation increases, therefore lateral deflection of higher CLT buildings may be the dimensioning key-parameter for this kind of structures. This supposition is also confirmed giving a look at maximum inter-storey drifts $d_{i-s,max}$ (Figure I.4-2), where it is possible to notice that higher CLT multi-storey buildings in seismic-prone areas with higher PGAs can exceed the inter-storey drift limit of 5 ‰ imposed by EC8 [111]. Red columns on histograms of Figure I.4-2 represent the slip contribution $d_{sl,max}$ to inter-storey drift, and it is possible to observe that its percentage contribution on the total maximum measured inter-storey drift displacement $d_{i-s,max}$ increments decreasing the number of storeys but it is anyway an exiguous value.

In conclusion, it is worth noting that lateral flexibility of CLT multi-storey buildings can be the dimensioning factor, since the maximum lateral displacement allowed by EC8 [111] can be exceeded. It is therefore paramount to carry out more studies on seismic drift demand on multi-storey CLT buildings, similarly to investigations presented by Demirci *et al.* [226] that provided formulas to derive inter-storey and maximum roof drifts to the vary of joint density, building aspect ratio, behaviour factor, principal period of the structure and frequency content of the earthquake action.

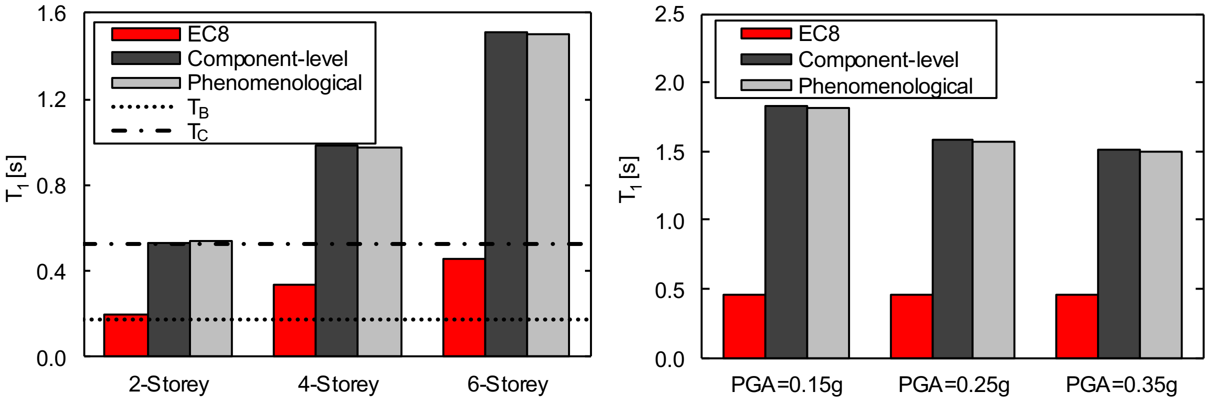

🟥	0.20	0.34	0.46
⬛	0.53	0.98	1.51
⬜	0.54	0.98	1.50

(*a*)

🟥	0.46	0.46	0.46
⬛	1.83	1.59	1.51
⬜	1.81	1.58	1.50

(*b*)

Figure I.4-1 – Comparison between linear modelling strategies in terms of principal elastic period T_1 (*a*) to the vary of building configuration for PGA=0.35 g and (*b*) to the vary of PGA level for 6-storey building configuration, with T_B and T_C respectively lower and upper limits of the constant spectral acceleration.

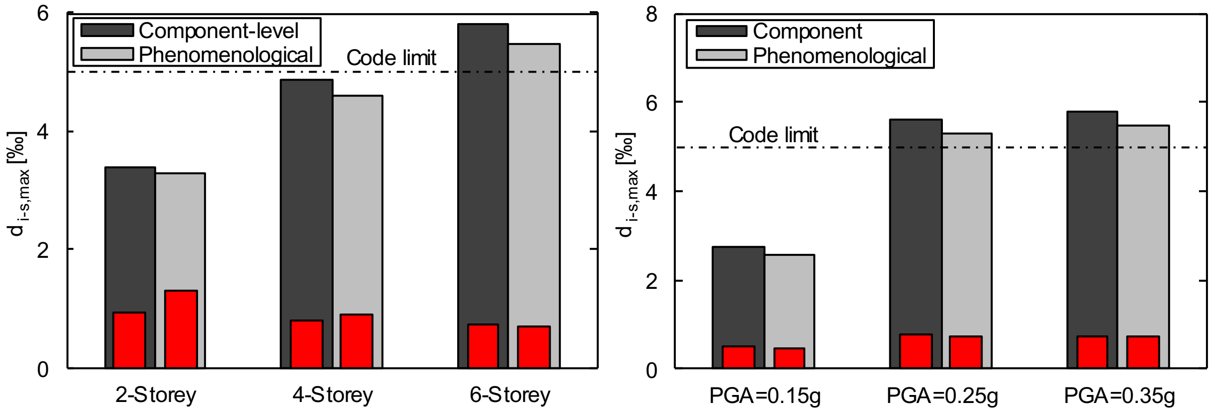

⬛	3.40	4.86	5.81
	0.93	*0.81*	*0.73*
⬜	3.30	4.61	5.46
	1.30	*0.90*	*0.71*

(*a*)

⬛	2.74	5.61	5.81
	0.49	*0.75*	*0.73*
⬜	2.58	5.29	5.46
	0.46	*0.73*	*0.71*

(*b*)

Figure I.4-2 – Comparison between linear modelling strategies in terms of maximum inter-storey drift $d_{i\text{-}s,max}$ (*a*) to the vary of building configuration for PGA=0.35 g and (*b*) to the vary of PGA level for 6-storey building configuration. Red bars of histograms and underlined italic values on tables represent the sliding contribution $d_{sl,max}$.

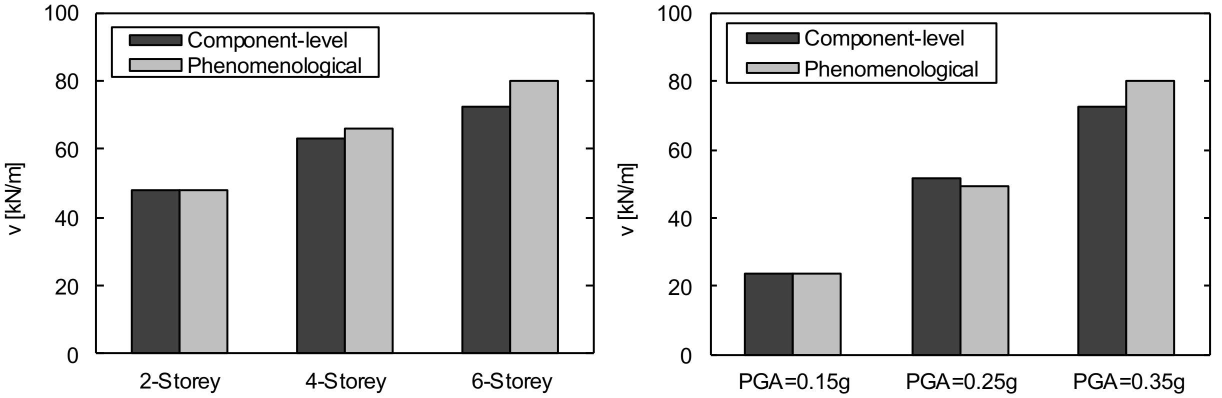

	2-Storey	4-Storey	6-Storey
■	48.22	62.96	72.60
□	48.08	66.20	80.33

(*a*)

	PGA=0.15g	PGA=0.25g	PGA=0.35g
■	23.96	51.82	72.60
□	23.61	49.10	80.33

(*b*)

Figure I.4-3 – Comparison between linear modelling strategies in terms of base shear per unity of length *v* (*a*) to the vary of building configuration for PGA=0.35 g and (*b*) to the vary of PGA level for 6-storey building configuration.

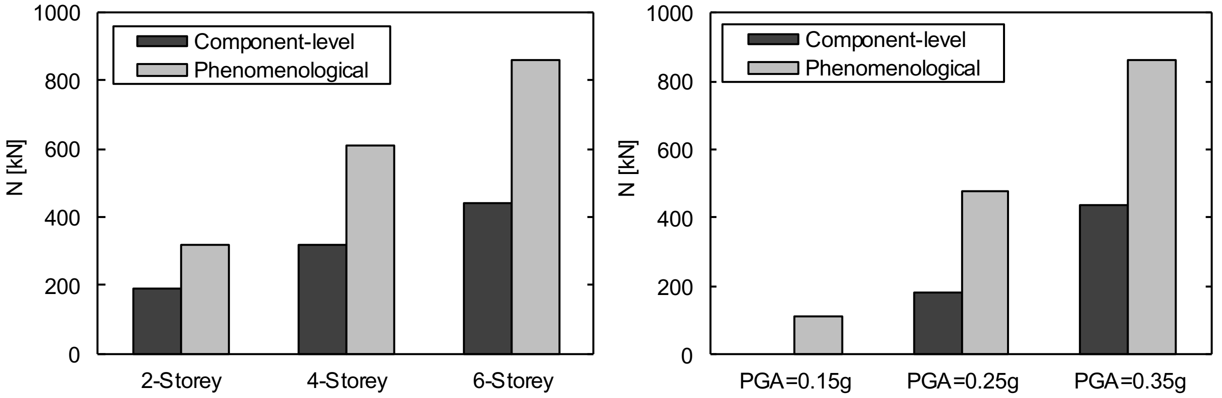

	2-Storey	4-Storey	6-Storey
■	191.28	320.02	438.88
□	318.37	610.03	863.16

(*a*)

	PGA=0.15g	PGA=0.25g	PGA=0.35g
■	0.00	179.47	438.88
□	110.59	477.38	863.16

(*b*)

Figure I.4-4 – Comparison between linear modelling strategies in terms of uplift force *N* (*a*) to the vary of building configuration for PGA=0.35 g and (*b*) to the vary of PGA level for 6-storey building configuration.

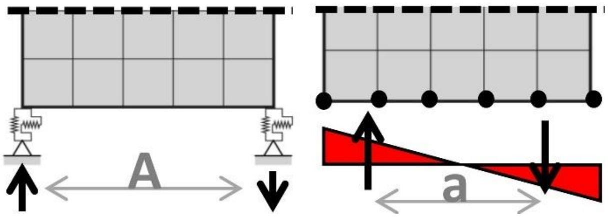

(*a*)

(*b*)

Figure I.4-5 – Comparison between linear modelling strategies in terms of uplift force *N* (*a*) to the vary of building configuration for PGA=0.35 g and (*b*) to the vary of PGA level for 6-storey building configuration (*image credits*: presentation at TSE 2017 by L. Pozza *et al.* [191]).

I.4.4 Comparison between non-linear models

The main findings of the investigations carried out on non-linear component-level (Section I.2.4.2) and phenomenological (Section I.3.4) modelling approaches and a comparison between them is presented in the following.

Analyses carried out on non-linear component-level approach showed that only by correctly modelling the local mechanical behavior of connections, taking into account for their actual failure modes and deformations in the global structure, it is possible to obtain a reliable numerical prediction of the structural response of CLT wall systems. Component-level approach requires an accurate comprehension of all the characteristics of the connection system because of the sensitivity of this approach to the numerical calibration of constitutive laws of its components. It can actually happen that the connection inserted in the global CLT wall system shows a different behavior from the one observed during tests carried out on the single connection. For instance, the wall system could develop out-of-plane displacement when subjected to lateral loads, as in the SOFIE project cyclic tests on CLT walls, and as a consequence also connections are subjected to out-of-plane movements. Anyway, tests carried out on single connections, usually adopted as reference to calibrate the components of the numerical model, do not develop out-of-plane displacements, as for connections tests of SOFIE project. The component-level model must take into account for this incongruity of behavior when the connections are calibrated, otherwise the simulation will give unreliable and misleading results, especially in the prediction of local uplift and slip displacements, as evidenced by the sensitivity analyses carried out in this work. In other words, component-level approach gives reliable results as long as the tests on single components used for calibration reflect their behavior in the global wall system [227]. If it does not happen, strategies to adapt the constitutive law of components to their actual behavior in the global system must be adopted. It has been shown that a simple damage model that takes into account the reduced strength in angle brackets due to out-of-plane movements can be effectively used to model this phenomenon.

On the other hand, phenomenological non-linear approach is able to take into account for friction and second-order effects without requiring any specific strategy, since the global behavior of the model is not function of local mechanisms at component level, but the global law is already calibrated to take into account for all the phenomena that govern the wall system behavior. Anyway, despite simplicity, the representativeness of results is only limited to the wall configuration used for calibration.

Therefore, both models can predict global behavior in terms of force-displacement curve and cumulative energy with excellent results, but which approach is the best choice to be adopted on the seismic analysis of a CLT building depends on the purpose. If a modular building has to be studied, phenomenological could be the right choice for easiness, while for with a lot of CLT wall system configurations (both in shapes and connections type and arrangement) a more general component-level approach could be preferable.

Comparison between the results obtained from the two different modelling strategies show that, for all the three analyzed wall system configurations, phenomenological approach can fit better cumulative energy (Figure I.4-6.b), but on the other hand component-level approach can predict with more accuracy the force-displacement curve (Figure I.4-6.a).

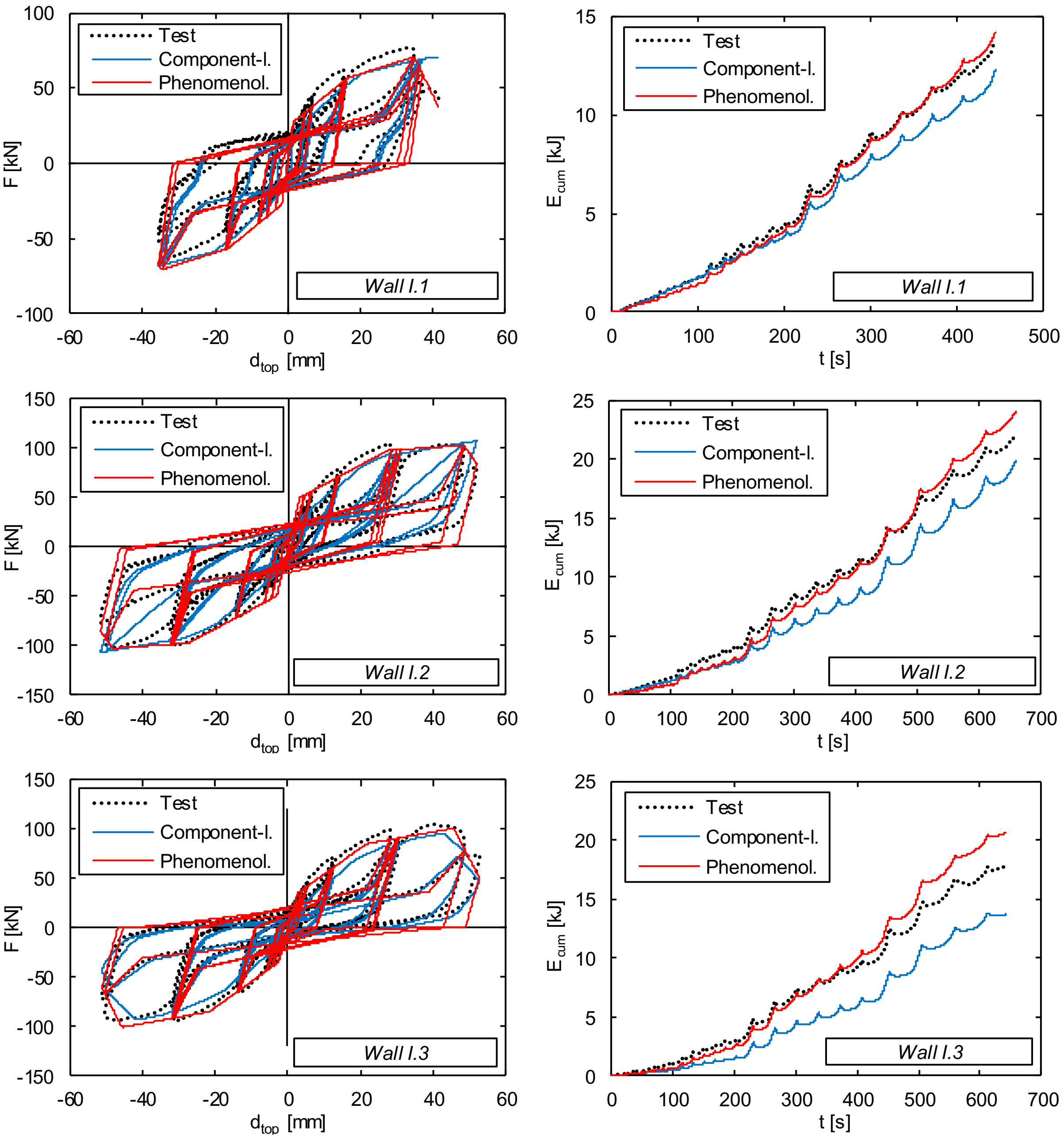

(*a*) (*b*)

Figure I.4-6 – Comparison between non-linear modelling strategies in terms of (*a*) force-displacement and (*b*) cumulative energy curves for CLT wall system configurations I.1, I.2 and I.3 tested at CNR-IVALSA [77].

Bibliography of Part I

[1] S. Pei, J. Berman, D. Dolan, J. Van De Lindt, J. Ricles, R. Sause, H. Blomgren, M. Popovski, D. Rammer, Progress on the development of seismic resilient tall buildings in the Pacific Northwest, in: World Conf. Timber Eng. 2014, 2014.

[2] K. Fujita, T. Hanazato, I. Sakamoto, Earthquake response monitoring and seismic performanceof five-storied timber pagoda, in: 13 Th World Conf. Earthq. Eng., Vancouver, B.C., Canada, 2004.

[3] M. Piazza, R. Tomasi, R. Modena, Strutture in legno - Materiale, calcolo e progetto secondo le nuove normative europee, Biblioteca Tecnica Hoepli, 2005.

[4] K. Mahapatra, L. Gustavsson, Multi-storey timber buildings: breaking industry path dependency, Build. Res. Inf. 36 (2008) 638–648. doi:10.1080/09613210802386123.

[5] Italian Ministry of Infrastructure and Transport, Norme Tecniche per le Costruzioni 2008 (in Italian), Decreto Minist. Gazz. Uff. (2008).

[6] D.M.LL.PP. 09/01/1996: “Norme tecniche per il calcolo, l’esecuzione ed il collaudo delle strutture in cemento armato, normale e precompresso e per le strutture metalliche.” (in Italian), Italian Ministry of Public Works, 1996.

[7] A. Buchanan, B. Deam, M. Fragiacomo, S. Pampanin, A. Palermo, Multi-Storey Prestressed Timber Buildings in New Zealand, Struct. Eng. Int. 18 (2008) 166–173. doi:10.2749/101686608784218635.

[8] Institute for Research in Construction - National Research Council of Canada, National Building Code of Canada, (2015).

[9] International Code Council, International Building Code 2015, International Code Council, 2014.

[10] W. Pang, D. V. Rosowsky, S. Pei, J.W. van de Lindt, Simplified Direct Displacement Design of Six-Story Woodframe Building and Pretest Seismic Performance Assessment, J. Struct. Eng. 136 (2010) 813–825. doi:10.1061/(ASCE)ST.1943-541X.0000181.

[11] T. Harley, G. White, A. Dowdall, J. Bawcombe, A. Mcrobie, R. Steinke, Dalston Lane - The world’s tallest CLT building, in: WCTE 2016 - World Conf. Timber Eng., Vienna, Austria, 2016.

[12] A. Rauf, R.H. Crawford, The Effect of Material Service Life on the Life Cycle Embodied Energy of Multi-Unit Residential Buildings, in: World SB14, Barcelona, Spain, 2014.

[13] J.W.G.V. De Kuilen, A. Ceccotti, Z. Xia, M. He, Very Tall Wooden Buildings with Cross Laminated Timber, Procedia Eng. 14 (2011) 1621–1628. doi:10.1016/j.proeng.2011.07.204.

[14] I. Sustersic, M. Fragiacomo, B. Dujic, Seismic Analysis of Cross-Laminated Multistory Timber Buildings Using Code-Prescribed Methods: Influence of Panel Size, Connection Ductility, and Schematization, J. Struct. Eng. 142 (2016). doi:10.1061/(ASCE)ST.1943-541X.0001344.

[15] Waugh Thistleton Architects Website, (2019). http://waughthistleton.com/dalston-works/.

[16] The possible website, (2019). https://www.the-possible.com/clt-high-rise-building-tall-with-engineered-timber/.

[17] R. Abrahamsen, Mjøstårnet-Construction of an 81 m tall timber building, in: Int. Holzbau-Forum - IHF 2017, Garmisch-Partenkirchen, Germany, 2017.

[18] R.B. Abrahamsen, K. Arne Malo, Structural design and assembly of “Treet” - A 14-storey timber residential building in Norway, in: World Conf. Timber Eng. 2014, Quebec, Canada, 2014.

[19] K.A. Malo, R.B. Abrahamsen, M.A. Bjertnæs, Some structural design issues of the 14-storey timber framed building “Treet” in Norway, Eur. J. Wood Wood Prod. 74 (2016) 407–424.

doi:10.1007/s00107-016-1022-5.

[20] W. Ferdous, Y. Bai, T.D. Ngo, A. Manalo, P. Mendis, New advancements, challenges and opportunities of multi-storey modular buildings – A state-of-the-art review, Eng. Struct. 183 (2019) 883–893. doi:10.1016/j.engstruct.2019.01.061.

[21] A. Asiz, I. Smith, Connection System of Massive Timber Elements Used in Horizontal Slabs of Hybrid Tall Buildings, J. Struct. Eng. 137 (2011) 1390–1393. doi:10.1061/(ASCE)ST.1943-541X.0000363.

[22] M. He, Z. Li, F. Lam, R. Ma, Z. Ma, Experimental Investigation on Lateral Performance of Timber-Steel Hybrid Shear Wall Systems, J. Struct. Eng. 140 (2014) 04014029. doi:10.1061/(ASCE)ST.1943-541X.0000855.

[23] R. Brandner, G. Flatscher, A. Ringhofer, G. Schickhofer, A. Thiel, Cross laminated timber (CLT): overview and development, Eur. J. Wood Wood Prod. 74 (2016) 331–351. doi:10.1007/s00107-015-0999-5.

[24] L. Muszynski, E. Hansen, S. Fernando, G. Schwarzmann, J. Rainer, Insights into the Global Cross-Laminated Timber Industry, Bioprod. Bus. 8 (2017) 77–92. doi:10.22382/bpb-2017-008.

[25] R. Brandner, Production and Technology of Cross Laminated Timber (CLT): A state-of-the-art Report, in: R. Harris, A. Ringhofer, G. Schickhofer (Eds.), Focus Solid Timber Solut. Conf. Cross Laminated Timber, The University of Bath, Bath, 2013.

[26] S. Aicher, M. Hirsch, Z. Christian, Hybrid cross-laminated timber plates with beech wood cross-layers, Constr. Build. Mater. 124 (2016) 1007–1018. doi:10.1016/j.conbuildmat.2016.08.051.

[27] V. Sebera, L. Muszyński, J. Tippner, M. Noyel, T. Pisaneschi, B. Sundberg, FE analysis of CLT panel subjected to torsion and verified by DIC, Mater. Struct. 48 (2015) 451–459. doi:10.1617/s11527-013-0195-1.

[28] R. Stürzenbecher, K. Hofstetter, J. Eberhardsteiner, Structural design of Cross Laminated Timber (CLT) by advanced plate theories, Compos. Sci. Technol. 70 (2010) 1368–1379. doi:10.1016/j.compscitech.2010.04.016.

[29] D. Ugalde, J.L. Almazán, H. Santa María, P. Guindos, Seismic protection technologies for timber structures: a review, Eur. J. Wood Wood Prod. 77 (2019) 173–194. doi:10.1007/s00107-019-01389-9.

[30] Moelven website, Moelven website, (2019). https://mediabank.moelven.com/mediaroom.html?keywords=Mjostarnet&company=MoelvenLimtre AS.

[31] D. Casagrande, P. Grossi, R. Tomasi, Shake table tests on a full-scale timber-frame building with gypsum fibre boards, Eur. J. Wood Wood Prod. 74 (2016) 425–442. doi:10.1007/s00107-016-1013-6.

[32] J.W. van de Lindt, S. Pei, S.E. Pryor, H. Shimizu, H. Isoda, Experimental Seismic Response of a Full-Scale Six-Story Light-Frame Wood Building, J. Struct. Eng. 136 (2010) 1262–1272. doi:10.1061/(ASCE)ST.1943-541X.0000222.

[33] A. Filiatrault, I.P. Christovasilis, A. Wanitkorkul, J.W. van de Lindt, Experimental Seismic Response of a Full-Scale Light-Frame Wood Building, J. Struct. Eng. 136 (2010) 246–254. doi:10.1061/(ASCE)ST.1943-541X.0000112.

[34] R. Tomasi, D. Casagrande, P. Grossi, T. Sartori, Shaking table tests on a three-storey timber building, Proc. Inst. Civ. Eng. - Struct. Build. 168 (2015) 853–867. doi:10.1680/jstbu.14.00026.

[35] R. Tomasi, T. Sartori, D. Casagrande, M. Piazza, Shaking Table Testing of a Full-Scale Prefabricated Three-Story Timber-Frame Building, J. Earthq. Eng. 19 (2015) 505–534. doi:10.1080/13632469.2014.974291.

[36] M. Follesa, M. Fragiacomo, M.P. Lauriola, A proposal for revision of the current timber part (Section 8) of Eurocode 8 Part 1, in: CIB-W18 Meet. 44, Alghero, Italy, 2011.

[37] D. Acar, Evolution and rationalization of timber frame design in Istanbul in the second half of the nineteenth century, J. Archit. Conserv. 23 (2017) 190–210. doi:10.1080/13556207.2017.1330384.

[38] R. Crocetti, M. Johansson, R. Kliger, H. Lidelöw, A. Mårtensson, B. Norlin, A. Pousette, Design of timber structures - Structural aspects of timber construction, 2:2016, Swedish Wood, Stockholm, Sweden, 2016.

[39] FPInnovations, CLT Handbook, Quebec, Canada, 2011.

[40] M. Li, F. Lam, Lateral Behaviour of Cross Laminated Timber Shear Walls under Reversed Cyclic Loads, in: Tenth Pacific Conf. Earthq. Eng., Sydney, Australia, 2015.

[41] S. Pei, J.W. van de Lindt, M. Popovski, Approximate R-Factor for Cross-Laminated Timber Walls in Multistory Buildings, J. Archit. Eng. 19 (2013) 245–255. doi:10.1061/(ASCE)AE.1943-5568.0000117.

[42] A. Ceccotti, M.P. Lauriola, M. Pinna, C. Sandhaas, SOFIE project - Cyclic tests on cross-laminated wooden panels, in: 9th World Conf. Timber Eng. 2006, Portland, Oregon, USA, 2006: pp. 805–812.

[43] G. Flatscher, K. Bratulic, G. Schickhofer, Experimental tests on cross-laminated timber joints and walls, Proc. Inst. Civ. Eng. - Struct. Build. 168 (2015) 868–877. doi:10.1680/stbu.13.00085.

[44] I. Gavric, G. Rinaldin, C. Amadio, M. Fragiacomo, A. Ceccotti, Experimental-numerical analyses of the seismic behaviour of cross-laminated wall systems, in: 15th World Conf. Earthq. Eng. WCEE 2012, Lisbon, Portugal, 2012.

[45] M. Popovski, I. Gavric, Performance of a 2-Story CLT House Subjected to Lateral Loads, J. Struct. Eng. 142 (2016) E4015006. doi:10.1061/(ASCE)ST.1943-541X.0001315.

[46] R. Tomasi, I. Smith, Experimental Characterization of Monotonic and Cyclic Loading Responses of CLT Panel-To-Foundation Angle Bracket Connections, J. Mater. Civ. Eng. 27 (2015) 04014189. doi:10.1061/(ASCE)MT.1943-5533.0001144.

[47] D. Casagrande, S. Rossi, T. Sartori, R. Tomasi, Proposal of an analytical procedure and a simplified numerical model for elastic response of single-storey timber shear-walls, Constr. Build. Mater. 102 (2016) 1101–1112. doi:10.1016/j.conbuildmat.2014.12.114.

[48] L. Pozza, R. Scotta, D. Trutalli, A. Polastri, I. Smith, Experimentally based q-factor estimation of cross-laminated timber walls, Proc. Inst. Civ. Eng. - Struct. Build. 169 (2016) 492–507. doi:10.1680/jstbu.15.00009.

[49] J.E. Martínez-Martínez, M. Alonso-Martínez, F.P.Á. Rabanal, J.J. del C. Díaz, Finite Element Analysis of Composite Laminated Timber (CLT), Proceedings. 2 (2018) 1454. doi:10.3390/proceedings2231454.

[50] T. Reynolds, D. Casagrande, R. Tomasi, Comparison of multi-storey cross-laminated timber and timber frame buildings by in situ modal analysis, Constr. Build. Mater. 102 (2016) 1009–1017. doi:10.1016/j.conbuildmat.2015.09.056.

[51] L. Pozza, Ductility and behaviour factor of wood structural systems. Theoretical and experimental development of a high ductility wood-concrete shearwall system, University of Padua, 2013. http://paduaresearch.cab.unipd.it/5637/.

[52] D. Trutalli, Insight into seismic behaviour of timber shear-wall systems, Università degli Studi di Padova, 2016. http://paduaresearch.cab.unipd.it/9143/.

[53] A. Ringhofer, R. Brandner, H.J. Blaß, Cross laminated timber (CLT): Design approaches for dowel-type fasteners and connections, Eng. Struct. 171 (2018) 849–861. doi:10.1016/j.engstruct.2018.05.032.

[54] M. Izzi, D. Casagrande, S. Bezzi, D. Pasca, M. Follesa, R. Tomasi, Seismic behaviour of Cross-Laminated Timber structures: A state-of-the-art review, Eng. Struct. 170 (2018) 42–52. doi:10.1016/j.engstruct.2018.05.060.

[55] Structural Timber Association, Cross-laminated timber construction - an introduction, 2015. http://www.structuraltimber.co.uk/assets/InformationCentre/eb11.pdf.

[56] A. Polastri, C. Loss, L. Pozza, I. Smith, CLT Buildings Laterally Braced With Core and Perimeter Walls, in: WCTE 2016 - World Conf. Timber Eng., Vienna, Austria, 2016.

[57] C.P. Devereux, T.J. Holden, A.H. Buchanan, S. Pampanin, NMIT Arts & Media Building - Damage Mitigation Using Post-tensioned Timber Walls, in: Ninth Pacific Conf. Earthq. Eng., Auckland, New Zealand, 2011.

[58] M.H. Ramage, H. Burridge, M. Busse-Wicher, G. Fereday, T. Reynolds, D.U. Shah, G. Wu, L. Yu, P. Fleming, D. Densley-Tingley, J. Allwood, P. Dupree, P.F. Linden, O. Scherman, The wood from the trees: The use of timber in construction, Renew. Sustain. Energy Rev. 68 (2017) 333–359. doi:10.1016/j.rser.2016.09.107.

[59] H.J. Blaß, C. Sandhaas, Timber Engineering - Principles for Design, KIT Scientific Publishing, 2017. doi:10.5445/KSP/1000069616.

[60] A. Klasson, R. Crocetti, The Effects on the Bracing Stiffness of Timber Structures of the Stiffness of Its Members, Structures. 19 (2019) 41–47. doi:10.1016/j.istruc.2018.12.003.

[61] J.M. Branco, T. Descamps, Analysis and strengthening of carpentry joints, Constr. Build. Mater. 97 (2015) 34–47. doi:10.1016/j.conbuildmat.2015.05.089.

[62] M. Ballerini, Sistemi di connessioni - Connessioni a gambo cilindrico, n.d.

[63] J.N. Karadelis, P. Brown, Punched metal plate timber fasteners under fatigue loading, Constr. Build. Mater. 14 (2000) 99–108. doi:10.1016/S0950-0618(00)00015-5.

[64] G. Tlustochowicz, E. Serrano, R. Steiger, State-of-the-art review on timber connections with glued-in steel rods, Mater. Struct. 44 (2011) 997–1020. doi:10.1617/s11527-010-9682-9.

[65] Weyerhaeuser website, (2015). https://www.weyerhaeuser.com/blog/the-built-up-column-conundrum/.

[66] K. Pintarič, M. Premrov, Mathematical modelling of timber-framed walls using fictive diagonal elements, Appl. Math. Model. 37 (2013) 8051–8059. doi:10.1016/j.apm.2013.02.050.

[67] Fastfix Website, (2018). https://www.fastenerandfixing.com/construction-fixings/heco-s-sustainable-connections/.

[68] M. Yurrita, J.M. Cabrero, P. Quenneville, Brittle failure in the parallel-to-grain direction of multiple shear softwood timber connections with slotted-in steel plates and dowel-type fasteners, Constr. Build. Mater. 216 (2019) 296–313. doi:10.1016/j.conbuildmat.2019.04.100.

[69] Setra Group Webpage, (2019). https://www.setragroup.com/en/glulam/design-solutions/.

[70] A. Ceccotti, C. Sandhaas, M. Yasumura, Seismic behaviour of multistory cross-laminated timber buildings, in: Int. Conv. Soc. Wood Sci. Technol. United Nations Econ. Comm. Eur. – Timber Comm., Geneva, Switzerland, 2010.

[71] A.J.M. Dunbar, S. Pampanin, A.H. Buchanan, Seismic Performance of Core-Walls for Multi-Storey Timber Buildings, in: New Zeal. Soc. Earthq. Eng., Auckland, New Zealand, 2014.

[72] T. Reynolds, Å. Bolmsvik, J. Vessby, W.-S. Chang, R. Harris, J. Bawcombe, J. Bregulla, Ambient vibration testing and modal analysis of multi-storey Cross-Laminated Timber buildings, in: World Conf. Timber Eng. 2014 - WCTE 2014, Quebec, Canada, 2014.

[73] T. Reynolds, R. Harris, W.-S. Chang, J. Bregulla, J. Bawcombe, Ambient vibration tests of a cross-laminated timber building, Proc. Inst. Civ. Eng. - Constr. Mater. 168 (2015) 121–131. doi:10.1680/coma.14.00047.

[74] T. Uibel, H.J. Blaß, Load carrying capacity of joints with dowel type fasteners in solid wood panels,

in: Int. Counc. Res. Innov. Build. Constr. - Work. Comm. W18 - Timber Struct. - Meet. Thirty-Nine, Florence, Italy, 2006.

[75] T. Uibel, H. Blaß, Edge Joints with Dowel Type Fasteners in Cross Laminated Timber, in: Int. Counc. Res. Innov. Build. Constr. Work. Comm. W18 - Timber Struct. - Meet. Forty, Bled, Slovenia, 2007.

[76] V. Mahdavifar, A.R. Barbosa, A. Sinha, L. Muszynski, R. Gupta, S.E. Pryor, Hysteretic Response of Metal Connections on Hybrid Cross-Laminated Timber Panels, J. Struct. Eng. 145 (2019) 04018237. doi:10.1061/(ASCE)ST.1943-541X.0002222.

[77] I. Gavric, M. Fragiacomo, A. Ceccotti, Cyclic Behavior of CLT Wall Systems: Experimental Tests and Analytical Prediction Models, J. Struct. Eng. 141 (2015) 04015034. doi:10.1061/(ASCE)ST.1943-541X.0001246.

[78] A. Hossain, M. Popovski, T. Tannert, Group Effects for Shear Connections with Self-Tapping Screws in CLT, J. Struct. Eng. 145 (2019) 04019068. doi:10.1061/(ASCE)ST.1943-541X.0002357.

[79] C. Loss, A. Hossain, T. Tannert, Simple cross-laminated timber shear connections with spatially arranged screws, Eng. Struct. 173 (2018) 340–356. doi:10.1016/j.engstruct.2018.07.004.

[80] M. Follesa, M. Brunetti, R. Cornacchini, S. Grasso, Mechanical in-plane joints between cross laminated timber panels, in: A. Ceccotti (Ed.), 11th World Conf. Timber Eng. 2010, WCTE 2010, Riva del Garda, Italy, 2010: pp. 1840–1845.

[81] I. Gavric, M. Fragiacomo, A. Ceccotti, Cyclic behavior of typical screwed connections for cross-laminated (CLT) structures, Eur. J. Wood Wood Prod. 73 (2015) 179–191. doi:10.1007/s00107-014-0877-6.

[82] L. Pozza, A. Saetta, M. Savoia, D. Talledo, Angle bracket connections for CLT structures: Experimental characterization and numerical modelling, Constr. Build. Mater. 191 (2018) 95–113. doi:10.1016/j.conbuildmat.2018.09.112.

[83] L. Pozza, A. Saetta, M. Savoia, D. Talledo, Coupled axial-shear numerical model for CLT connections, Constr. Build. Mater. 150 (2017) 568–582. doi:10.1016/j.conbuildmat.2017.05.141.

[84] Progetto Energia Zero website, (2017). http://www.progettoenergiazero.com/2017/11/17/x-lam-modalita-e-tipologie-di-connessione/.

[85] Timber-Online website, (2018). https://www.timber-online.net/holzprodukte/2018/11/developments-for-the-entire-sector.html.

[86] L.-M. Ottenhaus, M. Li, T. Smith, Structural performance of large-scale dowelled CLT connections under monotonic and cyclic loading, Eng. Struct. 176 (2018) 41–48. doi:10.1016/j.engstruct.2018.09.002.

[87] D. Trutalli, L. Marchi, R. Scotta, L. Pozza, Capacity design of traditional and innovative ductile connections for earthquake-resistant CLT structures, Bull. Earthq. Eng. 17 (2019) 2115–2136. doi:10.1007/s10518-018-00536-6.

[88] R. Scotta, L. Marchi, D. Trutalli, L. Pozza, A Dissipative Connector for CLT Buildings: Concept, Design and Testing, Materials (Basel). 9 (2016) 139. doi:10.3390/ma9030139.

[89] A. Polastri, I. Giongo, A. Angeli, R. Brandner, Mechanical characterization of a pre-fabricated connection system for cross laminated timber structures in seismic regions, Eng. Struct. 167 (2018) 705–715. doi:10.1016/j.engstruct.2017.12.022.

[90] A. Kraler, J. Kögl, R. Maderebner, M. Flach, Sherpa-CLT-connector for Cross Laminated Timber (CLT) elements, in: World Conf. Timber Eng. 2014 - WCTE 2014, Quebec, Canada, 2014.

[91] M. Latour, G. Rizzano, Seismic behavior of cross-laminated timber panel buildings equipped with traditional and innovative connectors, Arch. Civ. Mech. Eng. 17 (2017) 382–399. doi:10.1016/j.acme.2016.11.008.

[92] T. Schmidt, H.J. Blaß, Recent development in CLT connections part II: In-plane shear connections for CLT bracing elements under cyclic loads, Wood Fiber Sci. 50 (2018) 58–67. doi:10.22382/wfs-2018-040.

[93] Forest Group website, (2019). http://www.gruppoforest.it/edifici-multipiano/.

[94] Centro Legno S.r.l. website, (2015). https://www.centrolegnosrl.com/avada_portfolio/hotel-7-piani/?portfolioCats=27.

[95] M. Lauriola, C. Sandhaas, Quasi-static and pseudo-dynamic tests on XLAM walls and buildings, in: Cost E29 Int. Work. Earthq. Eng. Timber Struct., Coimbra, Portugal, 2006: pp. 119–133.

[96] A. Ceccotti, New Technologies for Construction of Medium-Rise Buildings in Seismic Regions: The XLAM Case, Struct. Eng. Int. 18 (2008) 156–165. doi:10.2749/101686608784218680.

[97] A. Ceccotti, C. Sandhaas, M. Okabe, M. Yasumura, C. Minowa, N. Kawai, SOFIE project - 3D shaking table test on a seven-storey full-scale cross-laminated timber building, Earthq. Eng. Struct. Dyn. 42 (2013) 2003–2021. doi:10.1002/eqe.2309.

[98] V. Hristovski, B. Dujic, M. Stojmanovska, V. Mircevska, Full-Scale Shaking-Table Tests of XLam Panel Systems and Numerical Verification: Specimen 1, J. Struct. Eng. 139 (2013) 2010–2018. doi:10.1061/(ASCE)ST.1943-541X.0000754.

[99] M. Popovski, J. Schneider, M. Schweinsteiger, Lateral load resistance of cross-laminated wood panels, in: 11th World Conf. Timber Eng. 2010, WCTE 2010, Riva del Garda, Italy, 2010.

[100] M. Yasumura, K. Kobayashi, M. Okabe, T. Miyake, K. Matsumoto, Full-Scale Tests and Numerical Analysis of Low-Rise CLT Structures under Lateral Loading, J. Struct. Eng. 142 (2016) E4015007. doi:10.1061/(ASCE)ST.1943-541X.0001348.

[101] G. Flatscher, G. Schickhofer, Shaking-table test of a cross-laminated timber structure, Proc. Inst. Civ. Eng. - Struct. Build. 168 (2015) 878–888. doi:10.1680/stbu.13.00086.

[102] I. Gavric, M. Fragiacomo, A. Ceccotti, Cyclic behaviour of typical metal connectors for cross-laminated (CLT) structures, Mater. Struct. 48 (2015) 1841–1857. doi:10.1617/s11527-014-0278-7.

[103] L. Pozza, M. Massari, M. Savoia, B. Ferracuti, Experimental campaign of mechanical CLT connections subjected to a combination of shear and tension forces, in: Struct. Archit., CRC Press, 2016: pp. 110–118. doi:10.1201/b20891-13.

[104] G. Rinaldin, C. Amadio, M. Fragiacomo, A component approach for the hysteretic behaviour of connections in cross-laminated wooden structures, Earthq. Eng. Struct. Dyn. 42 (2013) 2023–2042. doi:10.1002/eqe.2310.

[105] D. Talledo, L. Pozza, A. Saetta, M. Savoia, Coupled shear-tension numerical model for modelling of CLT connections, in: M.P. J. Eberhardsteiner, W. Winter, A. Fadai (Ed.), Proc. World Conf. Timber Eng. (WCTE 2016), Vienna University of Technology, Austria, Vienna, Austria, 2016.

[106] L. Pozza, R. Scotta, Influence of wall assembly on behaviour of cross-laminated timber buildings, Proc. Inst. Civ. Eng. - Struct. Build. 168 (2015) 275–286. doi:10.1680/stbu.13.00081.

[107] B. Dujic, K. Strus, R. Zarnic, A. Ceccotti, Prediction of Dynamic Response of a 7-storey Massive XLam Wooden Building Tested on a Shaking Table, in: 11th World Conf. Timber Eng. 2010, WCTE 2010, Riva del Garda, Italy, 2010: pp. 3450–3457.

[108] O. Espinoza, V.R. Trujillo, M. Fernanda, L. Mallo, U. Buehlmann, Cross-Laminated Timber: Status and Research Needs in Europe, 2016.

[109] H.J. Blass, A. Ceccotti, C. Dyrbye, M. Gnuschke, K.F. Hansen, J. Nielsen, S. Ohlsson, M. Parche, E. Reyer, C.K.A. Stieda, A. Vergne, A. Vignoli, M. Yasumura, J.D. Dolan, Timber structures in seismic regions - RILEM state-of-the-art report, 1994.

[110] European Committee for Standardisation, EN 1995-1-1 - Eurocode 5: Design of timber structures - Part 1-1: General - Common rules and rules for buildings, 2004.

[111] European Committiee for Standardization, ed., EN 1998-1: Eurocode 8: Design of structures for earthquake resistance—Part 1: general rules, seismic actions and rules for buildings., 2004.

[112] Italian Ministry of Infrastructure and Transport, NTC 2018 - D.M. 17.01.18: Aggiornamento delle “Norme Tecniche per le costruzioni” (in Italian), (2018).

[113] M. Follesa, M. Fragiacomo, D. Casagrande, R. Tomasi, M. Piazza, D. Vassallo, D. Canetti, S. Rossi, The new provisions for the seismic design of timber buildings in Europe, Eng. Struct. 168 (2018) 736–747. doi:10.1016/j.engstruct.2018.04.090.

[114] M. Fragiacomo, B. Dujic, I. Sustersic, Elastic and ductile design of multi-storey crosslam massive wooden buildings under seismic actions, Eng. Struct. 33 (2011) 3043–3053. doi:10.1016/j.engstruct.2011.05.020.

[115] Canadian Standards Association, CSA O86 - Engineering design in wood, Ottawa, Canada, 2014.

[116] American Society of Civil Engineers, Minimum Design Loads for Buildings and Other Structures: ASCE Standards ASCE/SEI 7-10, American Society of Civil Engineers, Reston, VA, 2013. doi:10.1061/9780784412916.

[117] A. Filiatrault, B. Folz, Performance-Based Seismic Design of Wood Framed Buildings, J. Struct. Eng. 128 (2002) 39–47. doi:10.1061/(ASCE)0733-9445(2002)128:1(39).

[118] BSL - Japan ministry of land, infrastructure, transport and tourism, building standard law, The Building Standard Law of Japan, Building Center of Japan, Tokyo, Japan, 2016.

[119] HOWTEC - Guideline for 2016 CLT relative notifications, Japan Housing and Wood Technology Center, Tokyo, Japan, 2016.

[120] HOWTEC - Design and construction manual for CLT buildings, Japan Housing and Wood Technology Center, Tokyo, Japan, 2016.

[121] Standards Association of New Zealand, NZS 3603:1993: Code of Practice for Timber Design, (1993).

[122] L.-M. Ottenhaus, M. Li, T. Smith, P. Quenneville, Overstrength of dowelled CLT connections under monotonic and cyclic loading, Bull. Earthq. Eng. 16 (2018) 753–773. doi:10.1007/s10518-017-0221-8.

[123] Ministry of Housing and Urban Planning (Minvu) of Chile, General Law of Urban Planning and Construction, Ministry of Housing and Urban Planning (Minvu) of Chile, 2018.

[124] Decreto 47 - Fija nuevo texto de la ordenanza general de la ley general de urbanismo y construcciones, Ministry of Housing and Urban Planning (Minvu) of Chile, 2019.

[125] Norma Chilena NCh1198-2006: Madera - Construcciones en madera - Càlculo, Instituto Nacional de Normalización, 2006.

[126] Norma Chilena NCh433-1996 Modificada en 2009: Diseño sísmico de edificios, Instituto Nacional de Normalización, 2009.

[127] National Standard of the People’s Republic of China GB 50011-2010: Code for Seismic Design of Buildings, (2010).

[128] Standardization Administration of China, GB/T 51226-2017: Technical standard for multi-story and high rise timber buildings, (2017).

[129] A.K. Chopra, Dynamics of Structures: Theory and Applications to Earthquake Engineering, 1995.

[130] E. Miranda, V. V. Bertero, Evaluation of Strength Reduction Factors for Earthquake-Resistant Design, Earthq. Spectra. 10 (1994) 357–379. doi:10.1193/1.1585778.

[131] P. Fajfar, Capacity spectrum method based on inelastic demand spectra, Earthq. Eng. Struct. Dyn. 28 (1999) 979–993. doi:10.1002/(SICI)1096-9845(199909)28:9<979::AID-EQE850>3.0.CO;2-1.

[132] P. Fajfar, Design spectra for the new generation of codes, in: Pergamon (Ed.), Elev. World Conf. Earthq. Eng., Acapulco, Mexico, 1996: p. Paper No. 2127. http://www.iitk.ac.in/nicee/wcee/article/11_2127.PDF.

[133] C. Uang, Establishing R (or Rw) and Cd Factors for Building Seismic Provisions, J. Struct. Eng. 117 (1991) 19–28. doi:10.1061/(ASCE)0733-9445(1991)117:1(19).

[134] D. Mitchell, P. Paultre, Ductility and overstrength in seismic design of reinforced concrete structures, Can. J. Civ. Eng. 21 (1994) 1049–1060. doi:10.1139/l94-109.

[135] J.L. Humar, M.A. Rahgozar, Concept of overstrength in seismic design, in: Elev. World Conf. Earthq. Eng., Elsevier Science Ltd, Acapulco, Mexico, 1996: p. Paper No. 639.

[136] R. Park, Explicit incorporation of element and structure overstrength in the design process, in: Elev. World Conf. Earthq. Eng., Elsevier Science Ltd, Acapulco, Mexico, 1996: p. Paper No. 2130.

[137] M. Popovski, E. Karacabeyli, Seismic Performance of Cross-Laminated Wood Panels, in: 44th CIB-W18 Meet., Alghero, Italy, 2011: pp. 44-15–7.

[138] L. Pozza, D. Trutalli, A. Polastri, A. Ceccotti, Seismic design of CLT buildings: Definition of the suitable q-factor by numerical and experimental procedures, in: P.J.S. Cruz (Ed.), Struct. Archit. Concepts, Appl. Challenges - Proc. 2nd Int. Conf. Struct. Archit. ICSA 2013, Taylor & Francis Group, London, Boca Raton, FL, 2013.

[139] W. Muñoz, M. Mohammad, A. Salenikovich, P. Quenneville, Need for a harmonized approach for calculations of ductility of timber assemblies, in: W18-Timber Struct. CIB, St. Andrews, Canada, 2008.

[140] L. Pozza, D. Trutalli, An analytical formulation of q-factor for mid-rise CLT buildings based on parametric numerical analyses, Bull. Earthq. Eng. 15 (2017) 2015–2033. doi:10.1007/s10518-016-0047-9.

[141] M. Popovski, S. Pei, J.W. Lindt, E. Karacabeyli, Force Modification Factors for CLT Structures for NBCC, in: Mater. Joints Timber Struct., Springer Netherlands, Dordrecht, 2014: pp. 543–553. doi:10.1007/978-94-007-7811-5_50.

[142] N. Newmark, W. Hall, Earthquake Spectra and Design, Earthquake Engineering Research Institute; First Edition (US) Third Printing edition (June 1, 1982), 1982.

[143] P. Fajfar, A Nonlinear Analysis Method for Performance-Based Seismic Design, Earthq. Spectra. 16 (2000) 573–592. doi:10.1193/1.1586128.

[144] M. Yasumura, N. Kawai, Evaluation of Wood Framed Shear Walls subjected to Lateral Load, in: CIB-W18, 30th Meet., Vancouver, Canada, 1997: p. paper 30-15-4.

[145] S. Pei, M. Popovski, J. van de Lindt, Performance Based Design and Force Modification Factors for CLT Structures, in: Int. Counc. Res. Innov. Build. Constr. Meet. 45, Växjö, Sweden, 2012: p. paper 45-15-1.

[146] A. Ceccotti, C. Sandhaas, A proposal for a standard procedure to establish the seismic behaviour factor q of timber buildings, in: 10th World Conf. Timber Eng. WCTE, Riva del Garda, Italy, 2010.

[147] L. Pozza, R. Scotta, D. Trutalli, A. Polastri, Behaviour factor for innovative massive timber shear walls, Bull. Earthq. Eng. 13 (2015) 3449–3469. doi:10.1007/s10518-015-9765-7.

[148] T. Smith, D. Moroder, F. Sarti, S. Pampanin, A.H. Buchanan, The Reality of Seismic Engineering in a Modern Timber World, in: R. Görlacher (Ed.), 48th Meet. Int. Netw. Timber Eng. Res. (INTER 2015), Timber Scientific Publishing KIT Holzbau und Baukonstruktionen Karlsruhe, Germany, Šibenik, Croatia, 2015: p. paper 48-102-3.

[149] T. Tannert, M. Follesa, M. Fragiacomo, P. Gonzalez, H. Isoda, D. Moroder, H. Xiong, J. van de Lindt, Seismic design of Cross-Laminated Timber buildings, Wood Fiber Sci. 50 (2018) 3–26. doi:10.22382/wfs-2018-037.

[150] D. Trutalli, L. Pozza, Seismic design of floor–wall joints of multi-storey CLT buildings to comply with regularity in elevation, Bull. Earthq. Eng. 16 (2018) 183–201. doi:10.1007/s10518-017-0193-8.

[151] D. Vamvatsikos, C.A. Cornell, Incremental dynamic analysis, Earthq. Eng. Struct. Dyn. 31 (2002) 491–514. doi:10.1002/eqe.141.

[152] A. Polastri, L. Pozza, Proposal for a standardized design and modeling procedure of tall CLT buildings, Int. J. Qual. Res. 10 (2016) 607–624. doi:10.18421/IJQR10.03-12.

[153] M. Izzi, A. Polastri, M. Fragiacomo, Investigating the Hysteretic Behavior of Cross-Laminated Timber Wall Systems due to Connections, J. Struct. Eng. 144 (2018) 04018035. doi:10.1061/(ASCE)ST.1943-541X.0002022.

[154] J.M. Kelly, R.I. Skinner, A.J. Heine, Mechanisms of energy absorption in special devices for use in earthquake resistant structures, Bull. New Zeal. Soc. Earthq. Eng. 5 (1972) 63–88.

[155] D. Moroder, T. Smith, A. Dunbar, S. Pampanin, A. Buchanan, Seismic testing of post-tensioned Pres-Lam core walls using cross laminated timber, Eng. Struct. 167 (2018) 639–654. doi:10.1016/j.engstruct.2018.02.075.

[156] A. Hashemi, P. Zarnani, R. Masoudnia, P. Quenneville, Seismic resistant rocking coupled walls with innovative Resilient Slip Friction (RSF) joints, J. Constr. Steel Res. 129 (2017) 215–226. doi:10.1016/j.jcsr.2016.11.016.

[157] W.Y. Loo, C. Kun, P. Quenneville, N. Chouw, Experimental testing of a rocking timber shear wall with slip-friction connectors, Earthq. Eng. Struct. Dyn. 43 (2014) 1621–1639. doi:10.1002/eqe.2413.

[158] M. Mohammad, H. Blaß, A. Salenikovich, A. Ringhofer, P. Line, D. Rammer, T. Smith, M. Li, Design approaches for CLT connections, Wood Fiber Sci. 50 (2018) 27–47. doi:10.22382/wfs-2018-038.

[159] A. Jorissen, M. Fragiacomo, General notes on ductility in timber structures, Eng. Struct. 33 (2011) 2987–2997. doi:10.1016/j.engstruct.2011.07.024.

[160] H.J. Blaß, P. Schädle, Ductility aspects of reinforced and non-reinforced timber joints, Eng. Struct. 33 (2011) 3018–3026. doi:10.1016/j.engstruct.2011.02.001.

[161] EN 12512, Timber structures, Test methods. Cyclic testing of joints made with mechanical fasteners, CEN, Brussels, Belgium, 2011.

[162] K. Kobayashi, M. Yasumura, Evaluation of plywood sheathed shear walls with screwed joints tested according to ISO 21581, in: Proc. 44th CIB-W18 Meet., Alghero, Italy, 2011: p. paper 44-15 – 8.

[163] ASTM E2126-11, ASTM E2126 - Standard test methods for cyclic (reversed) load test for shear resistance of vertical elements of the lateral force resisting systems for buildings, (2011).

[164] Comité Européen de Normalisation (CEN), prEN 14592: Timber structures — Dowel-type fasteners — Requirements, (2017).

[165] M. Izzi, A. Polastri, Low cycle ductile performance of screws used in timber structures, Constr. Build. Mater. 217 (2019) 416–426. doi:10.1016/j.conbuildmat.2019.05.087.

[166] D. Casagrande, S. Bezzi, G. D'Arenzo, S. Schwendner, A. Polastri, W. Seim, M. Piazza, A methodology to determine the seismic low-cycle fatigue strength of timber connections, Constr. Build. Mater. 231 (2020) 117026. doi:10.1016/j.conbuildmat.2019.117026.

[167] K.W. Johansen, Theory of Timber Connections, Int. Assoc. Bridg. Struct. Eng. 9 (1949) 249–262. doi:10.5169/seals-9703.

[168] M. Izzi, G. Flatscher, M. Fragiacomo, G. Schickhofer, Experimental investigations and design

provisions of steel-to-timber joints with annular-ringed shank nails for Cross-Laminated Timber structures, Constr. Build. Mater. 122 (2016) 446–457. doi:10.1016/j.conbuildmat.2016.06.072.

[169] U.T. Blaß HJ, Tragfähigkeit von stiftförmigen Verbindungsmitteln in Brettsperrholz, 2007.

[170] R. Brandner, A. Ringhofer, M. Grabner, Probabilistic models for the withdrawal behavior of single self-tapping screws in the narrow face of cross laminated timber (CLT), Eur. J. Wood Wood Prod. 76 (2018) 13–30. doi:10.1007/s00107-017-1226-3.

[171] A. Ringhofer, R. Brandner, G. Schickhofer, A Universal Approach for Withdrawal Properties of Self - Tapping Screws in Solid Timber and Laminated Timber Products, in: R. Görlacher (Ed.), INTER 2015- Int. Netw. Timber Eng. Res., Timber Scientific Publishing KIT Holzbau und Baukonstruktionen Karlsruhe, Germany, Šibenik, Croatia, 2015: p. paper 48-07-01.

[172] C. Sandhaas, R. Görlacher, Nailed joints : Investigation on parameters for Johansen model, in: R. Görlacher (Ed.), INTER 2017- Int. Netw. Timber Eng. Res., Timber Scientific Publishing KIT Holzbau und Baukonstruktionen Karlsruhe, Germany, Kyoto, Japan, 2017: p. paper 50-07-3.

[173] P. Park, T. Paulay, Reinforced concrete structers, John Wiley & Sons, Inc., 1975.

[174] M. Follesa, M. Fragiacomo, D. Vassallo, M. Piazza, R. Tomasi, S. Rossi, D. Casagrande, A proposal for a new Background Document of Chapter 8 of Eurocode 8, in: R. Görlacher (Ed.), 48th Meet. Int. Netw. Timber Eng. Res. (INTER 2015), Timber Scientific Publishing KIT Holzbau und Baukonstruktionen Karlsruhe, Germany, Šibenik, Croatia, 2015: pp. 48-102–01.

[175] Y. Plüss, R. Brandner, Untersuchungen zum Tragverhalten von axial beanspruchten Schraubengruppen in der Schmalseite von Brettsperrholz (BSP), in: Int. Holzbau-Forum IHF 2014, Garmisch-Partenkirchen, Germany, 2014.

[176] I. Gavric, M. Fragiacomo, A. Ceccotti, Capacity seismic design of X-LAM wall systems based on connection mechanical properties, in: R. Görlacher (Ed.), CIB-W18 Meet. 46, Timber Scientific Publishing KIT Holzbau und Baukonstruktionen Karlsruhe, Germany, Vancouver, Canada, 2013: p. paper 46-15-2.

[177] C. Loss, D. Zonta, M. Piazza, On Estimating the Seismic Displacement Capacity of Timber Portal-Frames, J. Earthq. Eng. 17 (2013) 879–901. doi:10.1080/13632469.2013.779333.

[178] F. Brühl, J. Schanzlin, U. Kuhlmann, Materials and Joints in Timber Structures, Springer Netherlands, Dordrecht, 2014. doi:10.1007/978-94-007-7811-5.

[179] C. Dickof, S.F. Stiemer, M.A. Bezabeh, S. Tesfamariam, CLT–Steel Hybrid System: Ductility and Overstrength Values Based on Static Pushover Analysis, J. Perform. Constr. Facil. 28 (2014) A4014012. doi:10.1061/(ASCE)CF.1943-5509.0000614.

[180] I. Sustersic, M. Fragiacomo, B. Dujic, Influence of connection properties on the ductility and seismic resistance of multi-storey cross-lam buildings, in: CIB-W18 Meet. 44, Alghero, Italy, 2012: p. paper 44-15 – 9.

[181] G. D’Arenzo, G. Rinaldin, M. Fossetti, M. Fragiacomo, An innovative shear-tension angle bracket for Cross-Laminated Timber structures: Experimental tests and numerical modelling, Eng. Struct. 197 (2019) 109434. doi:10.1016/j.engstruct.2019.109434.

[182] F. Benedetti, V. Rosales, A. Opazo, Cyclic testing and simulation of Hold-Down connections in radiata pine CLT shear walls, in: WCTE 2016 - World Conf. Timber Eng., Vienna, Austria, 2016.

[183] European Organisation for Technical Approvals, European Technical Assessment ETA-06/0106 of 06/12/2016: Three-dimensional nailing plate (timber-to-timber/timber-to- concrete angle bracket), 2016.

[184] European Organisation for Technical Approvals, European Technical Assessment ETA-11/0086 of 2015-01-26: Three-dimensional nailing plate (Angle brackets and hold-downs for timber-to-timber or

timber-to-concrete or steel connections), 2015.

[185] L. Pozza, B. Ferracuti, M. Massari, M. Savoia, Axial – Shear interaction on CLT hold-down connections – Experimental investigation, Eng. Struct. 160 (2018) 95–110. doi:10.1016/j.engstruct.2018.01.021.

[186] J. Liu, F. Lam, Experimental test of Cross Laminated Timber connections under bi-directional loading, in: World Conf. Timber Eng. 2016 (WCTE 2016), Vienna, Austria, 2016.

[187] J. Liu, F. Lam, Experimental test of coupling effect on CLT hold-down connections, Eng. Struct. 178 (2019) 586–602. doi:10.1016/j.engstruct.2018.10.063.

[188] M. Izzi, A. Polastri, M. Fragiacomo, Modelling the mechanical behaviour of typical wall-to-floor connection systems for cross-laminated timber structures, Eng. Struct. 162 (2018) 270–282. doi:10.1016/j.engstruct.2018.02.045.

[189] M. Shahnewaz, T. Tannert, M.S. Alam, M. Popovski, Performance of Cross Laminated Timber Shear Walls under Cyclic Loading, in: Can. Soc. Civ. Eng. Annu. Conf. Gen. Meet. 2017 Leadersh. Sustain. Infrastruct., Canadian Society for Civil Engineering (CSCE), Vancouver, Canada, 2017.

[190] I.P. Christovasilis, L. Riparbelli, G. Rinaldin, G. Tamagnone, Methods for practice-oriented linear analysis in seismic design of Cross Laminated Timber buildings, Soil Dyn. Earthq. Eng. 128 (2020) 105869. doi:10.1016/j.soildyn.2019.105869.

[191] L. Pozza, M. Savoia, L. Franco, A. Saetta, D. Talledo, Effect of different modelling approaches on the prediction of the seismic response of multi-storey CLT buildings, Int. J. Comput. Methods Exp. Meas. 5 (2017) 953–965. doi:10.2495/CMEM-V5-N6-953-965.

[192] J. Schneider, Y. Shen, S.F. Stiemer, S. Tesfamariam, Assessment and comparison of experimental and numerical model studies of cross-laminated timber mechanical connections under cyclic loading, Constr. Build. Mater. 77 (2015) 197–212. doi:10.1016/j.conbuildmat.2014.12.029.

[193] L. Franco, L. Pozza, A. Saetta, M. Savoia, D. Talledo, Strategies for structural modelling of CLT panels under cyclic loading conditions, Eng. Struct. 198 (2019) 109476. doi:10.1016/j.engstruct.2019.109476.

[194] G. Rinaldin, M. Fragiacomo, Non-linear simulation of shaking-table tests on 3- and 7-storey X-Lam timber buildings, Eng. Struct. 113 (2016) 133–148. doi:10.1016/j.engstruct.2016.01.055.

[195] H.J. Blaß, P. Fellmoser, Design of solid wood panels with cross layers, in: 8th World Conf. Timber Eng. WCTE 2004, Finnish Assoc. of Civil Engineers, Lahti, Finland, 2004.

[196] Y.-L. Shen, J. Schneider, S. Tesfamariam, S.F. Stiemer, Z.-G. Mu, Hysteresis behavior of bracket connection in cross-laminated-timber shear walls, Constr. Build. Mater. 48 (2013) 980–991. doi:10.1016/j.conbuildmat.2013.07.050.

[197] R. Brandner, P. Dietsch, J. Dröscher, M. Schulte-Wrede, H. Kreuzinger, M. Sieder, G. Schickhofer, S. Winter, Shear Properties of Cross Laminated Timber (CLT) under in-plane load: Test Configuration and Experimental Study, in: R. Görlacher (Ed.), 48th Meet. Int. Netw. Timber Eng. Res. (INTER 2015), Timber Scientific Publishing KIT Holzbau und Baukonstruktionen Karlsruhe, Germany, Šibenik, Croatia, 2015: p. paper 48-12-02.

[198] T. Ehrhart, R. Brandner, G. Schickhofer, A. Frangi, Rolling Shear Properties of some European Timber Species with Focus on Cross Laminated Timber (CLT): Test Configuration and Parameter Study, in: R. Görlacher (Ed.), 48th Meet. Int. Netw. Timber Eng. Res. (INTER 2015), Timber Scientific Publishing KIT Holzbau und Baukonstruktionen Karlsruhe, Germany, Šibenik, Croatia, 2015: p. paper 48-6-1. doi:10.3929/ethz-a-010548168.

[199] R. Steiger, A. Gülzow, C. Czaderski, M.T. Howald, P. Niemz, Comparison of bending stiffness of cross-laminated solid timber derived by modal analysis of full panels and by bending tests of strip-shaped specimens, Eur. J. Wood Wood Prod. 70 (2012) 141–153. doi:10.1007/s00107-011-0521-7.

[200] E. Serrano, B. Enquist, Compression strength perpendicular to grain in Cross-Laminated Timber (CLT), in: 11th World Conf. Timber Eng. 2010 (WCTE 2010), Riva del Garda, Italy, 2010.

[201] M. Andreolli, R. Tomasi, A. Polastri, Experimental investigation on in-plane behaviour of cross-laminated timber elements, in: 45th CIB-W18 Meet., Växjö, Sweden, 2012: p. paper 45-12-4.

[202] T. Bogensperger, T. Moosbrugger, G. Silly, Verification of CLT-plates under loads in plane, in: 11th World Conf. Timber Eng. 2010, WCTE 2010, Riva del Garda, Italy, 2010.

[203] O. Perret, A. Lebée, C. Douthe, K. Sab, The Bending–Gradient theory for the linear buckling of thick plates: Application to Cross Laminated Timber panels, Int. J. Solids Struct. 87 (2016) 139–152. doi:10.1016/j.ijsolstr.2016.02.021.

[204] B. Van Damme, S. Schoenwald, A. Zemp, Modeling the bending vibration of cross-laminated timber beams, Eur. J. Wood Wood Prod. 75 (2017) 985–994. doi:10.1007/s00107-016-1152-9.

[205] J. Schneider, S.F. Stiemer, S. Tesfamariam, E. Karacabeyli, M. Popovski, Damage assessment of cross laminated timber connections subjected to simulated earthquake loads, in: World Conf. Timber Eng. 2012 (WCTE 2012), Auckland, New Zealand, 2012.

[206] J. Schneider, E. Karacabeyli, M. Popovski, S.F. Stiemer, S. Tesfamariam, Damage Assessment of Connections Used in Cross-Laminated Timber Subject to Cyclic Loads, J. Perform. Constr. Facil. 28 (2014) A4014008. doi:10.1061/(ASCE)CF.1943-5509.0000528.

[207] F. Benedetti, V. Rosales, A. Opazo, Cyclic behavior of foundation – wall connection in cross laminated timber shear walls, in: 16th World Conf. Earthquake, 16WCEE 2017, Santiago, Chile, 2017: p. paper 1906.

[208] M. Izzi, A. Polastri, M. Fragiacomo, Advanced modelling of CLT wall systems for earthquake resistant timber structures, in: R. Görlacher (Ed.), Meet. 49 Int. Netw. Timber Eng. Res., Timber Scientific Publishing KIT Holzbau und Baukonstruktionen Karlsruhe, Germany, Graz, Austria, 2016: p. paper 49-15-6.

[209] M. Izzi, G. Rinaldin, M. Fragiacomo, A. Polastri, Numerical modelling of steel-to-timber joints and connectors for CLT structures, in: World Conf. Timber Eng. 2016, Vienna, Austria, 2016.

[210] G. Flatscher, Evaluation and approximation of timber connection properties for displacement-based analysis of CLT wall systems, Graz University of Technology, 2017.

[211] Strand7 Pty. Ltd, Strand7 - Theoretical Manual, (2005). http://www.strand7.com/html/docu_theoretical.htm.

[212] I. Gavric, A. Ceccotti, M. Fragiacomo, Experimental cyclic tests on cross-laminated timber panels and typical connections, in: 15th Conf. Ital. Natl. Assoc. Earthq. Eng. (ANIDIS 2011), Bari, Italy, 2011.

[213] A. Ceccotti, M. Follesa, M.P. Lauriola, C. Sandhaas, Sofie Project – Test Results on the Lateral Resistance of Cross-Laminated Wooden Panels, in: Proc. First Eur. Conf. Earthq. Eng. Seism., Geneva, Switzerland, 2006: p. paper 1912.

[214] European Organisation for Technical Approvals, European Technical Assessment ETA-07/0285 of 2015-12-03: Three-dimensional nailing plate (timber to timber and timber to concrete/steel hold downs and post bases), 2015.

[215] T. Moosbrugger, W. Guggenberger, T. Bogensperger, Cross-Laminated Timber Wall Segments under homogeneous Shear - With and without Openings, in: WCTE 2006 - Word Conf. Timber Eng., Portland, Oregon, USA, 2006: pp. 219–228.

[216] R. Brandner, T. Bogensperger, G. Schickhofer, In Plane Shear Strength Of Cross Laminated Timber (CLT): Test Configuration, Quantification and Influencing Parameters, in: R. Görlacher (Ed.), Proc. 46th CIB-W18 Meet., Timber Scientific Publishing KIT Holzbau und Baukonstruktionen Karlsruhe, Germany, Vancouver, Canada, 2013: p. paper 46-12-2.

[217] R. Stürzenbecher, K. Hofstetter, J. Eberhardsteiner, Cross Laminated Timber: a multi-layer, shear compliant plate and its mechanical behavior, in: Word Conf. Timber Eng. 2010 (WCTE 2010), Riva del Garda, Italy, 2010.

[218] Computers & Structures Inc., CSI Analysis Reference Manual For SAP2000®, ETABS®, SAFE® and CSiBridge®, rev. 15, Berkeley, California, USA, 2016.

[219] S. Mazzoni, F. McKenna, M.H. Scott, G.L. Fenves, OpenSees command language manual, Pacific Earthq. Eng. Res. Cent. (2006).

[220] L.N. Lowes, A. Altoontash, Modeling Reinforced-Concrete Beam-Column Joints Subjected to Cyclic Loading, J. Struct. Eng. 129 (2003) 1686–1697. doi:10.1061/(ASCE)0733-9445(2003)129:12(1686).

[221] G.C. Foliente, Stochastic dynamic response of wood structural systems, Virginia Polytechnic Institute and State University, 1993. http://scholar.lib.vt.edu/theses/available/etd-05042006-164535/.

[222] J.P. Judd, Analytical modeling of wood-frame shear walls and diaphragms, Brigham Young University, 2005.

[223] W.M. McKenzie, H. Karpovich, The frictional behaviour of wood, Wood Sci. Technol. 2 (1968) 139–152. doi:10.1007/BF00394962.

[224] M. Seki, H. Sugimoto, T. Miki, K. Kanayama, Y. Furuta, Wood friction characteristics during exposure to high pressure: influence of wood/metal tool surface finishing conditions, J. Wood Sci. 59 (2013) 10–16. doi:10.1007/s10086-012-1295-1.

[225] C. Aranha, J.M. Branco, P. Lourenço, G. Flatscher, G. Schickhofer, Finite Element Modelling of the Cyclic Behaviour of CLT Connectors and Walls, in: WCTE 2016 - World Conf. Timber Eng., Vienna, Austria, 2016.

[226] C. Demirci, C. Málaga-Chuquitaype, L. Macorini, Seismic drift demands in multi-storey cross-laminated timber buildings, Earthq. Eng. Struct. Dyn. 47 (2018) 1014–1031. doi:10.1002/eqe.3003.

[227] F. Lam, R. 0. Foschi, H. Prion, Needs in Modeling and Analysis of Seismic Resistance of Woodframe Construction, in: F. Seible, A. Filiatrault, C.-M. Uang (Eds.), Proc. Invit. Work. Seism. Testing, Anal. Des. Woodframe Constr., California Universities for Research in Earthquake Engineering, San Diego, California, 1999: pp. 125–127.

II

Design methods for CLT wall systems

II.1 State-of-the-art of design methods for CLT wall systems

Abstract

Analytical models capable of describing the mechanical behavior of CLT wall systems subjected to horizontal loads are necessary in order to provide tools that can easily be used by practitioners for the seismic design of CLT buildings avoiding overdesign due to lack of knowledge about this novel constructive technology. Scope of this Section is to give an overview on the state-of-the-art of analytical design methods for platform-frame CLT walls subjected to horizontal loads. These methods, available in the scientific literature and handbooks, are characterized by heterogeneity of hypotheses, thus not giving to practitioners an unambiguous effective support in the design of CLT multi-storey buildings. As a result, often design methods vary among practitioners. In the following, the different methods available on scientific literature to derive shear strength of CLT shear walls will be compared in terms of basic assumptions, in order to define advantages and drawbacks that can help practitioners to find the best method that suits the design of a CLT structure. Their limits will also be highlighted pointing out the necessity of an enhancement of available methods in order to meet the requirements of modern design criteria for structures.

II.1.1 Chapter contents

In this Chapter a state-of-the-art of analytical methods to predict the lateral resistance of CLT wall systems is reported. Methods for monolithic and coupled CLT walls are presented in Section II.1.2 and II.1.3. The main limits of the described models will be illustrated in Section II.1.4. Finally, in Section II.1.5 an overview on coupling methods for connections will be given.

II.1.2 Methods for strength assessment of monolithic CLT shear walls

Different analytical models characterized by different levels of complexity [1] have been developed in the last years for the evaluation of the shear capacity of CLT walls. These models can be subdivided between methods that disregard ([2, 3]) or consider ([4, 5]) the axial strength of angle-bracket connections against rocking kinematics of the shear wall. All these models consider the CLT panel as rigid and most of them do not take into account the interaction between axial and lateral strength of connections.

The lateral load-carrying capacity of CLT shear walls is simply assumed as the minimum between the horizontal force corresponding to two independent failure mechanisms, namely (i) the rocking and (ii) the sliding kinematics given by respectively the axial and lateral strength of connections. An extensive comparison between analytical models to predict both strength and stiffness of CLT shear walls in platform-frame configuration has been carried out by Lukacs *et al.* [1, 6]

In this Section an overview of the different analytical methods available on scientific literature – to author's knowledge – for the design of lateral in-plane response of CLT single-storey monolithic platform-frame wall systems loaded with an upper horizontal force is presented (Figure II.1-1.a). For balloon frame or multi-panel CLT wall systems the reader is referred to literature, e.g. respectively the model by Chen & Popovski [7] and the one by Sandoli *et al.* [8], since both topics are out of the scope if this thesis.

For all the models, connections do not give neither strength nor stiffness contribution in compression, timber do not resist to tension and CLT panel is considered rigid, vis. no bending and shear elastic deformations are considered. Two types of constitutive laws for axial tensile resistance of connections are considered: (i) an elasto-brittle (labelled as "El-Br") and a (ii) constant one (labelled as "Const") if the relationship between the axial strength N_i and displacement $\delta_{N,i}$ of the i-th connection is respectively linear or constantly equal to the yielding strength $N_{i,y,0}$ (Figure II.1-1.b). Since no plastic behavior for connections is considered in none of the models presented in this sub-section, force redistribution among axially-loaded connections for their plastic behavior and redundancy is not allowed. A more refined model developed in Section II.3 will also take into account for this aspect. In the shear direction connections have a constant constitutive law, with a resistance equal to the yielding one $V_{i,y,0}$ for every value of the shear displacement $\delta_{V,i}$. Three alternative coupling criteria are assumed for connections with a biaxial resistance: (i) rectangular (labelled as "Rect"), (ii) linear (labelled as "Linear") and (iii) elliptic (labelled as "Elliptic"), see Section II.1.5 for further details.

The bottom ground timber interface can deform to either one of three following constitutive laws (Figure II.1-1.b and .c): (i) rigid material (labelled as "Rig") that develops no strains in the compressed area (with the compressive force F_c being concentrated in the corner), (ii) a stress-block (labelled as "Str-Bl") with a smeared uniform compressive stress in the compressed area equal to the maximum one f_c and (iii) an elasto-brittle one (labelled as "El-Br") with f_c reached only at the compressed corner. All the methods consider a rigid support, work within the hypothesis of bottom plane section and, except for the one from Pei *et al.* [5], they consider the lateral resistance of the wall V as the minimum between the one horizontal force that activates a rocking mechanism of the wall system V_{rock} (correlated to the uplift displacement d_{up} of the wall system) and the one associated to sliding failure V_{sl} (correlated to the slip displacement d_{sl} of the wall system), accordingly to:

$$V = min\{V_{rock}; V_{sl}\} \qquad (II.1\text{-}1)$$

The strength that connections can develop is uniaxial (labelled as “Uni”) or biaxial (labelled as “Bi”) if the resistance in their secondary direction (vis. shear direction for hold-downs and axial direction for angle brackets) is respectively disregarded or considered.

Table II.1-1 and Table II.1-2 respectively show and compare the assumptions and the two shear strength components of Equation (II.1-1) for different design methods available in literature that will be synthetically illustrated in the following. Table II.1-2 shows the formulations for a monolithic wall system large l, high h and thick t, anchored to ground floor through n connections, n_{AB} angle-brackets (AB) placed among n_{HD} lateral hold-downs (HD) evenly distributed among the two edges of the CLT panel. The reference configuration used to illustrate the various models is represented in Figure II.1-2, where connections 1 and 6 are hold-downs and connections 2 to 5 are angle brackets. Each i-th connection is placed at a distance x_i from the compressed corner, has an uncoupled axial stiffness $k_{N,i,0}$ and the parameter n_i stands for the number of connections placed in same position x_i. A horizontal force V at the top of the wall and a vertical distributed load q are present, while dead load of CLT panel is disregarded for all the models, therefore the resulting vertical force is equal to $N = q \cdot l$. The models that include friction contribution to shear sliding strength V_{sl} consider a Coulomb model with a coefficient of friction μ. In the formulations by Reynolds *et al.* [4] n_{trax} is the number of connections active in tension.

Schickhofer *et al.* [9] propose three different solutions to derive the lateral resistance of CLT wall systems. The first one #1 (Figure II.1-3.a) assumes a linear distribution of tension and compression stresses, and a fictious position of tensioned hold-down on the balance point of the tensioned area assumed having an extension l_T equal to:

$$l_T = \frac{l}{2} - \frac{q \cdot l^3}{12 \cdot F \cdot h} \tag{II.1-2}$$

The second model #2 proposed by Schickhofer (Figure II.1-3.b) considers gap opening without considering tensile strength of connections while the third one #3 (Figure II.1-3.c) also considers both gap opening and tensile strength of connections. The method #1 requires the iterative solution of a nonlinear equation in order to derive V_{rock}, while the method #3 derives the rocking resistance as the minimum between the one related to failure of axially loaded connection $V_{rock,I}$ and the one related to compression failure of timber $V_{rock,II}$:

$$V_{rock,I} = \frac{n_{HD}}{2} \cdot \frac{N_{HD,y,0} \cdot x_1}{h} + \frac{l}{2h}\left(N + \frac{n_{HD}}{2} \cdot N_{HD,y,0}\right) - \frac{2N(N + n_{HD} \cdot N_{HD,y,0}) - N_{HD,y,0}^2 \cdot n_{HD}}{3 f_c t_{ef} \cdot 1m \cdot h} \tag{II.1-3}$$

$$V_{rock,II} = \frac{n_{HD} \cdot N_{HD,y,0}}{6h}(3x_1 - x) + \frac{N}{6h}(3l - 2\,x) \tag{II.1-4}$$

where $1m$ stays for a strip of one meter of the bottom interface of the CLT panel and x is the neutral axis position to be derived accordingly to the following equation where t is the CLT panel thickness:

$$x = \frac{3x_1 \cdot f_c - \sqrt{\frac{3}{t}} \cdot \sqrt{-8\,V_{rock,II} \cdot h \cdot f_c \cdot t + 3x_1^2 \cdot f_c^2 - 8x_1 \cdot l \cdot f_c \cdot q + 4l^2 \cdot f_c \cdot q}}{2f_c} \tag{II.1-5}$$

Sustersic & Dujic [10] (Figure II.1-3.d) consider a simple model where all connections resist both to shear and axial loads without considering reduction of resistance for interaction of forces in the two directions (rectangular coupling domain, see Section II.1.5). A rigid behavior of timber at the bottom interface is considered but, in order to take into account in a fictious way for the reduction of the vertical internal forces lever-arm due to plasticization of compressed timber, a coefficient β ranging from 0.90 to 0.95 to move the rocking pivoting point of the panel from the corner inwards is assumed. The same assumption will also be used by Casagrande *et al.* [2]. Axial loads are linearly distributed along longitudinal direction with the connections subjected to maximum uplift reaching its yielding strength $N_{HD,y,0}$. Friction effect is considered to determine the shear strength of CLT wall system, and both hold-down and angle bracket connections contribute to shear resistance.

Also Pei *et al.* [5] (Figure II.1-3.e) consider all connections resisting in both axial and shear direction and a CLT panel behaving rigidly. Axial loads are linearly distributed along longitudinal direction with the connections subjected to maximum uplift reaching its yielding strength $N_{HD,y,0}$. Shear resistance V_{sl} is back-designed after calculation of rocking resistance V_{rock}, differently from all the other approaches here illustrated where V_{sl} is calculated independently from V_{rock}.

Waller-Novak *et al.* [11] (Figure II.1-3.f) present a simplified[1] approach where only tensioned hold-downs resist to axial loads, while angle brackets resist to shear. A stress-block constitutive law for compressed timber is considered assuming a compressed zone $x = \frac{l}{4}$. Friction effect is considered to determine the shear strength.

Gavric & Popovski [3] (Figure II.1-3.g and .h) proposed an approach that considers a CLT panel rigid in compression, all connections resisting to tension and only angle brackets resisting to shear. Since angle brackets are subjected to a biaxial tensional state, in order to take into account for the interaction between strengths in axial and shear directions two types of coupling criteria are considered (see Section II.1.5 for further details): a linear one (Equation (I.1-4), method #1) and an elliptic one (Equation (II.1-7), method #2).

$$\frac{N_i}{N_{i,y,0}} + \frac{V_i}{V_{i,y,0}} \leq 1 \qquad (II.1\text{-}6)$$

$$\left(\frac{N_i}{N_{i,y,0}}\right)^2 + \left(\frac{V_i}{V_{i,y,0}}\right)^2 \leq 1 \qquad (II.1\text{-}7)$$

Tomasi *et al.* [12] (Figure II.1-3.i) considered a stress-block constitutive law for compressed timber at bottom interface extending for a length equal to $0.8 \cdot x$, where x is the depth of neutral axis respect to the compressed corner and it is derived imposing vertical equilibrium:

$$x = \frac{N + \frac{n_{HD}}{2} \cdot N_{HD,y,0}}{0.8\, t_{ef} \cdot f_c} \qquad (II.1\text{-}8)$$

where t_{ef} is the effective thickness given by the sum of the thickness of layers with vertically-oriented grains.

Casagrande *et al.* [2] (Figure II.1-3.j) proposed a model with a CLT panel assumed rigid in compression, only hold-downs resisting to uplift forces and angle brackets resisting to shear. The compressive force F_c is assumed acting on the compressive hold-down in a fictious way.

Reynolds *et al.* [4] propose four different types of analytical models, each considering friction effects to calculate V_{rock}. The first one #1 (Figure II.1-3.k) considers a triangular distribution of tensile forces acting on connections, with the one subjected to maximum uplift reaching the yielding strength $N_{HD,y,0}$. The second model #2 (Figure II.1-3.l) considers the panel as rigid in compression at the bottom, with all the connections yielded (constant constitutive law, Figure II.1-1.b) except for the ones closest to the compressed corner, and only these connections that are not resisting to tension are active in the shear direction. The third model proposed by Reynolds #3 (Figure II.1-3.m) assumes in a fictious way that the compression area is extended for a depth $x = \frac{l}{3}$ and that only the connections comprised within a distance $\frac{l}{3}$ from the uplifted corner resist to tension with a constant constitutive law. Finally, the fourth model proposed by Reynolds #4 (Figure II.1-3.n) assumes a constant and a stress-block constitutive law respectively for connections and timber with a depth of the neutral axis that, given n_{trax} the number of connections active in axial direction, is equal to:

$$x = \frac{N + \sum_{i=1}^{n_{trax}} N_i}{t_{ef} \cdot f_c} \qquad (II.1\text{-}9)$$

---

[1] The internal lever arm e is assumed to be $e \simeq x_1 - \frac{l}{4}$ while the correct value is $e = x_1 - \frac{l}{8}$ (Figure II.1-3.f).

Table II.1-1 – Assumptions of different design methods for CLT shear-walls available in literature.

Model	*Connections*		*Constitutive laws*		*Friction*
	Resistance	*Coupling*	*Timber**	*Connections*	
Schickhofer et al. #1 (2010) [9]	Uni		El-Br	El-Br	✗
Schickhofer et al. #2 (2010) [9]	Only AB to shear		El-Br	✗[d]	✗
Schickhofer et al. #3 (2010) [9]	Uni		El-Br	El-Br	✗
Sustersic & Dujic (2012) [10]	Bi	Rect	Rig	El-Br	✓
Pei et al. (2013) [5]	Bi	Rect	Rig	El-Br	✗
Waller-Novak et al. (2014) [11]	Uni		Str-Bl	Const	✓
Gavric & Popovski #1 (2014) [3]	HD: Uni - AB: Bi	Linear[c]	Rig	El-Br	✗
Gavric & Popovski #2 (2014) [3]	HD: Uni - AB: Bi	Elliptic[c]	Rig	El-Br	✗
Tomasi et al. (2014) [12]	Uni		Str-Bl	Const	✗
Casagrande et al. (2016) [2]	Uni		Rig	Const	✗
Reynolds et al. #1 (2017) [4]	Uni		Str-Bl	El-Br	✓
Reynolds et al. #2 (2017) [4]	Uni		Rig	Const [a]	✓
Reynolds et al. #3 (2017) [4]	Uni		Str-Bl	Const [b]	✓
Reynolds et al. #4 (2017) [4]	Uni		Str-Bl	Const	✓

* *At bottom interface*

[a] *Connection closest to compressed corner has no shear resistance*

[b] *Active axial resistance of connections only within a distance b/3 from tensioned corner of the shear wall*

[c] *Only for angle-brackets*

[d] *Connections do not resist in tension*

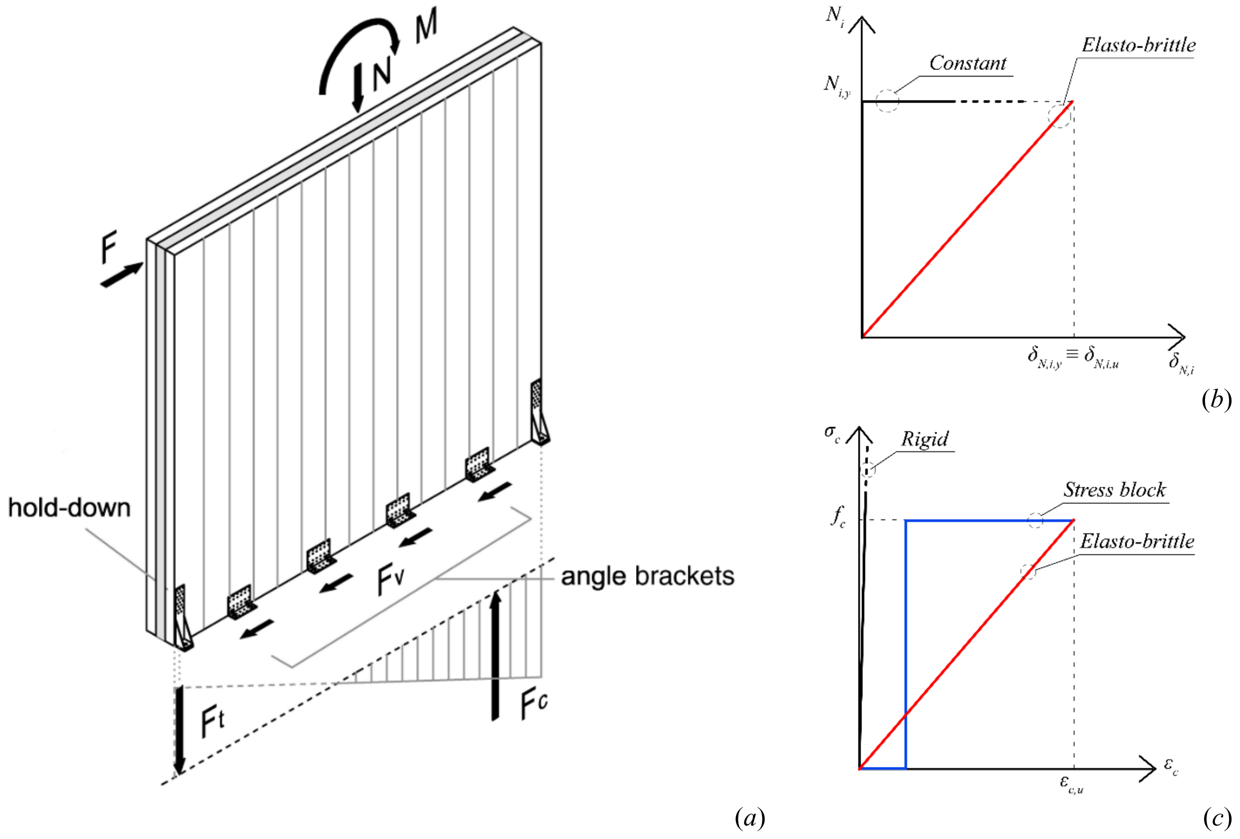
M
N
F
hold-down
Fv
angle brackets
Ft
Fc
(a)
N_i
$N_{i,y}$
Constant
Elasto-brittle
$\delta_{N,i,y} \equiv \delta_{N,i,u}$
$\delta_{N,i}$
(b)
σ_c
Rigid
Stress block
f_c
Elasto-brittle
$\varepsilon_{c,u}$
ε_c
(c)

Figure II.1-1 – Design approaches for CLT wall systems: (*a*) schematic representation of a model that disregards the resistance of connections in their secondary direction (*image credits*: Tomasi & Smith [13]), (*b*) elasto-brittle (red line) and constant (black line) constitutive laws for connections and (*c*) rigid (black line), stress-block (blue line) and elasto-brittle (red line) constitutive laws for timber.

Table II.1-2 – Lateral strength formulations of CLT shear-walls for different analytical models

Model	*Wall system strength*	
	Rocking failure V_{rock}	*Sliding failure* V_{sl}
Schickhofer et al. #1 (2010) [9]	$\frac{n_{HD}}{2} \cdot N_{HD,y,0} = \frac{3V_{rock} \cdot h - N \cdot l}{2l} + \frac{N^2 \cdot l}{24V_{rock} \cdot h}$	$n_{AB} \cdot V_{AB,y,0}$
Schickhofer et al. #2 (2010) [9]	$\frac{q \cdot l^2}{2h} \leq \frac{q \cdot l}{h}\left(\frac{l}{2} - \frac{x}{3}\right)$	$n_{AB} \cdot V_{AB,y,0}$
Schickhofer et al. #3 (2010) [9]	$min\{V_{rock,I}, V_{rock,II}\}$	$n_{AB} \cdot V_{AB,y,0}$
Sustersic & Dujic (2012) [10]	$\frac{\frac{n_{HD}}{2} \cdot N_{HD,y,0} \cdot \{\sum_{i=1}^{n} k_{N,i,0} \cdot [x_i - (1-\beta)l]^2\}}{k_{N,HD,0} \cdot h \cdot [x_1 - (1-\beta)l]} + \frac{q(\beta l)^2}{2h}$	$n_{HD} \cdot V_{HD,y,0} + n_{AB} \cdot V_{AB,y,0} + N \cdot \mu$
Pei et al. (2013) [5]	$\frac{1}{h}\left(\sum_{i=1}^{n'} n_i \cdot N_i \cdot x_i + \frac{N \cdot l}{2}\right), with\ N_1 = N_{HD,y,0}$	$\sum_{i=1}^{n_{AB}} n_i \cdot V_{i,y,0} > V_{rock}$
Waller-Novak et al. (2014) [11]	$\simeq \frac{1}{h}\left[\left(\frac{n_{HD}}{2} \cdot N_{HD,y,0} + \frac{0.9q \cdot l}{2}\right)\left(x_1 - \frac{l}{4}\right)\right]$	$\sum_{i=1}^{n_{AB}} n_i \cdot V_{i,y,0}$
Gavric & Popovski #1 & #2 (2014) [3]	$\frac{l}{2h} \cdot N + \frac{\frac{n_{HD}}{2} \cdot N_{HD,y,0} \cdot x_1}{h} + \frac{N_{AB,y}}{h \cdot x_1} \sum_{i=1+\frac{n_{HD}}{2}}^{n-\frac{n_{HD}}{2}} n_i \cdot x_i^2$	$\sum_{i=1+\frac{n_{HD}}{2}}^{n-\frac{n_{HD}}{2}} V_i$
Tomasi et al. (2014) [12]	$\frac{1}{h} \cdot \left[\frac{n_{HD}}{2} \cdot N_{HD,y,0}\left(x_1 - \frac{l}{2}\right) + \left(N + \frac{n_{HD}}{2} \cdot N_{HD,y,0}\right)\left(\frac{l}{2} - \frac{N + \frac{n_{HD}}{2} \cdot N_{HD,y,0}}{2f_c \cdot t_{ef}}\right)\right]$	$\sum_{i=1}^{n_{AB}} n_i \cdot V_{i,y,0}$
Casagrande et al. (2016) [2]	$\beta\frac{l}{h}\left(\frac{n_{HD}}{2} \cdot N_{HD,y,0} + \frac{N}{2}\right)$	$\sum_{i=1}^{n_{AB}} n_i \cdot V_{i,y,0}$
Reynolds et al. #1 (2017) [4]	$\frac{1}{h}\left[\sum_{i=1}^{n_{trax}} n_i \cdot N_i\left(x_i - \frac{x}{2}\right) + \frac{N}{2}(l - x)\right], with\ N_1 = N_{HD,y,0}$	$\sum_{j=n_{trax}+1}^{n} n_i \cdot V_{j,y,0} + \mu\left(\sum_{i=1}^{n_{trax}} n_i \cdot N_i + N\right)$
Reynolds et al. #2 (2017) [4]	$\frac{1}{h}\left[\sum_{i=1}^{n_{trax}} n_i \cdot N_{i,y,0} \cdot x_i + N \cdot \frac{l}{2}\right]$	$\sum_{j=n_{trax}+1}^{n} n_i \cdot V_{j,y,0} + \mu\left(\sum_{i=1}^{n_{trax}} n_i \cdot N_i + N\right)$
Reynolds et al. #3 (2017) [4]	$\frac{1}{h}\left[\sum_{i=1}^{n_{trax}} n_i \cdot N_{i,y,0}\left(x_i - \frac{l}{6}\right) + N \cdot \frac{l}{3}\right]$	$\sum_{j=n_{trax}+1}^{n} n_i \cdot V_{j,y,0} + \mu\left(\sum_{i=1}^{n_{trax}} n_i \cdot N_i + N\right)$
Reynolds et al. #4 (2017) [4]	$\frac{1}{h}\left[\sum_{i=1}^{n_{trax}} n_i \cdot N_{i,y,0}\left(x_i - \frac{x}{2}\right) + \frac{N}{2}(l - x)\right]$	$\sum_{j=n_{trax}+1}^{n} n_i \cdot V_{j,y,0} + \mu\left(\sum_{i=1}^{n_{trax}} n_i \cdot N_i + N\right)$

The models proposed by Sustersic [10], Pei [5] and the method #1 by Reynolds [4] assume that the CLT shear-wall reaches its rocking resistance V_{rock} when the connection furthest from the compressed corner is yielded. Anyway, it must be noticed that in seismic-prone areas connections are usually arranged so that the furthest connection from the compressed corner (connection number 1 in Figure II.1-2) is a hold-down, while the connection closest to it is an angle bracket (connection number 2 in Figure II.1-2) characterized by a different and usually less performant constitutive law to axial loads. Therefore, even if not explicitly declared by authors, the aforementioned methods should be considered valid only if the failure of the angle bracket due to an axial displacement $\delta_{N,2}$ exceeding the maximum yielding one $\delta_{N,2,y,0}$ is prevented. Hence, defined $\delta_{N,HD,y,0}$ and $\delta_{N,AB,y,0}$ the yielding displacement of respectively hold-down and angle bracket connections, the method proposed by Sustersic [10] is valid if:

$$\frac{\delta_{N,AB,y,0}}{\delta_{N,HD,y,0}} \geq \frac{x_2 + \beta \cdot l - l}{x_1 + \beta \cdot l - l} \qquad (II.1\text{-}10)$$

Similarly, the method by Pei [5] can be applied only if the following condition is satisfied:

$$\frac{\delta_{N,AB,y,0}}{\delta_{N,HD,y,0}} \geq \frac{x_2}{x_1} \qquad (II.1\text{-}11)$$

The condition to be satisfied for the validity of the method Reynolds #1 [4] is:

$$\frac{\delta_{N,AB,y,0}}{\delta_{N,HD,y,0}} \geq \frac{x_2 - x}{x_1 - x} \qquad (II.1\text{-}12)$$

On the other hand, methods #2 and #4 by Reynolds [4] are based on the assumption that all the connections subjected to tension are able to withstand their maximum resistance prior that the connection subjected to maximum axial displacement (connection 1 of Figure II.1-2) reaches its ultimate displacement. This condition is quite unrealistic and may lead to overestimation of effective wall resistance as pointed out in [1].

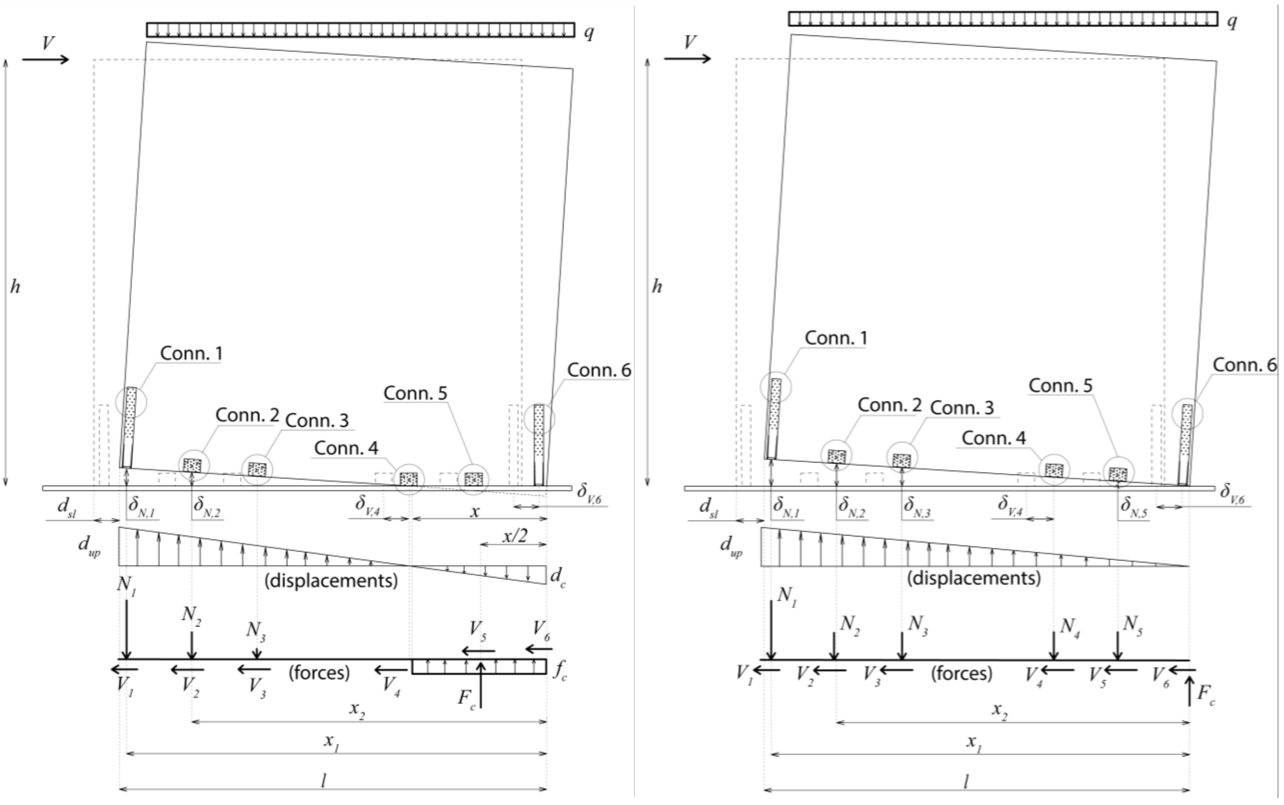

(*a*) (*b*)

Figure II.1-2 – Schematic representation of models with (*a*) a stress block and linear constitutive law of axial forces and (*b*) with assumed a rigid behavior of compressed timber and a constant distribution of tensile forces on connections.

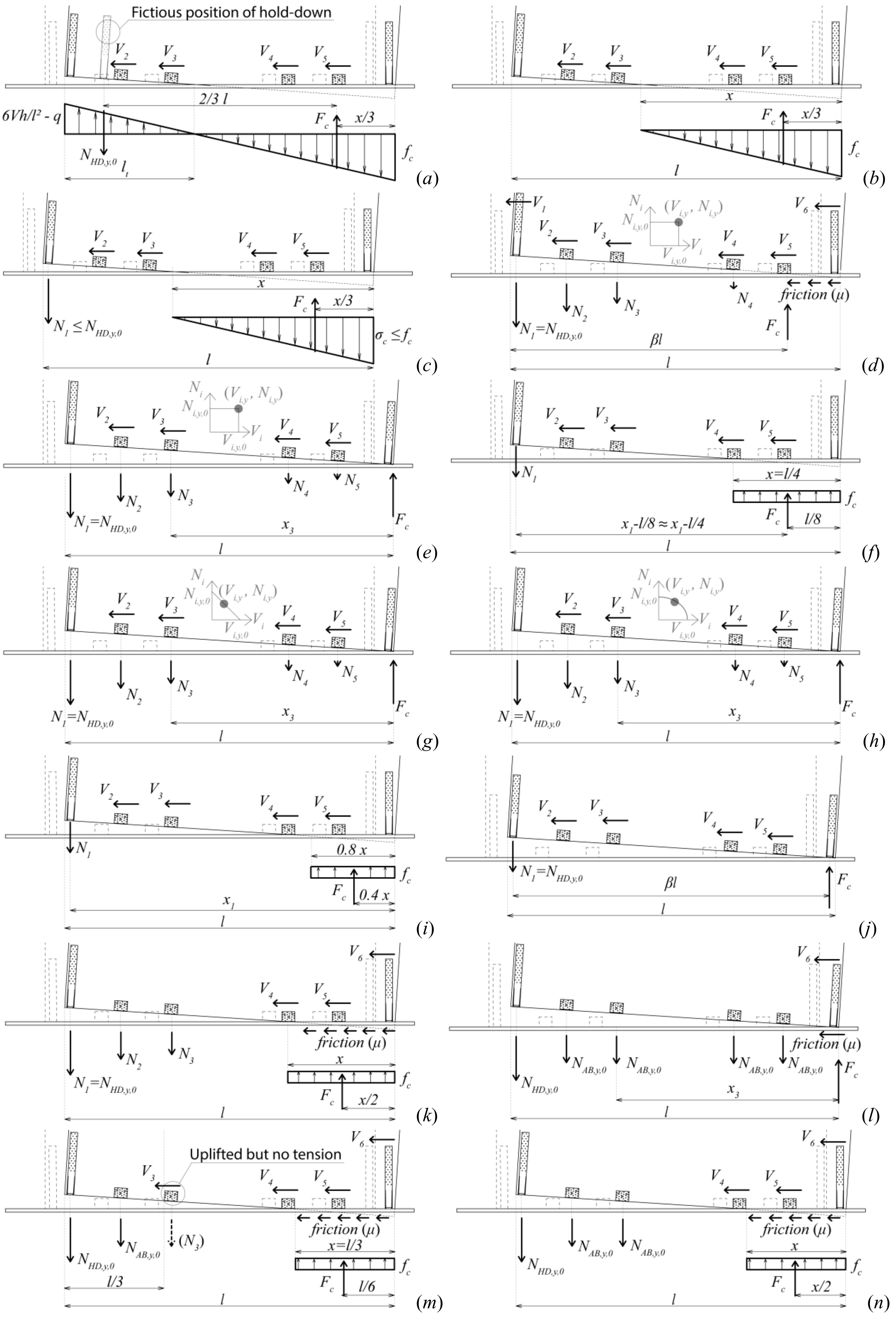
Fictious position of hold-down
V_2
V_3
V_4
V_5
$2/3\ l$
$6Vh/l^2 - q$
F_c
$x/3$
f_c
$N_{HD,y,0}$
l_t
(a)
x
l
(b)
$N_1 \leq N_{HD,y,0}$
$\sigma_c \leq f_c$
(c)
V_1
V_6
N_i
$(V_{i,y}, N_{i,y})$
$N_{i,y,0}$
V_i
$V_{i,y,0}$
friction (μ)
N_2
N_3
N_4
N_5
$N_1 = N_{HD,y,0}$
βl
(d)
x_3
(e)
$x = l/4$
$l/8$
$x_1 - l/8 \approx x_1 - l/4$
(f)
(g)
(h)
$0.8\ x$
$0.4\ x$
x_1
(i)
(j)
$x/2$
(k)
$N_{HD,y,0}$
$N_{AB,y,0}$
(l)
Uplifted but no tension
(N_3)
$x = l/3$
$l/3$
$l/6$
(m)
(n)

Figure II.1-3 – Forces at bottom interface at rocking failure for each model: (*a*) Schickhofer #1, (*b*) Schickhofer #2, (*c*) Schickhofer #3, (*d*) Sustersic & Dujic, (*e*) Pei, (*f*) Waller-Novak, (*g*) Gavric & Popovski #1, (*h*) Gavric & Popovski #2, (*i*) Tomasi, (*j*) Casagrande, (*k*) Reynolds #1, (*l*) Reynolds #2, (*m*) Reynolds #3 and (*n*) Reynolds #4.

II.1.3 Methods for strength assessment of coupled CLT shear walls

Casagrande *et al.* [14] developed a refined analytical model for the assessment of elastic behaviour (strength and stiffness) of multi-panel CLT wall systems adopting the minimum total potential energy principle. The model considers uniaxial resistance of connections, with hold-downs resisting only to tension and angle-brackets only to shear. Therefore, the behaviour of connections is uncoupled, therefore rocking and sliding behaviour of wall systems are considered to be independent. Different kinematic models have been derived to the vary of the ratio between the axial stiffness of hold-downs and vertical joints between panels.
Nolet *et al.* [15] proposed an analytical procedure to determine the elasto-plastic force-displacement behavior of coupled multi-panel CLT shear walls. The method allows for the prediction of ultimate strength and displacement of the wall system and the determination of sequence of yielding and failure of connections.
Sandoli *et al.* [8] proposed an equivalent frame models to predict the lateral in-plane behavior of multi-panel CLT shear walls schematized as a cantilever beam fixed at the base through a rotational spring. The model was built in two versions: a more refined one that considers a rigid material behavior of timber at bottom interface, and a more refined one that considers timber deformability in compression.
The analysis of coupled multi-panel CLT wall systems is anyway out of the scope of this thesis, therefore for further details of their analytical models the reader is referred to the scientific literature.

II.1.4 Main limits of models for monotonic CLT shear walls

The models for the prediction of strength of laterally-loaded CLT shear walls (Section II.1.2) present some limits. First of all, most of them (Table II.1-1) assume a uniaxial behaviour of connections, disregarding the fact that, especially for angle-brackets, considering a biaxial behaviour is necessary to correctly predict their strength and stiffness contribution to the wall system [16, 17]. When a biaxial model for connections is considered, the analytical methods - except for the one by Gavric & Popovski [3] - do not properly consider the coupling effects on strength of connections (see Section II.1.5). Many of them do not take into account for the ductile elasto-plastic behavior of compressed timber, fact that limits the effective strength capacity offered by this material. Some models are based on extremely simplified assumptions, especially the methods #1 and #2 by Schickhofer [9] where axial strength of connections is totally disregarded or considered in a fictious way. In add, all of them do not consider an elasto-plastic behavior of connections unlike experimental evidences (e.g. [18]). This fact does not allow for a redistribution of forces among connections subjected to tension after the first one has reached yielding strength, limiting the effective shear-wall capacity. Finally, all of them (except for method #3 by Schickhofer [9]) assume the rocking failure happening because of balanced tensile failure of connections and compressed timber, without considering other failure mechanisms.
These assumptions and simplifications could lead to overdesign of CLT structures, reason why a more refined non-linear iterative model for the design of CLT wall systems that remove some of the limits just exposed has been implemented by Tamagnone *et al.* [19–21] adopting a multifailure criterion similar to the one adopted for the design of reinforced concrete structures. This model will be analysed in depth in Section II.2 and it will serve as background for the development of a furtherly advanced model illustrated in Section II.3.

II.1.5 Coupling models for CLT connections

When a biaxial tensional state for CLT connections is considered, vis. both its axial and shear strengths are considered, it should be necessary to consider that interaction between forces in the two different directions may decrease the maximum resistance respect to the case of uniaxial tensional state. In other words, hold downs and angle brackets subjected to a shear force are able to undergo an ultimate axial strength (and displacement) less than the value that could be measured when the same connection is subjected to pure traction. Similarly, these connections are able to furnish lower shear resistance and stiffness when subjected also to traction respect to the case where no axial loads are applied. Nevertheless, it is important noticing that a combined axial and shear tensional state on connections is common for CLT wall systems subjected to seismic loads, but analytical models provided by codes and standards (e.g. Eurocode 5 [22]) or by academic literature (e.g. formulations by Blaß [23]) apply only to uniaxial lateral loading conditions. Similarly, tests on connections, often taken as reference for calibration of numerical models, are usually carried out with uniaxial load patterns (e.g. [13, 18, 24]). For this reason, in the last years there has been a growing interest in analyzing the behavior of connections subjected simultaneously to axial and shear loads. This mutual interaction phenomenon is usually referred to as *coupling* of connections strength and stiffness. Some experimental evidences of tests carried out in the last years have investigated this phenomenon, like the tests carried out by Pozza *et al.* at University of Bologna on hold-down connections subjected to monotonic and cyclic axial loadings to the vary of the imposed lateral displacement (Figure II.1-4) [25]. A similar experimental campaign on angle-brackets subjected to monotonic and cyclic lateral loads to the vary of the imposed axial displacements have been carried out by Pozza *et al.* [26]. Also Liu & Lam [27, 28] carried out experimental campaigns both on hold-downs and angle brackets to the vary of a constant force level applied on the other direction. Furthermore Izzi *et al.* [29] investigated the coupled behavior of CLT connections through advanced parametric numerical simulations by varying the inclination of the applied load.

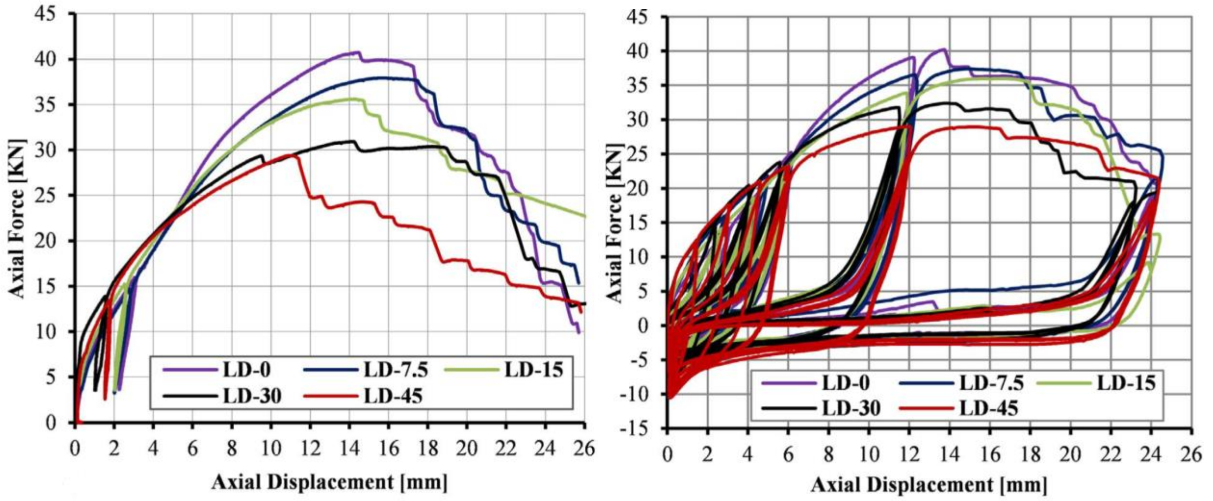

(*a*) (*b*)

Figure II.1-4 – Coupling phenomenon on connections: decay of strength and stiffness of hold-down axially-loaded connections for different levels of imposed lateral displacements (LD, values in mm) for (*a*) monotonic and (*b*) cyclic loading conditions (*image credits*: Pozza *et al.* [25]).

No design criteria to take into account for coupling phenomenon is available on codes and standards, and only ETAs (e.g. ETA-06/0106 [30] and ETA-11/0086 [31]) furnish a simple elliptical coupling criterion (Equation (II.1-7)). A coupling method derived from the elliptical criterion of ETAs has been presented by Rinaldin *et al.* [32]. The method applies a reduction of the backbone curve of constitutive laws of connections only once, when the domain boundary is first reached. The scaling of the backbone curve is carried out in terms of forces keeping constant the displacements.

Pozza *et al.* recently developed a novel hybrid force-displacement based coupling method to take into account for coupling phenomena of hold-down [33] and angle-bracket [26] connections. The model takes into account for the modification of the constitutive law in the considered direction due to displacements in the secondary direction (Figure II.1-5.a). The model can predict both monotonic and cyclic behavior of connections also accounting for degradation of strength and stiffness. The formulation of the coupling model for axially-loaded hold-downs (HDs) subjected to lateral displacement and laterally-loaded angle brackets (ABs) subjected to axial displacement is reported in Table II.1-3. Subscript t denotes the current configuration with a displacement orthogonal respect to the direction of the constitutive law and subscript *0* stands for the reference configuration with no displacement applied in the perpendicular direction. The parameters α, β, γ, m_i and q_i for $i \in [1;4]$ have been calibrated through linear regression analysis of experimental results of tests on connections subjected to bidirectional tensional state (Figure II.1-5.b).

Table II.1-3 – Hybrid force-displacement based coupling model formulation.

	N-law for HD	*V-law for AB*
$P_{I,y1,t}$	$\delta_{N,y1,t} = \delta_{N,y1,0}$ $F_{N,y1,t} = F_{N,y1,0}$	$\delta_{V,y1,t} = \delta_{V,y1,0}$ $F_{V,y1,t} = F_{V,y1,0}$
$P_{I,y2,t}$	$\delta_{N,y2,t} = \alpha \cdot \delta_{V,t} + \delta_{N,y2,0}$ $F_{N,y2,t} = \beta \cdot \delta_{V,t} + F_{N,y2,0}$	$\delta_{V,y2,t} = \left(1 + \frac{m_1}{q_1} \cdot \delta_{N,t}\right) \delta_{V,y2,0}$ $F_{V,y2,t} = \kappa \left(1 + \frac{m_2}{q_2} \cdot \delta_{N,t}\right) F_{V,y2,0} \ (for\ \ t > 0)$
$P_{I,max,t}$	$\delta_{N,F_{max},t} = \delta_{N,F_{max},0}$ $F_{N,max,t} = \gamma \cdot \delta_{V,t} + F_{N,max,0}$	$\delta_{V,F_{max},t} = \left(1 + \frac{m_3}{q_3} \cdot \delta_{N,t}\right) \delta_{V,F_{max},0}$ $F_{V,max,t} = \left(1 + \frac{m_4}{q_4} \cdot \delta_{N,t}\right) F_{V,max,0}$
$P_{I,u,t}$	$\delta_{N,u,t} = \delta_{N,u,0}$ $F_{N,u,t} = 0$	$\delta_{V,u,t} = \delta_{v,u,0}$ $F_{V,u,t} = 0$

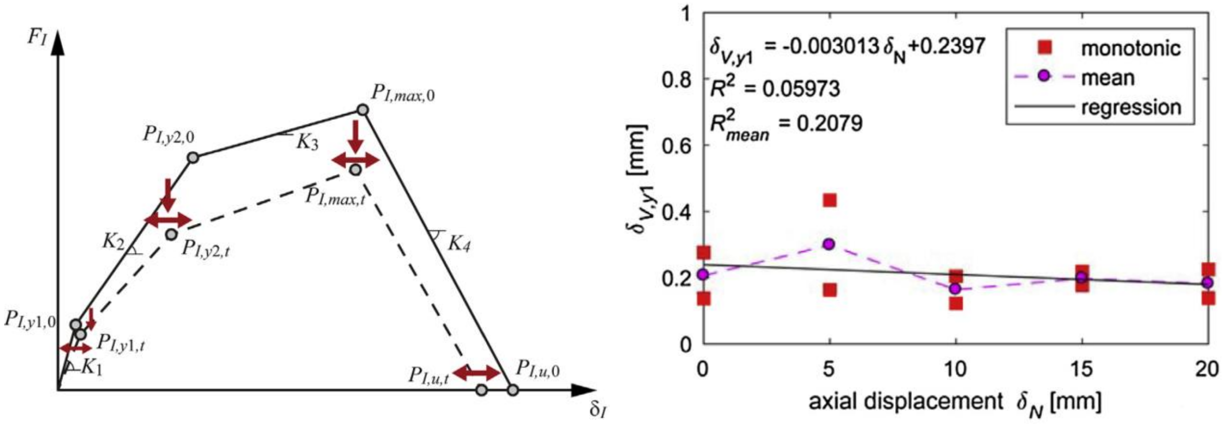

(*a*) (*b*)

Figure II.1-5 – Hybrid force-displacement based coupling method: (*a*) example of variation of the backbone envelope curve of axially-loaded hold-downs due to displacements in the secondary direction (subscripts *0* and *t* respectively stand for uncoupled and coupled conditions) and (*b*) example of linear regression analysis on experimental outcomes to derive the parameter $\delta_{V,y,1}$ (first yielding shear displacement) of laterally-loaded angle brackets to the vary of axial displacement δ_N (*image credits*: (*a*) Pozza *et al.* [33] and (*b*) Pozza *et al.* [26]).

II.2 State-of-the-art of advanced non-linear design methods for CLT wall systems

Abstract

The analytical design models for CLT shear walls showed in the previous Section II.1 suffer of some limitative assumptions, like constitutive laws of connections that do not properly consider the effective elasto-plastic-like behavior of connections. In add, most of them assume the rocking failure occurring with balanced tensile failure of both connections and compressed timber, without considering other possible failure mechanisms. In this Section an advanced method to derive V-N interaction domains available in literature is presented. The method determines the resistance of the CLT wall analyzing its failure conditions for five different sub-domains, similarly to the techniques adopted to derive interaction domains for reinforced concrete sections. The model has been developed for single-storey platform frame CLT walls connected at the bottom through hold-downs and angle brackets and assumes the rocking mechanism as the only failure mode disregarding shear failure of the wall system. This method will be used as basis for an enhanced method to derive interaction domains for CLT wall systems illustrated in Section II.3.

II.2.1 Chapter contents

In this Chapter a promising design procedure developed by Tamagnone *et al.* [19–21] for the definition of the shear capacity of a CLT wall system is presented. This procedure allows to define the *N*-*V* interaction domains of the CLT shear wall, where *N* is the axial load - assumed positive in the case of compression - and *V* is the shear force acting on the wall. In Section II.2.2 the model assumptions and hypotheses will be illustrated, highlighting their main limits. In Section II.2.3 a stress distribution coefficient will be described. Finally, in Section II.2.4 the five sub-domains of the model and their relative formulations will be shown.

II.2.2 Assumptions and hypotheses

In order to derive the method to define the *N*-*V* interaction domains, different assumptions on the mechanical behavior of the components of the CLT wall system have been considered by Tamagnone *et al.* [19–21]. These hypotheses will be listed in the following highlighting, if any, their limits.

The model has been developed referring to a platform-frame CLT wall system configuration (Section I.1.2.2.3), therefore a single-storey wall with a horizontal force applied at the top has been considered. Connections do not resist in compression and an elasto-plastic constitutive law has been assumed to describe their tensile behaviour (Figure II.2-1.b). Timber resists only in compression with a conservative elasto-brittle constitutive law (Figure II.2-1.c), despite timber subjected to compression stresses behaves in a ductile way [34]. By comparing Figure II.2-1.b and Figure II.2-1.c it is possible to observe that the constitutive law of timber is expressed in terms of stress vs. strains (σ-ε), while the one adopted for connections is a force vs. displacements (F-d) law. It is therefore necessary the adoption of a special coefficient k of compressive stress distribution (see Section II.2.3) in order to convert compressive strain of timber ε_c into an equivalent displacement d_c. In this way, working within the hypothesis of plane sections for the bottom interface section of the CLT panel, it is possible to define different sub-domains (Section II.2.4) to the vary of the displacements of compressed corner and tensioned connections.

The shear resistance of connections is assumed to be infinite, therefore no sliding failure of the wall system is considered regardless of the entity of the axial load N applied at the top of the timber panel. It must be highlighted that this is a great limit of the method proposed by Tamagnone *et al.* [19–21], since for high values of N a failure of the wall system associated to rocking kinematic is unlikely and, conversely, a sliding failure is expected. Assuming an infinite shear resistance of connections can therefore lead to unconservative results, on one hand because the effective resistance of the wall system can be overestimated for high values of the applied vertical load N, and on the other hand because disregarding the shear failure mechanism is unsafe since it is a brittle-type failure to which practitioners designing CLT structures in seismic-prone areas should guard against. A uniaxial stress state is considered for connections, therefore no coupling criteria have been considered. Contribution of friction on the shear resistance of the CLT wall system is disregarded on the safe side. Finally, the CLT panel is considered to behave rigidly, vis. no bending or shear lateral deformations are considered. It should be noted that anyway timber can deform (only) at its bottom interface accordingly to the assumed elasto-plastic constitutive law.

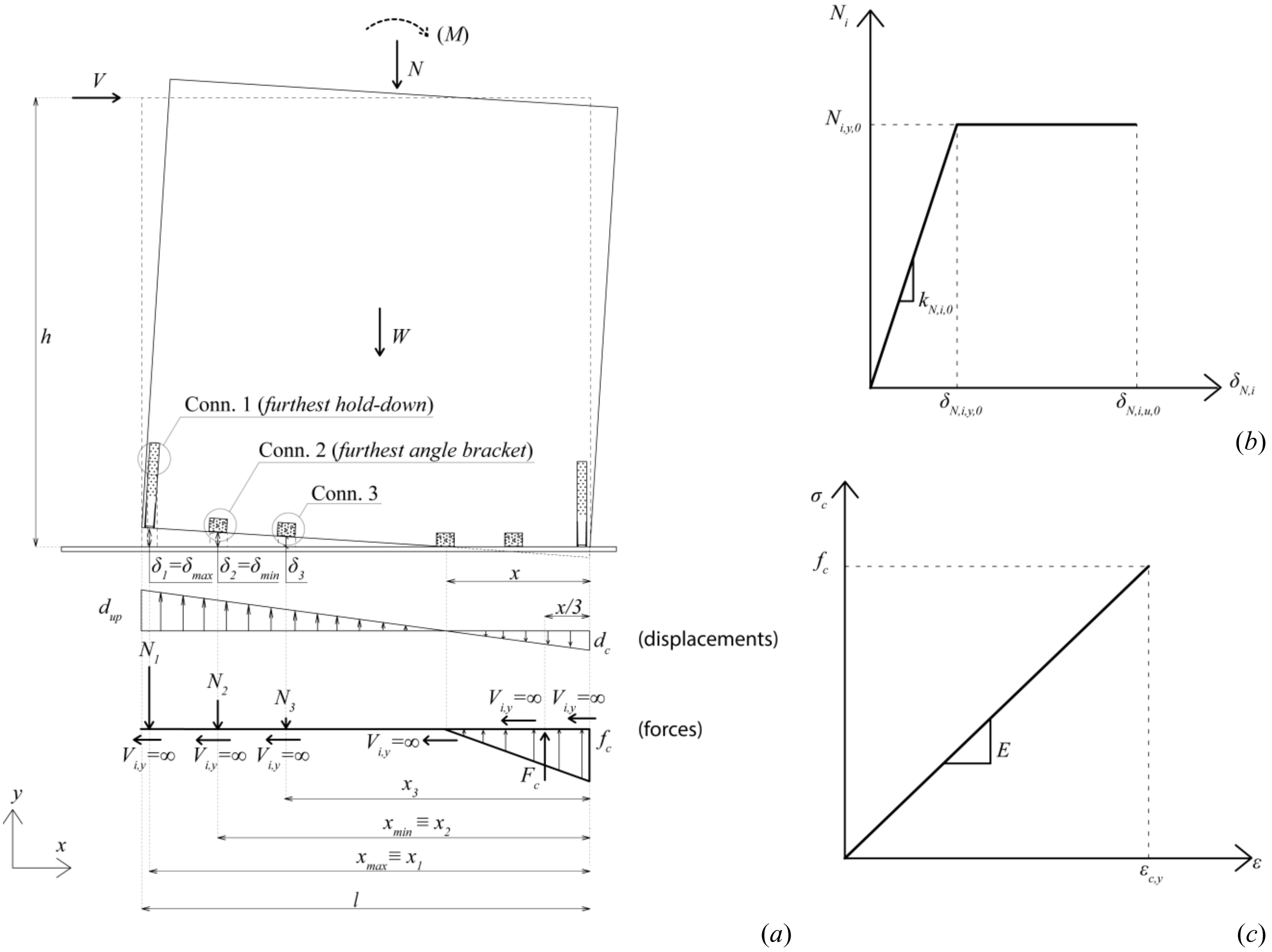
(M)
N
V
h
W
Conn. 1 (furthest hold-down)
Conn. 2 (furthest angle bracket)
Conn. 3
$\delta_1=\delta_{max}$
$\delta_2=\delta_{min}$
δ_3
x
d_{up}
x/3
d_c
(displacements)
N_1
N_2
N_3
$V_{i,y}=\infty$
(forces)
f_c
F_c
x_3
$x_{min} \equiv x_2$
$x_{max} \equiv x_1$
l
y
x
(a)
N_i
$N_{i,y,0}$
$k_{N,i,0}$
$\delta_{N,i}$
$\delta_{N,i,y,0}$
$\delta_{N,i,u,0}$
(b)
σ_c
f_c
E
ε
$\varepsilon_{c,y}$
(c)

Figure II.2-1 – Model by Tamagnone *et al.* [19–21]: (*a*) schematic representation of the: geometrical layout and force and displacement patterns, (*b*) constitutive law of connections and (*c*) timber.

II.2.3 Definition of the stress distribution coefficient

As previously stated, the model requires to convert the compressive strains of timber into displacements by means of the stress distribution coefficient k defined according to the following Equation:

$$k = \frac{\int_0^h \sigma_c(y)dy}{f_c \cdot h} \qquad (II.2\text{-}1)$$

where $\sigma_c(y)$ is the compressive stress distribution on CLT panel along its height h and f_c is the timber compressive strength.

The distribution coefficient k values have been obtained through FEM non-linear static analyses varying (i) the applied loads (ii) the height-to-length ratios and (iii) the support conditions considering both a rigid and a deformable support. The values, obtained respectively for walls subjected to an upper horizontal force V and a bending moment M, are graphically represented for different panel geometrical ratios $\frac{H}{l}$ in Figure II.2-1, where Vh stands for the overturning moment due to horizontal load V.

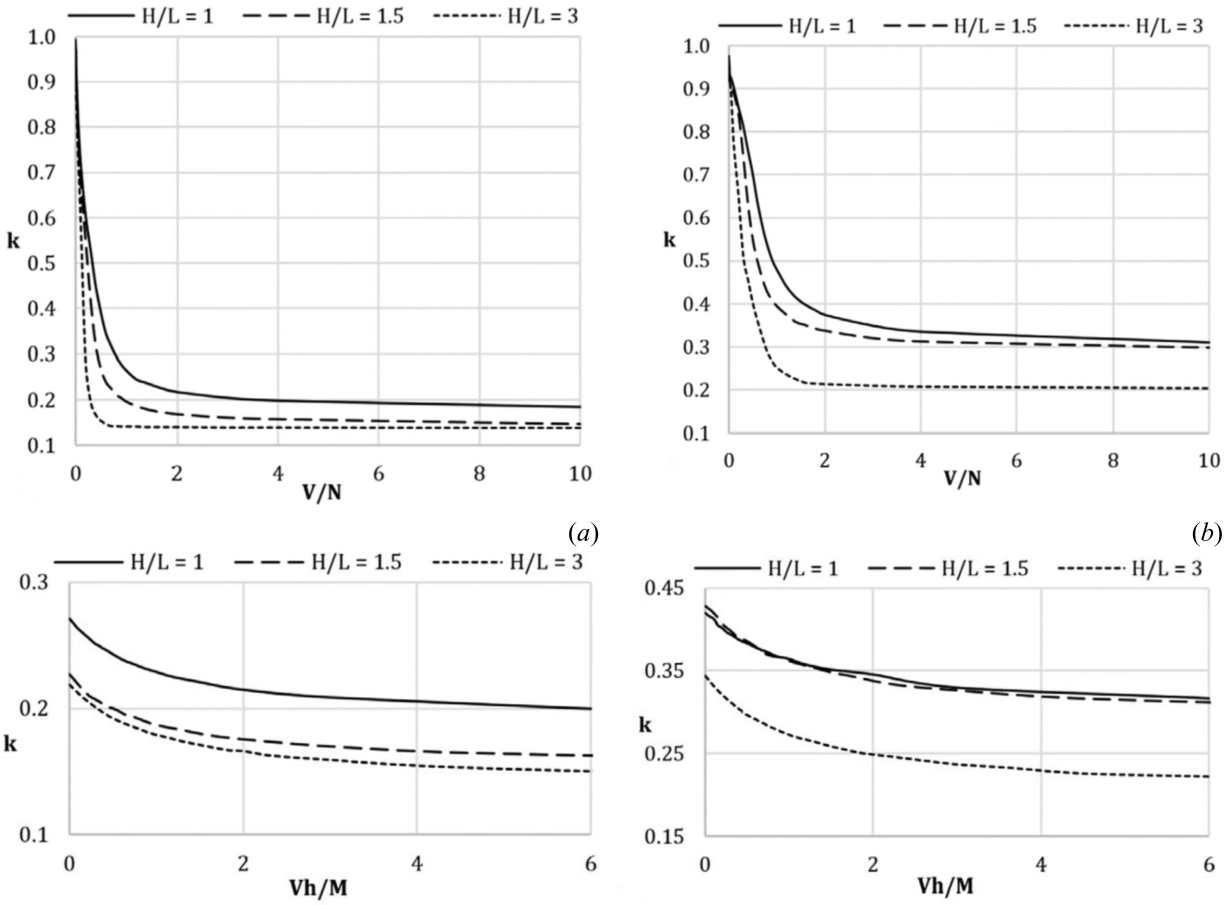

(*a*) (*b*)

(*c*) (*d*)

Figure II.2-2 – Stress distribution coefficient *k* for CLT walls subjected to (*a-b*) horizontal force *V* and (*c-d*) bending moment *M* for (*a-c*) rigid and (*b-d*) CLT flexible supports (*image credits*: Tamagnone *et al.* [19]).

II.2.4 Sub-domains definition and formulations

In analogy with the analysis of reinforced concrete (RC) sections subjected to combined axial and bending forces, different sub-domains that describe all the failure modes that the bottom section of the CLT panel can undergo have been defined. In particular, the section can reach its strength capacity or because of failure of connections in tension, or since the maximum timber capacity in compression has been reached, or for a combination of these two failure states.

The five sub-domains are defined as follows (Figure II.2-3.a):

- sub-domain 1 (*pure tension*): at least one connection reaches its ultimate uncoupled displacement $\delta_{N,i,u,0}$ and timber is not compressed;
- sub-domain 2: the failure of the wall system happens for the attainment of ultimate displacement $\delta_{N,i,u,0}$ of one of the connections, timber is compressed but with a compression stress at the corner σ_c lower than the ultimate one f_c;
- sub-domain 3 (*balanced failure*): at least one of the connections is subjected to tension and timber reaches its ultimate resistant stress f_c;
- sub-domain 4: stress at panel corner σ_c is equal to f_c, none of the connections is subjected to tension and the corner opposite to the compressed one is uplifted;
- sub-domain 5 (*pure compression*): timber attains its maximum resistant stress f_c at the compressed corner, all the bottom panel section is compressed.

The subscripts *0* stand for the uncoupled mechanical parameters of connections, since the model by Tamagnone *et al.* [19] disregards interaction between axial and shear strength of connections.

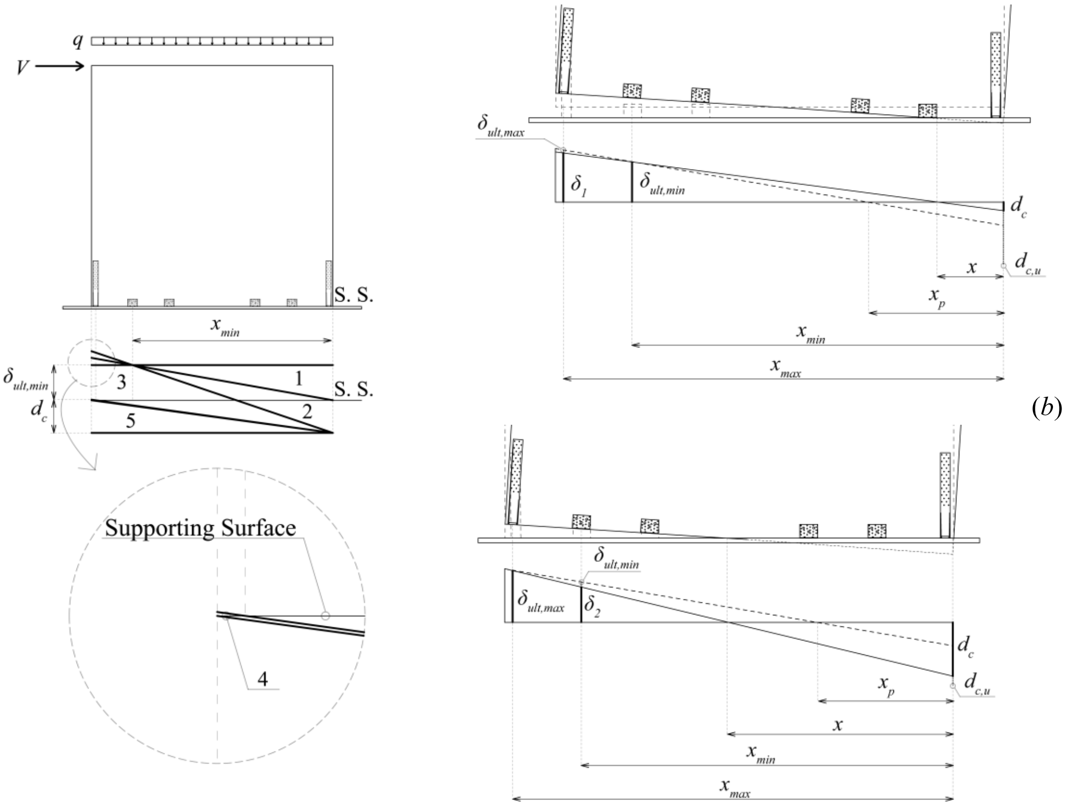

(*b*)

(*a*) (*c*)

Figure II.2-3 – Failure sub-domains: (*a*) sub-domains definition, (*b*) failure condition for sub-domains 1 and 2 for attainment of ultimate condition on furthest angle bracket and (*c*) furthest hold-down.

Sub-domains 1,2 and 3 require an iterative solution because of non-linearity of constitutive law of the tensioned connections, while sub-domains 4 and 5 have a closed-form solution. It must be anyway noticed that the solutions at the boundaries between sub-domains 1-2 and 2-3 do not require iterations since the position of the neutral axis x can be simply derived geometrically.

Hold-down and angle-brackets connections are characterized by different ultimate failure displacements, respectively $\delta_{ult,max}$ and $\delta_{ult,min}$, with usually $\delta_{ult,max} \geq \delta_{ult,min}$ Therefore, for sub-domains 1 and 2 the failure can happen in one or the other connections as a function of their position and their mechanical characteristics. In particular, failure happens in angle-brackets if the following condition is satisfied (Figure II.2-3.b):

$$x \leq x_p = \frac{\delta_{ult,max} \cdot x_{min} - \delta_{ult,min} \cdot x_{max}}{\delta_{ult,max} - \delta_{ult,min}} \qquad (II.2\text{-}2)$$

where x is the position of the neutral axis (measured respect to the compressed corner and positive in the direction opposite to the applied horizontal force V) and x_{min} and x_{max} are the position of the farthest connection from the compressed corner having respectively $\delta_{ult,min}$ and $\delta_{ult,max}$ as ultimate condition.

If the value of x is greater than the limit given in Equation (II.2-2) the failure of the wall in sub-domains 1 and 2 happens for the attainment of ultimate conditions of hold-down $\delta_{ult,max}$ (Figure II.2-3.c) if the following condition is satisfied:

$$x_p \leq \frac{x_{min} \cdot d_{c,u}}{\delta_{ult,min} \cdot d_{c,u}} \tag{II.2-3}$$

where $d_{c,u}$ is the ultimate timber compressive deformation. The condition (II.2-3) is necessary to guarantee that timber has not reached its ultimate condition in compression.

Defined x_i the position of the i-th connection from the compressed corner (Figure II.2-1.a), it is possible to define in the following the formulations for the five sub-domains.

The axial deformation of the i-th connection δ_i for sub-domains 1 and 2 is defined accordingly to Equation (II.2-4) while for sub-domain 3 it is defined by Equation (II.2-5):

$$\delta_i = \begin{cases} \dfrac{\delta_{ult,min}(x_i - x)}{x_{min} - x} & for\ x \leq x_p \\ \dfrac{\delta_{ult,max}(x_i - x)}{x_{max} - x} & for\ x > x_p \end{cases} \tag{II.2-4}$$

$$\delta_i = \frac{d_{c,u}(x_i - x)}{x} \tag{II.2-5}$$

The correspondent axial force N_i acting on the i-th connection is equal to (Figure II.2-1.b):

$$N_i = \begin{cases} N_{i,y,0} & for\ \delta_i > \delta_{N,i,y,0} \\ k_{N,i,0} \cdot \delta_i & for\ \delta_i \leq \delta_{N,i,y,0} \end{cases} \tag{II.2-6}$$

The compressive resultant force F_c for sub-domains 2 and 3 is respectively given by Equation (II.2-7) and (II.2-8):

$$F_c = \frac{\sigma_c \cdot t \cdot x}{2} \tag{II.2-7}$$

$$F_c = \frac{f_c \cdot t \cdot x}{2} \tag{II.2-8}$$

where σ_c is the stress at the compressed corner and t is the thickness of the CLT panel.

The position of the neutral axis x for sub-domains 1, 2 and 3 can be derived iteratively imposing the vertical equilibrium:

$$N = F_c(x) - \sum_{1}^{n_{trax}} N_i(x) - W \tag{II.2-9}$$

where n_{trax} is the number of connections subjected to tension and W is the dead load.

For sub-domains 4 and 5 it is possible to derive x in a closed form solution, respectively accordingly to Equations (II.2-10) and (II.2-11):

$$x = \frac{2(N + W)}{f_c \cdot t} \tag{II.2-10}$$

$$x = \frac{f_c \cdot t \cdot l^2}{2(f_c \cdot t \cdot l - N - W)} \tag{II.2-11}$$

It is therefore possible to derive the resistant shear force V by imposing the equilibrium to rotation of the wall system. For sub-domains 1 to 4, the resistant shear force V is:

$$V = \frac{F_c}{h}\left(\frac{l}{2} - \frac{x}{3}\right) - \sum_{1}^{n_{trax}} N_i\left(\frac{l}{2} - x_i\right) \tag{II.2-12}$$

For sub-domain 5 the resistant shear force V is equal to:

$$V = \frac{F_c}{h}\left(\frac{l}{2} - \frac{l}{3}\frac{2\,\sigma_d + f_c}{\sigma_d + f_c}\right) \qquad (II.2\text{-}13)$$

where σ_d is the timber compression stress on the corner of the CLT panel opposite to the direction of the horizontal force V (i.e. the left corner in Figure II.2-4), whose value can be derived accordingly to:

$$\sigma_d = f_c\left(1 - \frac{l}{x}\right) \qquad (II.2\text{-}14)$$

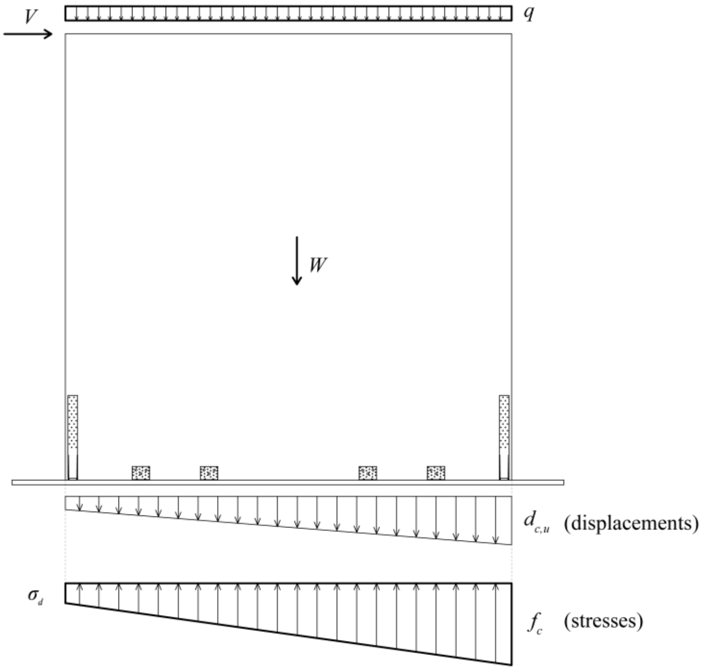

Figure II.2-4 – Displacements and stresses distributions at bottom interface for sub-domain 5.

Figure II.2-6 shows as case study the interaction domains and the correspondent five sub-domains obtained with the method by Tamagnone *et al.* [19] for walls I.1, I.2 and I.3 (Figure II.2-5) tested at CNR-IVALSA within the SOFIE project [35]. The three walls are characterized by the same geometry and connection arrangement while different vertical loads are applied (i.e. 9.25 kN/m for walls I.1.and I.2, and 18.5 kN/m for Wall I.3). It is possible to observe that for sub-domains 4 and 5 the two diagrams are coincident, since the CLT shear wall response is not function of connections behavior for that two dub-domains. The differences for the other three sub-domains are minimal for the *N-V* curve and it is possible to observe also a slight change of the boundary limits of the sub-domains. It is worth noting that for wall configuration I.1 the method by Tamagnone overestimates the effective strength measured in the experimental campaign while, on the contrary, the method is on the safe side for configurations I.2 and I.3. This is due to the fact that the analytical method disregards the shear failure of the CLT wall-system, and as pointed out in [35], while walls I.2 and I.3 are characterized by a combined rocking-sliding failure, wall I.1 fails because of shear, therefore its failure cannot be correctly captured by this model. This is one of the main limits of the model by Tamagnone that will be removed in the enhanced design method presented in the following chapter II.3.

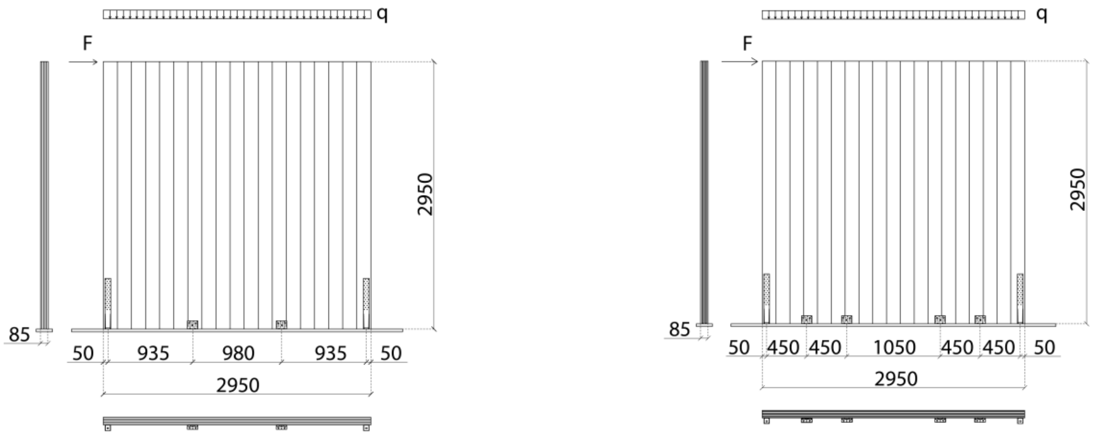
q
F
2950
85
50
935
980
935
50
2950
q
F
2950
85
50
450
450
1050
450
450
50
2950

(*a*) (*b*)

Figure II.2-5 – Wall configurations (*a*) I.1 with 2 angle-brackets and configurations (*b*) I.2-I.3 with 4 angle-brackets tested within the SOFIE project [35].

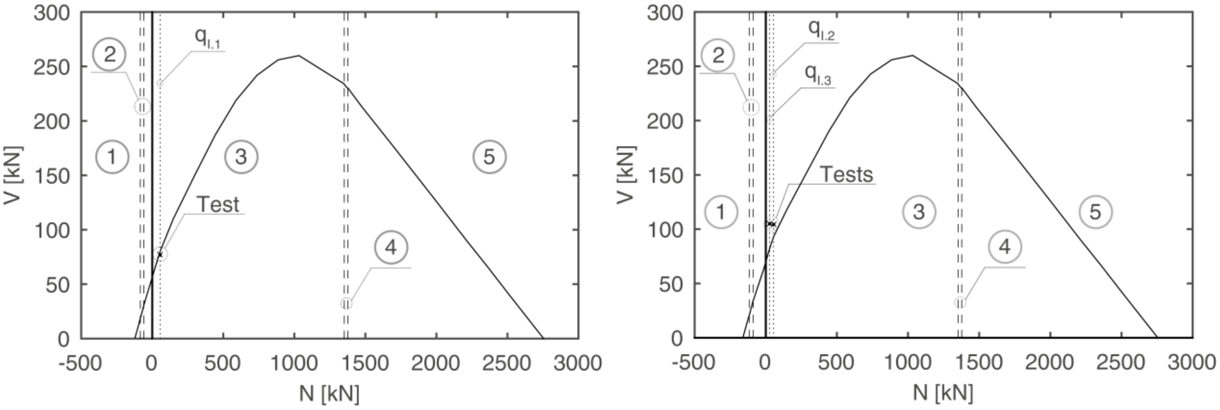

(*a*) (*b*)

Figure II.2-6 – Interaction domains of wall configurations (*a*) I.1 and (*b*) I.2-I.3 derived with the method proposed by Tamagnone *et al.* [19]. Dashed vertical lines delimit the boundaries of the five sub-domains. Dotted vertical lines are indicative of the value of the vertical load *N* for each configuration. The markers denote the experimental tests outcomes.

II.3 Interaction Domains for CLT Shear Walls with Coupled Constitutive Laws of Connections

Abstract

The seismic design of a CLT shear wall is currently based on the evaluation of the forces acting on the single components of the system. This can be performed by using linear or nonlinear numerical models requiring the implementation of the constitutive law of each individual component of the shear wall for the different loading condition. In the last years, alternative design procedures have been developed by many researchers to provide simplified design methods best suited for practitioners. One of the most promising is derived from the well-known cross-sectional analysis techniques currently adopted for reinforced concrete and is based on the N-V interaction domains. The present Section, starting from one of these design method of CLT shear wall based on the N-V interaction domain available in literature, proposes an enhanced procedure, which considers the ductile behaviour of the timber panel in compression and introduces the failure mechanism of the connection elements according to the most reliable axial-shear coupling criteria. The basic assumptions and the novelty aspects of the enhanced N-V interaction domain model are presented and discussed with special attention to the criteria adopted for the linearization of the connection load-displacement response and the correspondent multicriteria failure mechanisms. The reliability of the improved model is demonstrated by means of refined analyses exploiting the ultimate failure condition of the materials both in terms of strength and displacement capacity. Finally, the N-V domain for a case study CLT shear-wall is presented and the impact of the different basic assumptions on the results are discussed in comparison with the experimental outcomes.

II.3.1 Chapter contents

The study presented in this Section aims at improving the model proposed by Tamagnone *et al.* [19] (Section II.2) to derive *N-V* interaction domains of CLT shear walls (where *N* and *V* are respectively the axial load assumed positive if in the case of compression, and shear force acting on the wall), considering more refined failure criteria of the CLT wall components in order to obtain more reliable results. Section II.3.2 reports the assumptions of the enhanced model. First of all an elastoplastic behavior of wood is considered instead of the linear one of the reference model by Tamagnone *et al.* [19]. In addition, the proposed model takes into account the coupling effect between the axial and lateral strength of connections, that has been proven to be crucial in defining the correct mechanical behavior of fastening system (i.e. hold-down and angle brackets) by different authors [4, 26, 33, 36]. Two bi-linearization methods (Section II.3.3.1) for the definition of the connections constitutive laws are implemented in the coupling axial-lateral strength model of connections ([26, 33]) in order to properly take into account the failure mechanism of the shear wall that is disregarded in the reference model [19]. The coupling methods adopted are presented in Sections II.3.3.2 and II.3.3.3.

Finally, a comparison between the N-V domain for a case study CLT shear-wall, chosen among the ones tested at the CNR-IVALSA laboratory during the so called "SOFIE project" [35] is presented and the impact of the different basic assumptions on the results are discussed in comparison with the experimental outcomes (Section II.3.4).

II.3.2 Assumptions

The model has been developed on the basis of the one proposed by Tamagnone *et al.* [19] which adopts for the study of CLT walls the well-known cross-sectional analysis techniques developed for RC cross sections, e.g. [37]. In detail, the timber panel is considered as the compressed element (like concrete in RC sections) and the connections as the only tension-resistant elements (like steel bars in RC sections). According to this approach, CLT shear wall panel is considered as rigid body and in direct contact with the ground surface. Connections are modelled as uniaxial elastoplastic elements [19] capable of exploiting only tensile resistance, since the contribution of the connections to the compression strength of the system is assumed as negligible.

The sectional analysis computes the resistant moment of the cross-section, which is then converted to shear force at top of the wall, by considering the entire wall height *h* and the actual boundary conditions (in this work, the wall is assumed to behave as a cantilever).

In this Section various improvements are performed to the constitutive laws proposed in [19] in order to better describe both the behavior of the timber in compression and the response of the connection elements when subjected to coupled axial-shear actions. In particular, concerning the behavior of timber in compression, an elastic-perfectly-plastic (EPP) constitutive law is adopted, accordingly to the response observed in many experimental studies (e.g. [34]). This assumption not only reflects more realistically the mechanical behavior of the timber in compression, but also allows to better exploit its ductility capabilities. As far as the behavior of connections is concerned, both axial and lateral directions are considered by assuming proper coupled constitutive laws, since recent experimental tests carried out on hold-downs and angle-brackets demonstrated a significant correlation between the strength and stiffness in both strong and weak direction (e.g. [26, 33, 36]). In fact, neglecting this effect could provide an overestimation of the effective strength of the shear wall, possibly leading to wrong and unsafe results.

A schematic representation of the model proposed in this work is depicted in Figure II.3-1, while Table II.3-1 summarizes all the symbols used together with a brief description. The main assumptions used in the proposed model are summarized in the following, respectively for timber and connection elements.

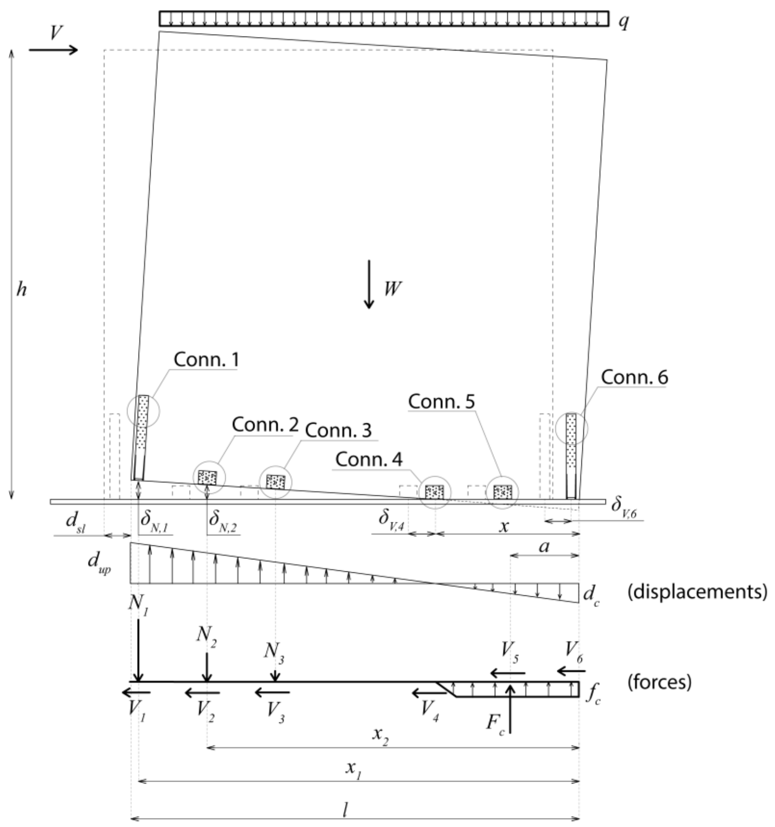

Figure II.3-1 – Schematic representation of the proposed model: geometrical layout and force and displacement patterns.

Table II.3-1 – List of symbols of Figure II.3-1 (alphabetical order).

Symbol	*Description*
a	Position of F_c respect to the compressed corner
d_c	Displacement of the compressed corner of CLT panel
d_{sl}	Global slip displacement of shear wall
d_{up}	Global uplift displacement of shear wall
F_c	Compressive force of timber
h	Height of CLT panel
l	Length of CLT panel
N_i	Axial force on *i-th* connection
V	Horizontal force acting at the top of the shear wall
V_i	Shear force on *i-th* connection
W	Dead load of the CLT panel
x	Neutral axis position from compressed edge
x_i	Position of *i-th* connection from compressed edge
$\delta_{N,i}$	Axial displacement of *i-th* connection
$\delta_{V,i}$	Lateral displacement of *i-th* connection

Timber: modeled with an EPP behavior (Figure II.3-2.a), characterized by Young modulus E, ultimate compressive stress f_c and ultimate strain $\varepsilon_{c,u}$. The stress-strain law is mapped to a force-displacement (N-d_c) law through the coefficient k, derived, coherently with [19], as a function of compressive stress distribution along the height of the panel h.

Connection elements: coupling between tensile and shear strengths of connections is considered according to both force-based approach, e.g. [32], and a more innovative hybrid force-displacement-based approach (in the following *Hybrid Method*), [26, 33]. Specifically, the axial behavior is modeled with an EPP constitutive law

(Figure II.3-2.b), defined by the three parameters: yielding force $N_{i,y}$, yielding displacement $\delta_{N,i,y}$ and ultimate displacement $\delta_{N,i,u}$. The shear behavior of the connections is also modeled through EPP law (Figure II.3-2.c), characterized by yielding force $V_{i,y}$, yielding displacement $\delta_{V,i,y}$ and ultimate displacement $\delta_{V,i,u}$. The shear forces are transferred only by metal connections (Figure II.3-1) since the friction at the interface between the CLT panel and the ground surface could be neglected, e.g. [38]. It's finally worth noting that the interaction domains are derived neglecting the buckling phenomena, which for high values of the vertical loads N could modify the failure mode of the CLT shear wall.

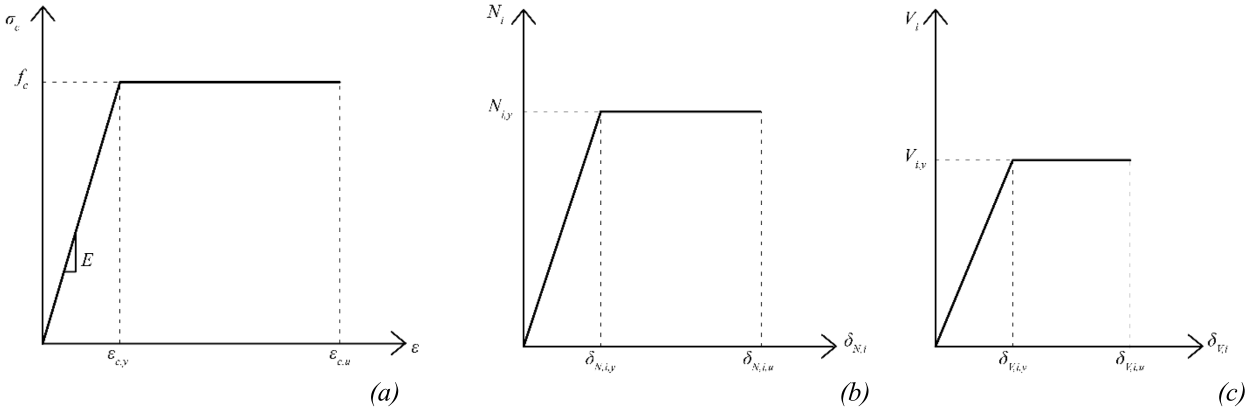

Figure II.3-2 – Constitutive laws for: (*a*) compressed timber at the bottom interface; (*b*) connections loaded in axial direction; (*c*) connections loaded in lateral direction.

II.3.3 Multicriteria ultimate conditions

Since the cross-section consists of different components and different materials, multiple failure modes should be considered to define the global ultimate strain profile corresponding to the conventional ultimate strength of the section. Therefore, the conventional failure is associated to the ultimate deformation profile that attains at least one of the two following conditions: *i*) failure of timber in compression; *ii*) failure of connection element (i.e. hold-down or angle bracket) in tension (*ii-a*) or in shear (*ii-b*).

According to the basic model assumption of the *N-V* interaction domain (Section II.3.2), timber is assumed to fail in compression when the ultimate displacement $d_{c,u}$ is reached, while for the definition of the connections failure, the axial-shear coupling is considered, [26, 33, 36]. As previously stated, in this work two different approaches characterized by increasing level of complexity are adopted, i.e. respectively a force-based and a hybrid force-displacement-based approach, and the results are critically compared. The two approaches are described in the following subsections II.3.3.2 and II.3.3.3, while the bi-linearization procedures of the experimental connections load-displacement curve used for the definition of the their constitutive law is briefly summarized in subsection II.3.3.1.

II.3.3.1 Bi-linearization of uniaxial constitutive laws of connections

The *N-V* diagram of a CLT wall can significantly be affected by the method adopted for the definition of the bilinear constitutive laws of the connection elements, [39]. Two different bi-linearization methods suitable to derive the parameters defining the corresponding bi-linear constitutive law (i.e. $N_{i,y}$, $\delta_{N,i,y}$, $\delta_{N,i,u}$ for axially-loaded connections, $V_{i,y}$, $\delta_{V,i,y}$ $\delta_{V,i,u}$ for laterally-loaded connections, Figure II.3-3) are adopted and compared in the present Section. Both the proposed criteria require a preliminary multi-linearization of the experimental envelope curve, according to the procedure defined in [26, 33].

The first criterion (Figure II.3-3.a), labelled as #1 in the following, considers the yielding point of the bilinear curve ($N_{i,y}$, $\delta_{N,i,y}$ and $V_{i,y}$, $\delta_{V,i,y}$ respectively for axially and laterally loaded connections) matching the second yielding point (P_2) of the backbone curve defined in [10,11] (dash-dot line in Figure II.3-3) and adopts a secant stiffness.

The second criterion (Figure II.3-3.b), labelled as #2 in the following, sets the bilinear curve to the maximum strength of the connection F_{max}, that is equal to the force corresponding to point P_3 of the backbone curve defined in [26, 33], and the stiffness is derived through an energy balance with the reference backbone. Both approaches define d_u as the displacement corresponding to a reduction of 20% of the maximum strength F_{max} in the softening branch, accordingly to EN 12512 [40].

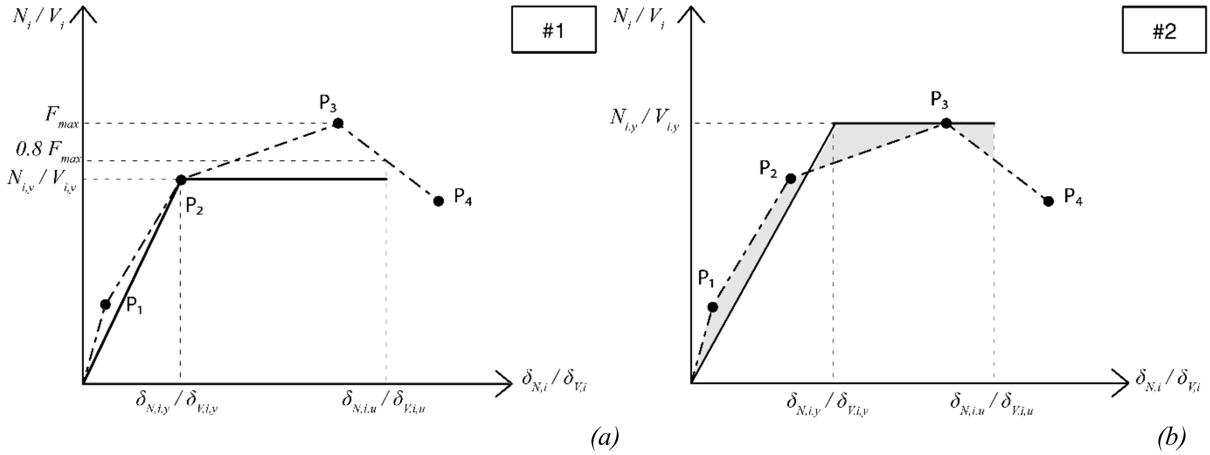

Figure II.3-3 – Bi-linearization method (solid lines) and backbone curve (dash-dot line) defined by points P1-P4 according to [26, 33]. (*a*) method 1 - #1; (*b*) method 2 - #2

II.3.3.2 Force-based connection strength domain

The force-based approach is currently used by design codes [22, 41] and by Technical Approval documents, e.g. [30] for the definition of the strength domain of connections subjected to biaxial loading condition. Two different strength domain formulation are available in literature and used in this work: an elliptical and a rectangular one, respectively represented in Figure II.3-4.a and Figure II.3-4.b. It is worth noting that, being the constitutive laws EPP, the failure and yielding domains in term of forces are exactly the same.

The first formulation is the one recommended by the Technical Approval documents of the connection elements [30] and was firstly used in [32] for the development of a coupled tension-shear numerical model of the CLT connections. Accordingly to [30], the elliptical domain (N_i, V_i) schematized in Figure II.3-4.a is represented by the following equation:

$$\left(\frac{N_i}{N_{i,y,0}}\right)^2 + \left(\frac{V_i}{V_{i,y,0}}\right)^2 = 1 \qquad (II.3\text{-}1)$$

where $N_{i,y,0}$ and $V_{i,y,0}$ represent respectively the maximum uniaxial axial and shear strengths of the connection. In detail, when the elliptical limit surface (in terms of forces) is reached at the point $V_{i,y}, N_{i,y}$, two different failure methods are proposed: in the first one, marked with a cross symbol in Figure II.3-4.a and named "*Refined*" in the following, the constitutive laws are scaled up to the $N_{i,y}$ and $V_{i,y}$ values, while maintaining the ultimate displacement as the same of the initial condition, as proposed in [32]. In the second case, marked with circular symbol in Figure II.3-4.a and named "*Simplified*" in the following, the constitutive laws are still scaled up to the $N_{i,y}$ and $V_{i,y}$ values, but reducing the ultimate displacements to the yielding one. The latter approach is simpler and more suitable for practitioners to design CLT shear-walls. It gives results on the safe side, since the connection is considered failed (i.e. attainment of one of the multi-failure criteria) when the limit surface is firstly reached, disregarding the possible forces redistribution among the connections due to their ductile behavior.

The rectangular domain is a basic approach typically used by practitioners in the design phase [4, 5] and in the numerical modelling [38, 42–45] of CLT structures to account for the biaxial strength of the connections. Differently form the elliptical domain, no interaction effects are accounted for, since the connection can exploit simultaneously both the maximum axial and shear strength. The rectangular domain depicted in Figure II.3-4.b is described by the following equations, where the symbols are the same as in Equation (II.*3-1*):

$$\begin{aligned} N_i &= N_{i,y,0} \quad \text{when } -V_{i,y,0} < V_i < V_{i,y,0} \\ V_i &= V_{i,y,0} \vee V_i = -V_{i,y,0} \quad \text{when } 0 < N_i < N_{i,y,0} \end{aligned} \qquad (II.3\text{-}2)$$

Similarly to the case of elliptical domain, also for the rectangular one, the two previously introduced approaches are adopted: the “*Simplified”* one (circular symbol in Figure II.3-4.b) is based on the assumption that ultimate displacement corresponds to the yielding one, even if no scaling of constitutive law in terms of force is considered, while in the “*Refined”* one (cross symbol in Figure II.3-4.b) the ultimate displacement is assumed equal to the one defined in the initial condition.

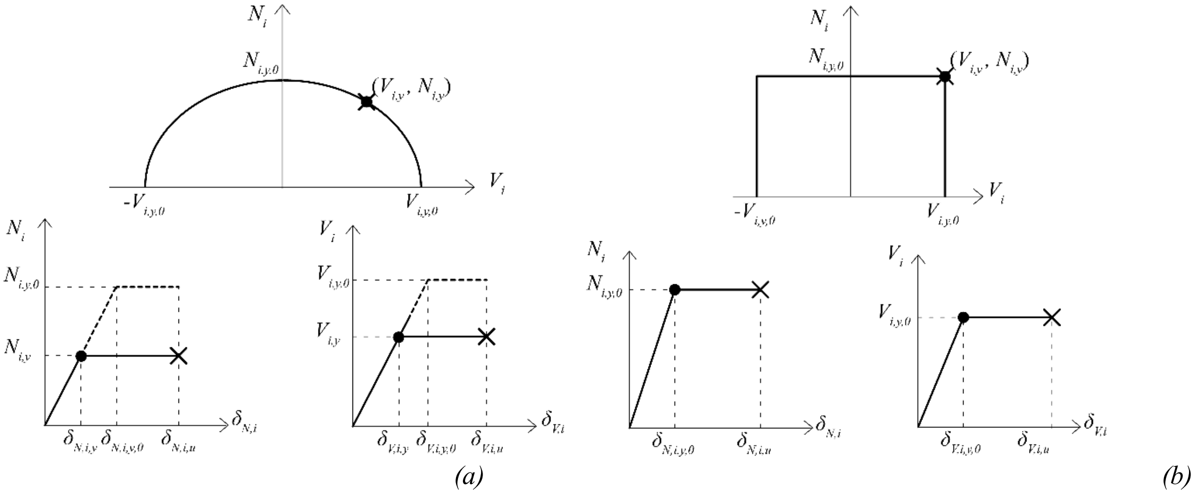

Figure II.3-4 – Coupling force-based strength domain of connections: (*a*) Elliptical domain; (*b*) Rectangular domain.

II.3.3.3 Hybrid force-displacement-based connection strength domain

The Hybrid force-displacement–based approach described in this section is an innovative procedure to account for the axial-shear coupling effect and it is based on the formulation developed by some of the authors in [26, 33]. According to this approach, the characteristic points of the connection constitutive laws in one direction are affected by the displacement reached in the orthogonal direction. Such an approach was derived from coupled experimental tests carried out on hold-down and angle brackets CLT connections [25, 26] and refers to the piece-wise linear function depicted in Figure II.3-3 for the definition of the coupling behavior in the two load-directions and characterized by the four points: first and second yielding points, P_1 and P_2, peak and ultimate points, P_3 and P_4. Since the general model for the definition of the *N-V* interaction domain of the CLT shear wall is based on a bi-linear schematization of the components, in this work the coupling model proposed in [26, 33] is adapted in order to allow the implementation of the bilinear connection constitutive laws described in Section II.3.3.1. Specifically, new regression equations that describe the influence of orthogonal displacement on the two characteristic points of the bilinear curve (i.e. yielding and ultimate points) are defined.

It is worth noting that the coupling effect is more pronounced in the main working direction of the connection (i.e. axial for hold-down and lateral for angle bracket) [26, 33] therefore in the following only a uniaxial coupling behaviour is considered, i.e. the effects of lateral displacement on the axial constitutive law of hold-down and of the axial displacement on the shear constitutive law of angle bracket are considered. The shear constitutive law of hold-down connections and the axial constitutive law of angle brackets will therefore be considered in their uncoupled formulation for the analyses carried out with the *Hybrid* coupling criterion.

The coupled bi-linear constitutive laws are obtained for increasing values of the orthogonal displacement starting from the multi-linear envelopes reported in [26, 33], see Figure II.3-5.

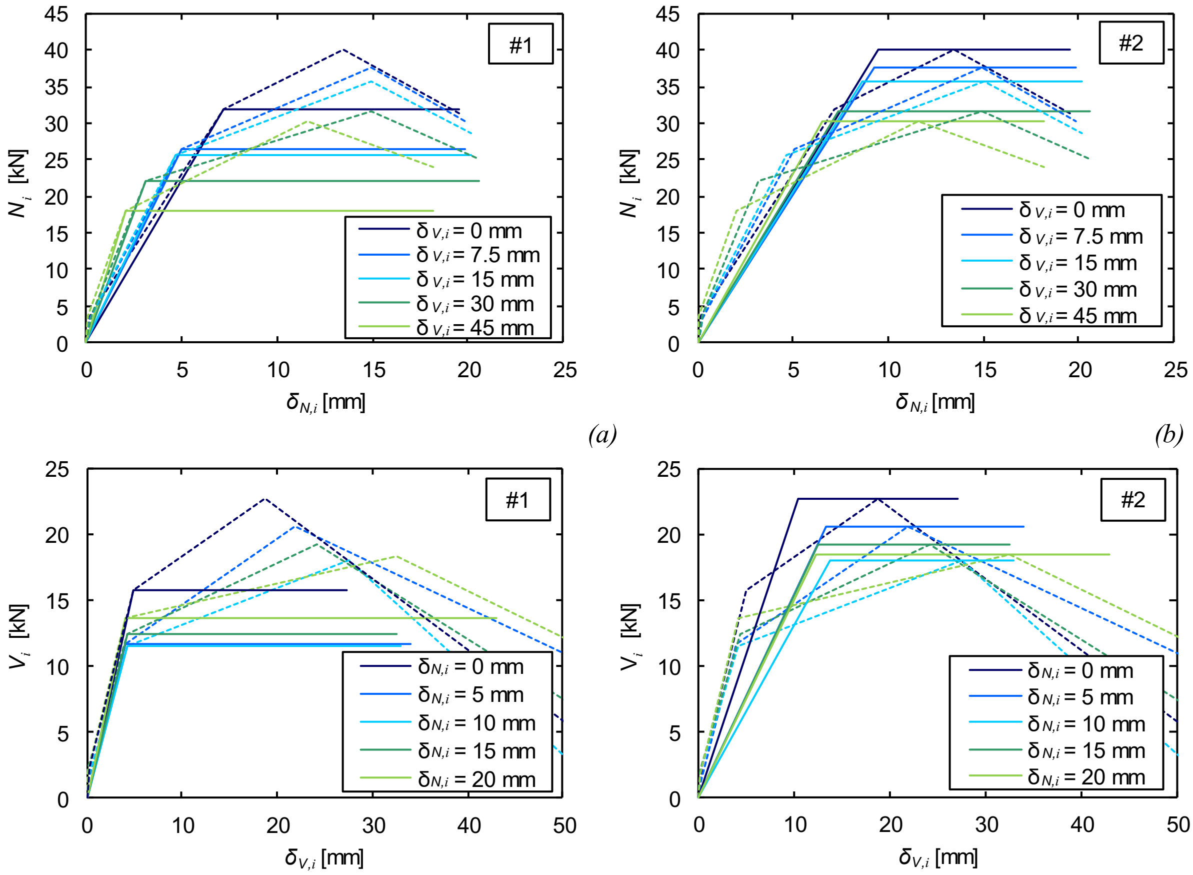

(a) (b)

(c) (d)

Figure II.3-5 – Coupled elasto-plastic constitutive laws (solid lines) and backbone curves (dashed lines) [26, 33] for different values of displacement in the orthogonal direction: axially-loaded hold-down connections calibrated with criterion (*a*) #1 and (*b*) #2; laterally-loaded angle bracket connections calibrated with criterion (*c*) #1 and (*d*) #2.

From the results of the bi-linearization procedure it is possible to observe that for axially-loaded hold-down connections the yielding force decreases with increasing lateral displacement (Figure II.3-5.a and b), while for laterally-loaded angle bracket connections, no specific trend is evident (Figure II.3-5.c and d). In addition, for axially-loaded hold-down constitutive law bi-linearized with method #1 (Figure II.3-5.a), the stiffness increases with increasing lateral displacement, while it is almost constant if bi-linearization #2 is adopted (Figure II.3-5.b).

The results of the linear regression analysis on the characteristic points are depicted in Figure II.3-6 to Figure II.3-8, where the relationships between the parameters that define the bi-linear laws ($N_{i,y}$, $\delta_{N,i,y}$, $\delta_{N,i,u}$ for axially-loaded hold-down connections, $V_{i,y}$, $\delta_{V,i,y}$ $\delta_{V,i,u}$ for laterally-loaded angle bracket connections) and the displacement in the orthogonal direction are reported. According to [26, 33], in order to define the parameters of the bi-linear curve, the slope of the regression lines m_i are normalized to the correspondent intercepts q_i

defining the ratios $r_i = m_i/q_i$ (Table II.3-2). These ratios r_i are representative of the variation of the mechanical properties for increasing orthogonal displacements.

The model proposed in [26, 33] characterized with the bi-linear constitutive laws is defined by the following equations:

$$N_{i,y} = (1 + r_1 \cdot |\delta_V|) N_{i,y,0} \tag{II.3-3}$$

$$\delta_{N,i,y} = (1 + r_2 \cdot |\delta_V|) \delta_{N,i,y,0} \tag{II.3-4}$$

$$\delta_{N,i,u} = (1 + r_3 \cdot |\delta_V|) \delta_{N,i,u,0} \tag{II.3-5}$$

$$V_{i,y} = (1 + r_4 \cdot \delta_N) V_{i,y,0} \tag{II.3-6}$$

$$\delta_{V,i,y} = (1 + r_5 \cdot \delta_N) \delta_{V,i,y,0} \tag{II.3-7}$$

$$\delta_{V,i,u} = (1 + r_6 \cdot \delta_N) \delta_{V,i,u,0} \tag{II.3-8}$$

where the parameters with subscript 0 (i.e. the reference parameters $N_{i,y,0}$, $\delta_{N,i,y,0}$, $\delta_{N,i,u,0}$, $V_{i,y,0}$, $\delta_{V,i,y,0}$, $\delta_{V,i,u,0}$) are those defining the bi-linear constitutive laws of the connections loaded in uniaxial conditions (i.e. their value for a null displacement in the orthogonal direction).

Table II.3-2 – Ratio r_i of the coupling equations (II.3-3) - (II.3-8) for bi-linearization methods #1 and #2 derived from linear regression analysis.

Ratio r_i=m_i/q_i	*#1*	*#2*
r_1	-0.0075	-0.0056
r_2	-0.0161	-0.0071
r_3	-0.0012	-0.0012
r_4	-0.0080	-0.0091
r_5	-0.0084	0.0116
r_6	0.0217	0.0217

In the case of a CLT shear wall fastened with connections different from those adopted in [26, 33], the reference parameters must be evaluated referring to the bilinear curves obtained by performing specific experimental uniaxial tests in tension and shear on the angle bracket and hold-down connections employed in the CLT wall, as done in section II.3.4.2.2.

From the results of regression analyses, it can be observed that yielding force reduces for increasing orthogonal displacement, in accordance with the outcomes obtained by using the reference backbone curve (see [26, 33]), for both the bi-linearization methods (Figure II.3-6). Yield displacement in axial direction decreases with increasing lateral displacement for both bi-linearization methods, while in lateral direction it decreases for bi-linearization method #1 and increases for bi-linearization method #2 (Figure II.3-7). Finally, ultimate displacement in axial direction slightly decreases with increasing lateral displacement, while in lateral direction it increases for increasing axial displacement for both bi-linearization methods (Figure II.3-8).

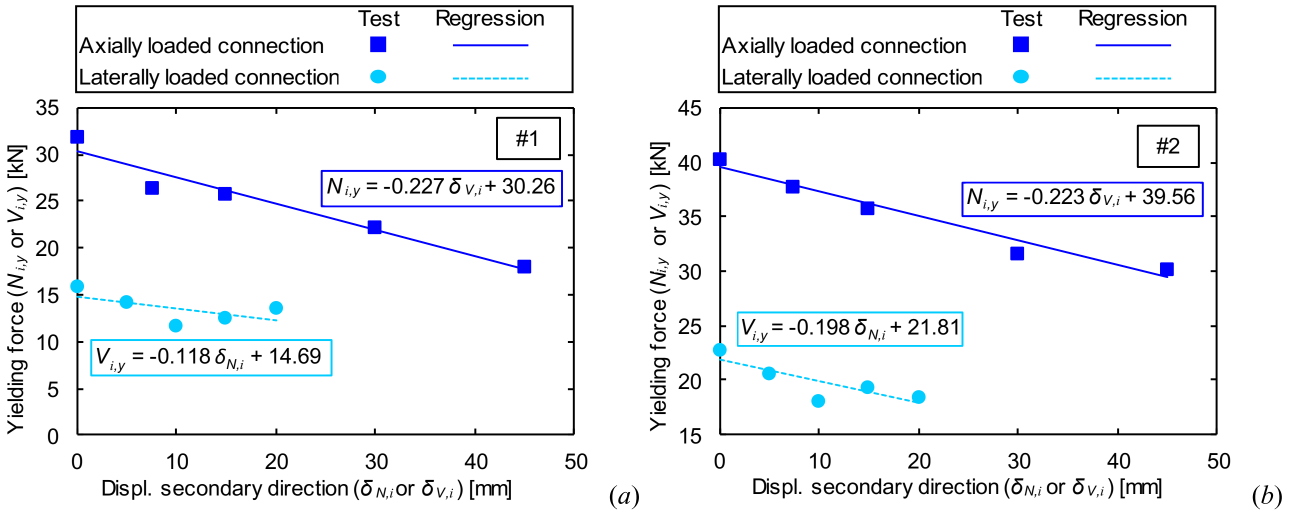

Figure II.3-6 – Regression analysis for axially-loaded hold-down (blue solid line and markers) and laterally-loaded angle bracket (light blue dashed line and markers) connections. Yielding force vs. displacement in the orthogonal direction: bi-linearization method (*a*) #1 and (*b*) #2.

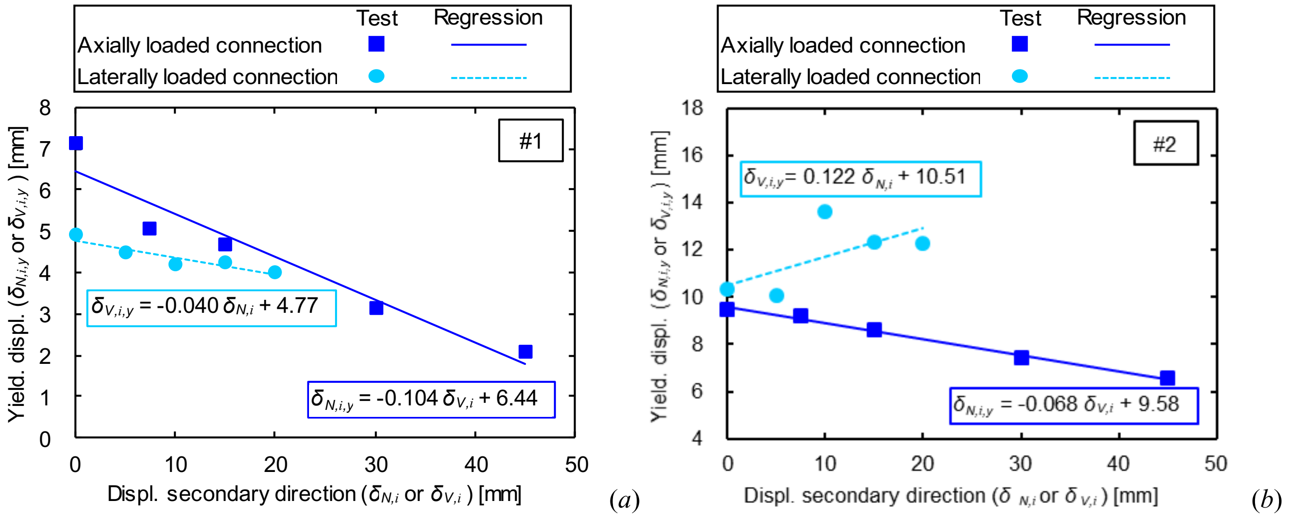

Figure II.3-7 – Regression analysis for axially-loaded hold-down (blue solid line and markers) and laterally-loaded angle bracket (light blue dashed line and markers) connections. Yielding displacement vs. displacement in the orthogonal direction: bi-linearization method (*a*) #1 and (*b*) #2.

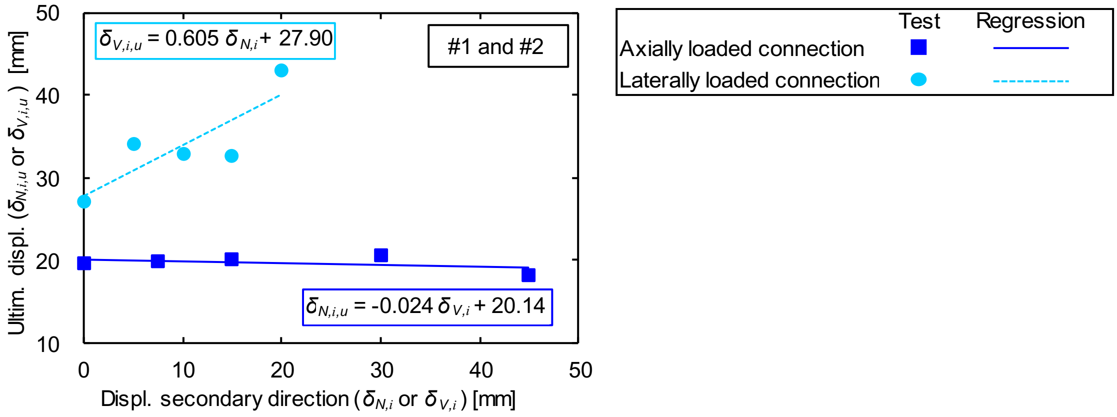

Figure II.3-8 – Regression analysis for axially-loaded hold-down (blue solid line and markers) and laterally-loaded angle bracket (light blue dashed line and markers) connections. Ultimate displacement vs. displacement in the secondary direction for bi-linearization methods #1 and #2.

II.3.4 Model calibration and validation

II.3.4.1 Case study

The shear wall configuration analyzed in this work (Figure II.3-9) presents a 5 layered 85 mm thick CLT panel, with two WHT540 hold-downs and four BMF 90x48x3x116 angle brackets whose mechanical characteristics are available in [18]. This shear wall is the one tested at the CNR-IVALSA mechanical laboratory within the SOFIE project with two different vertical load values *q*, equal to 18.5 kN/m and 9.25 kN/m respectively for configurations labelled as I.2 and I.3 [35]. The results of these tests have already been widely used to create and calibrate both numerical [16, 17, 38] and analytical [35] models.

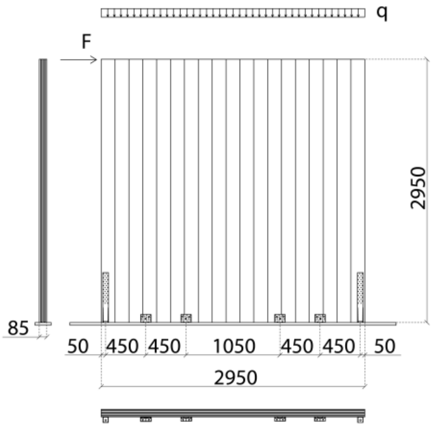

Figure II.3-9 – Case study CLT shear wall (measures in millimeters).

II.3.4.2 Definition of model mechanical parameters

In this section the model calibration is presented both in terms of timber and connection elements and the mechanical parameters assumed in the model are detailed. CLT panel is modelled through an equivalent homogenization approach [46], while connections mechanical characteristics are obtained with the two different bi-linearization criteria described in Section II.3.3.1.

II.3.4.2.1 CLT panel

The mechanical parameters of timber panel are the ones declared in [20], namely Young Modulus E=5700 MPa (obtained using the equivalent homogenization approach proposed in [46]), timber density ρ=400 kg/m^3 and compressive strength f_c=11 MPa. The ultimate deformation of timber is assumed equal to $\varepsilon_{c,u}$=0.05, accordingly to [47], observing that this value has been inferred from tests conducted on 5-layered 171.5 mm thick CLT panels (i.e. [48]). Finally, the distribution coefficient k is assumed equal to the value proposed in [19].

II.3.4.2.2 Connections

The uniaxial experimental load displacement curves of hold-down and angle bracket connections tested at the CNR-IVALSA mechanical laboratory within the SOFIE project [18] are firstly multi-linearized according to the procedure described in [26, 33] in order to define the point P_1, P_2, P_3 and P_4 of the reference backbone. Then the obtained multilinear backbones are bi-linearized using the methods #1 and #2 presented in Section II.3.3.1. Figure II.3-10 reports, for each type of connection (hold-down and angle bracket) and each load direction (axial and lateral) the bilinear curves superimposed to the experimental load displacement cyclic curves and to the averaged multilinear backbone curve.

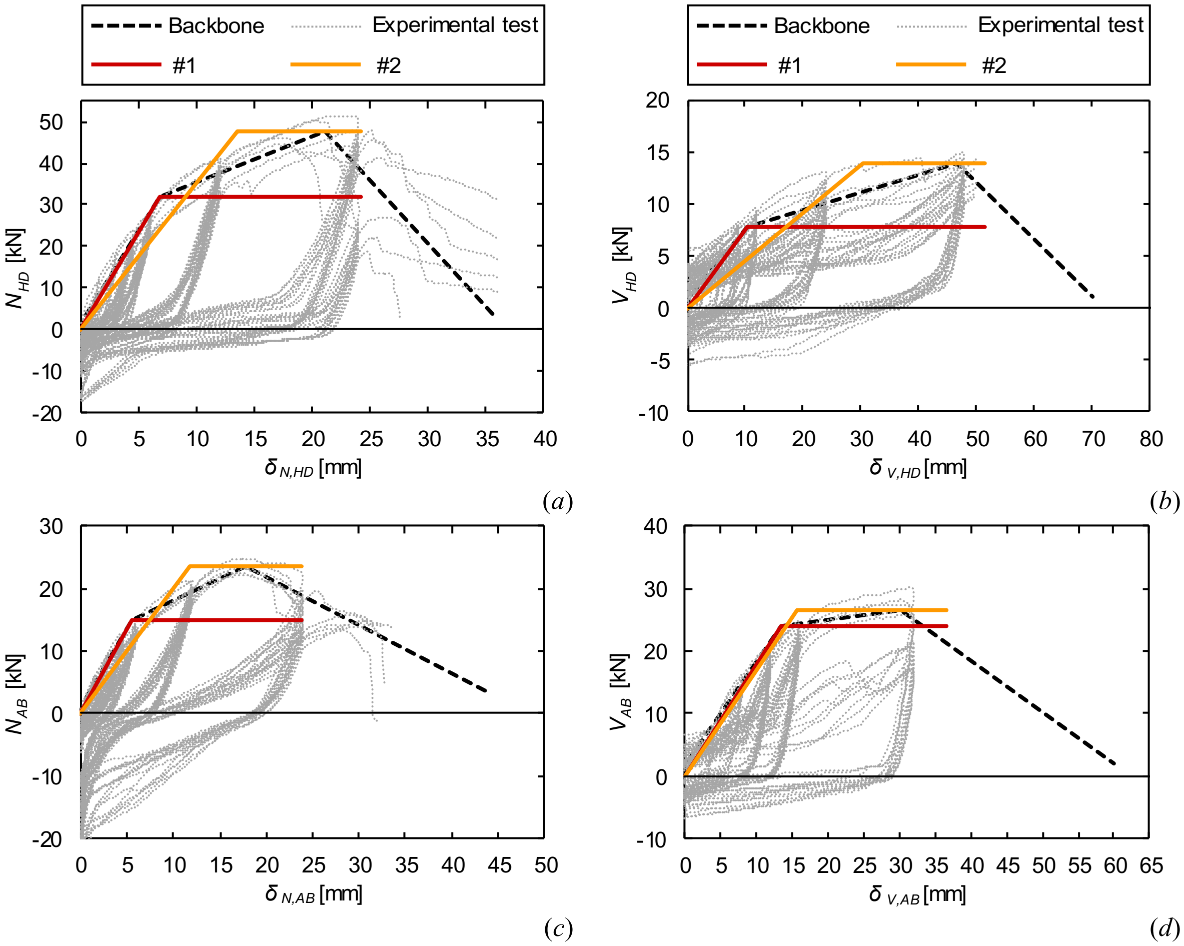

Figure II.3-10 – Bi-linear curves obtained with calibration criterion #1 (red) and #2 (orange): (*a*) hold-down in axial direction: (*b*) hold-down in lateral direction; (*c*) angle brackets in axial direction; (*d*) angle brackets in lateral direction.

The results of the bi-linearization of the connections experimental curves are reported in Table II.3-3, that lists the reference parameters (i.e. $N_{i,y,0}$, $\delta_{N,i,y,0}$, $\delta_{N,i,u,0}$, $V_{i,y,0}$, $\delta_{V,i,y,0}$, $\delta_{V,i,u,0}$) of the elasto-plastic constitutive laws, used in the global model to define the *N*-*V* interaction domain of the case study CLT shear wall.

Table II.3-3 – Reference parameters of the constitutive laws of connections for bi-linearization methods #1 and #2.

Parameter	*#1*		*#2*	
$N_{i,y,0}$	31.86	kN	47.49	kN
$\delta_{N,i,y,0}$	6.89	mm	13.56	mm
$\delta_{N,i,u,0}$	24.18	mm	24.18	mm
$V_{i,y,0}$	23.94	kN	26.68	kN
$\delta_{V,i,y,0}$	13.50	mm	15.58	mm
$\delta_{V,i,u,0}$	36.53	mm	36.53	mm

As it was expected, bi-linearization method #1 is on the safe side, since it tends to underestimate the maximum strength of connections, while method #2 could lead to an overestimation of the strength of connections, but on the other hand it could underestimates the elastic stiffness of connections. However, in case of angle bracket loaded in the lateral direction, the two methods provide similar results both in terms of maximum strength and initial elastic stiffness since the connection load displacement curve is characterized by limited hardening in the post yielding branch.

II.3.4.3 Results

In this section the impact of the different hypotheses assumed for the model formulation (i.e. method of bi-linearization, multi-failure criterion adopted, etc.) on the reliability of the *N*-*V* interaction domain is presented and critically discussed. Figure II.3-11.a and Figure II.3-11.b show the results, respectively for bi-linearization methods #1 and #2 in terms of:

- the reference model proposed by *Tamagnone et al.*[19] (*Reference*, black line);
- the proposed model enhanced considering the elastic-plastic behavior of timber in compression and with infinite shear strength of connections ("$V_y = \infty$", grey line);
- the proposed model accounting for the axial-shear coupling phenomena in the connection elements (magenta, green and blue curves respectively for *Rectangular*, *Elliptical* and *Hybrid* methods) implemented with *Refined* (solid lines) and *Simplified* (dashed lines) coupling criteria.

It is evident the strong influence of the shear strength of connections on the effective strength of the shear wall horizontally limiting the *N*-*V* interaction domain at the maximum shear capacity of the connections themselves. The adoption of the EPP constitutive law for timber allows to obtain strengths of the shear wall higher than the one of the *Reference* model. The *Simplified* force-based approach gives lower strength of the shear wall with respect to the *Refined* one, since it disregards the force redistribution allowed by the ductility of the connections.

It can then be noticed that the *force-based* coupling criteria and the *Hybrid* one differ only if at least one connection is loaded in tension, since when the base section of the shear wall is totally compressed, the behavior of the system is governed only by the uncoupled lateral strength of connections and the compressive constitutive law of timber.

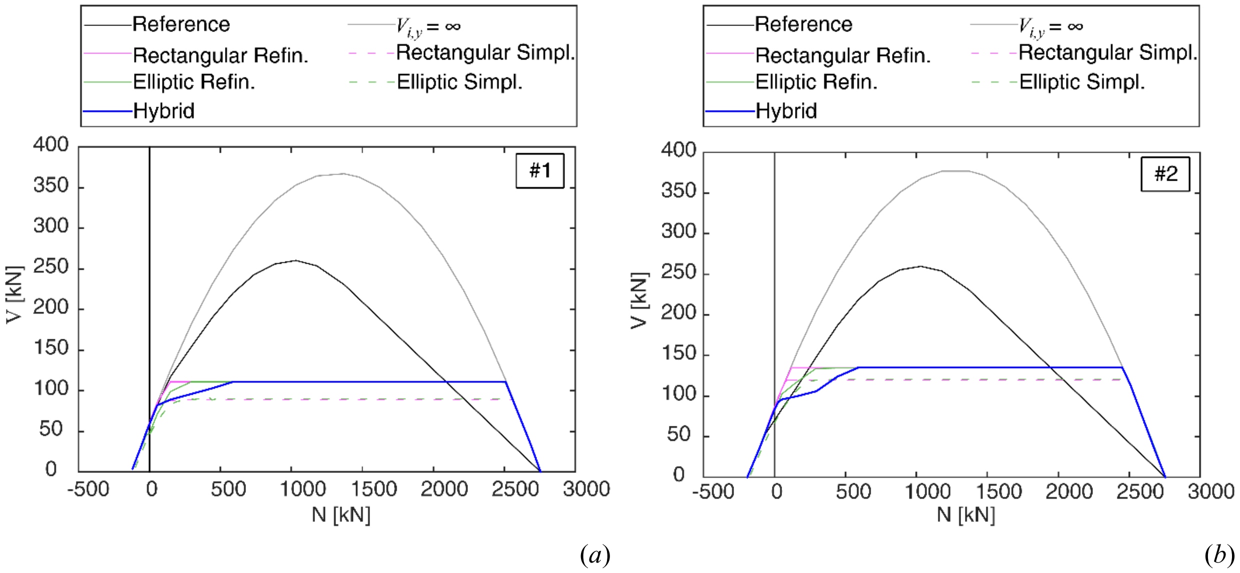

(*a*) (*b*)

Figure II.3-11 – Comparison between the different multifailure criteria, the reference model (black line) and the uncoupled model (grey line): (*a*) bi-linearization method 1 - #1; (*b*) bi-linearization method 2 - #2.

II.3.4.3.1 Timber constitutive law effect

The interaction domain obtained by considering an elastic-plastic behavior of timber in compression ("$V_y = \infty$", grey line in Figure II.3-11) is almost symmetrical, while the model proposed by Tamagnone *et al.* [19] (*Reference,* black line in Figure II.3-11) provides a domain with a peak point shifted towards the left. In addition, the peak strength obtained with the EPP constitutive law is about 40% higher than the *Reference* one and in general, as previously stated, the "$V_y = \infty$" interaction domain is significantly greater than the *Reference* one.

For small or negative values of the axial load N, the difference between the two domains is almost negligible, since the behavior of the shear wall is mainly governed by the strength of connections. On the contrary, the difference is significant for higher values of the axial load N, that corresponds to the typical compression force working range of CLT walls.

II.3.4.3.2 Coupling criteria effect

Independently from the adopted coupling criterion, the choice of the axial-shear strength interaction law of the connection is a key-aspect in the correct definition of the interaction domains of CLT shear walls. Actually, the models that disregard the axial-shear coupling (i.e. *Reference* and "$V_y = \infty$") significantly overestimate the strength of the shear wall, since they do not consider the shear failure mechanism of connections. Looking more closely to the results obtained with the different coupling criteria (Figure II.3-11), it is possible to observe that:

- for high levels of the axial load N, the lateral load-carrying capacity V of the shear wall is given by the lateral strength of connections, independently from the adopted coupling criterion.
- for negative or very low levels of the axial load N, the elliptical method (both implemented in a *Refined* or *Simplified* way) gives lower load carrying capacity than the *Hybrid* one (Figure II.3-12). This behaviour is opposite when the shear failure mechanism of connections is activated within the *Hybrid method*: this occurs because this criterion penalizes the shear strength of connections more than the elliptical one (see Eq. (15b) of [26]).
- the elliptical strength domain provides lower load carrying capacity V than the rectangular criterion, as it was expected since in the former hypothesis, the strength of connections is reduced due to coupling effect.
- the *Simplified* models provide a lower load-carrying capacity with respect to the corresponding *Refined* formulations. This is because the *Simplified* approaches do not allow for plastic force redistribution in the connections, since they are considered failed once yielded.

In general, the force-based *Simplified* models are on the safe side with respect to the *Refined* ones, and the *Hybrid* criterion is anyway the most precautionary, since it takes into account the axial-shear strength interaction, even for small values of displacement in the orthogonal direction.

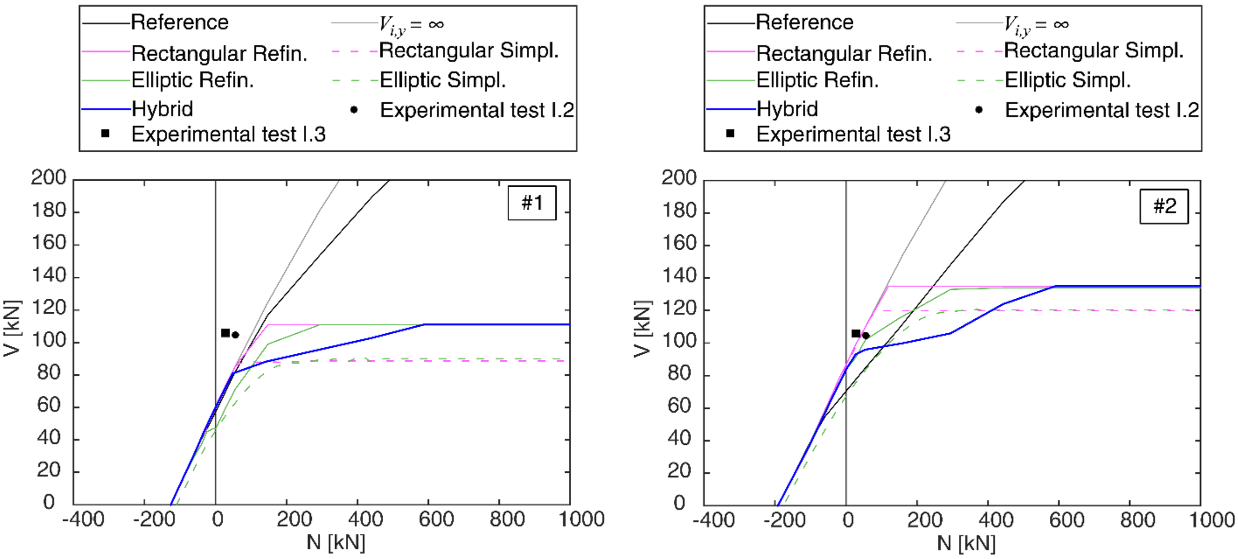

(*a*) (*b*)

Figure II.3-12 – Comparison between the different criteria, the reference model (black line), the uncoupled model (grey line) and the experimental tests obtained within the SOFIE project ([35], wall I.2 and I.3) for low values of axial load N: (*a*) bi-linearization method 1 - #1; (*b*) bi-linearization method 2 - #2.

II.3.4.3.3 Bi-linearization method of connections constitutive laws effect

Bi-linearization method *#1* provides results that are on the safe side if compared to the ones obtained with method #2 (see Figure II.3-11.a and Figure II.3-11.b respectively), even if method *#1* could excessively underestimate the effective strength of the shear wall. In order to verify which of the two bi-linearization methods provides the most reliable results, the experimental results obtained within the SOFIE project cyclic tests [35] for walls I.2 and I.3 is used as reference case. The reliability of these experimental results in terms of global response is also supported by the outcomes reported in [38].

As summarized in Table II.3-4, almost all the analyzed combinations of coupling methods and linearization criteria underestimate the experimental results, even if method *#2* fits better the experimental outcomes than method *#1*, that systematically underestimates the effective strength of the shear wall irrespectively to the coupling criterion used. It is worth noting that this underestimation is probably due to the friction strength contribution that is disregarded in this work.

Table II.3-4 – Percentage gap between numerical and experimental tests obtained within the SOFIE project ([35]), wall I.2 and I.3 for bi-linearization methods #1 and #2 to the vary of the bi-linearization method.

Coupling criterion	*Configuration I.2*		*Configuration I.3*	
	#1	*#2*	*#1*	*#2*
Rectangular Refined	-20%	4%	-30%	-6%
Elliptic Refined	-33%	-4%	-44%	-13%
Hybrid	-22%	-9%	-33%	-12%
Rectangular Simplified	-20%	4%	-32%	-7%
Elliptic Simplified	-41%	-21%	-48%	-28%

Figure II.3-12, showing an enlargement of the initial region of Figure II.3-11, reports also the points corresponding to the failure of the two walls I.2 and I.3 [35]. Comparing experimental evidences with the various results obtained using the bi-linearization method #1, it is possible to observe that the lower differences are provided by the force-based method employing rectangular domain (with both the *Refined* and *Simplified* approaches) even if the *Hybrid* method ensures slightly higher differences. On the contrary, the force-based method employing elliptical domain shows higher differences with a significant underestimation of the wall capacity. This suggests that the use of elliptical domain in combination with the bi-linearization method #1 should be avoided.

Results are quite different when the bi-linearization method #2 is used, since the percentage differences reported in Table II.3-4 are significantly smaller, demonstrating the capability of this method in reproducing these experimental evidences. In this case, the elliptical *Refined* force-based method provides results similar to those obtained using the rectangular force-based and the *Hybrid* method. The elliptical *Simplified* force-based method provides the worst results also in this case.

II.3.5 Conclusions

In this Section, a method for the design of CLT shear wall based on *N-V* interaction domain is proposed focusing particularly on the effects of the different criteria used for the definition of the failure condition of the wall components (i.e. timber panel and connections). Differently from other reference methods available in literature, the one developed in this work consider an elastoplastic behaviour of the timber panel and a coupled axial-shear behaviour of the connection elements to derive *N-V* interaction domains.

In the first part of the research, the multicriteria ultimate conditions used for a reliable reproduction of the behaviour of the system is presented with particular regard to the elastoplastic behaviour of the timber panel, to the procedure adopted for the bilinearization of the connection constitutive laws and to the type of axial-shear coupling. Two bilinearization procedures (#1 and #2), that differ in the definition of the yielding point, are considered and two different coupling approaches are analyzed. Specifically, the conventional force-based approach with elliptical and rectangular force domain (here implemented considering two different ultimate displacement capacities of the connections – *Simplified* and *Refined*) is compared with the more innovative *Hybrid* force-displacement-based one. The procedure to specify the *Hybrid* force-displacement approach, that is based on a multi-linear backbone envelope curve of the connections, to the use of bilinear constitutive laws of the connection, required by the general method for the *N-V* interaction domain, is given and discussed.

The basic assumptions of the proposed model are then applied to derive *N-V* interaction domains of a CLT shear wall case study chosen among the ones tested at the CNR-IVALSA laboratory during the so called "SOFIE project" and a sensitivity analysis is carried out to verify the impact on results of the constitutive laws of the timber panel, of the different bi-linearization procedure and of the different axial-shear coupling criteria of connection elements.

Results obtained from the analyses firstly demonstrate that for small or negative values of the axial load N the behavior of the shear wall is mainly governed by the strength of connections. On the contrary, for higher values of the axial load N, the *N-V* domain carried out using an EPP constitutive laws of timber is about 40% higher than the one obtained with the *Reference* approach based on an elastic-brittle law.

Results clearly demonstrate that bi-linearization method #*1* excessively underestimates the effective load capacity of the CLT shear wall regardless of the coupling approach used. Moreover, the force-based *Simplified* models are on the safe side with respect to the *Refined* ones, and the *Hybrid* approach is anyway the most precautionary, since it takes into account the axial-shear interaction, even for small values of displacement in the orthogonal direction.

Based on results obtained in this work, it is possible to conclude that the set of assumptions that guarantees the best reliability of the *N-V* interaction domain consists of an EPP constitutive law for timber, connections with constitutive laws according to method #*2* and axial-shear coupling criterion of the connections according to force-based elliptical *Refined* approach or to the *Hybrid* one.

The results also show that coupling effects are significant only for those values of the ratio between the applied vertical load and shear load capacity that lies among 0.1 and 0.2. It's anyway worth to note that these values could vary with the geometrical and connection configurations of the examined shear wall, as well as with the boundary conditions. Future works will investigate the *N-V* interaction domain to vary of both the geometrical and connection characteristics, and the boundary conditions of the shear wall.

The model will be employed to derive interaction domains with mechanical parameters of connections defined accordingly to the most common codes and standards for timber structures, e.g. using the strength and stiffness formulations for connections provided by Eurocode 5 [22]. This model specification is of direct implementation by practitioners for the seismic design of CLT shear walls.

Bibliography of Part II

[1] I. Lukacs, A. Björnfot, R. Tomasi, Strength and stiffness of cross-laminated timber (CLT) shear walls: State-of-the-art of analytical approaches, Eng. Struct. 178 (2019) 136–147. doi:10.1016/j.engstruct.2018.05.126.

[2] D. Casagrande, S. Rossi, T. Sartori, R. Tomasi, Proposal of an analytical procedure and a simplified numerical model for elastic response of single-storey timber shear-walls, Constr. Build. Mater. 102 (2016) 1101–1112. doi:10.1016/j.conbuildmat.2014.12.114.

[3] I. Gavric, M. Popovski, Design models for CLT shearwalls and assemblies based on connection properties, in: Timber Scientific Publishing KIT Holzbau und Baukonstruktionen (Ed.), Meet. 47 Int. Netw. Timber Eng. Res., Bath, United Kingdom, 2014: pp. 47-15–4. doi:10.13140/RG.2.1.3845.0728.

[4] T. Reynolds, R. Foster, J. Bregulla, W.-S. Chang, R. Harris, M. Ramage, Lateral-Load Resistance of Cross-Laminated Timber Shear Walls, J. Struct. Eng. 143 (2017) 06017006. doi:10.1061/(ASCE)ST.1943-541X.0001912.

[5] S. Pei, J.W. van de Lindt, M. Popovski, Approximate R-Factor for Cross-Laminated Timber Walls in Multistory Buildings, J. Archit. Eng. 19 (2013) 245–255. doi:10.1061/(ASCE)AE.1943-5568.0000117.

[6] I. Lukacs, A. Björnfot, R. Tomasi, State-of-the-art: Cross Laminated Timber shear wall capacity and stiffness assessment methods, COST Action FP1402. (2018) 203–216.

[7] Z. Chen, M. Popovski, Mechanics-based analytical models for balloon-type cross-laminated timber (CLT) shear walls under lateral loads, Eng. Struct. (2019) 109916. doi:10.1016/j.engstruct.2019.109916.

[8] A. Sandoli, D. Moroder, S. Pampanin, B. Calderoni, Simplified analitycal models for coupled CLT walls, in: WCTE 2016 - World Conf. Timber Eng., Vienna, Austria, 2016.

[9] G. Schickhofer, T. Bogensperger, T. Moosbrugger, M. Augustin, H. Blaß, H. Ebner, A. Et, BSPhandbuch Holz-Massivbauweise in Brettsperrholz Nachweise auf Basis des neuen europäischen Normenkonzepts. 2. Auflage, Verlag der Technischen Universität Graz, (2010).

[10] I. Sustersic, B. Dujic, Simplified cross-laminated timber wall modelling for linear-elastic seismic analysis, in: 45th CIB-W18 Meet., Växjö, Sweden, 2012: pp. 45-15–6.

[11] M. Wallner-Novak, J. Koppelhuber, K. Pock, Cross-Laminated Timber Structural Design - Basic design and engineering principles according to Eurocode, 1st editio, proHolz Austria, 2014.

[12] R. Tomasi, CLT course at FPS COST Action FP1004 – Enhance mechanical properties of timber, engineered wood products and timber structures. CLT Training School, University of Trento, (2014).

[13] R. Tomasi, I. Smith, Experimental Characterization of Monotonic and Cyclic Loading Responses of CLT Panel-To-Foundation Angle Bracket Connections, J. Mater. Civ. Eng. 27 (2015) 04014189. doi:10.1061/(ASCE)MT.1943-5533.0001144.

[14] D. Casagrande, G. Doudak, L. Mauro, A. Polastri, Analytical Approach to Establishing the Elastic Behavior of Multipanel CLT Shear Walls Subjected to Lateral Loads, J. Struct. Eng. 144 (2018) 04017193. doi:10.1061/(ASCE)ST.1943-541X.0001948.

[15] V. Nolet, D. Casagrande, G. Doudak, Multipanel CLT shearwalls: an analytical methodology to predict the elastic-plastic behaviour, Eng. Struct. 179 (2019) 640–654. doi:10.1016/j.engstruct.2018.11.017.

[16] L. Pozza, M. Savoia, L. Franco, A. Saetta, D. Talledo, Effect of different modelling approaches on the prediction of the seismic response of multi-storey CLT buildings, Int. J. Comput. Methods Exp. Meas. 5 (2017) 953–965. doi:10.2495/CMEM-V5-N6-953-965.

[17] M. Izzi, A. Polastri, M. Fragiacomo, Investigating the Hysteretic Behavior of Cross-Laminated Timber Wall Systems due to Connections, J. Struct. Eng. 144 (2018) 04018035. doi:10.1061/(ASCE)ST.1943-541X.0002022.

[18] I. Gavric, M. Fragiacomo, A. Ceccotti, Cyclic behaviour of typical metal connectors for cross-laminated (CLT) structures, Mater. Struct. 48 (2015) 1841–1857. doi:10.1617/s11527-014-0278-7.

[19] G. Tamagnone, G. Rinaldin, M. Fragiacomo, A novel method for non-linear design of CLT wall systems, Eng. Struct. 167 (2018) 760–771. doi:10.1016/j.engstruct.2017.09.010.

[20] G. Tamagnone, G. Rinaldin, M. Fragiacomo, A Simplified Non−Linear Procedure for Seismic Design of CLT Wall Systems, in: Proc. WCTE 2016 World Conf. Timber Eng., Vienna, Austria, 2016.

[21] Tamagnone, Rinaldin, Fragiacomo, A simplified procedure for non − linear design of the metal connectors in XLam timber walls subjected to gravity and lateral loads, in: XVI Convegno ANIDIS

L'Aquila 2015, 2015.

[22] European Committee for Standardisation, EN 1995-1-1 - Eurocode 5: Design of timber structures - Part 1-1: General - Common rules and rules for buildings, 2004.

[23] T. Uibel, H.J. Blaß, Load carrying capacity of joints with dowel type fasteners in solid wood panels, in: Int. Counc. Res. Innov. Build. Constr. - Work. Comm. W18 - Timber Struct. - Meet. Thirty-Nine, Florence, Italy, 2006.

[24] F. Benedetti, V. Rosales, A. Opazo, Cyclic testing and simulation of Hold-Down connections in radiata pine CLT shear walls, in: WCTE 2016 - World Conf. Timber Eng., Vienna, Austria, 2016.

[25] L. Pozza, B. Ferracuti, M. Massari, M. Savoia, Axial – Shear interaction on CLT hold-down connections – Experimental investigation, Eng. Struct. 160 (2018) 95–110. doi:10.1016/j.engstruct.2018.01.021.

[26] L. Pozza, A. Saetta, M. Savoia, D. Talledo, Angle bracket connections for CLT structures: Experimental characterization and numerical modelling, Constr. Build. Mater. 191 (2018) 95–113. doi:10.1016/j.conbuildmat.2018.09.112.

[27] J. Liu, F. Lam, Experimental test of Cross Laminated Timber connections under bi-directional loading, in: World Conf. Timber Eng. 2016 (WCTE 2016), Vienna, Austria, 2016.

[28] J. Liu, F. Lam, Experimental test of coupling effect on CLT hold-down connections, Eng. Struct. 178 (2019) 586–602. doi:10.1016/j.engstruct.2018.10.063.

[29] M. Izzi, A. Polastri, M. Fragiacomo, Modelling the mechanical behaviour of typical wall-to-floor connection systems for cross-laminated timber structures, Eng. Struct. 162 (2018) 270–282. doi:10.1016/j.engstruct.2018.02.045.

[30] European Organisation for Technical Approvals, European Technical Assessment ETA-06/0106 of 06/12/2016: Three-dimensional nailing plate (timber-to-timber/timber-to- concrete angle bracket), 2016.

[31] European Organisation for Technical Approvals, European Technical Assessment ETA-11/0086 of 2015-01-26: Three-dimensional nailing plate (Angle brackets and hold-downs for timber-to-timber or timber-to-concrete or steel connections), 2015.

[32] G. Rinaldin, C. Amadio, M. Fragiacomo, A component approach for the hysteretic behaviour of connections in cross-laminated wooden structures, Earthq. Eng. Struct. Dyn. 42 (2013) 2023–2042. doi:10.1002/eqe.2310.

[33] L. Pozza, A. Saetta, M. Savoia, D. Talledo, Coupled axial-shear numerical model for CLT connections, Constr. Build. Mater. 150 (2017) 568–582. doi:10.1016/j.conbuildmat.2017.05.141.

[34] A. Reiterer, S.E. Stanzl-Tschegg, Compressive behaviour of softwood under uniaxial loading at different orientations to the grain, Mech. Mater. 33 (2001) 705–715. doi:10.1016/S0167-6636(01)00086-2.

[35] I. Gavric, M. Fragiacomo, A. Ceccotti, Cyclic Behavior of CLT Wall Systems: Experimental Tests and Analytical Prediction Models, J. Struct. Eng. 141 (2015) 04015034. doi:10.1061/(ASCE)ST.1943-541X.0001246.

[36] J. Liu, F. Lam, Experimental test of coupling effect on CLT angle bracket connections, Eng. Struct. 171 (2018) 862–873. doi:10.1016/j.engstruct.2018.05.013.

[37] B.R.W. Furlong, Ultimate Strength of Square Columns Under Biaxially Eccentric Loads, ACI J. Proc. 57 (1961) 1129–1140. doi:10.14359/8061.

[38] L. Franco, L. Pozza, A. Saetta, M. Savoia, D. Talledo, Strategies for structural modelling of CLT panels under cyclic loading conditions, Eng. Struct. 198 (2019) 109476. doi:10.1016/j.engstruct.2019.109476.

[39] W. Muñoz, M. Mohammad, A. Salenikovich, P. Quenneville, Need for a harmonized approach for calculations of ductility of timber assemblies, in: W18-Timber Struct. CIB, St. Andrews, Canada, 2008.

[40] EN 12512, Timber structures, Test methods. Cyclic testing of joints made with mechanical fasteners, CEN, Brussels, Belgium, 2011.

[41] Institute for Research in Construction - National Research Council of Canada, National Building Code of Canada, (2015).

[42] M. Fragiacomo, B. Dujic, I. Sustersic, Elastic and ductile design of multi-storey crosslam massive wooden buildings under seismic actions, Eng. Struct. 33 (2011) 3043–3053. doi:10.1016/j.engstruct.2011.05.020.

[43] I. Sustersic, M. Fragiacomo, B. Dujic, Seismic Analysis of Cross-Laminated Multistory Timber Buildings Using Code-Prescribed Methods: Influence of Panel Size, Connection Ductility, and Schematization, J. Struct. Eng. 142 (2016). doi:10.1061/(ASCE)ST.1943-541X.0001344.

[44] Y.-L. Shen, J. Schneider, S. Tesfamariam, S.F. Stiemer, Z.-G. Mu, Hysteresis behavior of bracket connection in cross-laminated-timber shear walls, Constr. Build. Mater. 48 (2013) 980–991. doi:10.1016/j.conbuildmat.2013.07.050.

[45] V. Hristovski, B. Dujic, M. Stojmanovska, V. Mircevska, Full-Scale Shaking-Table Tests of XLam Panel Systems and Numerical Verification: Specimen 1, J. Struct. Eng. 139 (2013) 2010–2018. doi:10.1061/(ASCE)ST.1943-541X.0000754.

[46] H.J. Blaß, P. Fellmoser, Design of solid wood panels with cross layers, in: 8th World Conf. Timber Eng. WCTE 2004, Finnish Assoc. of Civil Engineers, Lahti, Finland, 2004.

[47] T. Akbas, R. Sause, J.M. Ricles, R. Ganey, J. Berman, S. Loftus, J.D. Dolan, S. Pei, J.W. van de Lindt, H.-E. Blomgren, Analytical and Experimental Lateral-Load Response of Self-Centering Posttensioned CLT Walls, J. Struct. Eng. 143 (2017) 04017019. doi:10.1061/(ASCE)ST.1943-541X.0001733.

[48] R. Ganey, J. Berman, T. Akbas, S. Loftus, J. Daniel Dolan, R. Sause, J. Ricles, S. Pei, J. van de Lindt, H.-E. Blomgren, Experimental Investigation of Self-Centering Cross-Laminated Timber Walls, J. Struct. Eng. 143 (2017) 04017135. doi:10.1061/(ASCE)ST.1943-541X.0001877.

III

Innovative timber-based composite structures

III.1 State-of-the-art of timber-based composite structures

Abstract

Timber-based composite structures represent a construction technique that has been successfully used for many years both to build new structures and for restoration purposes. Its mechanical characterization is anyway still a hot issue since the structural behaviour is influenced by many parameters, primarily the efficiency of connections to create a composite action. In this Section, a selection of available literature references about the state-of-the-art of timber-based composite structures is given, in order to provide an overview on this building technology. After describing the different types of timber-based constructions highlighting the advantages of the system, hints of their mechanical behavior will be furnished. A description of the available types of connections, their modelling and their behavior will then be provided, comparing the advantages and drawbacks of each one. Finally, analytical and numerical modelling of these structures will also be discussed.

III.1.1 Chapter contents

In this Chapter a state-of-the-art of timber-based composite structures is reported. In Section III.1.2 an overview on timber-based composite structures typologies and their mechanical behaviour is given. In Section III.1.3 an in-depth focus on the state-of-the-art of timber-steel composite structures will be given. In Section III.1.4 the typical connections employed for timber-based composite structures are illustrated, focusing in particular on dowel-type fasteners (Section III.1.4.1), notched shear connections (Section III.1.4.2), glued connections (Section III.1.4.3) and innovative ones (Section III.1.4.4). Finally, in Sections III.1.5 and III.1.6 an overview of analytical and numerical models available for the analysis of this kind of structures is given

III.1.2 Overview on timber-based composite structures

Timber–Based Composite (or Hybrid, sometimes referred to as Mixed) Structures (TBCSs) are systems composed by a timber member connected to an element of another material in order to resist external loads with mutual interaction. The load transfer between the two materials can be guaranteed or at a structural component level, creating composite elements such as composite slabs or composite frame beams, or at a building system level, obtaining composite building systems such as composite shear wall systems [1]. The arguments exposed in this thesis are referred to the first case of composite structural elements.

III.1.2.1 Timber-based composite structures typologies

It is possible to define three main types of TBCSs. The first one is represented by the Timber-Concrete Composite Structures (TCCSs), that are composed by a timber member connected to a concrete slab, so that the timber primarily resists tensile forces and the concrete resists compressive forces generated from flexure.

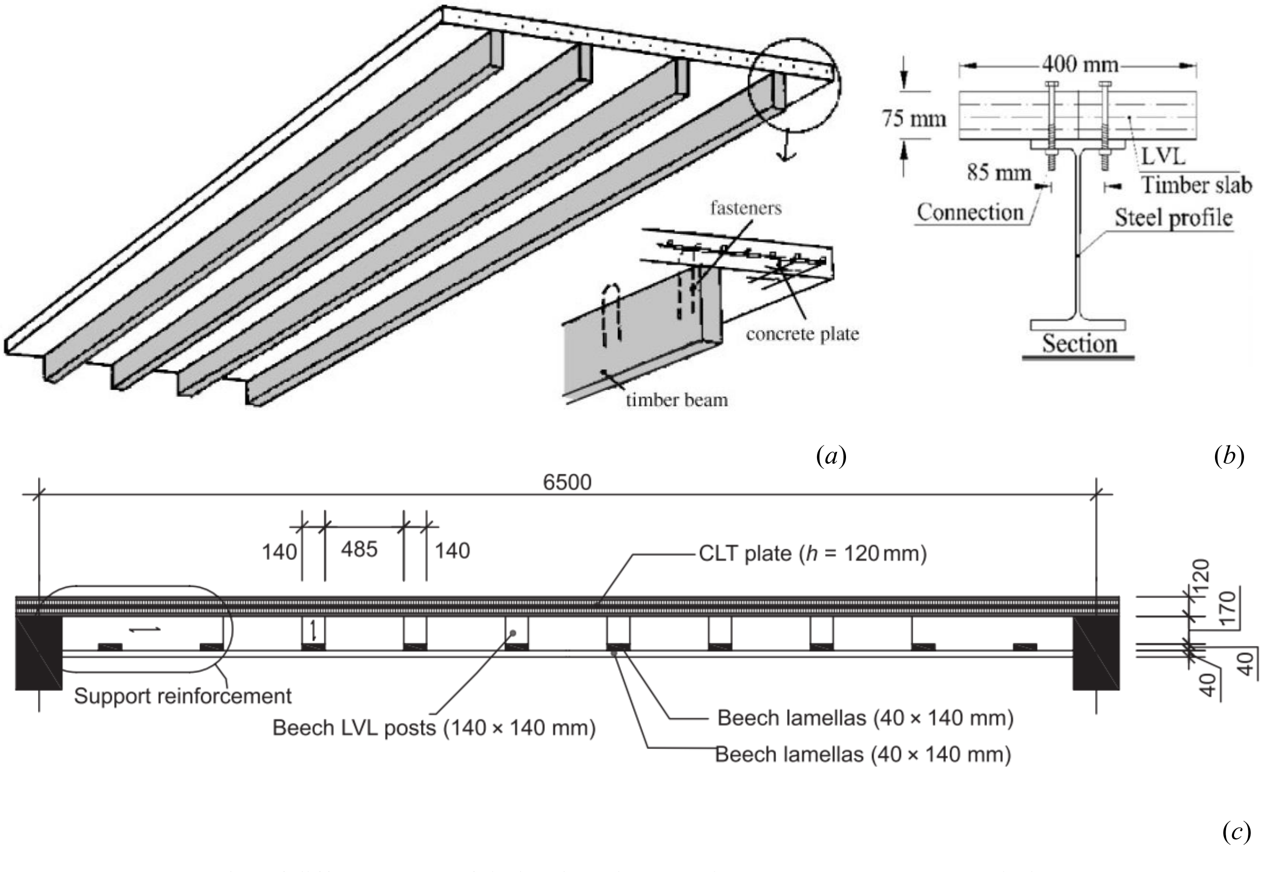
fasteners
concrete plate
timber beam
400 mm
75 mm
85 mm
LVL
Timber slab
Connection
Steel profile
Section
6500
140
485
140
CLT plate (h = 120 mm)
120
170
40
40
Support reinforcement
Beech LVL posts (140 × 140 mm)
Beech lamellas (40 × 140 mm)
Beech lamellas (40 × 140 mm)

(*a*) (*b*)

(*c*)

Figure III.1-1 – Examples of different types of timber-based composite structures TBCSs: (*a*) Timber-Concrete TCCSs, (*b*) Timber-Steel TSCSs and (*c*) Timber-Timber composite structures TTCSs (*image credits*: (*a*) Ceccotti [2], (*b*) Hassanieh *et al.* [3] and (*c*) Leyder *et al.* [4]).

An exhaustive presentation of the state of the art of TCCSs is presented by Yeoh *et al.* [5]. On the other hand, Timber-Steel Composite Structures (TSCSs) are composed by a timber member connected to a steel one [3]. It's finally possible to define a third type of TBCSs, the Timber-Timber Composite Strictures (TTCSs), that are composed of two or more timber elements of different grade or specie jointed together [4, 6]. Other types of TBCSs are also present, like the Timber-Glass Composite Structures [7] or the ones that use timber with Fiber-Reinforced-Polymers (FRP) [8]. This thesis will focus TSCSs at a component level, presenting an analytical model for design and optimization of an innovative timber-steel composite beam proposed by Crocetti (see Section III.2).

TBCSs are a structural solution that is gaining success in the construction of multi-storey timber buildings (see Section I.1.1) thanks to many advantages that add up to the ones of timber structures like low carbon footprint, rapidity of execution and good seismic performance thanks to high strength-to-weight ratio [9]. Applications of this technology also extends to bridges [10], factories and domestic houses [11]. TBCSs technology is gaining interest not only for new constructions, but also for refurbishment interventions during restoration of existing buildings, with successful applications since 80s [12]. TBCSs allow to obtain stiffer and more damped structures, so that it's easier to satisfy SLS deflection and vibration requirements [13]. On the other hand, the efficient usage of the two different materials allows for higher strength than pure timber elements. Crocetti *et al.* proposed an innovative solution for TCCSs that uses precast concrete slab that adds other advantages, like less time required to complete the structure since no time is needed for the concrete to cure, reduced creep effects due to young-aged concrete and more cost-efficiency thanks to higher prefabrication level [14]. Lukaszewska *et al.* [15] also proposed a TCCS with prefabricated slab and carried out an experimental survey in order to analyze the efficiency of different connectors between concrete and timber. It's in add important to underline the fact that TCCSs allow to reuse both timber beam and concrete slab at the end of their service life, making it a very promising structural system.

The most widespread TBCS typology is the Timber-Concrete one (TCCS), therefore most of the knowledge and literature available on TBCSs focuses on this type, and an extensive state-of-the-art is available in [5]. In TCCSs upper concrete slab acts as a barrier against fire propagation, enhancing therefore fire performance respect to normal timber structures [2]. Natter [16] points out that TBCSs also have better fire performances than concrete structures. O'Neill [17] carried out fire tests on two 4 m span specimens accordingly to ISO 834 protocol [18], finding that the failure mode is governed by the size reduction of timber beams exposed to fire. Frangi *et al.* [19] developed a method for the calculation of TCCSs subjected to fire, on the basis of the theory of the mechanically jointed beams [20] and the reduced section method [21]. The method also takes into account the effect of temperature on strength and stiffness of shear screwed connections though simplified formulae. An extensive literature review on the structural performance of TCCSs subjected to fire is reported by Hozjan *et al.* [22].

III.1.2.2 Mechanical behavior

Considering mechanical behavior of TBCSs, these systems are internally statically indeterminate, and their behavior is strongly related to both material properties and connection systems adopted to join the two different materials that compose the structural element. Since generally the connection between the two materials is not rigid, a relative slip displacement is expected at the interface between them, therefore the assumption of plane sections in the deformed configuration of the composite structure does not apply to the whole composite section. The short-term mechanical behavior of these structures subjected to vertical loadings in simply-supported conditions, synthetically represented in Figure III.1-2, is characterized by a relative sliding v at layer interface that is maximum at the extremities and null at the mid-section. Considering a mechanical connection between the two layers with dowel-type connections spaced of a quantity s (Section III.1.4), it is evident that the maximum shear loads Q acting on connectors is maximum at extremities and null in the mid-section. In order to guarantee the horizontal equilibrium of the sections of the two layers, axial forces N_1 and N_2 with a lever arm r are present, with maximum values at the mid-section and null at extremities (if no external axial load N is applied to the composite beam), accordingly to the following equation:

$$N_i(x) = N\frac{E_i \cdot A_i}{E_1 \cdot A_1 + E_2 \cdot A_2} + \int_0^x Q\,dx, \qquad i \in [1,2] \wedge x \in [0,l] \qquad (III.1\text{-}1)$$

The two layers are also subjected to bending moments M_1 and M_2 in order to guarantee the rotational equilibrium of their cross-sections, and the global bending moment acting on the composite beam is:

$$M(x) = M_1(x) + M_2(x) + N \cdot r, \qquad x \in [0,l] \qquad (III.1\text{-}2)$$

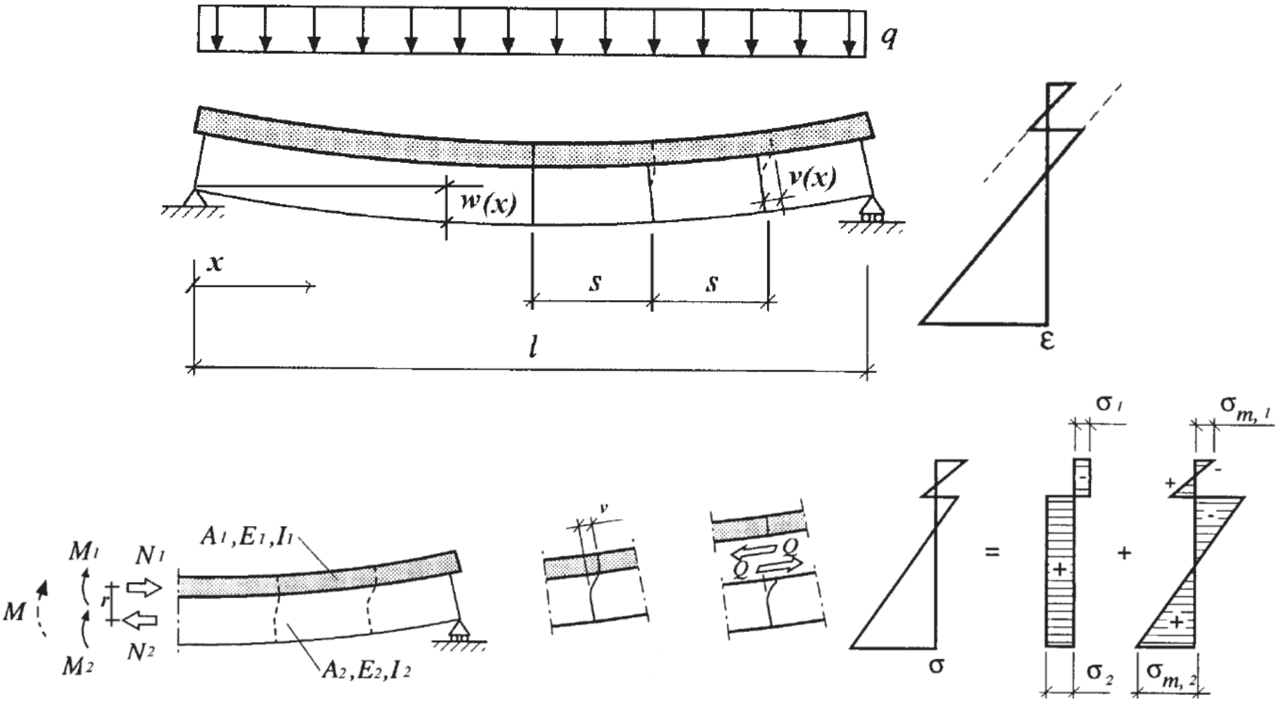

Figure III.1-2 – Mechanical behavior of timber-based composite structural elements (*image credits*: Ceccotti [2]).

The stiffer the shear connectors are, the lower are the bending moments M_i and the higher are the axial loads N_i.

It is worth noting that the neutral axis of the composite structure should be located near the interface between the two layers in order to ensure that both materials behave efficiently, with concrete purely compressed in TCCSs and timber purely compressed in TSCSs. An extensive experimental campaign to investigate the behavior of TCCSs and their connections has been carried out in [11].

Code provisions for SLS and ULS design of these structures are given in EC5 parts 1-1 [20] and part 2 [23].

One of the main hot topics about this kind of structures is the analysis of the long-term behavior [24], that led many authors to develop models to study the phenomenon [25, 26]. An experimental study conducted by Balogh *et al.* [27] evidenced how the long-term behavior of TCCSs are significantly affected by repeated and sustained loadings in the long-term, probably because of plastic strains developed in the wood notches, with an increase in deflections of 18% for cyclic loadings and 59% for sustained ones. Actually, TBCSs are composed by materials that develop time-dependent strains due to long-term effects like creep and shrinkage. Timber is a viscoelastic material characterized by creep and mechano-sorptive effects due to cyclic variations of humidity [28], and the strains due to this phenomenon can also be five times the short-term elastic ones [29]. In add, concrete presents shrinkage and creep phenomena [30] and connections present creep and mechano-sorptive effects as well [31].

Besides, the mechanical characterization of the connection is still subjected to a huge amount of research, since it plays a primary role in the definition of the composite actions, hence on the global behaviour of the structure, as it will be shown in the following Section.

III.1.3 Timber-steel composite structures

In this Section an overview on the state-of-the-art of timber-steel composite structures is given, aspect that will be investigated further in Section III.2 with the study of a novel timber-steel composite beam prototyped at KTH Royal Institute of Technology of Stockholm.

An in-depth study on an innovative modular hybrid steel-timber system has been carried out by Loss *et al.* [32, 33]. The authors carried out an extensive experimental study on different connections systems to allow for a composite action between linear steel elements (i.e. beams and columns) and CLT panels in order to detect the ones more performant both for strength and stiffness [32]. A numerical study on a novel modular hybrid steel-timber systems has also been carried to investigate the effect of the local performance of connections on the global composite behaviour [33]. The novel proposed composite floors and shear walls have many advantages thanks to a high level of prefabrication – that allows both for better quality controls and less problems thanks to no casting of concrete on site – and a quick assembly on site that considerably reduces the global building costs. In add timber-steel composite structures satisfy the need of architectural freedom thanks to easily obtainable open spaces and thanks to the possibility to add or modify building modules. In order to guarantee the advantages of high prefabrication level, the different connections systems proposed by Loss (Figure III.1-3.b and c) have been optimized and their clearances have been engineered also for being easy to install. The connections of the proposed steel-timber composite floor system (Figure III.1-3.a) have been investigated with a wide experimental campaign in order to guarantee good performances both in the out-of-plane and in-plane directions for respectively vertical and horizontal seismic (or wind) loads. Different connection technologies to join steel and timber elements have been investigated through monotonic and cyclic non-linear tests, namely (*i*) mechanical (*ii*) glued with epoxy resin and (*iii*) hybrid mechanical-glued connections. The adjacent CLT panels are jointed through inclined screws, and different angles of insertion have been analyzed. Loss also carried out numerical analyses on composite steel-timber wall-systems and floors in order to investigate the possibility of creating rigid diaphragms and ductile shear walls. The models developed assume a lumped plasticity with plastic hinges at the end of beams and columns and adopting link elements to take into account for interaction between adjacent panels. The hybrid floor system proposed by Loss is characterized by good ductility in the out-of-plane direction, with inelastic capacity primarily activated in the steel beam and then also in the connections. The numerical outcomes showed a good efficiency of the composite action for the out-of-plane behavior with most of the proposed connections. In addition, the structural collaboration of the steel beams allows to increase the performances of the CLT panels both avoiding brittle failures and instability for compressive forces. From the numerical analyses on in-plane behavior of composite floors it resulted that the type of beam-to-panel connection influences both its load-carrying capacity and its stiffness. The non-linear static analyses carried out on the proposed composite shear-wall system (Figure III.1-3.a) showed that the response is affected by the number and type of column-to-panel connections and that the connections placed at the corners are the first to yield while internal ones are subjected to a lower entity of slip displacements.

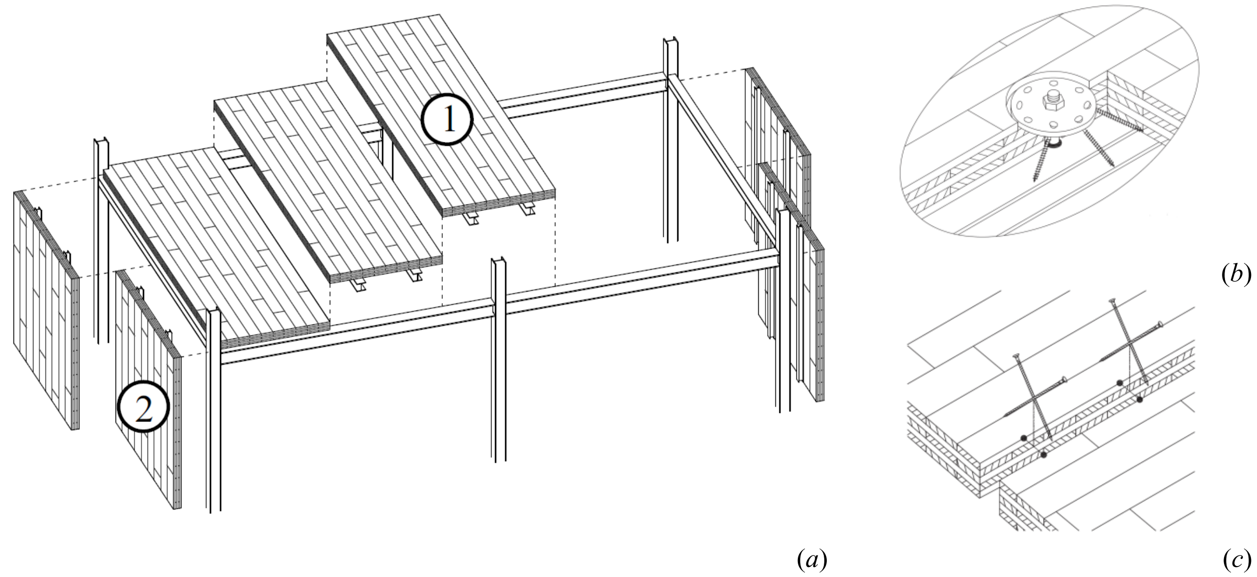

Figure III.1-3 – Hybrid steel-timber structure proposed by Loss *et al.* [32, 33]: (*a*) axonometric view with indicated by the number 1 is the composite floor system and with number 2 is the wall system, (*b*) example of beam-to-panel connection and (c) example of panel-to-panel connection (*image credits*: (*a*) and (*c*) Loss *et al.* [33], (*b*) Loss *et al.* [32]).

Hassanieh *et al.* [6] investigated the short-term behavior of CLT-steel composite beams (Figure III.1-4) both through numerical analyses and experimental campaigns. The numerical studies have been carried out both with models that employ one-dimensional (Figure III.1-5) and bidimensional finite elements (Figure III.1-6). Both the modelling strategies have been proven to capture the short-term behavior of CLT-steel composite beams with high accuracy. The numerical outcomes have then been compared with the results of four-point bending tests. The experimental dataset has been analyzed in terms of (*i*) load-displacement curves, (*ii*) initial stiffness, (*iii*) peak strength and (*iv*) failure modes. In addition, the structural composite efficiency has been investigated comparing results obtained from numerical simulations and experimental tests. Similarly to Loss *et al.* [32, 33] Hassanieh investigated the behavior of the composite steel-timber structure adopting both mechanical and glued epoxy connections, where in the latter also coach screws were used to connect the two materials in order to avoid brittle failures typical of glued connections (see Section III.1.4). Hassanieh also proposed and tested a new connection composed of bolts inserted in pockets filled with high-strength cementitious grout. This novel connection has been engineered in order to allow both for easiness in its installation and high component efficiency. From the results of the study carried out by the author it resulted an efficiency of the composite action of 73 and 91% respectively for mechanical and glued connections. It has finally been found that the composite action increases the peak strength of the structural members of about 40% respect to the case of bare steel structures.

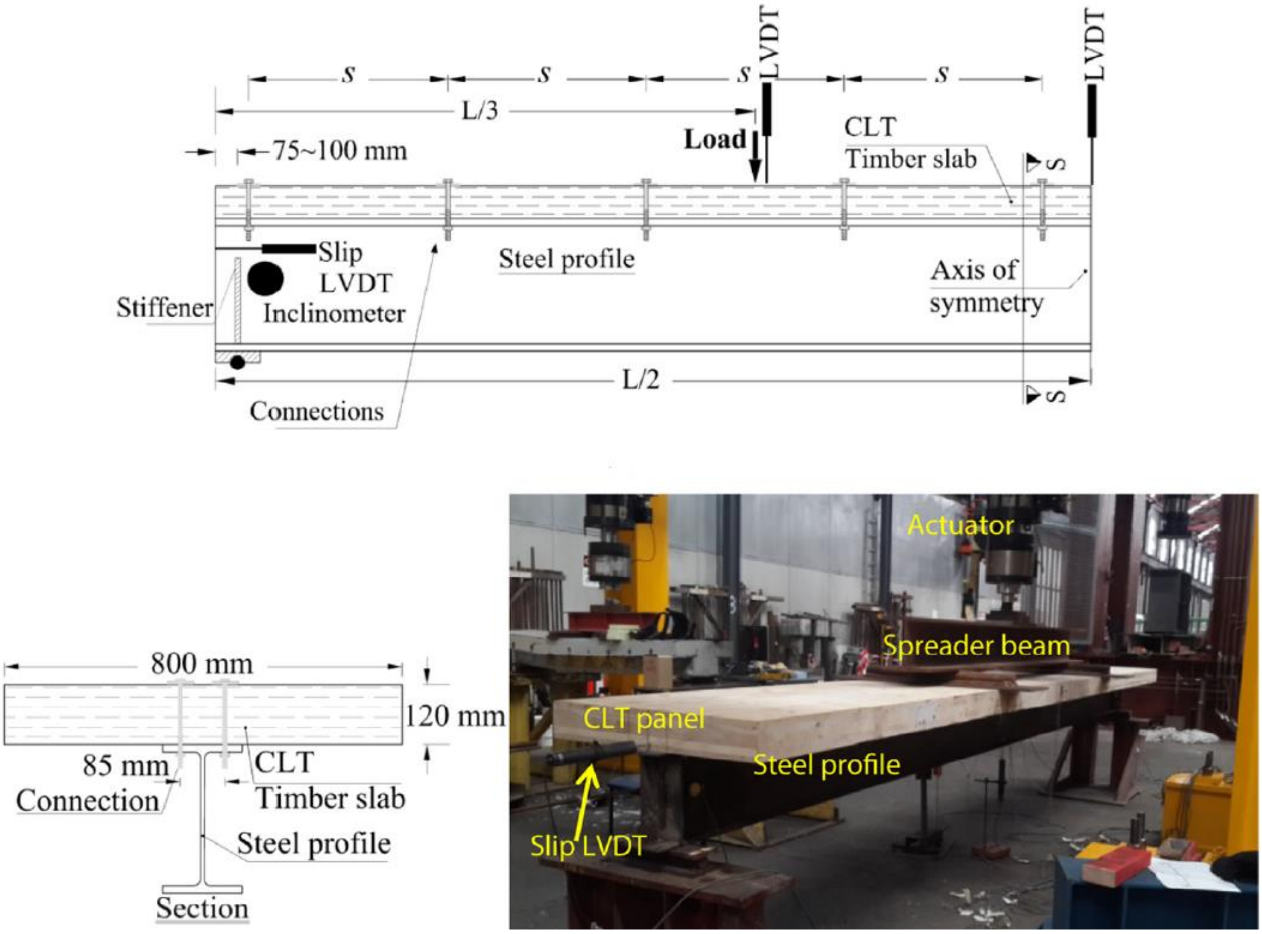
s
s
s
s
LVDT
LVDT
L/3
75~100 mm
Load
CLT
Timber slab
S
Slip
LVDT
Steel profile
Axis of
symmetry
Stiffener
Inclinometer
L/2
S
Connections
800 mm
120 mm
85 mm
Connection
CLT
Timber slab
Steel profile
Section
Actuator
Spreader beam
CLT panel
Steel profile
Slip LVDT

Figure III.1-4 – CLT-steel hybrid beam proposed by Hassanieh *et al.* [6] (*image credits*: Hassanieh *et al.* [6]).

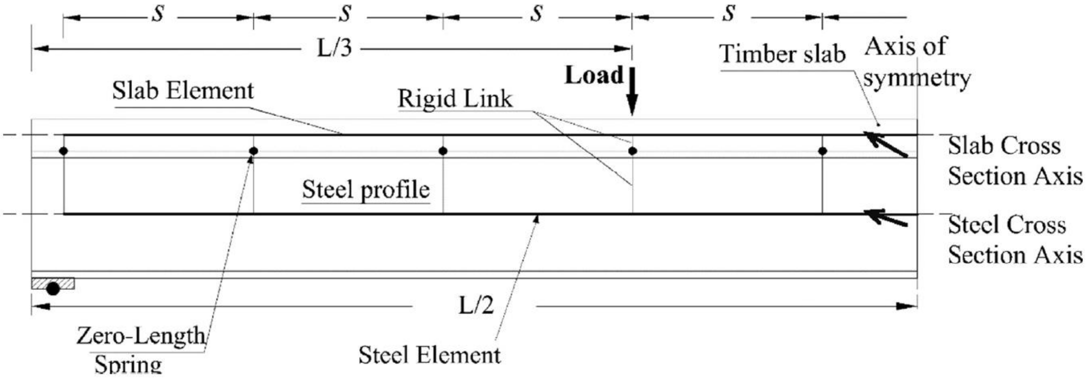
s
s
s
s
L/3
Timber slab
Axis of
symmetry
Slab Element
Rigid Link
Load
Slab Cross
Section Axis
Steel profile
Steel Cross
Section Axis
L/2
Zero-Length
Spring
Steel Element

Figure III.1-5 – One-dimensional FEM model by Hassanieh *et al.* [6] (*image credits*: Hassanieh *et al.* [6]).

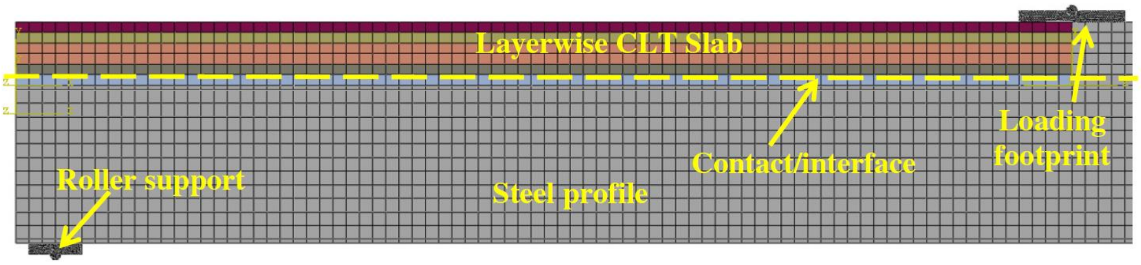
Layerwise CLT Slab
Loading
footprint
Contact/interface
Roller support
Steel profile

Figure III.1-6 – Bidimensional FEM model by Hassanieh *et al.* [6] (*image credits*: Hassanieh *et al.* [6]).

Keipour *et al.* [34] investigated through an experimental campaign the strength, stiffness and rotational capacity of beam-to-column flush end-plate connections between steel-timber composite beams and steel columns (Figure III.1-7). Six full-scale cruciform beam-to-column connection specimens have been tested with a static push-down displacement procedure, where vertical load is applied to the column on the upside-down specimen in simple support condition (Figure III.1-8). The behavior has been investigated to the vary of (*i*) spacing of the shear connectors used to join the CLT panel and the steel beam, (*ii*) usage of glue together with the mechanical connections, (*iii*) CLT panel width and (*iv*) type of connectors between adjacent CLT slabs. Results from the experimental campaign showed that both connections between CLT panels and the beam-to-column connections influence the stiffness of the hybrid structure. The ultimate strength is higher respect to a bare steel structure, provided that the connection between adjacent CLT panels is strong enough to transmit loads between the beam and the column. Keipour finally observed that all the tested configurations showed a good rotational capacity and that the usage of glued connections between CLT panels increases the initial stiffness but decreases the rotational capacity of the hybrid connection.

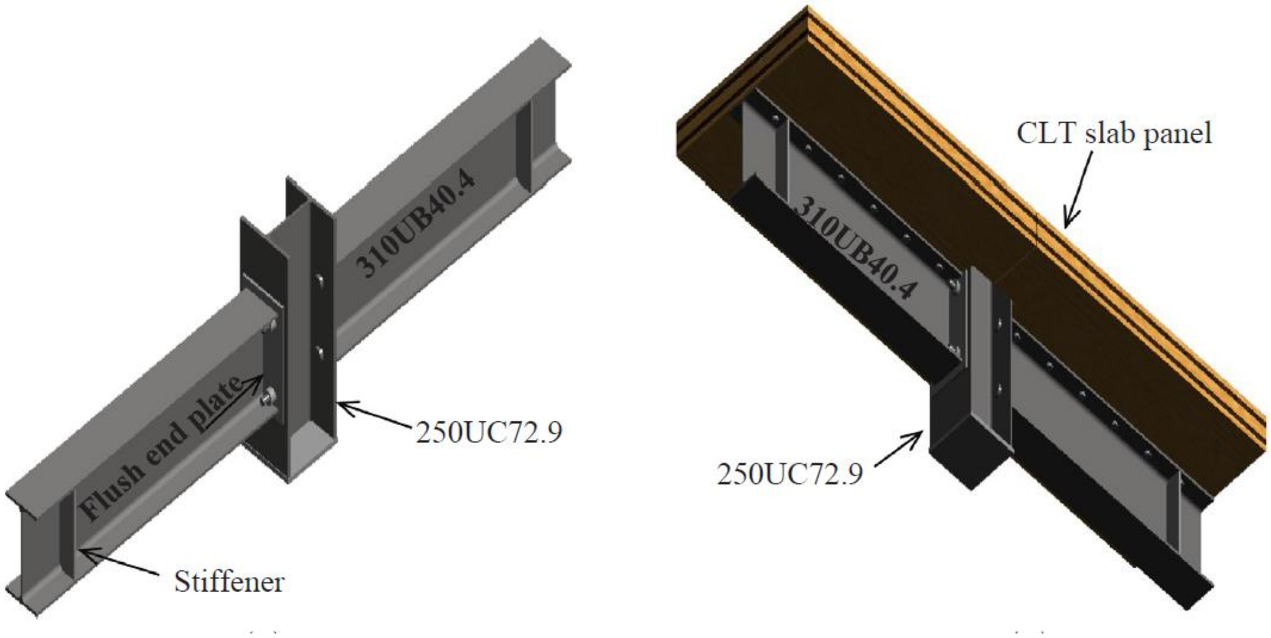
310UB40.4
Flush end plate
250UC72.9
Stiffener
CLT slab panel
310UB40.4
250UC72.9

Figure III.1-7 – Beam-to-column hybrid joints tested by Keipour *et al.* [34] (*image credits*: Keipour *et al.* [34]).

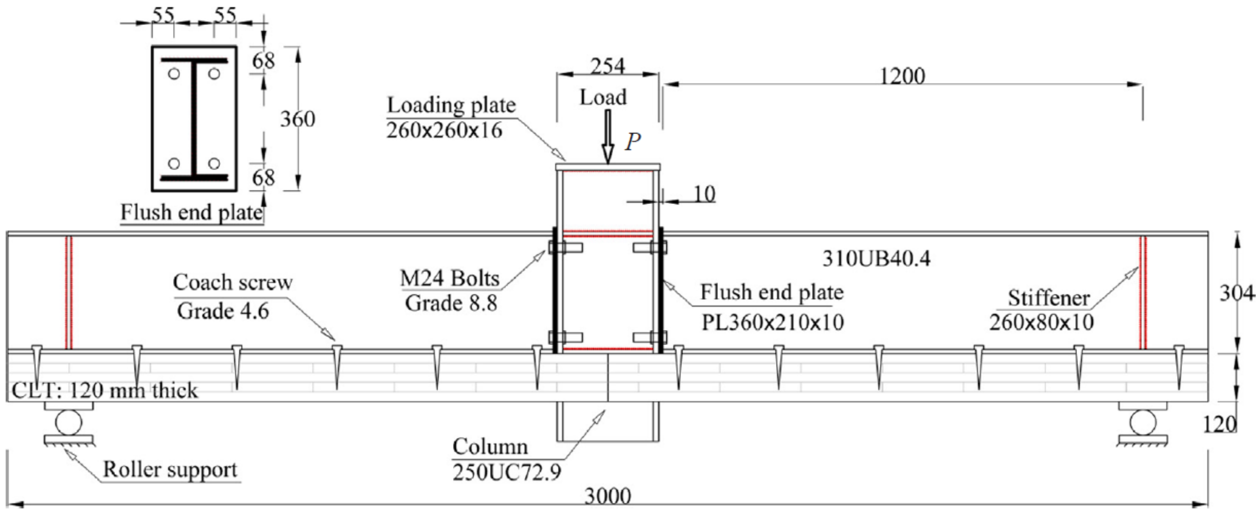
55
55
68
360
68
Flush end plate
Loading plate
260x260x16
254
Load
P
1200
10
310UB40.4
Coach screw
Grade 4.6
M24 Bolts
Grade 8.8
Flush end plate
PL360x210x10
Stiffener
260x80x10
304
CLT: 120 mm thick
120
Roller support
Column
250UC72.9
3000

Figure III.1-8 – Static push-down displacement test setup for the experimental campaign carried out by Keipour *et al.* [34] (*image credits*: Keipour et al. [34]).

Chiniforush *et al.* [35] carried out an experimental characterization of the viscoelastic and mechano-sorptive long-term behavior of two types of connections for CLT-steel composite structures, vis. hexagonal coach screws and dog screws. The tests have been carried out on symmetric steel-timber composite connection specimens (Figure III.1-9). The symmetry is necessary to guarantee a pure-shear loading condition on mechanical fasteners. Long-term push-out tests have been carried out applying a load correspondent to 40% or 60% of the shear capacity of connections for one year at ambient conditions assuming different load-to-grain orientations for the CLT panels. In addition, both static and dynamic short-term tests have been executed, the former to determine the initial stiffness and the peak loads for both joint solutions, and the later to evaluate the performance of connections to cyclic loadings. Finally, a three-parameter analytical model fitted on experimental data to estimate the long-term behavior of steel-timber composite connections has been proposed. Results showed that lower loads led to higher final-to-initial slip ratio. It was than observed that shrinkage and swelling deformations due to moisture variations are negligible, while creep and mechano-sorptive effects give the greatest contribution to long term deformations. Finally, it resulted that after one year the deformation of the tested connections was about 3 times the initial one.

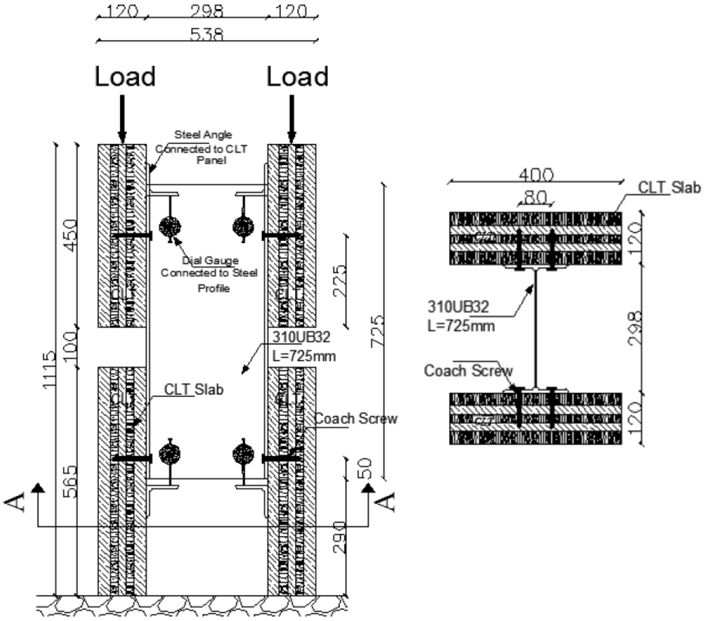

Figure III.1-9 – Experimental setup of tests on CLT-steel composite structural members carried out by Chiniforush *et al.* [35] (*image credits*: Chiniforush *et al.* [35])

III.1.4 Connections

Connections between the different layers of composite structures play a fundamental role, since the collaboration between different components is primarily function of their stiffness and strength. Besides, the behavior of connections strongly affects both strength and stiffness of these structures, hence their correct mechanical characterization is necessary to reliably predict the structural behavior of composite structures.

Different types of connections are available for TBCSs, and the most common are (*i*) notched connections [36, 37]), (*ii*) dowel-type fasteners [5] and (*iii*) glued interfaces [38]. Generally dowel-type connectors are less stiff and resistant than notched and glued connections, but they usually are more ductile [5] (Figure III.1-10). In the following, advantages and drawbacks of different types of connections and methods to predict their mechanical behavior will be discussed.

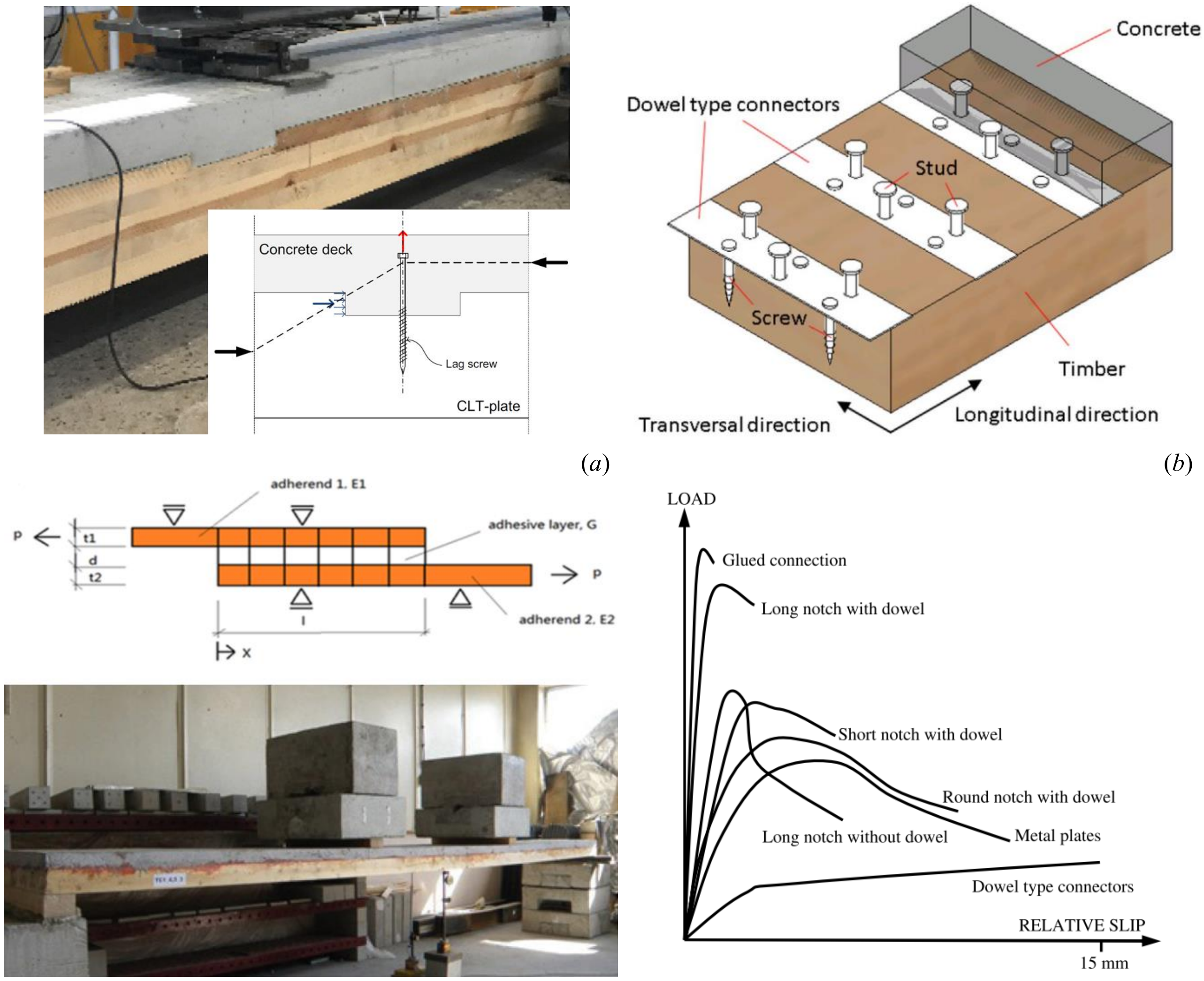
Concrete deck
Lag screw
CLT-plate
Concrete
Dowel type connectors
Stud
Screw
Timber
Transversal direction
Longitudinal direction
adherend 1, E1
adhesive layer, G
adherend 2, E2
P
t1
d
t2
l
x
LOAD
Glued connection
Long notch with dowel
Short notch with dowel
Round notch with dowel
Long notch without dowel
Metal plates
Dowel type connectors
RELATIVE SLIP
15 mm

(*a*) (*b*)

(*c*) (*d*)

Figure III.1-10 – Connections typologies for of TBCSs: (*a*) notched connection, (*b*) dowel-type connection, (*c*) glued connection and (*d*) typical load-slip curves for the different type of connections (*image credits*: (*a*) Jiang *et al.* [39] (*b*) Lyu *et al.* [40] (*c*) Shengmin *et al.* [41] and Kanócz *et al.* [38], (*d*) Yeoh *et al.* [5]).

III.1.4.1 Dowel-type fasteners

Dowel-type fasteners, used in timber structures from early days, are the most commonly used in TCCSs, because they are easy to use, relatively affordable, available everywhere and they have good mechanical performances [42]. The main shortcoming of these connections is the low stiffness if compared to other types of connectors for TBCSs (Figure III.1-10). Their behavior is highly influenced by their arrangement [2], by the characteristics of materials they are connected to, by the depth of insertion and by the type and dimensions of dowelled connections used (Figure III.1-11). The mechanical characterization of these connections can be carried out in different ways. One of these is given by analytical models [43], some of these based on Johansen theory [44] like the one presented in [45]. The mechanical characterization of dowel-type fasteners can also be derived from experimental tests outcomes, like the study conducted by Ahmadi [46] for seven different types of nails and three different penetration depths on timber side.

In order to determine the strength of dowel-type connectors in TBCSs, the Johansen theory [44] can be adapted to the specific case. Particularly, for TCCSs, Dias *et al.* [42] proposed a model to determine the load carrying capacity of dowel-type connections assuming and comparing three different types of constitutive laws for timber: (*i*) elastic perfectly plastic, (*ii*) elastic perfectly rigid and (*iii*) elastic with a gap between the two materials. The comparison with experimental result showed that the best model to predict the strength of dowel-type connectors is the one that assumes an elasto-plastic behavior of concrete, even if it is underestimated respect to test results, probably because of secondary effects (e.g. friction phenomenon and rope effect) not considered in the model and whose influence could be not negligible [47].

One of the parameters that mostly impact on the performance of composite structures is the load-slip constitutive law, since it influences the way the internal forces are transferred between the two different materials. Many ways are given to predict its value for dowel-type fasteners: a first one is given by analytical models based on the solution of a beam on elastic foundation, originally developed by Kuenzi [48] and then extended to consider an interlayer between the connected elements by Gelfi *et al.* [49]. Other methods are given by the empirical model contained into EC5 [21] and by carrying out experimental tests with the protocol described in EN 26891:1991 [50]. An extensive comparison between the methods is presented by Dias [51]. Jiang *et al.* [52] derived an analytical method that can predict the load-slip behaviour of dowel-type shear connectors of TCCSs before the complete curing of concrete [52]. Chiniforush *et al.* [35] proposed an analytical model, whose parameters are calibrated on experimental results using a Genetic Algorithm [53], to predict the long-term behaviour of TCCSs. He *et al.* [54] and Xie *at al.* [55] proposed theoretical shear capacity equations for dowel-type connectors in TCCSs based on Johansen theoretical model [44]. Finally, Marchi *et al.* [56] reported a simplified theoretical approach to define stiffness and strength of joints made with inclined screws.

An experimental campaign conducted by Ceccotti *et al.* [26] on TCCSs connected through corrugated rebars placed inside holes drilled in the timber and filled with epoxy resin showed that the analytical models proposed by Eurocodes underestimate the actual connection stiffness and strength, and it's therefore necessary to evaluate these properties through testing. It's important to observe that an experimental campaign of push-out tests on five different mechanical connectors showed that dowel-type fasteners show a non-linear behaviour even for low load values [57], therefore their modelling should be non-linear, since this markedly plastic behavior may significantly influence the mechanical behaviour of the composite structure and criteria reported by standards to determine the elastic stiffness k_{ser} could be misleading [58].

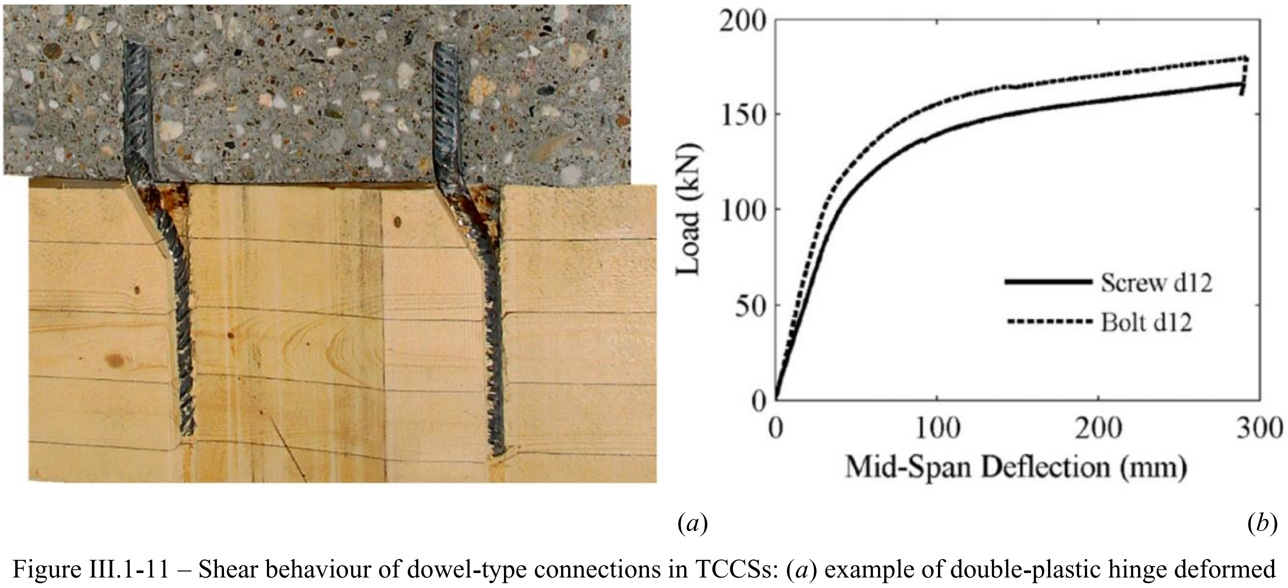

(*a*) (*b*)

Figure III.1-11 – Shear behaviour of dowel-type connections in TCCSs: (*a*) example of double-plastic hinge deformed configuration and (*b*) load vs. mid-span deflection of a TCC beam to the wary of the dowel-type connector (image credits: (*a*) Dias *et al.* [47] and (*b*) Hassanieh *et al.* [3]).

III.1.4.2 Notched shear key connections

Notched connections are very efficient [27], thanks to cost-effectiveness, strength and a stiffness that allows a nearly composite action [39]. One of the main drawbacks of this type of connections respect to the dowel-type ones illustrated in Section III.1.4.1 is the brittle behavior they usually exhibit at ULS - unless their spacing is limited – with the risk that this local behavior can affect the ductility of the whole composite structure [59], hence the robustness requirements might be jeopardized [60].

The notch sawn in the timber element can have different shapes, e.g. it can be rectangular (the most common and efficient, Figure III.1-12.a), circular (Figure III.1-12.b) or bird-mouth (Figure III.1-12.c) [61, 62]. A dowel-type fastener can also be placed in notched connections of TCCSs in order to avoid the separation at the interface between the two materials due to eccentricities of internal forces [39]. This type of connection has proven to be extremely efficient in terms of resistance, stiffness and post-peak behaviour [62].

An analytical model to derive the strength of notched connections, derived considering all the possible failure modes, is proposed in [63]. Analytical models to derive the non-linear load-slip behavior of these connections are available in [63, 64].

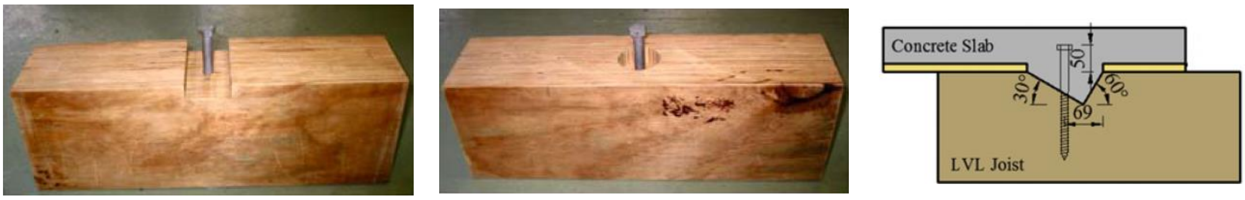

(*a*) (*b*) (*c*)

Figure III.1-12 – Different notched types: (*a*) rectangular, (*b*) circular and (*c*) bird-mouth (*image credits*: (*a-b*) Deam *et al.* [62], (*c*) Khorsandnia *et al.* [61]).

III.1.4.3 Glued connections

Glued interface between the two components of TBCSs create a continuous connection, as opposite to the discrete one offered by the notched- and the dowel-type illustrated in the previous Sections III.1.4.1 and III.1.4.2. Glued connection offers the main advantage of being stiffer respect to notched and dowel-type connectors, resulting before in an extreme performant solution, so that the connection can be considered rigid guaranteeing a full composite action [3]. The main drawbacks are on one hand an increased effect of concrete shrinkage on the deflection of TCCSs [38], and on the other hand the fact that glue requires a curing time (specified by the producer) unlike dowel-type connectors and notched connections. It is in add worth noting that glued connections require carefulness in predicting their behaviour to long-term actions, especially for outdoor sheltered climate, since premature failure of bond lines can happen as evidenced in the studies carried out by Larsson *et al.* [65].

An extensive experimental and numerical study on TSCSs connected with a hybrid connection system made up of non-sag epoxy glue and dowel-type fasteners has been carried out by Hassanieh *et al.* [3]. The outcomes show that glued connections are able to guarantee a nearly full composite action, increment the initial stiffness of the structure while its effect on its strength is negligible, and finally that glued connection may cause a brittle failure of the structural system.

III.1.4.4 Other innovative connections types

Other innovative less common connection types in add to the ones cited in Sections III.1.4.1-III.1.4.3 exist to guarantee the collaboration between materials in TBCSs. For example, Yeoh *et al.* [66] proposed a connection for TCCSs made of a double-sided toothed metal plate embedded in the concrete mesh and enclosed between two vertical layers that form the timber component (Figure III.1-13). Crocetti *et al.* [67] proposed two innovative dry shear connection systems to be used in TCCSs with prefabricated slabs, in particular a wooden shear anchor-key (Figure III.1-14.a) and a connection made with special inclined steel tubes (Figure III.1-14.b).

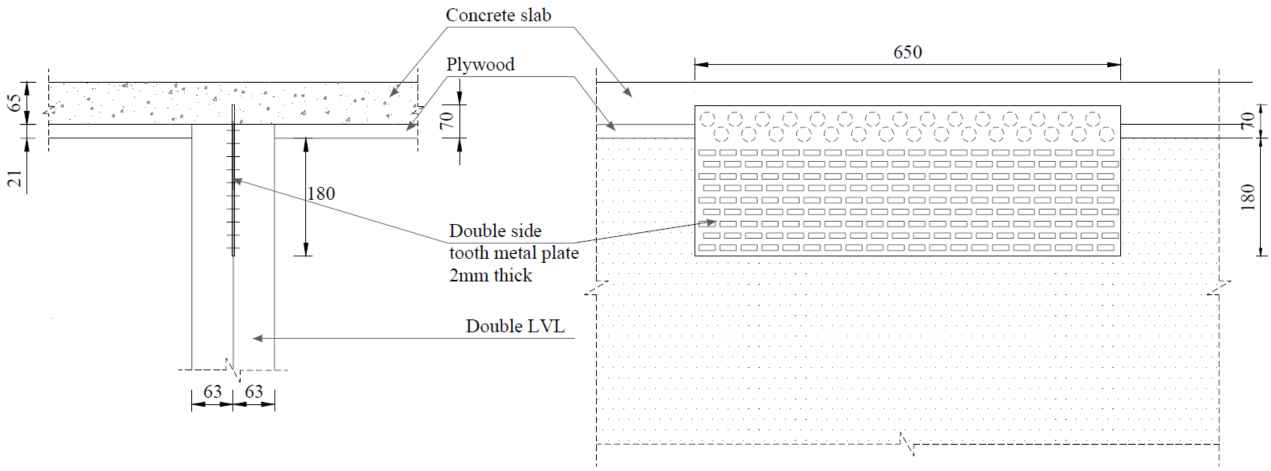
Concrete slab
Plywood
650
65
21
70
180
Double side
tooth metal plate
2mm thick
Double LVL
63
63
70
180

(*a*) (*b*)

Figure III.1-13 – Shear connection proposed by Yeoh *et al.* [66] (*image credits*: Yeoh *et al.* [66]).

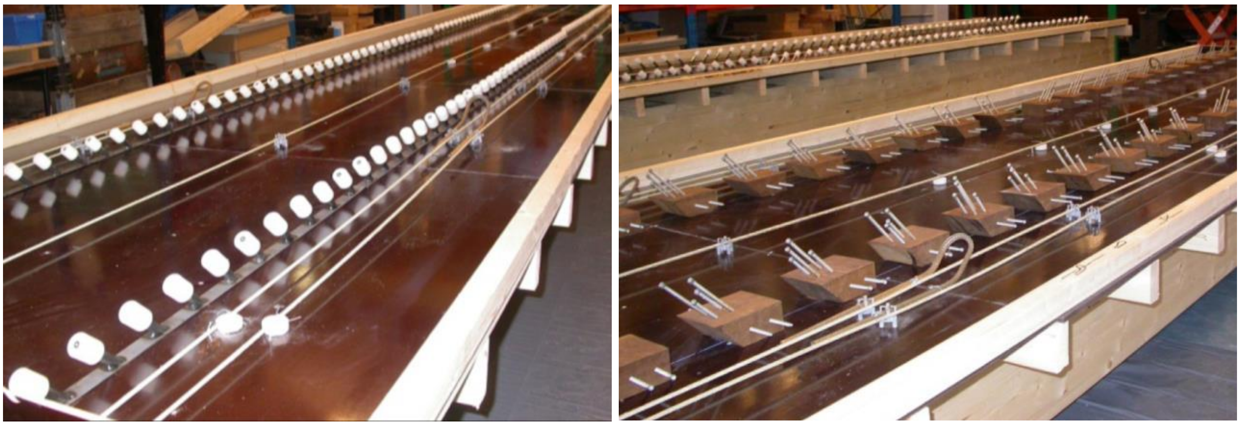

(*a*) (*b*)

Figure III.1-14 – Innovative dry shear connection systems by Crocetti *et al.* [14]: (*a*) inclined steel tubes and (*b*) wooden shear anchor-key (*image credits*: Crocetti *et al.* [14]).

III.1.5 Analytical modelling of timber-based composite structures

Analytical models are available in literature for the calculation of composite structures [68, 69], and for TBCSs most of them are based on the mechanically jointed beams theory of EC5 [15, 21, 70]. For example, for composite CLT-concrete floors, a modified γ method [20] that uses a combined distributed stiffness has been proposed in [39] for both SLS and ULS design. Bajzecerová [71] carried out a comparison between γ-method and the theory of Timoshenko for the calculation of composite CLT-concrete beams through a parametric analysis, finding out that the former methodology is preferable since it gives similar results than the Timoshenko theory but it also allows to take into account for flexibility between CLT and concrete components. More refined analytical solutions have also be proposed, like the one by Focacci *at al.* [72], that can predict both stresses and strains for composite beams generally connected by removing two assumptions usually present in analytical models for composite structures, namely (*i*) shear stresses do not depend on the cross-section rotations of the components and (*ii*) distribution of the global shear force in the components does not depend on the interface (longitudinal) shear stresses. The main drawback of this method is that it is non-linear and requires numerical solutions of the differential equations of the model. Zhang *et al.* [73] proposed an analytical method to predict the non-linear load-deflection behavior of TCCSs with ductile discrete connections obtained from the supposition of a series of linear models.

An experimental survey conducted by Ceccotti *et al.* [26] on TCCSs has shown that the analytical approximate models reported in EC5 are not conservative to describe the long term behaviour. More refined mathematical models to properly take into account for the rheological behaviour of TCCSs are available in literature, like the one recently proposed by Perkowski *et al.* [74], carried out assuming the standard linear solid model of viscoelasticity, also taking into account for interlayer uplift phenomenon.

III.1.6 Numerical modelling of timber-based composite structures

So far, it's mainly possible to find two numerical modelling strategies for composite structures: a 1D frame FE models, that uses unidimensional finite elements, and a 2D continuum-based models that use quadrilateral elements. In the former one, two parallel linear elements placed on the barycentric axis of the two components are connected through rigid links and horizontal springs to model the slip stiffness of the connectors (Figure III.1-15.a) [75, 76]. The 2D strategy is used to create more sophisticated models, able to take into account for phenomena like the separation between the elements, discontinuities, friction and local non-linear behaviour of materials when non-linear constitutive laws are assumed (Figure III.1-15.c) [64]. It is the best choice when an interlayer of plaster or filler material is inserted between concrete and timber in TCCSs. The 2D modelling strategy has the main drawback of being more time-consuming and computationally-costly than the 1D one, reason why it should be used only when a high accuracy of result is needed. For practitioners, the 1D strategy is usually sufficient, since in case the structure is isostatic, the load distribution is not unusual and the connection characteristics are uniform, the obtained results are satisfactory [2]. It is worth noting that, when plate or solid finite elements are adopted to model one or both the materials of the composite structure, the solution is influenced by the quality of the mesh, especially in the connections area where there is a concentration of stresses.

Connections are conventionally modelled with linear or non-linear springs (e.g. [64, 77]), since it is a computationally efficient approach once the constitutive law is properly calibrated. More refined models for connections exist, like the beam-to-solid model [78], where the dowel-type screw is modelled as a beam embedded in a mesh of 3D solid elements that model concrete and timber components (Figure III.1-15.b). Another refined modelling strategy for TCCSs is the Cohesive Zone Modelling method [79], that allows to take into account for local damaging at connection level thanks to a soft layer with cohesive damage interactions. A numerical model for connections of TSCSs is presented by Hassanieh *et al.* in [80], where a refined FE model that takes into account for steel yielding, combination of brittle and ductile failure modes of timber and non-linear behaviour of the contact interface is considered.

Khorsandnia *et al.* [81] developed a simple frame finite element model to study the long-term behaviour of TCCSs. Finally, Mascia *et al.* [82] carried out a numerical investigation on TCCSs through a model derived using the principle of virtual works.

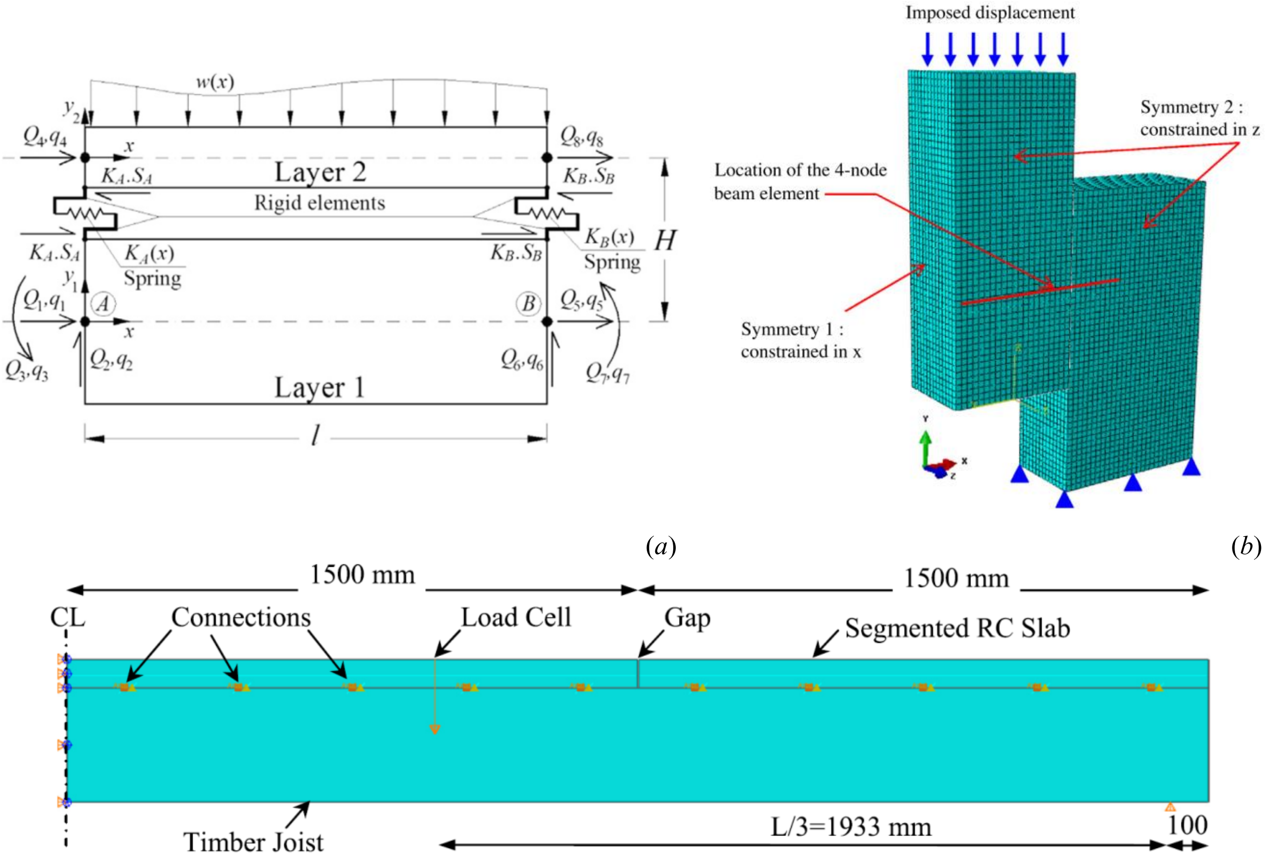
w(x)
y2
Q4,q4
x
Layer 2
Q8,q8
KA.SA
KB.SB
Rigid elements
KA.SA
KA(x)
Spring
KB.SB
KB(x)
Spring
H
y1
Q1,q1
A
B
Q5,q5
x
Q3,q3
Q2,q2
Layer 1
Q6,q6
Q7,q7
l
Imposed displacement
Symmetry 2 :
constrained in z
Location of the 4-node
beam element
Symmetry 1 :
constrained in x
Y
X
Z
1500 mm
1500 mm
CL
Connections
Load Cell
Gap
Segmented RC Slab
Timber Joist
L/3=1933 mm
100

(*a*) (*b*)

(*c*)

Figure III.1-15 – Modelling strategies for composite timber-based structures: (*a*) 1D modelling approach, (*b*) beam-to-solid modelling of dowel-type connectors and (*c*) 2D modelling approach (*image credits*: (*a*) Khorsandnia *et al.* [76], (*b*) Oudjene *et al.* [78], (*c*) Khorsandnia *et al.* [64]).

III.2 A mechanics-based analytical model for an innovative timber-steel composite beam

Abstract

In order to satisfy the current demand of large open spaces, architectural flexibility and higher buildings, timber construction industry must face the problem of producing bigger and bigger structural members. Modern timber technology allows to cover very large spans with long glulam beams, but these structural elements have many drawbacks: they are difficult to transport from factory to site, their installation is complicated requiring big lifting machinery, they are difficult to produce and, as a consequence, they increase the construction cost of the building. In order to find a solution to these problems, an innovative timber-steel composite beam has been prototyped at KTH Royal Institute of Technology of Stockholm. This structural member is composed of separated timber joists then joint together on site through a steel system composed of notched shear-keys and tensioned cables. Thus, this technology allows to obtain longer structural elements starting from smaller ones, allowing a considerable decrease of the total construction cost thanks to easiness in the transportation and handling on site.

In this Section, after an overview on this innovative structural element, a mechanics-based analytical model able to describe its mechanical behaviour – both in term of internal forces and deflections- is presented. The model is then compared with the results obtained with a numerical model showing a very good agreement. It has finally been used to carry out a preliminary parametric analysis to investigate the performance of the system to the vary of the main mechanical and geometrical properties of the beam.

The proposed analytical model is a reliable tool to predict the structural performance of the innovative composite system and it allows for a better comprehension of the mechanical phenomena involved in the structural response respect to analyses carried out with numerical models.

III.2.1 Chapter contents

The main goal of this Section is to develop an analytical model able to predict both internal forces and displacements of an innovative composite timber-steel structure prototyped at KTH Royal Institute of Technology (Sweden) and studied through numerical analyses and a preliminary experimental campaign with four-point bending tests by Wang *et al.* [83].

After an opening description of the structural system, the basic assumptions used to develop the model and its mathematical formulation will be described. The validation of the analytical model, carried out through comparison with numerical results, has shown the high accuracy provided in predicting the structural behavior of the composite beam. The analytical model will be used to identify the parameters that affect the structural behaviour and to evaluate how much each of them affect the structural performance of the beam. Finally, in order to show the potentiality of the model, a simple parametric analysis is carried out in order analyze the influence of different parameters on Serviceability Limit States (SLS) performance.

The analytical model presented in this Section constitutes a powerful and versatile tool to rapidly carry out studies on the mechanical behavior of this novel technology, to design it and to accomplish parametric analyses for structural performance improvement and optimization. Actually, the tested configurations in a preliminary experimental campaign carried out at Moelven Industrier ASA (Töreboda, Sweden) [83] have been considered failed because of excessive deflections. Therefore, a reliable and manageable tool like an analytical model can be used to easily detect lacks in the innovative structural systems and to design structural improvements. The model will therefore be used to define which geometrical characteristics the experimental setup must have - given loads and materials – in order to obtain satisfiable deflections. The analytical model can also be used to carry out multi-parametric analyses for structural optimization - once implemented into a script - much faster respect to parametric analyses carried out with computationally-costly finite elements.

III.2.2 Overview

III.2.2.1 Description of the novel structural system

Modern building conception require buildings with large open spaces and architectural flexibility. Traditional timber structures could not face these problems, mainly because the maximum dimensions of the structural elements were limited by the size of trees trunks from where the members where extruded by sawn. New engineered timber products, like glulam, allowed to create longer and higher structural members, overcoming the problems of create structural elements that were long the enough to cover the desire span and that had big moment of inertia. Anyway, these big timber structural elements have many drawbacks: they are difficult to transport from factory to site, their installation is complicated requiring big lifting machinery, they are difficult to produce and, as a consequence, they considerably increase the construction cost of the building. In order to solve these problems, an innovative timber-based hybrid system has been developed and studied by Crocetti R., Wang Y. & Wang T. [83] (Figure III.2-1).

The composite timber-steel structural system is composed of timber joists connected together on site with a dry head-to-head joint (Figure III.2-2.a), steel shear-keys (Figure III.2-2.b) inserted in notches shaped on timber joists on production site (Figure III.2-2.c) and steel cables (Figure III.2-2.d). At the head-to-head interface it is inserted a steel plate in order to avoid the loss of strength and stiffness due to end grain contact compression [84] and on the upper lateral sides two steel plates are bolted to the timber in order to provide stabilization against relative lateral sliding between the two pieces of timber (Figure III.2-2.a). The steel strand has the structural function of adsorbing the tensile stresses necessary to guarantee the equilibrium in the mid-jointed section, where timber presents a material discontinuity (Section III.2.3).

The system allows to split the beams into two (or more) parts of equal length for easiness of transportation, and then easily assemble them on site with the use of shear-key connectors and an unbonded steel rod. This system can also be applied to continuous timber beam in order to increase their strength and stiffness, especially for restoration purposes, but this aspect is out of the scopes of this Thesis and the reader is referred to Wang *et al.* [83] for further details.

In order to properly design the notched connections, some recommendations should be followed [47]:

- minimum notch depth of 2.0 cm and 1.5 cm respectively for softwood and hardwood;
- minimum length of the notch of 15 cm;
- inclination of 90° of notch cuts;
- screws with a minimum diameter of 6 mm.

Given h_{notch} the height of the timber notch (Figure III.2-2.c), it should be respected a minimum distance of $0.8 \cdot h_{notch}$ between the end of the two internal notches and the beam mid-span section (Figure III.2-1), accordingly to EN 1995-1-1, NCI NA.12.1 (NA.4) [85], in order to achieve the maximum longitudinal shear strength without risk of brittle failure of timber.

Preliminary experimental tests to explore the behavior of this composite structure have been carried out by Wang *et al.* [83]. The specimens of composite structures have been tested in a four-point loading condition, with a simply supported configuration and a quasi-static load with monotonic increment applied through a hydraulic jack with an integrated gauge to measure the applied pressure.

III.2.2.2 Advantages and drawbacks of the novel technology

There is an increased interest and demand within the construction sector to use timber-based composite structures. Timber is widely recognized as one of the most sustainable materials for construction purposes, and its engineered products (e.g. CLT and glulam) make possible to overcome the issue of dimensional limit of timber structural elements, allowing these structures to span to lengths similar to traditional materials (i.e. steel and concrete).

There are anyway some issues relating these structures, like lower resistances and greater expense to transport and install big-size structural members. The composite timber-steel element proposed in [83] allows to work around these problems, since the desired span can be simply obtained by joining together smaller timber joists through steel cables and shear-keys. The main drawback of this technology may be represented by its potentially low resistance to fire action because of exposed steel at the intrados. A possible solution may be represented by coverage steel parts with timber caps, but further studies (out of the scope of this Thesis) are necessary.

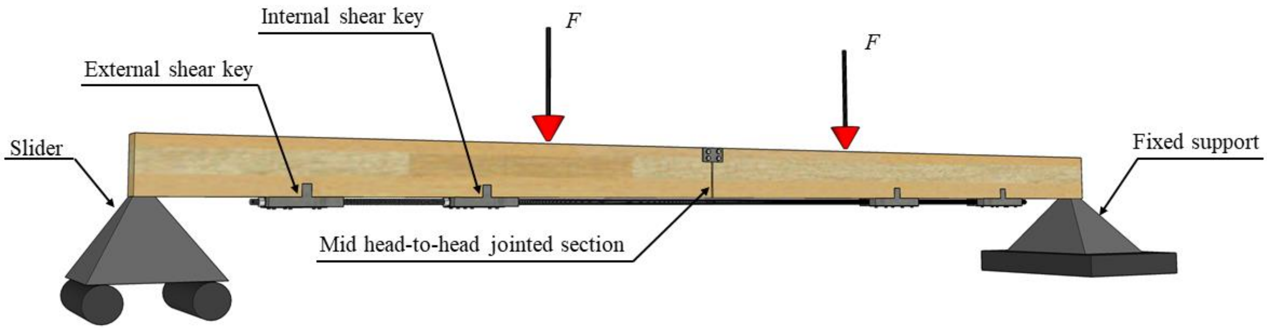

Figure III.2-1 – View of the timber-steel composite beam in a four-point loading simply-supported configuration.

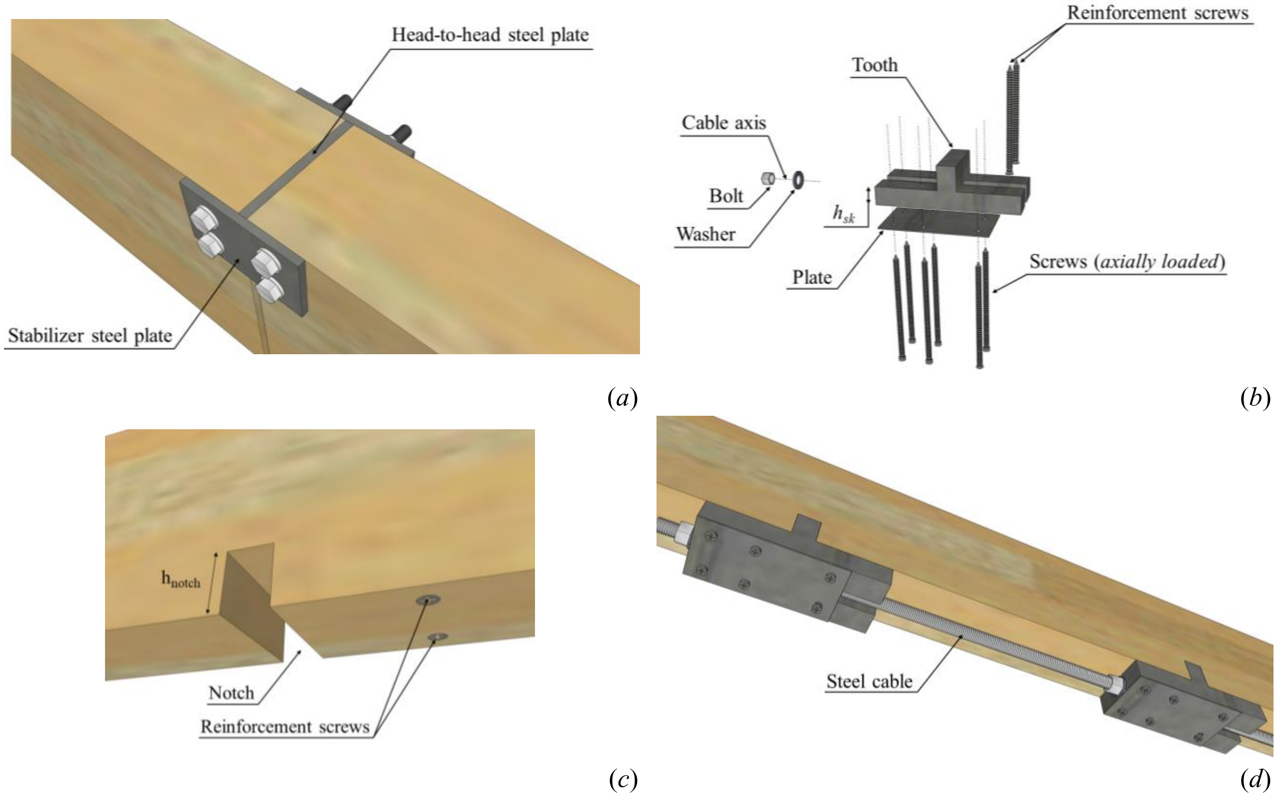
Head-to-head steel plate
Stabilizer steel plate
Reinforcement screws
Tooth
Cable axis
Bolt
Washer
h_{sk}
Plate
Screws (*axially loaded*)
h_{notch}
Notch
Reinforcement screws
Steel cable

(*a*) (*b*)

(*c*) (*d*)

Figure III.2-2 – Details of the hybrid timber-steel beam: (*a*) joint plates, (*b*) steel shear-key, (*c*) timber notch and (*d*) anchorage of shear keys on timber beam.

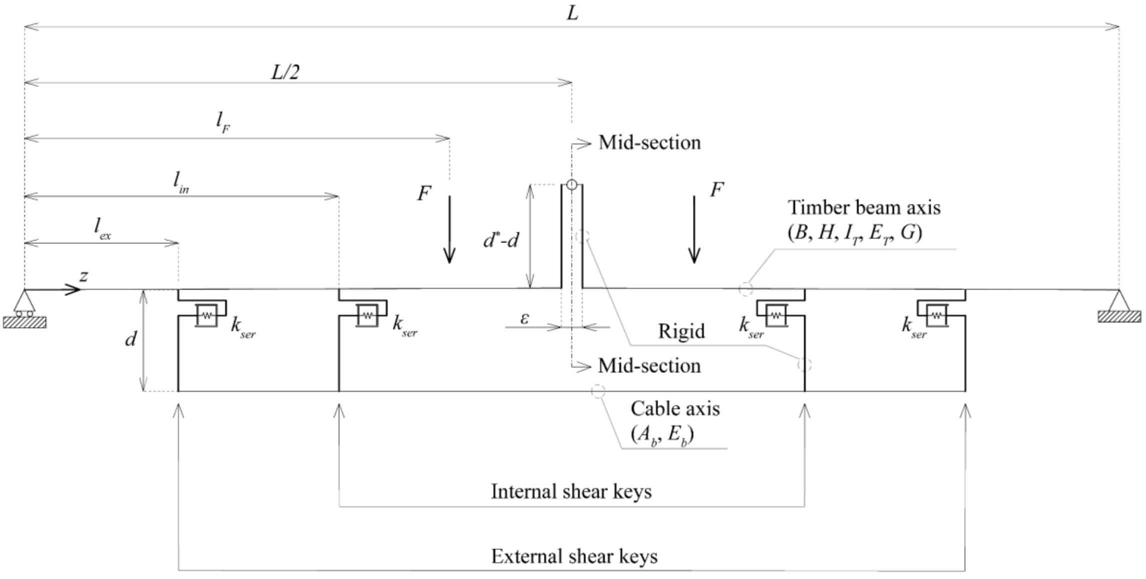
L
$L/2$
l_F
l_{in}
l_{ex}
z
F
d^*-d
F
Mid-section
Timber beam axis
(B, H, I_T, E_T, G)
d
k_{ser}
k_{ser}
ε
Rigid
k_{ser}
k_{ser}
Mid-section
Cable axis
(A_b, E_b)
Internal shear keys
External shear keys

Figure III.2-3 – Global mechanical model of the composite timber-steel structure used to define the analytical model.

III.2.3 Analytical model description

In the following, an analytical model used to derive in a closed-form solution both internal forces and short-term deflections of the composite timber-steel structure illustrated in Section III.2.2.1 will be illustrated. A list of the symbols is reported in Table III.2-1. The model has been built assuming the same boundary and loading conditions adopted for the preliminary tests illustrated in Wang *et al.* [83], vis. a four-point loading structural scheme with two vertical forces comprised between the internal shear keys is assumed. (Figure III.2-1). This choice is primarily due to the fact that the analytical model has been ideated with the purpose of being a support tool to optimize and design future experimental tests that will be carried out on the novel composite structure. In add, guaranteeing the same loading conditions and boundaries of the test configuration, comparison between analytical and experimental outcomes will be possible providing a further validation of the model. With minor modifications it will be possible to extend the analytical model here developed to a general configuration of loads and boundaries (i.e. with concentrated forces placed outer the inner shear keys, distributed load q or a generic number of shear key connections).

The simply supported composite beam behaviour has been schematized in the mechanical model represented in Figure III.2-3, adapting to the specific case the Vierendeel model usually suggested for isostatic composite structures with standard load distributions and uniform characteristics of connections [2].

The composite timber-steel structure is loaded with two vertical concentrated loads F placed within the two internal shear keys, accordingly to the four-point loading configuration assumed in the preliminary experimental campaign [83]. The left load is placed at a longitudinal position z equal to l_F, while the right one is symmetrically placed respect to the mid-section.

The timber joist has been analytically modelled as a beam-type linear element, positioned along the barycentric axis of the wooden component. Therefore, the mechanical and geometrical characteristic that define its behaviour are the width and height of timber cross-section B and H, the modulus of inertia I_T, the modulus of elasticity E_T (equal to the modulus of elasticity of timber in the direction parallel to grain) and the shear modulus G. The steel cable component, positioned at a distance d from the timber beam, is assumed to be placed at the middle of the height h_{sk} of the plinth of the shear keys (Figure III.2-2.b) and has been modelled as a truss-type linear element. Therefore, the mechanical and geometrical characteristic that define its behaviour are the area of the cable A_b and its modulus of elasticity E_b. The cross-sectional area of the steel cable A_b and the cross-section dimensions of timber beam B and H are assumed constant for every position z along the structure.

The shear key connections are four, two external and two internal, placed symmetrically respect to the mid-section. The positions of the left external and internal shear keys are respectively l_{ex} and l_{in}. The shear keys have been modelled as rigid bodies connected to the upper timber beam and the lower steel cable. The partial interaction between timber beam and steel cable is modelled through discrete linear springs with a stiffness k_{ser}. This stiffness value is due to the compression of timber of the notch by the steel shear key, considering negligible the shear contribution of the screws (Figure III.2-2.d).

A hinge is placed at mid-span with an eccentricity $d^* - d$ respect to the timber beam axis, where d^* is the distance between the axis itself and the resultant compressive force F_c acting at the interface between the two pieces of beam. Actually, the timber material discontinuity at mid-span is able to transmit only axial compression loads (and some shear because of friction in case of asymmetrical loading conditions), therefore the mechanical behaviour can be represented by a hinge placed on the resultants of the compressive force F_c.

Table III.2-1– List of notations used in the analytical model.

Symbol	*Description*
a	*Position of the bending moment* m *respect to the left support*
A_b	*Cross-sectional area of the steel cable*
B	*Width of the timber beam section*
C	*Barycentre of the timber beam section*
$c_{\delta_{ex}}$	*Displacement of the stiff bar of model in Figure III.2-9 due to* δ_{ex}
$c_{\delta_{in}}$	*Displacement of the stiff bar of model in Figure III.2-9 due to* δ_{in}
d	*Distance between the barycentre of the timber beam and the axis of the cable*
d^*	*Lever arm between tensile and compressive forces in the mid-section*
E_b	*Elastic modulus of the steel of the cable*
E_T	*Elastic modulus of timber in parallel to grain direction*
F	*Vertical load*
f_b	*Yielding strength of steel of cable*
F_c	*Compressive force acting on the mid-section*
f_c	*Yielding strength of timber material in parallel to grain direction*
G	*Timber shear modulus*
H	*Height of the timber beam cross- section*
h_{notch}	*Notch height*
h_{sk}	*Height of the plinth of the shear key*
I_{id}	*Moment of inertia of the area of the composite timber-steel beam*
I_T	*Moment of inertia of timber beam section*
$k_{a,ex}$	*Axial stiffness of timber beam portion comprised between the external shear keys*
$k_{a,in}$	*Axial stiffness of timber beam portion comprised between the internal shear keys*
k_b	*Axial stiffness of cable portion between external and internal shear keys*
k_{ex}	*Axial stiffness of external equivalent spring of the mechanical model in Figure III.2-9*
k_{in}	*Axial stiffness of internal equivalent spring of the mechanical model in Figure III.2-9*
k_{rot}	*Elastic rotational stiffness of the timber beam at a generic cross-section*
$k_{rot,ex}$	*Elastic rotational stiffness of the timber cross-section beam placed at* $z = l_{ex}$
$k_{rot,in}$	*Elastic rotational stiffness of the timber cross-section beam placed at* $z = l_{in}$
k_{ser}	*Notch stiffness*
k_T	*Axial stiffness of half of the timber beam part between the internal shear keys*
$k_{T,ex}$	*Axial stiffness at the cable level due to the elastic rotational stiffness* $k_{rot,ex}$
$k_{T,in}$	*Axial stiffness at the cable level due to the elastic rotational stiffness* $k_{rot,in}$
L	*Beam span*
l_{ex}	*Position of the external shear key connection measured from the left support*
l_F	*Position of the concentrated load F*
l_{in}	*Position of the internal shear key connection measured from the left support*
M	*Bending moment on timber beam*
m	*Concentrated bending moment acting on timber beam*
M_E	*Bending moment acting in the composite timber-steel mid-section*
m_{ex}	*Bending moment acting on timber beam due to force* T_{ex} *on external shear key*
m_{F_c}	*Localized bending moment at mid-span due to eccentricity of force* F_c
m_{in}	*Bending moment acting on timber beam due to force* T_{ex} *on internal shear key*
$M_{R,el}$	*Resistant bending elastic moment of mid-section of the composite structure*
$M_{T,E}$	*Bending moment acting in the timber beam mid-section*
N	*Axial force on timber beam*
n	*Composite steel to timber material homogenization coefficient*
T	*Tensile force in the part of the cable comprised between the internal shear keys*
T^*_{ex}	*Shear force on the external shear key when displacements* δ_{ex} *and* δ_{in} *are null*
T^*_{in}	*Shear force on the internal shear key when displacements* δ_{ex} *and* δ_{in} *are null*
T_{ex}	*Tensile force in the cable part between external and internal shear keys*
v	*Timber beam vertical deflection*
V	*Shear force on timber beam*

(continued on next page)

(continued from the previous page)

v_{el}	*Elastic vertical deflection contribution*
v_{F_c}	*Timber beam elastic deflection due to the eccentricity of the compressive force* F_c
$v_{m_{ex}}$	*Elastic deformation of timber beam due to* m_{ex}
$v_{m_{in}}$	*Elastic deformation of timber beam due to* m_{in}
v_{max}	*Timber beam vertical deflection measured at mid-span section*
v_{rig}	*Rigid vertical deflection contribution*
$v_{rig,max}$	*Rigid vertical deflection measured at mid-span*
v_{sh}	*Shear deformation of timber beam*
x	*Neutral axis position at mid-section respect to the compressed side*
z	*Position of the generic cross-section of the timber beam measured from the left support*
δ_{ex}	*Horizontal displacement at the cable level due to rotation* φ_{ex}
δ_{in}	*Horizontal displacement at the cable level due to rotation* φ_{in}
Δl_b	*Half elongation of steel cable part comprised between the two internal shear keys*
Δl_{mid}	*Half of the maximum (at lower level) gap opening at mid-span interface*
Δl_{notch}	*Horizontal displacement due to timber compression in the internal notch*
Δl_{sk}	*Horizontal displacement due to rotation of the internal shear key*
Δl_T	Elastic shortening of half of the timber beam axis due to force F_c
$\delta_m(z)$	*Horizontal displacement at the level of the cable due to rotation* $\varphi_m(z)$
ΔT_{ex}	*Variation of shear force on external shear keys due to displacements* δ_{ex} *and* δ_{in}
$\Delta T_{ex,\delta_{ex}}$	*Variation of shear force on external shear keys due to* δ_{ex}
$\Delta T_{ex,\delta_{in}}$	*Variation of shear force on internal shear keys due to* δ_{in}
ε	*Arbitrarily small little value*
ε_b	*Tensile strain of steel of the cable*
$\varepsilon_{b,y}$	*Yielding tensile strain of steel of the cable*
ε_T	*Compressive strain of timber*
$\varepsilon_{T,y}$	*Yielding compressive strain of timber*
σ_b	*Tensile stress on the steel cable*
$\sigma_{b,y}$	*Yielding tensile stress of steel of the cable*
σ_T	*Compressive stress on timber*
φ	*Cross-section rotation of the beam*
φ_{el}	*Timber beam cross-section elastic rotation*
φ_{ex}	*Elastic rotation of the external shear key due to* F_c *and* m_{in}
φ_{F_c}	*Elastic rotation of timber beam cross-section due to* F_c
$\varphi_{F_c}(z)$	*Elastic rotation of timber beam cross-section placed in* z *due to* F_c
φ_{in}	*Elastic rotation of the internal shear key due to* F_c *and* m_{ex}
$\varphi_m(z)$	*Elastic rotation of timber beam section placed at position* z *due to* m
$\varphi_{m_{ex}}$	*Elastic rotation of timber beam cross-section due to* m_{ex}
$\varphi_{m_{ex}}(z)$	*Elastic rotation of timber beam cross-section placed in* z *due to* m_{ex}
$\varphi_{m_{in}}$	*Elastic rotation of timber beam cross-section due to* m_{in}
$\varphi_{m_{in}}(z)$	*Elastic rotation of timber beam cross-section placed in* z *due to* m_{in}
φ_{rig}	*Rigid rotation contribution of the beam*
$\chi_{el,max}$	*Maximum curvature of the mid-section that allow materials to behave elastically*
Φ_b	*Steel cable diameter*

III.2.3.1 Basic assumptions

In order to develop the analytical model, some assumptions, developed fulfilling the compatibility and equilibrium conditions of the composite section, have been made:

- Euler-Bernoulli beam theory is assumed to describe the behaviour of the timber beam;
- little displacements are assumed;
- linear behaviour of materials, geometry and boundaries are assumed, but elasto-plastic behaviour of timber (Figure III.2-4.a) and steel of the cable (Figure III.2-4.b) is assumed for the calculation of the position of the neutral axis respect to compressed corner of the cross-section x, see Section III.2.3.2.1;
- rheological behaviour of timber (i.e. creep and mechano-sorptive phenomena) is disregarded;
- the effects of swelling and shrinkage of timber are disregarded;
- vertical deformation of supports and local crushing or deformations due to compression perpendicular to grain at supports is disregarded.

As previously mentioned, the model has been developed within the boundary and load conditions of the experimental setup [83], therefore with a total of four shear keys - two external and two internal - and two vertical loads F placed within the two internal shear keys (Figure III.2-3).

III.2.3.2 Composite beam internal forces

III.2.3.2.1 Tensile force on the cable

To determine the value of the tension force T acting on the portion of the steel cable comprised between the internal shear keys, it is firstly necessary to derive the position of the neutral axis x respect the compressed corner of the mid-span composite section. As stated in Section III.2.3.1, the constitutive laws of both timber and steel materials are elasto plastic (Figure III.2-4).

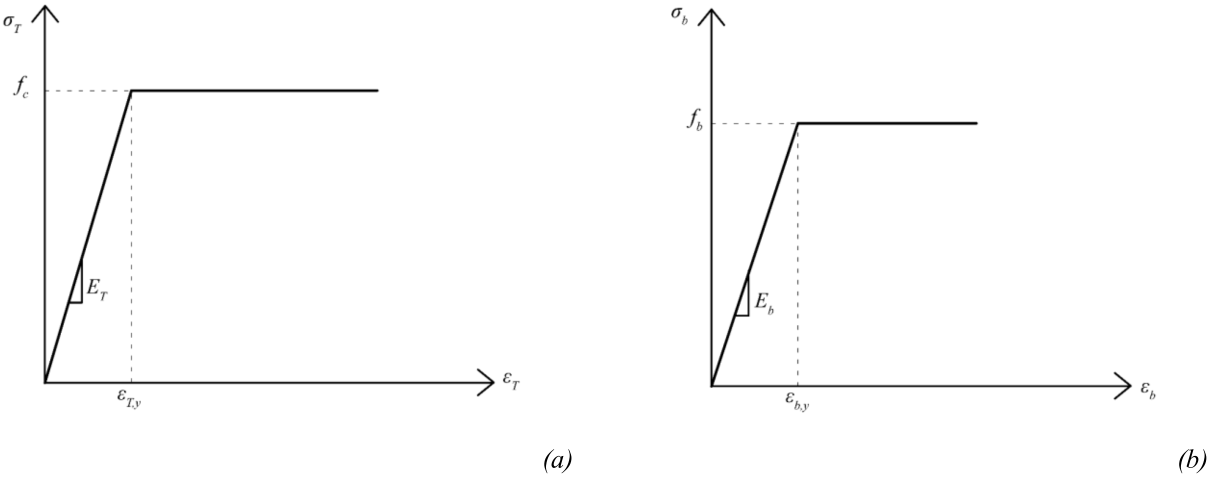

(a) *(b)*

Figure III.2-4 – Elasto-plastic constitutive laws of (a) timber and (b) steel of the cable for the calculation of the neutral axis position on the composite mid-section.

It must therefore firstly be distinguished whether the mid-span composite section reacts elastically or plastically to resist the applied external force. Hence, the maximum resistant elastic bending moment $M_{R,el}$ of the composite beam is firstly derived. To do this, it is necessary to evaluate the maximum curvature of the composite mid-section that allows to react elastically $\chi_{el,max}$. Its value is given as the minimum one between the two possible cases (Figure III.2-5). In the first one, named “Case 1”, the elastic limit is reached by the upper compressed timber fiber of the mid-section, while in the second one, named “Case 2”, the elastic limit is reached by the tensioned steel cable.

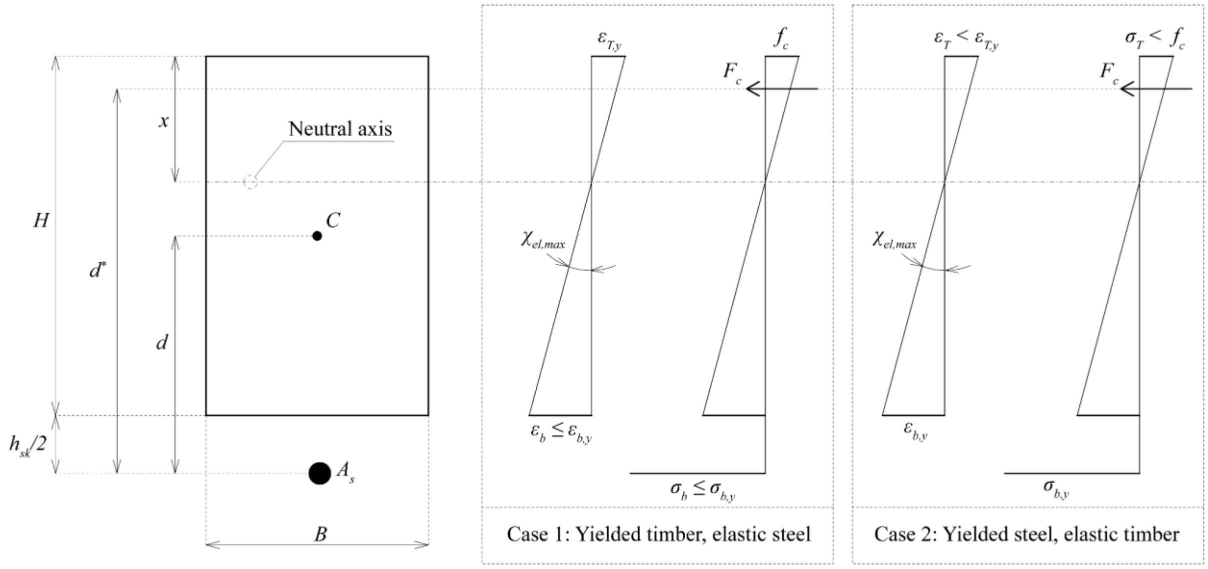
x
Neutral axis
H
C
d*
d
h_sk/2
A_s
B
ε_T,y
f_c
F_c
χ_el,max
ε_b ≤ ε_b,y
σ_b ≤ σ_b,y
Case 1: Yielded timber, elastic steel
ε_T < ε_T,y
σ_T < f_c
F_c
χ_el,max
ε_b,y
σ_b,y
Case 2: Yielded steel, elastic timber

Figure III.2-5 – Maximum elastic curvature $\chi_{el,max}$ of the composite mid-section: Case 1 (yielded timber) and Case 2 (yielded steel).

It is therefore possible to write the equation of the maximum elastic curvature of the composite mid-section $\chi_{el,max}$ as:

$$\chi_{el,max} = min\left(\frac{\varepsilon_{T,y}}{x};\frac{\varepsilon_{b,y}}{H+\frac{h_{sk}}{2}-x}\right) \qquad (III.2\text{-}1)$$

where $\varepsilon_{T,y}$ is the yielding compressive strain of timber, $\varepsilon_{b,y}$ is the yielding compressive strain of the steel cable, x is the position of the neutral axis, H is the height of the section and h_{sk} is the height of the plinth of the shear key.

The maximum resisting elastic bending moment of the composite beam is therefore:

$$M_{R,el} = \chi_{el,max} \cdot E_T \cdot I_{id} \qquad (III.2\text{-}2)$$

where E_T is the elastic modulus of the timber parallel to the grain (that can therefore be assumed equal to $E_{0,mean}$) and I_{id} is the moment of inertia of the area homogenized to timber material:

$$I_{id} = \frac{1}{12}B \cdot x^3 + n \cdot A_b\left(H+\frac{h_{sk}}{2}-x\right)^2 \qquad (III.2\text{-}3)$$

where $n = \frac{E_b}{E_T}$ is the section homogenization coefficient, E_b is the elastic modulus of the steel of the cable and A_b is the cross-sectional area of the steel cable.

Given M_E the bending moment acting on the composite mid-section, the value of the position of the neutral axis x if the section behaves elastically (i.e. if $M_E<M_{R,el}$) is equal to:

$$x = \frac{n \cdot A_b}{B} \cdot \left[-1+\sqrt{1+\frac{2B(H+h_{sk}/2)}{n \cdot A_b}}\right] \qquad (III.2\text{-}4)$$

If the section behaves plastically (i.e. $M_E \geq M_{R,el}$) with materials beyond the yielding limit, the position of the neutral axis x, assumed a stress-block behaviour of timber with a depth of $0.8 \cdot x$ accordingly to "Method B" of [86] (Figure III.2-6), is equal to:

$$x = \frac{H + \frac{h_{sk}}{2}}{0.8}\left(1 - \sqrt{1 - \frac{2M_E}{B \cdot f_c \left(\frac{h_{sk}}{2} + H\right)^2}}\right) \qquad (III.2\text{-}5)$$

where f_c is the yielding strength of timber material.

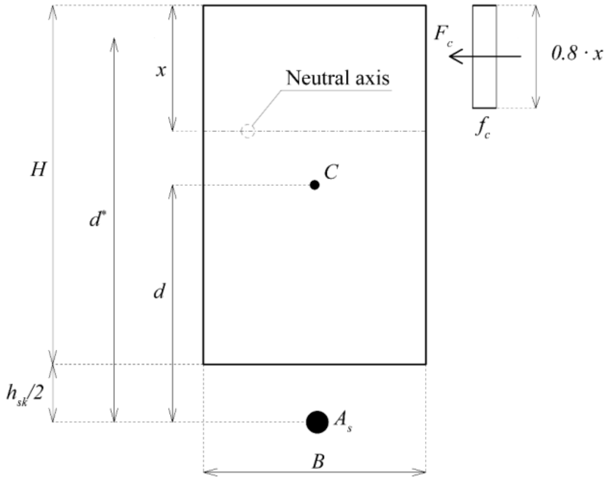

Figure III.2-6 –Position of the neutral axis *x* in the mid-section with plastic behavior of the composite mid-section.

The lever arm d^* between the compressive and tensile forces of the mid-section of the composite timber-steel structure in case of elastic and plastic behavior (Figure III.2-6) is given respectively by equations (III.2-6) and (*III.2-7*):

$$d^* = H + \frac{h_{sk}}{2} - \frac{x}{3} \qquad (III.2\text{-}6)$$

$$d^* = H + \frac{h_{sk}}{2} - 0.4 \cdot x \qquad (III.2\text{-}7)$$

Finally, the tensile stress T in the internal part of the cable (i.e. the one comprised between the two internal shear keys) is equal to:

$$T = \frac{M_E}{d^*} \qquad (III.2\text{-}8)$$

III.2.3.2.2 Shear force on connections

In order to derive the entity of the shear forces acting on the shear keys it is necessary to analyze the behavior of each component of the composite beam, i.e. cable, shear keys and timber beam. Therefore, differently from the previous Section III.2.3.2.1 where to derive the tensile force T the structure has been analyzed with a composite cross-sectional analysis, in the current Section and in the following Section III.2.3.2.3 a component approach is adopted, analyzing the mutual mechanical interactions between each component of the timber-steel hybrid member. The tensile force T acting on the internal portion of cable (i.e. the one comprised between the two internal shear keys) is distributed as shear forces among the external and internal shear keys proportionally to the stiffness of the external portion of the cable (i.e. the one comprised between the external and internal shear keys) and inversely proportionally to the shear key deformability. Actually, shear keys are modelled as rigid elements (see Section III.2.3), but they move horizontally because of timber notch deformability with stiffness k_{ser}, and they rotate respectively of φ_{ex} and φ_{in} because of elastic deflections of the timber beam to which the shear keys are anchored (Figure III.2-11 and Figure III.2-12).

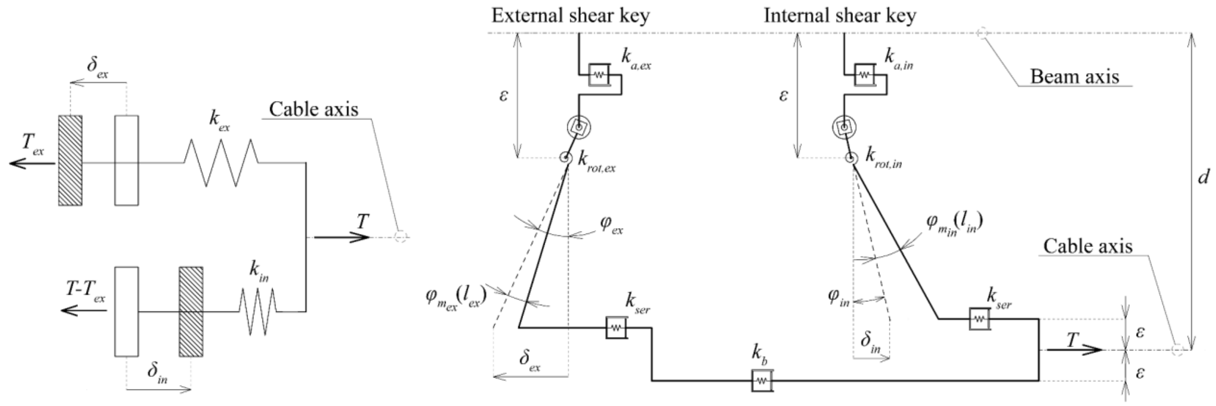

(*a*) (*b*)

Figure III.2-7 – Mechanical model to determine the distribution of the tensile force acting on the cable between the external and internal shear keys: (*a*) general and (*b*) detailed representation.

It is therefore possible to reproduce the mechanical behaviour of the composite structure with a mechanical model composed of two parallel springs with the stiffness k_{ex} and k_{in}, each holding an amount of tension respectively equal to T_{ex} for the external shear key and $T - T_{ex}$ for the internal one (Figure III.2-7.a), with both springs anchored to supports that displace of δ_{ex} and δ_{in} because of rotations of timber beam φ_{ex} and φ_{in} (Figure III.2-7.a). Stiffnesses k_{ex} and k_{in} can be derived from a more detailed model, represented in Figure III.2-7.b, where:

- $k_{rot,ex}$ and $k_{rot,in}$ are the rotational stiffness of the timber beam, respectively at $z = l_{ex}$ and $z = l_{in}$;
- ε is an arbitrarily small little value, meaning that its distance is reported in the figure only for merely graphical purposes, and it is considered null when doing calculations on the forces acting on the mechanical model;
- k_{ser} is the stiffness of the notched shear connection, whose values are derived accordingly to [87];
- k_b is the stiffness of the portion cable between the external and the internal shear key;
- $k_{a,ex}$ is the axial stiffness of the portion of timber beam comprised between the external shear keys;
- $k_{a,in}$ is the axial stiffness of the portion of timber beam comprised between the internal shear keys;
- φ_{ex} is the elastic rotation of the external shear key due to F_c and m_{in};
- φ_{in} is the elastic rotation of the internal shear key due to F_c and m_{ex};
- $\varphi_{m_{ex}}(l_{ex})$ is the elastic rotation of the external shear key due to m_{ex};
- $\varphi_{m_{in}}(l_{in})$ is the elastic rotation of the internal shear key due to m_{in};
- δ_{ex} and δ_{in} are the horizontal displacement at the cable level due respectively to rotation φ_{ex} and φ_{in}.

The mechanical model represented in Figure III.2-7.b can hence be transformed in a new one, represented in Figure III.2-8, where the rotational stiffnesses $k_{rot,ex}$ and $k_{rot,in}$ have been converted into the corresponding translational ones $k_{T,ex} = \frac{k_{rot,ex}}{d^2}$ and $k_{T,in} = \frac{k_{rot,in}}{d^2}$, where d is the distance between the barycentre of the timber beam C and the cable axis.

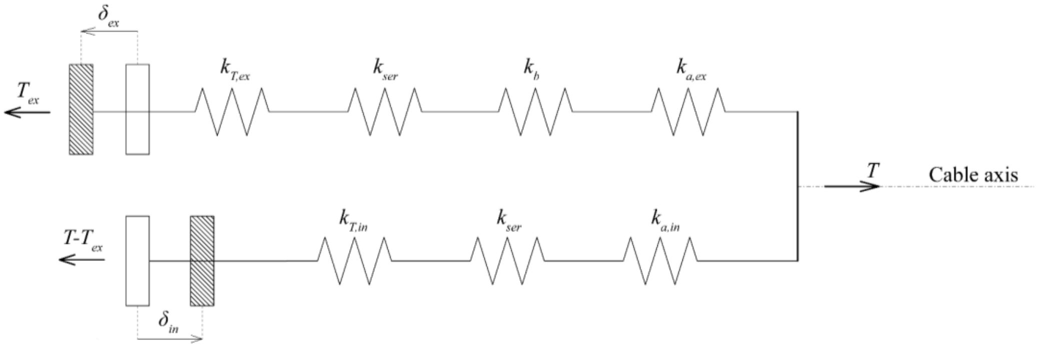

Figure III.2-8 – Mechanical model of axial springs only to determine the distribution of tensile force T in the portion of cable among the internal shear keys.

Therefore, the stiffness contributions that affect the distribution of the tensile force in the mid-section among the external and internal shear keys are:

- k_{ser}, notch stiffness;
- $k_{a,ex} = \frac{E_T \cdot B \cdot H}{\frac{L}{2} - l_{ex}}$, axial stiffness of the portion of timber beam comprised between the external shear keys;
- $k_{a,in} = \frac{E_T \cdot B \cdot H}{\frac{L}{2} - l_{in}}$, axial stiffness of the portion of timber beam comprised between the internal shear keys;
- $k_b = \frac{E_b \cdot A_b}{l_{in} - l_{ex}}$, axial stiffness of the portion of cable comprised between the external and the internal shear keys, where E_b is the modulus of elasticity of the cable and A_b is the cross-sectional area of the cable;
- $k_{T,ex}$ and $k_{T,in}$, axial stiffnesses contribution at the cable level due to the elastic rotational stiffnesses of timber beam in the section of the shear key $k_{rot,ex}$ and $k_{rot,in}$ (see Equations (*III.2-17*) and (*III.2-18*)).

It is therefore possible to derive[2] the total axial stiffnesses k_{ex} and k_{in} of the two shear keys (Figure III.2-7.a):

$$k_{ex} = \frac{k_{T,ex} \cdot k_{ser} \cdot k_b \cdot k_{a,ex}}{k_{T,ex} \cdot k_{ser} \cdot k_b + k_{T,ex} \cdot k_{a,ex} \cdot k_b + k_{T,ex} \cdot k_{ser} \cdot k_{a,ex} + k_{a,ex} \cdot k_{ser} \cdot k_b} \qquad (III.2\text{-}9)$$

$$k_{in} = \frac{k_{ser} \cdot k_{T,in} \cdot k_{a,in}}{k_{ser} \cdot k_{T,in} + k_{T,in} \cdot k_{a,in} + k_{ser} \cdot k_{a,in}} \qquad (III.2\text{-}10)$$

In add to the stiffnesses k_{ex} and k_{in} of each shear key, their horizontal displacements δ_{ex} and δ_{in}, due respectively to the elastic rotations $\varphi_{el}(l_{ex})$ and $\varphi_{el}(l_{in})$ (see Equations (*III.2-25*) and (*III.2-26*)), affect the distribution of T among the connections. In order to evaluate this effect, the mechanical models represented in Figure III.2-9.a and b are considered. This model is derived from the one shown in Figure III.2-7.a once one of the two moving support is fixed[3]. Given T_{ex}^* and T_{in}^* the forces acting on the springs of the mechanical models of Figure III.2-9 when the movable support has a null displacement ($\delta_{ex} = 0$ and $\delta_{in} = 0$), it is possible to obtain[4] the variation of the force T^*_{ex} due to displacements δ_{ex} and δ_{in}, respectively $\Delta T_{ex,\delta_{ex}}$ and $\Delta T_{ex,\delta_{in}}$:

---

[2] Since they are springs in series, it is possible to write for the external shear key: $\frac{1}{k_{ex}} = \frac{1}{k_{T,ex}} + \frac{1}{k_{ser}} + \frac{1}{k_b} + \frac{1}{k_{a,ex}}$. Similarly, the calculation can be carried out for the internal shear key.

[3] This mechanical model neglects the mutual effect of the displacements at supports. The variation of forces acting on the springs of the mechanical model in Figure III.2-9 due to displacement of the movable support may cause an elastic displacement of the other support, that in this mechanical model is considered rigid but in the real case is elastic. Anyway, this assumption does not affect the accuracy of results, since this effect can be considered negligible, as proved by the good agreement of results with the numerical model (Section III.2.4.1.2).

$$\Delta T_{ex,\delta_{ex}} = -\delta_{ex} \cdot \frac{k_{ex} \cdot k_{in}}{k_{ex} + k_{in}} \qquad (III.2\text{-}11)$$

$$\Delta T_{ex,\delta_{in}} = \delta_{in} \cdot \frac{k_{ex} \cdot k_{in}}{k_{ex} + k_{in}} \qquad (III.2\text{-}12)$$

Hence, the variation of the shear force on the external shear key ΔT_{ex} due to the horizontal displacements of both the shear keys δ_{ex} and δ_{in} (Equations (*III.2-25*) and (*III.2-26*)) is:

$$\Delta T_{ex} = \Delta T_{ex,\delta_{ex}} + \Delta T_{ex,\delta_{in}} = (\delta_{ex} - \delta_{in}) \cdot \frac{k_{ex} \cdot k_{in}}{k_{ex} + k_{in}} \qquad (III.2\text{-}13)$$

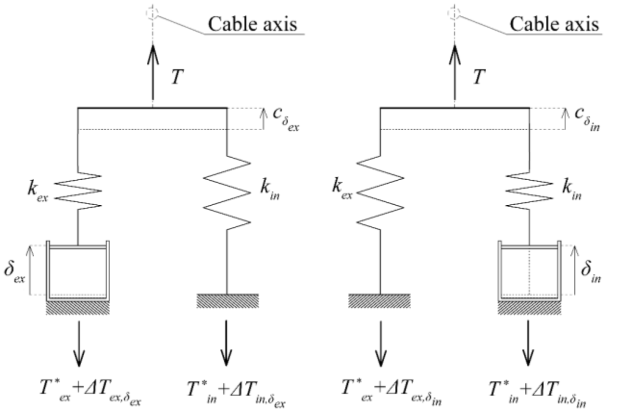
Cable axis
T
$c_{\delta_{ex}}$
k_{ex}
k_{in}
δ_{ex}
$T^*_{ex}+\Delta T_{ex,\delta_{ex}}$
$T^*_{in}+\Delta T_{in,\delta_{ex}}$
Cable axis
T
$c_{\delta_{in}}$
k_{ex}
k_{in}
δ_{in}
$T^*_{ex}+\Delta T_{ex,\delta_{in}}$
$T^*_{in}+\Delta T_{in,\delta_{in}}$

(*a*) (*b*)

Figure III.2-9 – Mechanical model to derive the variation of shear force in the external shear key due to elastic displacements (*a*) δ_{ex} and (*b*) δ_{in}.

It is therefore finally possible to derive the shear force acting on the external shear keys:

$$T_{ex} = T \cdot \frac{k_{ex}}{k_{ex} + k_{in}} + \Delta T_{ex} = [T + k_{in} \cdot (\delta_{in} - \delta_{ex})] \cdot \frac{k_{ex}}{k_{ex} + k_{in}} \qquad (III.2\text{-}14)$$

In order to define the elastic rotational stiffnesses $k_{rot,ex}$ and $k_{rot,in}$ of timber beam sections placed at $z = l_{ex}$ and $z = l_{in}$, it is firstly necessary to analyze the loads acting on the beam, represented in Figure III.2-10.a for one of the two symmetrically loaded parts. The eccentricity d of the forces T_{ex} and $T - T_{ex}$ transmitted by the cable to the timber joist through respectively the external and the internal shear keys determine two localized

---

[4] Given $c_{\delta_{ex}}$ and $c_{\delta_{in}}$ the displacements of the stiff bar of models in Figure III.2-9 due to the respectively the displacement δ_{ex} and δ_{in}, from linear constitutive laws it is possible to write:

$$\Delta T_{ex,\delta_{in}} = c_{\delta_{in}} \cdot k_{ex}$$
$$\Delta T_{in,\delta_{in}} = \left(c_{\delta_{in}} - \delta_{in}\right) \cdot k_{in}$$
$$\Delta T_{in,\delta_{ex}} = c_{\delta_{ex}} \cdot k_{in}$$
$$\Delta T_{ex,\delta_{ex}} = \left(c_{\delta_{ex}} - \delta_{ex}\right) \cdot k_{ex}$$

Then, for equilibrium:

$$\Delta T_{ex,\delta_{in}} = -\Delta T_{in,\delta_{in}}$$
$$\Delta T_{ex,\delta_{ex}} = -\Delta T_{in,\delta_{ex}}$$

It is therefore possible to derive the displacements $c_{\delta_{ex}}$ and $c_{\delta_{in}}$:

$$c_{\delta_{in}} = \delta_{in} \cdot \frac{k_{ex} \cdot k_{in}}{k_{ex} + k_{in}}$$
$$c_{\delta_{ex}} = \delta_{ex} \cdot \frac{k_{ex} \cdot k_{in}}{k_{ex} + k_{in}}$$

from which Equations (III.2-11) and (III.2-12) can be finally derived.

bending moments $m_{ex} = -T_{ex} \cdot d$ and $m_{in} = (T_{ex} - T) \cdot d$, respectively placed at $z = l_{ex}$ and $z = l_{in}$. In add, the eccentricity $d - d^*$ of the compressive force F_c acting at mid-span produces a bending moment on the timber beam equal to $m_{F_c} = F_c \cdot (d - d^*) = T \cdot (d - d^*)$, placed at $z = l_F$. These three localized bending moments are balanced by a torque given by two forces F with lever arm l_F. It is therefore worth noting that this loading configuration is statically equivalent to the isostatic one represented in Figure III.2-10.b, obtained placing a support at position $z = l_F$ where the vertical load F is located.

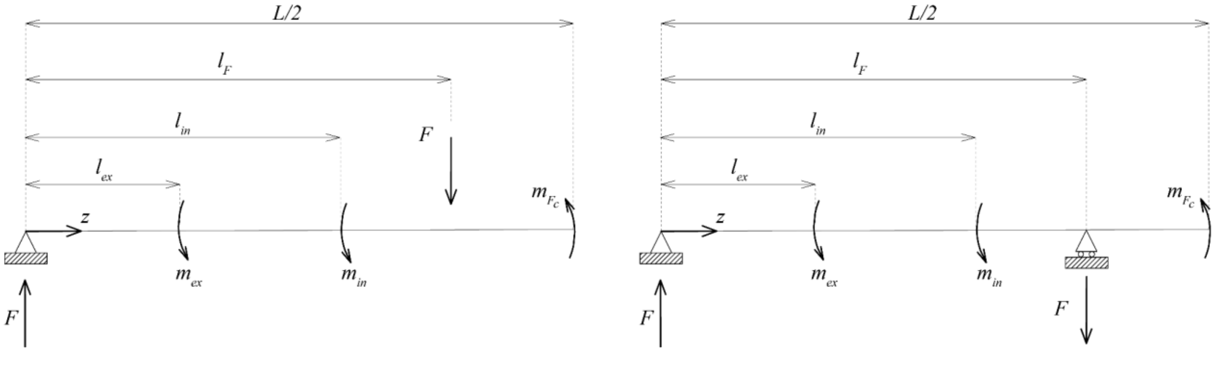

(*a*) (*b*)

Figure III.2-10 – (*a*) Forces acting on one of the two parts of the symmetrically loaded timber beam and (*b*) its statically equivalent isostatic system.

Considered therefore a localized bending moment m acting at a distance a from the left support (Figure III.2-11), and given I_T the modulus of inertia of the timber beam, it is possible to derive[5] the rotation of the section of the timber beam $\varphi_m(a)$ where a concentrated bending moment m is acting:

$$\varphi_m(a) = \frac{m}{E_T I_T} \cdot \left(\frac{l_F}{3} - a + \frac{a^2}{l_F} \right) \tag{III.2-15}$$

Therefore, imposing $a = l_{ex}$, it is possible to obtain the elastic rotation of the timber beam section placed where the external shear key is positioned due to a bending moment m acting on that section:

$$\varphi_m(l_{ex}) = \frac{m}{E_T I_T} \cdot \left(\frac{l_F}{3} - l_{ex} + \frac{{l_{ex}}^2}{l_F} \right) \tag{III.2-16}$$

Imposing therefore a unitary value for the rotation $\varphi_m(l_{ex})$, the rotational stiffness of the timber beam in the section of the external shear key connection $k_{rot,ex}$ can be derived:

$$k_{rot,ex} = \frac{3 E_T I_T l_F}{l_F^2 - 3 l_{ex} l_F + 3 l_{ex}^2} \tag{III.2-17}$$

Similarly, the rotational stiffness of the timber beam in the section of the internal shear key connection is equal to:

$$k_{rot,in} = \frac{3 E_T I_T l_F}{l_F^2 - 3 l_{in} l_F + 3 l_{in}^2} \tag{III.2-18}$$

---

[5] The elastic rotation $\varphi_m(z)$ of a section of the timber beam placed at a generic coordinate z due to the bending moment m acting at a coordinate a is equal to:

$$\varphi_m(z) = \frac{m}{2 E_T I_T l_F} \cdot z^2 + \frac{m}{E_T I_T} \cdot (a - z) + \frac{m}{6 E_T I_T l_F} \cdot (2 l_F^2 - 6 a l_F + 3 a^2)$$

from which Equation (III.2-15) can be derived by simply imposing $z = a$.

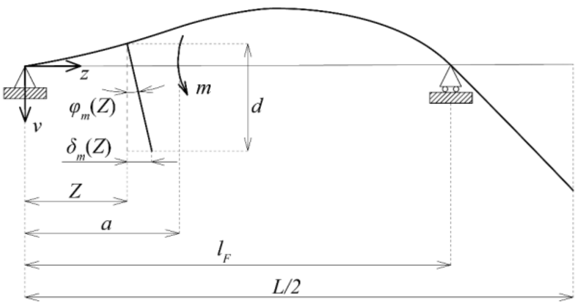

Figure III.2-11 – Elastic deformation of the timber beam due to a concentrated bending moment m at distance a from the left support.

The displacements at the cable level δ_{ex} and δ_{in} (Figure III.2-12) are due to the elastic rotations of the timber beam where respectively the external and internal shear keys are placed, φ_{ex} and φ_{in}. These rotations can be derived as the sum of two different force contributions that elastically bend the timber beam: (i) the compressive force F_c acting in the mid-section and (ii) the forces acting on the shear keys, T_{ex} and $T_{ex}-T$ respectively for the external and internal one. It is actually possible to write the following two equations:

$$\varphi_{ex}=\varphi_{m_{in}}(l_{ex})+\varphi_{F_c}(l_{ex}) \qquad (III.2\text{-}19)$$

$$\varphi_{in}=\varphi_{m_{ex}}(l_{in})+\varphi_{F_c}(l_{in}) \qquad (III.2\text{-}20)$$

where $\varphi_{m_{in}}(l_{ex})$ is the rotation of the external shear key caused by the bending moment m_{in}, $\varphi_{m_{ex}}(l_{in})$ is the rotation of the internal shear key caused by the bending moment m_{ex}, while $\varphi_{F_c}(l_{ex})$ and $\varphi_{F_c}(l_{in})$ are the rotations of respectively the external and the internal shear keys due to the eccentric force F_c acting on the mid-section.

The compressive force F_c actually has an eccentricity $d-d^*$ to the neutral axis (Figure III.2-5 and Figure III.2-6), causing therefore a bending moment $m_{F_c}=F_c\cdot(d-d^*)=T\cdot(d-d^*)$ whose deflection can be calculated using the model in Figure III.2-12, that, for the reasons previously exposed assumes the right support being placed where the concentrated vertical load F is positioned in the composite timber-steel structure (Figure III.2-3).

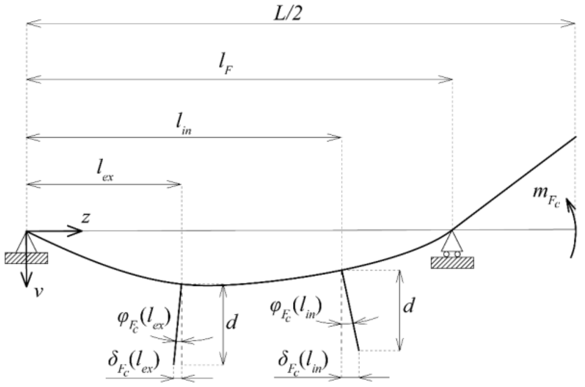

Figure III.2-12 – Elastic deformation of the timber beam due to eccentric force F_c.

Therefore, the horizontal displacements $\delta_{F_c}(l_{ex})$ and $\delta_{F_c}(l_{in})$ at the cable level due to F_c, respectively at the external and internal shear keys, are equal to:

$$\delta_{F_c}(l_{ex})=\frac{T\cdot(d-d^*)}{2E_TI_T}\left(\frac{l_F}{3}-\frac{l_{ex}^2}{l_F}\right) \qquad (III.2\text{-}21)$$

$$\delta_{F_c}(l_{in})=\frac{T\cdot(d-d^*)}{2E_TI_T}\left(\frac{l_F}{3}-\frac{l_{in}^2}{l_F}\right) \qquad (III.2\text{-}22)$$

where d^* is the lever arm between the compressive and tensional forces in the mid-section.

In addition to the contribution of F_c, it must also be considered that the forces acting on the shear keys have an eccentricity d respect to the axis of the timber joist (Figure III.2-3) that determines bending moments $m_{ex} = -T_{ex} \cdot d$ and $m_{in} = (T_{ex} - T) \cdot d$, respectively for the external and internal shear keys. These concentrated bending moments determine horizontal displacements $\delta_{m_{in}}(l_{ex})$ and $\delta_{m_{ex}}(l_{in})$, respectively on the external and internal shear keys (see Figure III.2-11), whose values are[6]:

$$\delta_{m_{in}}(l_{ex}) = \frac{(T - T_{ex}) \cdot d^2}{E_T \cdot I_T}\left(\frac{l_{in}^2}{2 \cdot l_F} + \frac{l_{ex}^2}{2 \cdot l_F} + \frac{l_F}{3} - l_{in}\right) \qquad (III.2\text{-}23)$$

$$\delta_{m_{ex}}(l_{in}) = \frac{T_{ex} \cdot d^2}{E_T \cdot I_T}\left(\frac{l_{in}^2}{2 \cdot l_F} + \frac{l_{ex}^2}{2 \cdot l_F} + \frac{l_F}{3} - l_{in}\right) \qquad (III.2\text{-}24)$$

where d is the distance between the cable axis and the timber beam axis (Figure III.2-3).

Therefore, the total horizontal displacements δ_{ex} and δ_{in} on the shear key connections can be simply calculated as the sum of the two contributions:

$$\delta_{ex} = \delta_{F_c}(l_{ex}) + \delta_{m_{in}}(l_{ex}) \qquad (III.2\text{-}25)$$

$$\delta_{in} = \delta_{F_c}(l_{in}) + \delta_{m_{ex}}(l_{in}) \qquad (III.2\text{-}26)$$

III.2.3.2.3 Bending moment on timber beam

Since the analytical model is developed within the hypothesis of linearity, the bending moment acting on the timber beam can be calculated as the sum of three contributions (Figure III.2-10):

- bending moment caused by the vertical concentrated loads F;
- bending moment transferred by external shear keys m_{ex};
- bending moment transferred by internal shear keys m_{in}.

From the resulting bending moment diagram of the timber component (Figure III.2-13) it can be noticed that the presence of the forces transmitted by the cable to the timber joist through the shear keys contribute to reduce the bending moment acting on timber respect to the case of a simple timber beam, highlighting that anyway this beneficial effect is only partial since there is an increment of axial compressive force acting on it. It is worth noting that in the mid-section there is not a null value of the bending moment, contrary to what it can be expected at a first glance for the presence of material discontinuity, and it is equal to:

$$M_{T,E} = F \cdot l_F + m_{ex} + m_{in} = F \cdot l_F \frac{d^* - d}{d^*} = T(d^* - d) \qquad (III.2\text{-}27)$$

This bending moment is actually due to the eccentricity $(d^* - d)$ of the compressive force $F_c = T$ in the mid-section.

---

[6] Actually, m_{in} causes a rotation on the external shear key $\varphi_{m_{in}}(l_{ex})$ and, vice-versa, m_{ex} causes a rotation $\varphi_{m_{ex}}(l_{in})$ on the internal shear key, whose values are:

$$\varphi_{m_{in}}(l_{ex}) = \frac{(T - T_{ex}) \cdot d}{E_T \cdot I_T}\left(\frac{l_{in}^2}{2 \cdot l_F} + \frac{l_{ex}^2}{2 \cdot l_F} + \frac{l_F}{3} - l_{in}\right)$$

$$\varphi_{m_{ex}}(l_{in}) = \frac{T_{ex} \cdot d}{E_T \cdot I_T}\left(\frac{l_{in}^2}{2 \cdot l_F} + \frac{l_{ex}^2}{2 \cdot l_F} + \frac{l_F}{3} - l_{in}\right)$$

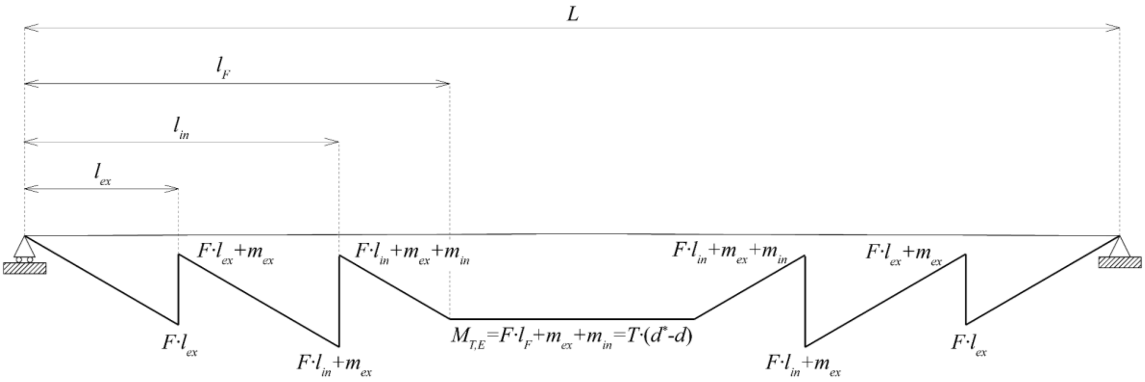
L
l_F
l_{in}
l_{ex}
$F \cdot l_{ex} + m_{ex}$
$F \cdot l_{in} + m_{ex} + m_{in}$
$F \cdot l_{in} + m_{ex} + m_{in}$
$F \cdot l_{ex} + m_{ex}$
$F \cdot l_{ex}$
$F \cdot l_{in} + m_{ex}$
$M_{T,E} = F \cdot l_F + m_{ex} + m_{in} = T \cdot (d^* - d)$
$F \cdot l_{in} + m_{ex}$
$F \cdot l_{ex}$

Figure III.2-13 – Bending moment on the timber component of the timber-steel hybrid beam.

III.2.3.3 Composite beam short-term deflections

The total beam deflection v is given by the sum of two contributions: a rigid displacement v_{rig}, due to the elongation of the cable between the internal shear keys (Section III.2.3.3.1), and the elastic deformation of the timber element v_{el}:

$$v = v_{rig} + v_{el} \tag{III.2-28}$$

Similarly, the rotation of a generic section φ is the sum of a rigid φ_{rig} and an elastic φ_{el} contribution:

$$\varphi = \varphi_{rig} + \varphi_{el} \tag{III.2-29}$$

In the following, the formulations to derive the addends of Equations (III.2-28) and (III.2-29) will be shown.

III.2.3.3.1 Rigid contribution

The rigid contribution to the vertical deflection of the beam is due to the elongation of the tensioned steel cable comprised between the two internal shear-keys. The elongation of this part of the cable determines a gap opening in the timber mid-section interface where two timber joists are placed side by side. Since the two segments of the cable placed among external and internal shear keys do not contribute in activating the rigid mechanism represented in Figure III.2-14, the contribution of the shear forces acting on the external shear keys and the tensile force acting on the external portions of the cable are disregarded in the current Section.

The rigid displacement in the mid-section of the beam $v_{rig,max} = v_{rig}\left(\frac{L}{2}\right) = \varphi_{rig} \cdot \frac{L}{2}$ is due to the rigid rotation φ_{rig} of the two pieces of the beam, that is equal to[7]:

$$\varphi_{rig} = \frac{\Delta l_b}{d^*} + \varphi_{el}\left(\frac{L}{2}\right) \cdot \left(1 - \frac{d}{d^*}\right) + \varphi_{el}(l_{in}) \cdot \frac{d}{d^*} + \frac{\Delta l_T}{d^*} + \frac{\Delta l_{notch}}{d^*} \tag{III.2-30}$$

---

[7] From the imposition of the displacements compatibility it is possible to write (Figure III.2-15):

$$\Delta l_b = \Delta l_{mid} + \Delta l_{sk} - \Delta l_T - \Delta l_{notch}$$

Therefore, since (Figure III.2-14):

- $\Delta l_{mid} = \varphi\left(\frac{L}{2}\right) \cdot (d^* - d)$
- $\varphi\left(\frac{L}{2}\right) = \varphi_{rig} - \varphi_{el}\left(\frac{L}{2}\right)$
- $\Delta l_{sk} = \varphi_{sk} \cdot d$
- $\varphi(l_{in}) = \varphi_{rig} - \varphi_{el}(l_{in})$

it is possible to write the following equation:

$$\Delta l_b = \left(\varphi_{rig} - \varphi_{el}\left(\frac{L}{2}\right)\right) \cdot (d^* - d) + \left(\varphi_{rig} - \varphi_{el}(l_{in})\right) \cdot d - \Delta l_T - \Delta l_{notch}$$

from which it is possible to derive the equation of φ_{rig}.

where (Figure III.2-14):

- $\Delta l_b = \frac{T}{k_b} = \frac{T}{\frac{\phi_b^2}{4}\pi E_b} \cdot \left(\frac{L}{2} - l_{in}\right)$ is the elongation of half of the part of the steel cable comprised between the two internal shear keys - with an axial stiffness k_b - due to the tensile force T;
- $\varphi_{el}\left(\frac{L}{2}\right) = \varphi_{F_c}\left(\frac{L}{2}\right) + \varphi_{m_{in}}\left(\frac{L}{2}\right) + \varphi_{m_{ex}}\left(\frac{L}{2}\right)$ is the elastic rotation in the mid-section of the timber beam, which is the sum of the following three contributions:
    - $\varphi_{F_c}\left(\frac{L}{2}\right) = \frac{T(d-d^*)}{E_T \cdot I_T} \cdot \left(\frac{2}{3} l_F - \frac{L}{2}\right)$, elastic rotation in the mid-section due to the eccentric compressive force F_c;
    - $\varphi_{m_{in}}\left(\frac{L}{2}\right) = \frac{(T_{ex}-T)\cdot d}{E_T \cdot I_T} \cdot \left(\frac{1}{6} l_F - \frac{l_{in}^2}{2l_F}\right)$, elastic rotation in the mid-section due to the bending moment acting on the internal sher key m_{in};
    - $\varphi_{m_{ex}}\left(\frac{L}{2}\right) = \frac{T_{ex}\cdot d}{E_T \cdot I_T} \cdot \left(\frac{l_{ex}^2}{2l_F} - \frac{1}{6} l_F\right)$, elastic rotation in the mid-section due to the bending moment acting on the external shear key m_{ex}.
- $\varphi_{el}(l_{in}) = \varphi_{F_c}(l_{in}) + \varphi_{m_{in}}(l_{in}) + \varphi_{m_{ex}}(l_{in})$ is the elastic rotation of the section of the timber beam placed where the internal shear key is positioned (in the following labelled as "shear key beam cross-section" for sake of simplicity), and it is the sum of the following three contributions:
    - $\varphi_{F_c}(l_{in}) = \frac{T(d-d^*)}{2\cdot E_T \cdot I_T} \cdot \left(\frac{l_F}{3} - \frac{l_{in}^2}{l_F}\right)$, elastic rotation of the internal shear key beam cross-section due to the eccentric compressive force F_c;
    - $\varphi_{m_{in}}(l_{in}) = \frac{(T_{ex}-T)\cdot d}{E_T \cdot I_T} \cdot (l_{in} - \frac{l_F}{3} - \frac{l_{in}^2}{l_F})$, elastic rotation of the internal shear key beam cross-section due to the bending moment m_{in};
    - $\varphi_{m_{ex}}(l_{in}) = \frac{T_{ex}\cdot d}{E_T \cdot I_T} \cdot (\frac{l_{in}^2}{2l_F} - l_{in} + \frac{l_{ex}^2}{2l_F} + \frac{l_F}{3})$, elastic rotation of the internal shear key beam cross-section due to the bending moment m_{ex}.
- $\Delta l_T = \frac{T}{k_T} = \frac{T}{E_T \cdot B \cdot H} \cdot \left(\frac{L}{2} - l_{in}\right)$ is the elastic shortening of half of the timber beam comprised between the internal shear keys - characterized by an axial stiffness k_T - due to the compression force $F_c = T$;
- $\Delta l_{notch} = \frac{(T-T_{ex})}{k_{ser}}$ is the horizontal displacement due to compression of timber of the internal notch.

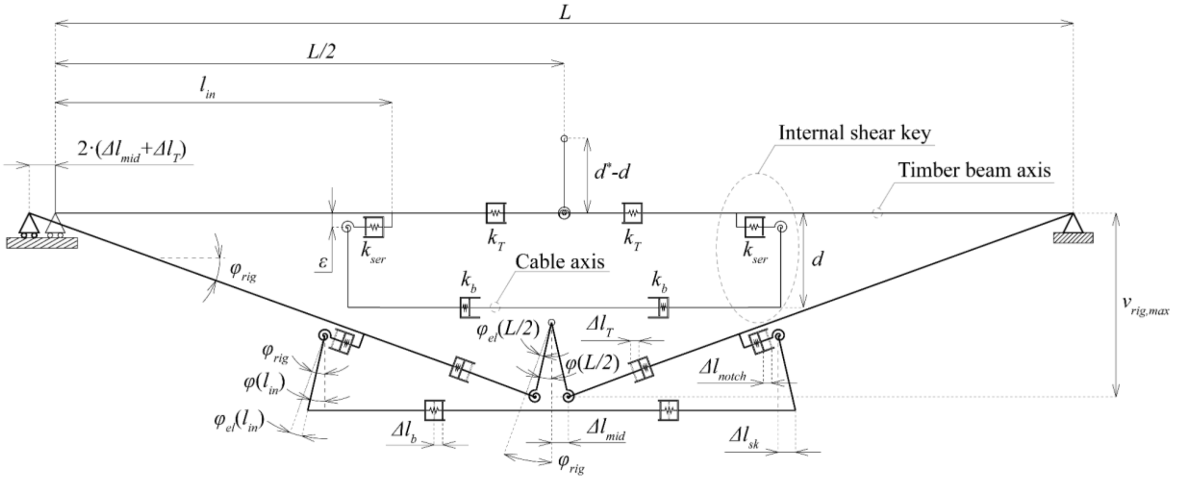

Figure III.2-14 – Mechanical model for the definition of the rigid contribution of deflections (ε is an arbitrarily small little distance).

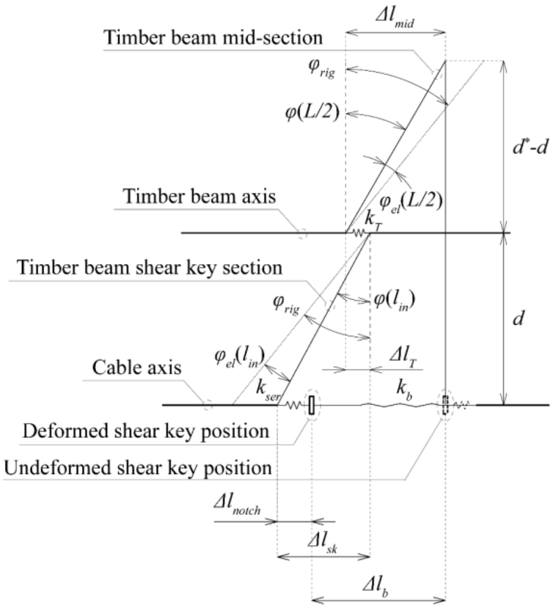
Δl_{mid}
Timber beam mid-section
φ_{rig}
$\varphi(L/2)$
d^*-d
Timber beam axis
$\varphi_{el}(L/2)$
k_T
Timber beam shear key section
φ_{rig}
$\varphi(l_{in})$
d
Cable axis
$\varphi_{el}(l_{in})$
Δl_T
k_{ser}
k_b
Deformed shear key position
Undeformed shear key position
Δl_{notch}
Δl_{sk}
Δl_b

Figure III.2-15 – Schematic representation of the displacement contributions to the rigid rotation of the beam derived from the mechanical model represented in Figure III.2-14.

III.2.3.3.2 Elastic contribution

The elastic displacement contribution v_{el} is due to the elastic deformations in the timber beam due both to bending moments and shear forces acting along its length, and it is the sum of four sub-contributions:

- bending deformation v_{F_c} due to the eccentricity of the compressive force F_c in the mid-section;
- bending deformation $v_{m_{ex}}$ due to the localized bending moment m_{ex} acting on the external shear key connection;
- bending deformation $v_{m_{in}}$ due to the localized bending moment m_{in} acting on the internal shear key;
- shear deformation v_{sh} due to shear force V acting on timber beam.

It is worth noting that the shear deformability contribution v_{sh} has been considered since it can be considerable also for quite stocky beams because of a low shear modulus G of wooden materials.

Therefore, it is possible to write the following equation:

$$v_{el} = v_{F_c} + v_{m_{ex}} + v_{m_{in}} + v_{sh} \qquad (III.2\text{-}31)$$

In the following the formulations of the three sub-contributions will be shown only for the left part of the composite beam, being easy to derive them for the right part for symmetry.

The equation of v_{F_c} for a generic cross-section at position z is:

$$v_{F_c}(z) = \begin{cases} \dfrac{T(d^* - d)z}{6 \cdot E_T \cdot I_T}\left(-\dfrac{z^2}{l_F} + l_F\right), & if\ z \in [0, l_F] \\ \dfrac{T(d^* - d)}{E_T \cdot I_T}\left(-\dfrac{z^2}{2} + \dfrac{2}{3} l_F z - \dfrac{{l_F}^2}{6}\right), & if\ z \in \left(l_F, \dfrac{L}{2}\right] \end{cases} \qquad (III.2\text{-}32)$$

The equation of $v_{m_{ex}}$ is:

$$v_{m_{ex}}(z) = \begin{cases} \dfrac{m_{ex}}{E_T \cdot I_T}\left[-\dfrac{z^3}{6l_F} + \left(l_{ex} - \dfrac{l_F}{3} - \dfrac{{l_{ex}}^2}{2l_F}\right) \cdot z\right], & if\ z \in [0, l_{ex}] \\ \dfrac{m_{ex}}{E_T \cdot I_T}\left[-\dfrac{z^3}{6l_F} + \dfrac{z^2}{2} - \left(\dfrac{l_F}{3} + \dfrac{{l_{ex}}^2}{2l_F}\right) \cdot z + \dfrac{{l_{ex}}^2}{2}\right], & if\ z \in (l_{ex}, l_F] \\ \dfrac{m_{ex}}{E_T \cdot I_T}\left(\dfrac{l_F}{6} - \dfrac{{l_{ex}}^2}{2l_F}\right)(z - l_F), & if\ z \in (l_F, \dfrac{L}{2}] \end{cases} \qquad (III.2\text{-}33)$$

Similarly, for $v_{m_{in}}$ it is possible to write:

$$v_{m_{in}}(z)=\begin{cases}\dfrac{m_{in}}{E_T\cdot I_T}\left[-\dfrac{z^3}{6l_F}+\left(l_{in}-\dfrac{l_F}{3}-\dfrac{{l_{in}}^2}{2l_F}\right)\cdot z\right], & if\ z\in[0,l_{in}]\\ \dfrac{m_{in}}{E_T\cdot I_T}\left[-\dfrac{z^3}{6l_F}+\dfrac{z^2}{2}-\left(\dfrac{l_F}{3}+\dfrac{{l_{in}}^2}{2l_F}\right)\cdot z+\dfrac{{l_{in}}^2}{2}\right], & if\ z\in(l_{in},l_F]\\ \dfrac{m_{in}}{E_T\cdot I_T}\left(\dfrac{l_F}{6}-\dfrac{{l_{in}}^2}{2l_F}\right)(z-l_F), & if\ z\in(l_F,\dfrac{L}{2}]\end{cases}\qquad (III.2\text{-}34)$$

Finally, the contribution v_{sh} is equal to:

$$v_{sh}(z)=\begin{cases}\dfrac{F\cdot z}{\frac{5}{6}\cdot B\cdot H\cdot G}, & if\ z\in[0;l_F]\\ \dfrac{F\cdot l_F}{\frac{5}{6}\cdot B\cdot H\cdot G}, & if\ z\in\left(l_F;\dfrac{L}{2}\right]\end{cases}\qquad (III.2\text{-}35)$$

Likewise, the elastic rotation of a generic cross-section φ_{el} is the sum of three sub-contributions:

- elastic rotation φ_{F_c} due to the eccentricity of the compressive force F_c in the mid-section;
- elastic rotation $\varphi_{m_{ex}}$ due to the localized bending moment m_{ex} acting on the external shear key;
- elastic rotation $\varphi_{m_{in}}$ due to the localized bending moment m_{in} acting on the internal shear key.

Therefore, it is possible to write the following equation:

$$\varphi_{el}=\varphi_{F_c}+\varphi_{m_{ex}}+\varphi_{m_{in}}\qquad (III.2\text{-}36)$$

The formulation of φ_{F_c} for a generic cross-section at position z is:

$$\varphi_{F_c}(z)=\begin{cases}\dfrac{T(d^*-d)}{2\cdot E_T\cdot I_T}(-\dfrac{z^2}{l_F}+\dfrac{l_F}{3}), & if\ z\in[0,l_F]\\ \dfrac{T(d^*-d)}{E_T\cdot I_T}(-z+\dfrac{2}{3}l_F), & if\ z\in(l_F,\dfrac{L}{2}]\end{cases}\qquad (III.2\text{-}37)$$

The equation of $\varphi_{m_{ex}}$ is:

$$\varphi_{m_{ex}}(z)=\begin{cases}\dfrac{m_{ex}}{E_T\cdot I_T}\left[-\dfrac{z^2}{2l_F}+l_{ex}-\dfrac{{l_{ex}}^2}{2l_F}-\dfrac{l_F}{3}\right], & if\ z\in[0,l_{ex}]\\ \dfrac{m_{ex}}{E_T\cdot I_T}\left[-\dfrac{z^2}{2l_F}+z-\dfrac{{l_{ex}}^2}{2l_F}-\dfrac{l_F}{3}\right], & if\ z\in(l_{ex},l_F]\\ \dfrac{m_{ex}}{E_T\cdot I_T}\left(\dfrac{l_F}{6}-\dfrac{{l_{ex}}^2}{2l_F}\right), & if\ z\in(l_F,\dfrac{L}{2}]\end{cases}\qquad (III.2\text{-}38)$$

Similarly, the equation of $\varphi_{m_{in}}$ is:

$$\varphi_{m_{in}}(z)=\begin{cases}\dfrac{m_{in}}{E_T\cdot I_T}\left[-\dfrac{z^2}{2l_F}+l_{in}-\dfrac{{l_{in}}^2}{2l_F}-\dfrac{l_F}{3}\right], & if\ z\in[0,l_{in}]\\ \dfrac{m_{in}}{E_T\cdot I_T}\left[-\dfrac{z^2}{2l_F}+z-\dfrac{{l_{in}}^2}{2l_F}-\dfrac{l_F}{3}\right], & if\ z\in(l_{in},l_F]\\ \dfrac{m_{in}}{E_T\cdot I_T}\left(\dfrac{l_F}{6}-\dfrac{{l_{in}}^2}{2l_F}\right), & if\ z\in(l_F,\dfrac{L}{2}]\end{cases}\qquad (III.2\text{-}39)$$

III.2.4 Results and comparison with numerical analyses

In order to evaluate the accuracy of outcomes of the proposed analytical model a comparison with the results of a numerical model will be carried out in the following.

III.2.4.1.1 Numerical model description

A comparison between the results obtained with the analytical model and the outcomes of FEM models is shown in the following for the configuration tested in [83].

The uniaxial finite element model strategy has been adapted to the specific case from the one presented by Fragiacomo *et al.* in [75], considering therefore two parallel linear finite elements connected by vertical rigid elements and horizontal springs where the shear keys are placed (Figure III.2-16 and Figure III.2-17).

The FEM analysis are carried out with Strand7 software [88], within the following hypotheses:

- timber beam (blue horizontal elements of Figure III.2-16) is modelled with “beam” elements (6 degrees of freedom DOFs, 3 translational and 3 rotational);
- steel cable (light green horizontal elements of Figure III.2-16) modelled with “truss” elements (3 translational DOFs);
- timber beam elements (blue ones of Figure III.2-16) is positioned along the barycentric axis of the timber beam;
- steel cable elements (light green ones of Figure III.2-16) is positioned along the axis of the cable;
- shear keys (lower vertical red elements of Figure III.2-16) are modelled with “beam” elements;
- shear keys are considered rigid, and this behavior is modelled through penalty method, vis. assigning a very high bending stiffness, through a big value of the area of the beam and a high modulus of elasticity;
- notch stiffness is modelled through end-releases with stiffness k_{ser} at the top of the shear key beams (see dark green attribute in Figure III.2-17.a);
- mid-hinge positioned with an offset $d^* - d$ (Figure III.2-3) respect to the beam axis (Figure III.2-16);
- mid-hinge modelled with a rotational end release on a little piece of horizontal beam placed at the position of the mid-hinge (Figure III.2-17.b);
- rigid offset connection between the mid-hinge and the beam axis modelled through two rigid vertical beams with the same properties as the shear key elements (upper red vertical elements close to Detail B in Figure III.2-16);
- one support is modelled as hinge, the other one is modelled as slider;
- plane model assumption (“2D beam” Freedom Case): 3 degrees of freedom (DOFs) considered, two translations in the plane and one for rotation in the plane.

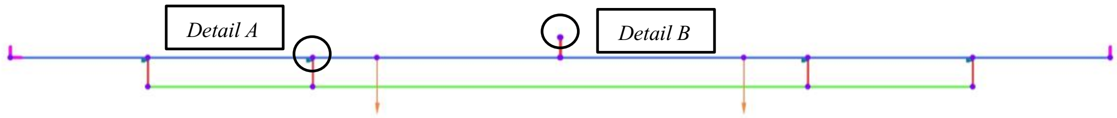

Figure III.2-16 – Global view of the FEM model.

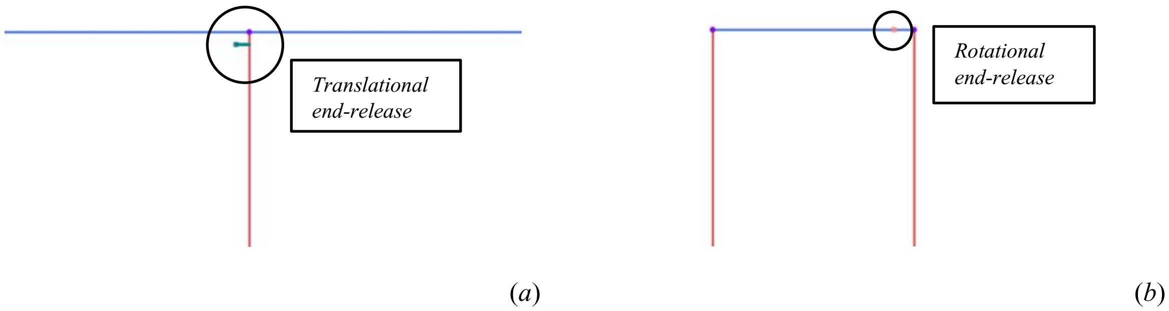

(*a*) (*b*)

Figure III.2-17 – Details of the FEM model: (a) detail A, translational end-release with stiffness k_{ser} to model the notch deformability, and (b) detail B, rotational end-release to model the mid-hinge.

The mean values of the mechanical properties are assigned, in order to allow a comparison with the experimental outcomes of the future tests that will be carried out on the composite structure. In order to determine the mean values, the probabilistic approach proposed in the JCSS Probabilistic Model Code [89] for prestressing steel [90] and timber [91] has been used. The cable used is a Dywidag $f_{y,k} = 830\ MPa\ /\ f_{p,k} = 1035\ MPa$ type having a mean yielding resistance of steel $f_{b,m} = 925.7\ MPa$ and a modulus of elasticity $E_b = 205\ GPa$.

For timber joist a strength class GL30 is assumed, characterized by a mean compressive resistance $f_{c,m} = 29.3\ MPa$, a modulus of elasticity $E_T = 13000\ MPa$ and a mean shear modulus $G = 650\ MPa$.

III.2.4.1.2 Comparison of results between analytical and numerical models

In the following the comparison of results obtained with analytical (Figure III.2-18) and numerical (Figure III.2-19) models for both deformations and forces will be shown. Since internal forces acting on the structures are symmetrical respect to the mid-section, for graphical reasons the numerical results are shown only for the left part of the structure.

The geometrical characteristic of the system configuration used for validation are the same used for the preliminary tests carried out in [83] and are summarized in Table III.2-2. A vertical concentrated force F = 10 kN is assumed.

From the comparison it is possible to observe that the results are in total accordance, therefore the analytical model gives reliable results comparable to the ones that can be obtained from simple FEM models.

From the analysis of the deflections reported in Figure III.2-18.c it is possible to notice that, as observed in the preliminary experimental campaign illustrated in [83] (Figure III.2-20), in the red area highlighted at mid-span there is contact between the steel cable and the intrados of the timber beam. This behavior of the composite member should be avoided, since it activates secondary resistant mechanisms difficult to predict and that rely on compressive strength on timber perpendicularly to the grain direction. It is finally possible to observe from the same figure a quite marked difference between the maximum deflection predicted by the analytical model and the one measured in the preliminary experimental campaign [83]. This discrepancy could be due to many reasons, like the fact that the value measured during the tests does not take into account for local deformations at supports both due to crushing perpendicular to grain and to possible deflections of the testing machine that is made of timber members [83]. In add it is possible that rigid movements due to clearances between timber notches and shear keys considerably contributed to the increment of the mid-span deflection respect to the analytical predictions. Further analyses on the discrepancy between analytical and experimental results will be carried out in future studies also carrying out new experimental tests.

III.2.4.1.3 Parameters affecting the structural performance of the system

From the analytical model it is possible to observe that, for given (*i*) mechanical characteristics (f_c, E_T and E_b), (*ii*) span L and (*iii*) vertical load F placed at position l_F, the geometrical characteristics that influence the behaviour of the system are:

- Φ_b: diameter of the cable;
- l_{ex}: longitudinal position of the external shear key connection;
- l_{in}: longitudinal position of the internal shear key connection;
- B: width of the timber beam cross-section;
- H: height of the timber beam cross-section;
- h_{sk}: height of the plinth of the shear key connection (Figure III.2-2.a);
- h_{notch}: height of the notch of the shear key connection.

Table III.2-2– Geometrical characteristic of the beam configuration numerically modelled (measurement unit: mm).

ϕ_b	l_{ex}	l_{in}	B	H	h_{sk}	h_{notch}	L
16	500	1100	90	180	30	40	4000

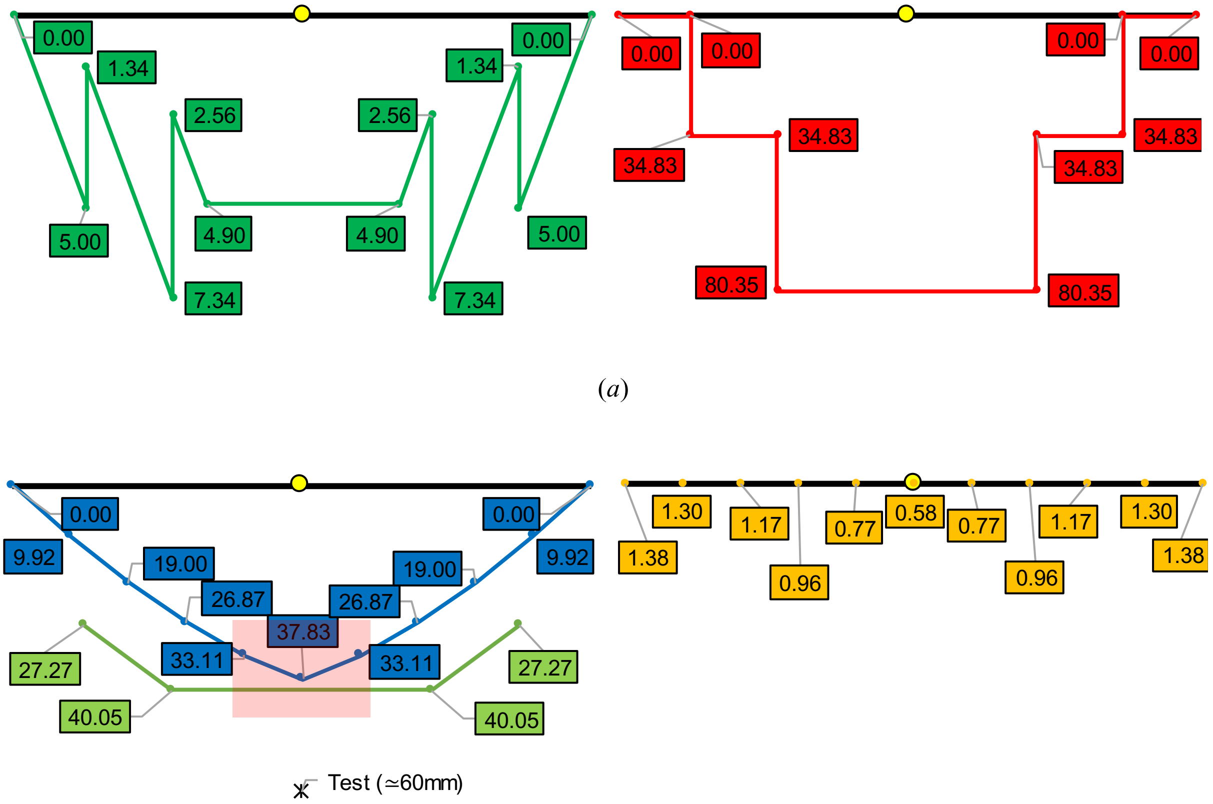

(*a*) (*b*)

(*c*) (*d*)

Figure III.2-18 – Results of analytical model: (*a*) bending moment on timber beam *M* (kNm), (*b*) axial force on timber beam *N* (kN), (*c*) vertical deflections *v* of the timber beam (blue line) and of the steel cable (green line) measured respect to the timber beam axis (mm) and (*d*) rotations *φ* (deg) of timber beam. The red patch in figure (*c*) highlights the area where there is contact between the steel cable and the intrados of the timber beam. The asterisk marker in figure (*c*) reports the tests value measured during the preliminary experimental campaign [83].

It is therefore possible to use the model to carry out parametric analyses in order to improve and optimize the performance of the system, both in term of SLS and ULS. It is finally worth noting that h_{notch} influences the performance of the system because the parameter k_{ser} is evaluated accordingly to the method presented by Dias *et al.* [87]. Under a general point of view, the parameter k_{ser} is a factor that could have a predominant role in influencing the performance of the composite timber-steel member, therefore, further investigations on its value may be necessary.

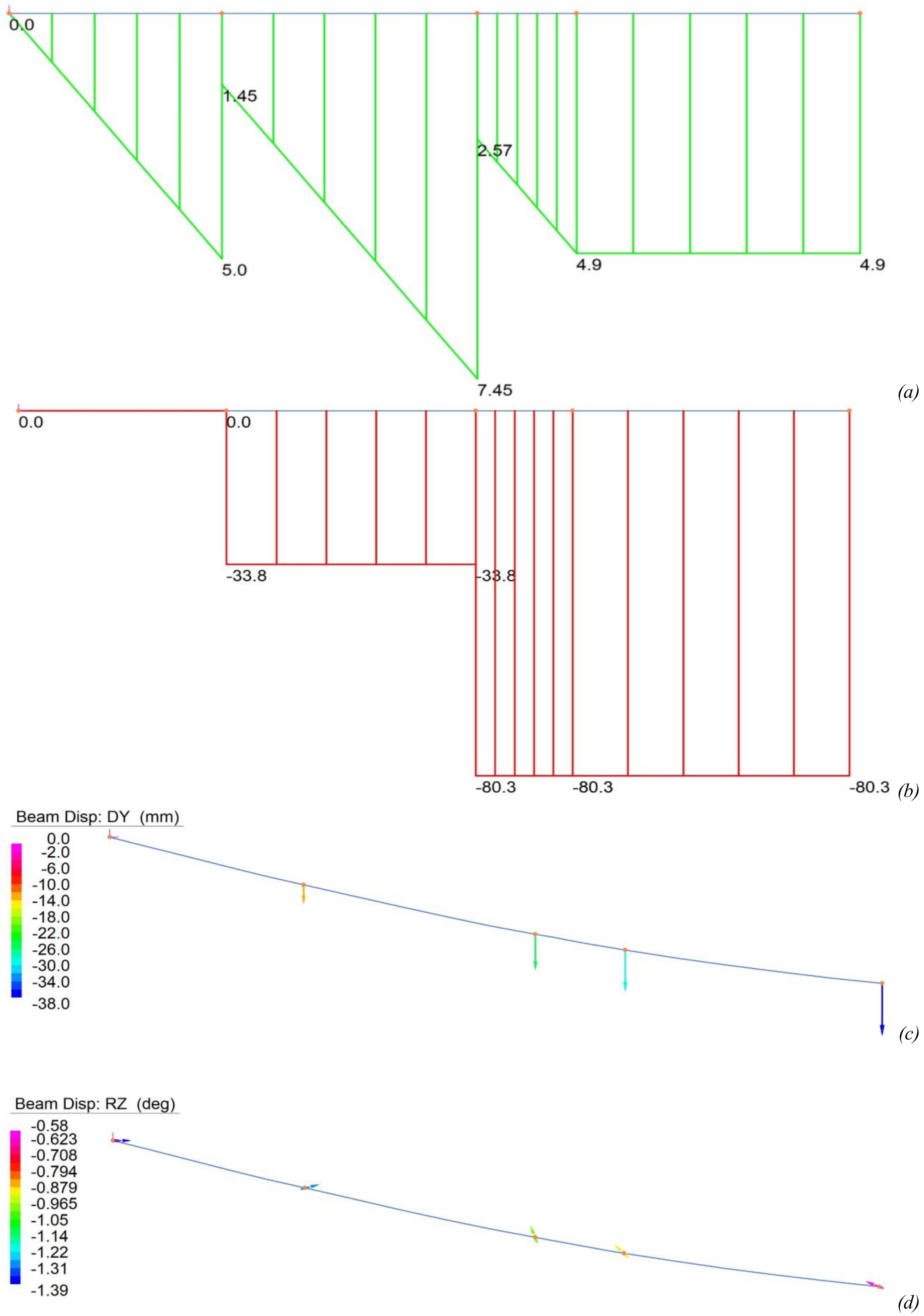

Figure III.2-19 – Results of numerical model: (*a*) bending moment on timber beam M (kNm), (*b*) axial force on timber beam N (kN), (*c*) vertical deflections v (mm) and (*d*) rotations φ (deg) of timber beam.

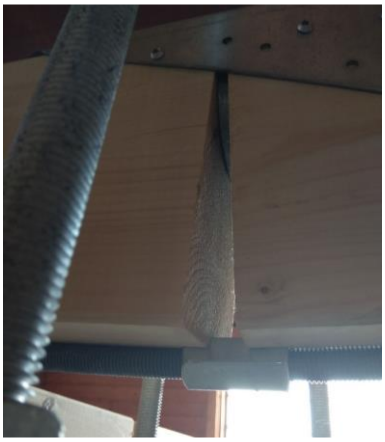

Figure III.2-20 – Contact between steel cable and timber beam during tests carried out in the preliminary experimental campaign presented in [83].

III.2.5 Parametric analysis for structural performance enhancement

From the results shown by Wang *et al.* [83] it is possible to observe that the main problem of this innovative structural system is represented by the high deflections measured during the experimental tests. Therefore, in order to analyze the effect of the mechanical and geometrical characteristic of the steel hardware (i.e. cable and shear keys) and of the timber beam on the SLS performances of a system given loads, a sensitivity analysis on the deflection measured at the mid-span of a reference beam configuration (Table III.2-3) to vary of parameters Φ_b, l_{ex}, l_{in} and h_{sk} has been carried out. An upper-bound limit is assigned to l_{in} in order to guarantee a distance equal or greater than $0.8 \cdot h_{notch}$ between the end of the notch and the mid-span section of the beam accordingly to EN 1995-1-1, NCI NA.12.1 (NA.4) [85], in order to achieve the maximum longitudinal shear strength and avoid brittle failures of timber. The results, shown in Figure III.2-21, are carried out imposing the absence of contact between the steel cable and the intrados of the timber beam (important condition not to alter the internal forces of the system with undesired second order effects), and assuming the following reference configuration of the beam:

Table III.2-3– Geometrical characteristic of the reference beam configuration of parametric analysis (measurement unit: mm).

ϕ_b	l_{ex}	l_{in}	B	H	h_{sk}	h_{notch}	L
26	500	1100	90	180	60	40	4000

A concentrated vertical load equal to F = 10 kN and mechanical parameters accordingly to Section III.2.4.1.1 are assumed. In add, SLS performances have been assumed satisfactory once the limit of $\frac{L}{180}$ (dashed lines of Figure III.2-21) is verified: the grey areas of Figure III.2-21 represent the unsatisfactory SLS performances.

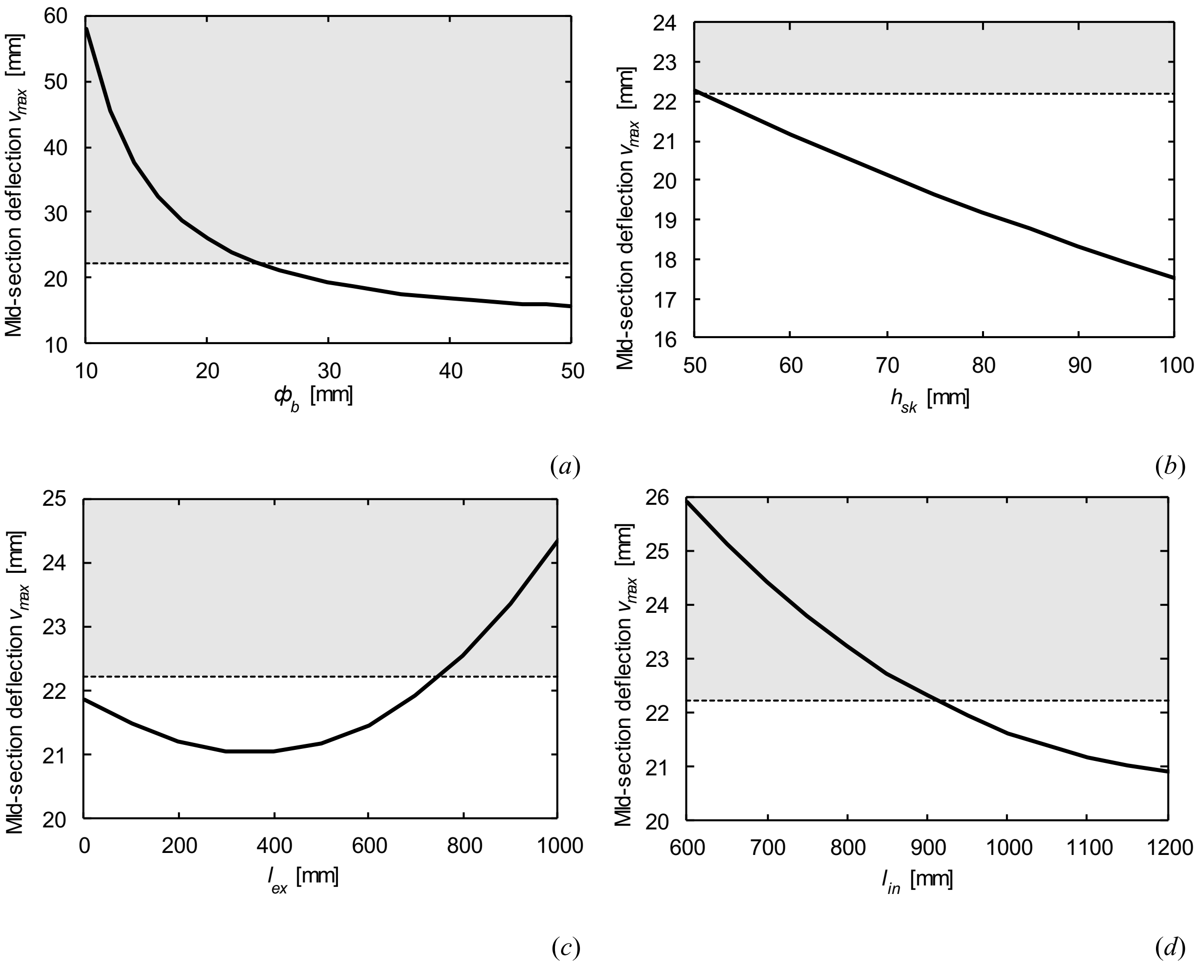

Figure III.2-21 – Parametric analysis on the SLS performance of the system to vary of steel hardware parameters: (*a*) diameter of the cable ϕ_b vs. mid-span deflection v_{max}, (*b*) height of the plinth of the shear key h_{sk} vs. mid-span deflection v_{max}, (*c*) position of the external shear key l_{ex} vs. mid-span deflection v_{max} and (*d*) position of the internal shear key l_{in} vs. mid-span deflection v_{max}.

It is firstly possible to observe that incrementing the value of all the parameters allows to improve the SLS performance of the system, except for the position of the external shear key l_{ex} (Figure III.2-21.c), for which exists an optimal point that allows to maximize the performance. On the contrary, parameters Φ_b and l_{in} present an asymptotic pattern, so that after a certain value their increment is useless, while h_{sk} presents almost a linear pattern even if it does not affect significantly the global deflection in the considered variation range. It is finally possible to conclude that the parameter that influences mostly the SLS performance is the diameter of the cable Φ_b (Figure III.2-21.a): actually, for little diameters (Φ_b<30 mm), little variations in its value can significantly decrement the deflection measured at the mid-span of the system.

Therefore, form Figure III.2-21 it is possible to conclude that (*i*) incrementing both the diameter of the cable, (*ii*) increasing the height of the plinth of the shear key and (*iii*) moving the internal shear key towards the mid-span improve the SLS performance of the system, with the biggest impact given by the diameter of the cable. On the other hand, the position of the external shear key has an optimal point that allow to maximize SLS performances.

The parametric analysis herein illustrated has proven the potentialities of the analytical model to carry out more refined multi-parametric analyses in order to improve and optimize the structural performances of the innovative composite beam.

Incidentally, it is finally important noticing from Figure III.2-18.a that to the vary of mechanical and geometrical parameters it is possible to obtain also negative bending moments acting on the timber.

III.2.6 Conclusions and future developments

A mechanics-based analytical model to predict the short-term structural behavior of an innovative timber-steel composite beam has been illustrated. The analytical model has been compared with FE outcomes showing a very good agreement both in terms of forces and deflections. A parametric analysis to investigate the deflection performance of the composite structure to the vary of its geometrical properties has been carried out, showing a predominant influence of the diameter of the steel cable in determining the entity of maximum deflection. Offset distance of the cable respect to the timber joist and positions of the shear keys are other geometrical parameters influencing the maximum deflection, and from the parametric analysis resulted that an optimum point for the position of the external shear-keys exists. The model constitutes a tool for practitioners to easily design the innovative timber-steel composite member. In add, it is a reliable and manageable model that can be used to carry out multi-parametric analyses for enhancement and optimization of the structural performance of the novel composite beam. The analytical model also allows for a better comprehension of the mechanical phenomena involved in the structural response respect to analyses carried out with numerical models, and it can be used as benchmark for refined numerical analyses of the composite structures.

The model has been built assuming a beam configuration with four shear keys and a simply-supported four-point loading condition with two vertical forces comprised between the two internal shear keys. Future developments can provide solutions for other boundary and loading conditions, for example considering a distributed load, an asymmetric load pattern and different configurations of the shear keys.

An enhancement of the proposed model can be obtained considering an elastic-gap constitutive law for the shear-key horizontal spring in order to take into account for allowance between the width steel tooth of the shear key and the timber notch width in which it is inserted. It is worth noting that, in this case, it is no more possible to carry out a linear solution of the system, since a non-linear constitutive law is adopted within the structural system. Another possible improvement of the analytical model can be obtained considering shrinkage and swelling phenomena, as long as creep and mechano-sorptive effects.

In add, an in-depth numerical and experimental investigation on the shear stiffness of the steel shear key connections is necessary, since the values available in literature are based on tests carried out on concrete-timber notched connections. Actually, the ratio between the elastic moduli of concrete and timber is about 3, while the same ratio between steel and timber is about 16, therefore a quite different stiffness can be expected. If experimental outcomes show a markedly plastic behavior of the connection, the model can be enhanced with an elasto-plastic constitutive law for the shear keys.

Finally, the model will be used to carry out multi-parametric analyses for structural optimization investigating the mutual effect of the variation of mechanical and geometrical properties on deflections and internal forces of the composite member.

Bibliography of Part III

[1] S. Tesfamariam, S.F. Stiemer, Special Issue on Performance of Timber and Hybrid Structures, J. Perform. Constr. Facil. 28 (2014) A2014001. doi:10.1061/(ASCE)CF.1943-5509.0000641.

[2] A. Ceccotti, Composite concrete-timber structures, Prog. Struct. Eng. Mater. 4 (2002) 264–275. doi:10.1002/pse.126.

[3] A. Hassanieh, H.R. Valipour, M.A. Bradford, Experimental and numerical study of steel-timber composite (STC) beams, J. Constr. Steel Res. 122 (2016) 367–378. doi:10.1016/j.jcsr.2016.04.005.

[4] C. Leyder, F. Wanninger, A. Frangi, E. Chatzi, Dynamic response of an innovative hybrid structure in hardwood, Proc. Inst. Civ. Eng. - Constr. Mater. 168 (2015) 132–143. doi:10.1680/coma.14.00043.

[5] D. Yeoh, M. Fragiacomo, M. De Franceschi, K. Heng Boon, State of the Art on Timber-Concrete Composite Structures: Literature Review, J. Struct. Eng. 137 (2011) 1085–1095. doi:10.1061/(ASCE)ST.1943-541X.0000353.

[6] A. Hassanieh, H.R. Valipour, M.A. Bradford, Experimental and numerical investigation of short-term behaviour of CLT-steel composite beams, Eng. Struct. 144 (2017) 43–57. doi:10.1016/j.engstruct.2017.04.052.

[7] M. Kozłowski, J. Hulimka, Load-bearing capacity of hybrid timber-glass beams, Archit. Civ. Eng. Environ. 7 (2014) 61–71.

[8] R. Lopez-Anido, H. Xu, Structural Characterization of Hybrid Fiber-Reinforced Polymer-Glulam Panels for Bridge Decks, J. Compos. Constr. 6 (2002) 194–203. doi:10.1061/(ASCE)1090-0268(2002)6:3(194).

[9] T. Herzog, J. Natterer, R. Schweitzer, M. Volz, W. Winter, Timber construction manual, Birkhauser Verlag AG, 2004.

[10] J.P. Wacker, A. Dias, T.K. Hosteng, Investigation of Early Timber-Concrete Composite Bridges in the United States, in: 3rd Int. Conf. Timber Bridg. (ICTB 2017), Skelleftea, Sweden, 2017.

[11] D.Y.E. Chuan, Behaviour and design of timber-concrete composite floor system, University of Canterbury, 2010.

[12] M.A. Parisi, M. Piazza, Restoration and Strengthening of Timber Structures: Principles, Criteria, and Examples, Pract. Period. Struct. Des. Constr. 12 (2007) 177–185. doi:10.1061/(ASCE)1084-0680(2007)12:4(177).

[13] K. Quang Mai, A. Park, K.T. Nguyen, K. Lee, Full-scale static and dynamic experiments of hybrid CLT–concrete composite floor, Constr. Build. Mater. 170 (2018) 55–65. doi:10.1016/j.conbuildmat.2018.03.042.

[14] R. Crocetti, T. Sartori, R. Tomasi, Innovative Timber-Concrete Composite Structures with Prefabricated FRC Slabs, J. Struct. Eng. 141 (2015) 04014224. doi:10.1061/(ASCE)ST.1943-541X.0001203.

[15] E. Lukaszewska, H. Johnsson, M. Fragiacomo, Performance of connections for prefabricated timber–concrete composite floors, Mater. Struct. 41 (2008) 1533–1550. doi:10.1617/s11527-007-9346-6.

[16] J.K. Natterer, New technologies for engineered timber structures, Prog. Struct. Eng. Mater. 4 (2002) 245–263. doi:10.1002/pse.119.

[17] J.W. O'Neill, The fire performance of timber-concrete composite floors, University of Canterbury, 2009.

[18] International Organization for Standardization (ISO), ISO 834-1: Fire-resistance tests. Elements of building construction. Part 1: General requirements., (1999).

[19] A. Frangi, M. Knobloch, M. Fontana, Fire Design of Timber-Concrete Composite Slabs with Screwed Connections, J. Struct. Eng. 136 (2010) 219–228. doi:10.1061/(ASCE)ST.1943-541X.0000101.

[20] European Committee for Standardisation, EN 1995-1-1 - Eurocode 5: Design of timber structures - Part 1-1: General - Common rules and rules for buildings, 2004.

[21] European Committee for Standardisation, EN 1995-1-2 -Eurocode 5: Design of timber structures - Part 1-2: General - Structural fire design, 2004.

[22] T. Hozjan, C. Bedon, A. Ogrin, M. Cvetkovska, M. Klippel, Literature Review on Timber–Concrete Composite Structures in Fire, J. Struct. Eng. 145 (2019) 04019142. doi:10.1061/(ASCE)ST.1943-541X.0002418.

[23] European Committee for Standardisation, EN 1995-2 - Eurocode 5: Design of timber structures - 2:

Bridges, 2004.

[24] L.F. Jorge, J. Schänzlin, S.M.R. Lopes, H. Cruz, U. Kuhlmann, Time-dependent behaviour of timber lightweight concrete composite floors, Eng. Struct. 32 (2010) 3966–3973. doi:10.1016/j.engstruct.2010.09.007.

[25] M. Fragiacomo, Long-Term Behavior of Timber–Concrete Composite Beams. II: Numerical Analysis and Simplified Evaluation, J. Struct. Eng. 132 (2006) 23–33. doi:10.1061/(ASCE)0733-9445(2006)132:1(23).

[26] A. Ceccotti, M. Fragiacomo, S. Giordano, Long-term and collapse tests on a timber-concrete composite beam with glued-in connection, Mater. Struct. 40 (2007) 15–25. doi:10.1617/s11527-006-9094-z.

[27] J. Balogh, M. Fragiacomo, R.M. Gutkowski, R.S. Fast, Influence of Repeated and Sustained Loading on the Performance of Layered Wood–Concrete Composite Beams, J. Struct. Eng. 134 (2008) 430–439. doi:10.1061/(ASCE)0733-9445(2008)134:3(430).

[28] A. Ranta-Maunus, The viscoelasticity of wood at varying moisture content, Wood Sci. Technol. 9 (1975) 189–205. doi:10.1007/BF00364637.

[29] T. Toratti, S. Svensson, Mechano-sorptive experiments perpendicular to grain under tensile and compressive loads, Wood Sci. Technol. 34 (2000) 317–326. doi:10.1007/s002260000059.

[30] R. Goel, R. Kumar, D.K. Paul, Comparative Study of Various Creep and Shrinkage Prediction Models for Concrete, J. Mater. Civ. Eng. 19 (2007) 249–260. doi:10.1061/(ASCE)0899-1561(2007)19:3(249).

[31] C. Amadio, A. Ceccotti, R. Di Marco, M. Fragiacomo, Long-term behaviour of a timber-concrete connection system, in: Proc. Int. RILEM Symp. Joints Timber Struct., Stuttgart, Germany, 2001: pp. 263–272.

[32] C. Loss, M. Piazza, R. Zandonini, Connections for steel–timber hybrid prefabricated buildings. Part I: Experimental tests, Constr. Build. Mater. 122 (2016) 781–795. doi:10.1016/j.conbuildmat.2015.12.002.

[33] C. Loss, M. Piazza, R. Zandonini, Connections for steel–timber hybrid prefabricated buildings. Part II: Innovative modular structures, Constr. Build. Mater. 122 (2016) 796–808. doi:10.1016/j.conbuildmat.2015.12.001.

[34] N. Keipour, H.R. Valipour, M.A. Bradford, Experimental study of steel-timber composite (STC) beam to steel column joints having a flush end-plate, Eng. Struct. 174 (2018) 906–918. doi:10.1016/j.engstruct.2018.08.009.

[35] A.A. Chiniforush, A. Akbarnezhad, H.R. Valipour, M.A. Bradford, Long-Term Behavior of Steel-CLT Connections, in: WCTE 2018 - World Conf. Timber Eng., Seoul, South Korea, 2018. https://www.researchgate.net/publication/328190381.

[36] B. Dujic, K. Strus, R. Zarnic, A. Ceccotti, Prediction of Dynamic Response of a 7-storey Massive XLam Wooden Building Tested on a Shaking Table, in: 11th World Conf. Timber Eng. 2010, WCTE 2010, Riva del Garda, Italy, 2010: pp. 3450–3457.

[37] R. Gutkowski, K. Brown, A. Shigidi, J. Natterer, Laboratory tests of composite wood–concrete beams, Constr. Build. Mater. 22 (2008) 1059–1066. doi:10.1016/j.conbuildmat.2007.03.013.

[38] J. Kanócz, V. Bajzecerová, Timber-concrete composite elements with various composite connections Part 3: adhesive connection, Wood Res. 60 (2015) 939–952.

[39] Y. Jiang, R. Crocetti, CLT-concrete composite floors with notched shear connectors, Constr. Build. Mater. 195 (2019) 127–139. doi:10.1016/j.conbuildmat.2018.11.066.

[40] Z. Lyu, C. Málaga-Chuquitaype, A.M. Ruiz-Teran, Design of timber-concrete composite (TCC) bridges with under-deck stay cables, Eng. Struct. 189 (2019) 589–604. doi:10.1016/j.engstruct.2019.03.059.

[41] X. Shengmin, T. Peiwei, Glued timber connections - Experimental and numerical study of tension behavior under various influencing parameters, Linnaeus University, 2015.

[42] A.M.P.G. Dias, S.M.R. Lopes, J.W.G. Van de Kuilen, H.M.P. Cruz, Load-Carrying Capacity of Timber–Concrete Joints with Dowel-Type Fasteners, J. Struct. Eng. 133 (2007) 720–727. doi:10.1061/(ASCE)0733-9445(2007)133:5(720).

[43] A. Hassanieh, H.R. Valipour, M.A. Bradford, Experimental and analytical behaviour of steel-timber composite connections, Constr. Build. Mater. 118 (2016) 63–75. doi:10.1016/j.conbuildmat.2016.05.052.

[44] K.W. Johansen, Theory of Timber Connections, Int. Assoc. Bridg. Struct. Eng. 9 (1949) 249–262. doi:10.5169/seals-9703.

[45] S. Kavaliauskas, A.K. Kvedaras, B. Valiūnas, Mechanical behaviour of timber-to-concrete connections

with inclined screws, J. Civ. Eng. Manag. 13 (2007) 201–207. doi:10.3846/13923730.2007.9636437.

[46] B.H. Ahmadi, M.P. Saka, Behavior of Composite Timber-Concrete Floors, J. Struct. Eng. 119 (1993) 3111–3130. doi:10.1061/(ASCE)0733-9445(1993)119:11(3111).

[47] A.M.P.G. Dias, U. Kuhlmann, K. Kudla, S. Mönch, A.M.A. Dias, Performance of dowel-type fasteners and notches for hybrid timber structures, Eng. Struct. 171 (2018) 40–46. doi:10.1016/j.engstruct.2018.05.057.

[48] E.W. Kuenzi, Theoretical Design of a Nailed or Bolted Joint Under Lateral Load, 1955.

[49] P. Gelfi, E. Giuriani, A. Marini, Stud Shear Connection Design for Composite Concrete Slab and Wood Beams, J. Struct. Eng. 128 (2002) 1544–1550. doi:10.1061/(ASCE)0733-9445(2002)128:12(1544).

[50] European Committee for Standardisation, EN 26891:1991: Timber structures — Joints made with mechanical fasteners — General principles for the determination of strength and deformation characteristics, (1991).

[51] A.M.P.G. Dias, H.M.P. Cruz, S.M.R. Lopes, J.W. van de Kuilen, Stiffness of dowel-type fasteners in timber–concrete joints, Proc. Inst. Civ. Eng. - Struct. Build. 163 (2010) 257–266. doi:10.1680/stbu.2010.163.4.257.

[52] Y. Jiang, W. Hong, X. Hu, R. Crocetti, L. Wang, W. Sun, Early-age performance of lag screw shear connections for glulam-lightweight concrete composite beams, Constr. Build. Mater. 151 (2017) 36–42. doi:10.1016/j.conbuildmat.2017.06.063.

[53] R.L. Haupt, S.E. Haupt, Practical Genetic Algorithms, Second Edi, Wiley-Interscience, Hoboken, New Jersey, U.S.A., 2004.

[54] G. He, L. Xie, J. Yi, L. Peng, P.J. Gustafsson, R. Crocetti, Shear Behavior Study on Timber-Concrete Composite Structures with Bolts, BioResources. 11 (2016) 9205–9218.

[55] L. Xie, G. He, P.J. Gustafsson, R. Crocetti, L. Chen, L. Li, W. Xie, Shear Capacity of Stud-Groove Connector in Glulam- concrete Composite Structure, BioResources. 12 (2017) 4690–4706.

[56] L. Marchi, R. Scotta, L. Pozza, Experimental and theoretical evaluation of TCC connections with inclined self-tapping screws, Mater. Struct. 50 (2017) 180. doi:10.1617/s11527-017-1047-1.

[57] E. Steinberg, R. Selle, T. Faust, Connectors for Timber–Lightweight Concrete Composite Structures, J. Struct. Eng. 129 (2003) 1538–1545. doi:10.1061/(ASCE)0733-9445(2003)129:11(1538).

[58] A.M.P.G. Dias, Analysis of the Nonlinear Behavior of Timber-Concrete Connections, J. Struct. Eng. 138 (2012) 1128–1137. doi:10.1061/(ASCE)ST.1943-541X.0000523.

[59] A.M.P.G. Dias, L.F.C. Jorge, The effect of ductile connectors on the behaviour of timber–concrete composite beams, Eng. Struct. 33 (2011) 3033–3042. doi:10.1016/j.engstruct.2011.05.014.

[60] P.H. Kirkegaard, J.D. Sørensen, D. Čizmar, V. Rajčić, System reliability of timber structures with ductile behaviour, Eng. Struct. 33 (2011) 3093–3098. doi:10.1016/j.engstruct.2011.03.011.

[61] N. Khorsandnia, H.R. Valipour, K. Crews, Experimental and analytical investigation of short-term behaviour of LVL–concrete composite connections and beams, Constr. Build. Mater. 37 (2012) 229–238. doi:10.1016/j.conbuildmat.2012.07.022.

[62] B.L. Deam, M. Fragiacomo, A.H. Buchanan, Connections for composite concrete slab and LVL flooring systems, Mater. Struct. 41 (2008) 495–507. doi:10.1617/s11527-007-9261-x.

[63] D. Yeoh, M. Fragiacomo, M. De Franceschi, A.H. Buchanan, Experimental Tests of Notched and Plate Connectors for LVL-Concrete Composite Beams, J. Struct. Eng. 137 (2011) 261–269. doi:10.1061/(ASCE)ST.1943-541X.0000288.

[64] N. Khorsandnia, H. Valipour, M. Bradford, Deconstructable timber-concrete composite beams with panelised slabs: Finite element analysis, Constr. Build. Mater. 163 (2018) 798–811. doi:10.1016/j.conbuildmat.2017.12.169.

[65] G. Larsson, P.J. Gustafsson, E. Serrano, R. Crocetti, Duration of load behaviour of a glued shear plate dowel joint, Eur. J. Wood Wood Prod. (2019). doi:10.1007/s00107-019-01474-z.

[66] D.E.C. Yeoh, M. Fragiacomo, P. Aldi, M. Mazzilli, U. Kuhlmann, Performance of Notched Coach Screw Connection for Timber-Concrete Composite Floor System, in: 10th World Conf. Timber Eng., Miyazaki, Japan, 2008.

[67] R. Crocetti, T. Sartori, M. Flansbjer, Timber-Concrete Composite Structures with Prefabricated FRC Slab, in: WCTE 2010 - Word Conf. Timber Eng., Riva del Garda, Italy, 2010.

[68] S. Schnabl, M. Saje, G. Turk, I. Planinc, Analytical Solution of Two-Layer Beam Taking into account Interlayer Slip and Shear Deformation, J. Struct. Eng. 133 (2007) 886–894. doi:10.1061/(ASCE)0733-9445(2007)133:6(886).

[69] A. Kroflic, I. Planinc, M. Saje, B. Cas, Analytical solution of two-layer beam including interlayer slip

and uplift, Struct. Eng. Mech. 34 (2010) 667–683. doi:10.12989/sem.2010.34.6.667.

[70] W.M.G. Burdzik, S. Skorpen, Experimental and analytical investigation into the stiffness of composite steel-reinforced timber beams with flexible shear connectors, J. South African Inst. Civ. Eng. 58 (2016) 11–20. doi:10.17159/2309-8775/2016/v58n4a2.

[71] V. Bajzecerová, Bending Stiffness of CLT-Concrete Composite Members - Comparison of Simplified Calculation Methods, Procedia Eng. 190 (2017) 15–20. doi:10.1016/j.proeng.2017.05.301.

[72] F. Focacci, P. Foraboschi, M. De Stefano, Composite beam generally connected: Analytical model, Compos. Struct. 133 (2015) 1237–1248. doi:10.1016/j.compstruct.2015.07.044.

[73] C. Zhang, P. Gauvreau, Timber-Concrete Composite Systems with Ductile Connections, J. Struct. Eng. 141 (2015) 04014179. doi:10.1061/(ASCE)ST.1943-541X.0001144.

[74] Z. Perkowski, M. Czabak, Description of behaviour of timber-concrete composite beams including interlayer slip, uplift, and long-term effects: Formulation of the model and coefficient inverse problem, Eng. Struct. 194 (2019) 230–250. doi:10.1016/j.engstruct.2019.05.058.

[75] M. Fragiacomo, C. Amadio, L. Macorini, Finite-Element Model for Collapse and Long-Term Analysis of Steel–Concrete Composite Beams, J. Struct. Eng. 130 (2004) 489–497. doi:10.1061/(ASCE)0733-9445(2004)130:3(489).

[76] N. Khorsandnia, H. Valipour, S. Foster, K. Crews, A force-based frame finite element formulation for analysis of two- and three-layered composite beams with material non-linearity, Int. J. Non. Linear. Mech. 62 (2014) 12–22. doi:10.1016/j.ijnonlinmec.2014.02.001.

[77] S. Lopes, L. Jorge, H. Cruz, Evaluation of non-linear behavior of timber–concrete composite structures using FE model, Mater. Struct. 45 (2012) 653–662. doi:10.1617/s11527-011-9787-9.

[78] M. Oudjene, E.-M. Meghlat, H. Ait-Aider, J.-L. Batoz, Non-linear finite element modelling of the structural behaviour of screwed timber-to-concrete composite connections, Compos. Struct. 102 (2013) 20–28. doi:10.1016/j.compstruct.2013.02.007.

[79] C. Bedon, M. Fragiacomo, Numerical analysis of timber-to-timber joints and composite beams with inclined self-tapping screws, Compos. Struct. 207 (2019) 13–28. doi:10.1016/j.compstruct.2018.09.008.

[80] A. Hassanieh, H.R. Valipour, M.A. Bradford, C. Sandhaas, Modelling of steel-timber composite connections: Validation of finite element model and parametric study, Eng. Struct. 138 (2017) 35–49. doi:10.1016/j.engstruct.2017.02.016.

[81] N. Khorsandnia, J. Schänzlin, H. Valipour, K. Crews, Coupled finite element-finite difference formulation for long-term analysis of timber–concrete composite structures, Eng. Struct. 96 (2015) 139–152. doi:10.1016/j.engstruct.2015.03.047.

[82] N.T. Mascia, N.C.S. Forti, J. Soriano, E.A. Nicolas, T.L.D. Forti, Study of concrete–timber composite beams using an analytical approach based on the principle of virtual work and experimental results, Eng. Struct. 46 (2013) 302–310. doi:10.1016/j.engstruct.2012.07.035.

[83] T. Wang, Y. Wang, Hybrid structures with shear-key connections, KTH - Royal Istitute of Technology, 2019.

[84] M. Flaig, T. Schmidt, H.J. Blass, Compressive strength and stiffness of end grain contact joints in glulam and CLT, in: INTER 2019- Int. Netw. Timber Eng. Res., Tacoma, USA, 2019.

[85] DIN EN 1995-1-1/NA. Eurocode 5: Bemessung und Konstruktion von Holzbauten – Teil 1–1 mit NA (2013): Allgemeines - Allgemeine Regeln und Regeln für den Hochbau., Germany: DIN - Deutsches Institut für Normung e. V., Berlin, 2010.

[86] I. Lukacs, A. Björnfot, R. Tomasi, Strength and stiffness of cross-laminated timber (CLT) shear walls: State-of-the-art of analytical approaches, Eng. Struct. 178 (2019) 136–147. doi:10.1016/j.engstruct.2018.05.126.

[87] A. Dias, J. Schänzlin, P. Dietsch, Design of timber-concrete composite structures, 2018.

[88] Strand7 Pty. Ltd, Strand7 - Theoretical Manual, (2005). http://www.strand7.com/html/docu_theoretical.htm.

[89] T. Vrouwenvelder, The JCSS probabilistic model code, Struct. Saf. 19 (1997) 245–251. doi:10.1016/S0167-4730(97)00008-8.

[90] JCSS, Probabilistic Model Code - Technical report 3.04: static properties of prestressing steel (prestressed concrete), 2006.

[91] JCSS—Joint Committee on Structural Safety, Probabilistic Model Code - Technical report 3.5: properties of timber, 2006.

Conclusions and future developments

In this work numerical modelling strategies and design methods for timber structures have been analyzed. In particular, three topics have been investigated in the three parts of the thesis: (*i*) strategies for structural modelling of CLT buildings under seismic actions, (*ii*) design methods for CLT wall systems subjected to horizontal actions and (*iii*) mechanical characterization and enhancement of an innovative composite timber-based beam. In the following, a summary of the main findings from each of the three topics covered in this work will be given.

As far as regards modelling strategies for CLT multi-storey buildings, two numerical approaches have been critically analyzed and compared, namely the component-level and the phenomenological ones. Results showed that both are feasible tools to reliably predict the seismic behavior of CLT wall systems provided that constitutive laws are subject to an accurate calibration phase. Component-level numerical models are the most complex to create, calibrate and use, but they are more powerful since they allow to analyze every configuration of CLT walls regardless of panel geometry, connections arrangements and vertical loads acting on them. They can also take into account for friction forces if appropriate contact elements are included in the numerical model. Moreover, they can consider secondary order effects - like out-of-plane movements of the laterally-loaded wall system - if constitutive laws of components are properly calibrated to consider these phenomena. Phenomenological models are easier and less-time consuming, but their versatility is limited from the dependency of their results from the specific loading, geometrical and connections configurations used for its calibration, therefore should be employed only for analyses of buildings presenting few homogeneous configurations of CLT walls. Tables for phenomenological models furnishing the equivalent elastic modulus to panel width ratio as a function of the number of storeys of the building and of the seismic intensity have been derived. From the comparison between linear dynamic analyses carried out with the two approaches it resulted that the phenomenological one overestimates uplift forces. The reason must be sought in an underestimation of the lever-arm between uplift and compression forces at the bottom interface. Actually, since fixed constraint condition at the bottom of the CLT wall system is considered in the phenomenological configuration, the distance between the two resultants forces is 2/3 the length of the wall. Instead, considering a uniaxial behavior of connections and a rigid behavior of compressed timber as usually assumed by practitioners when performing linear dynamic analyses, the lever arm when a component-level approach is approximately equal to the length of the panel. The analysis of the principal elastic period values obtained with linear analyses showed on one hand a perfect agreement between the two approaches in the prediction of the dynamic behavior of CLT multi-storey buildings, and on the other hand a high discrepancy between the numerical results and the values that can be obtained from codes especially for higher buildings. This fact highlights the lack of current building codes and standards in furnishing reliable tools for the design of CLT structures. It has in add been noticed that for higher buildings the principal period falls over the end of the spectral plateau, therefore on one hand they have the advantage of lower seismic induced forces, but on the other hand they are prone to develop high displacements, therefore the lateral deformability can be the dimensioning key-factor for seismic design of higher multi-storey CLT buildings. This fact is also corroborated from the values of inter-storey drifts obtained from the spectral analyses that for higher values of PGA exceed the inter-storey drift limit of 5 ‰ imposed by Eurocode 8. As far as regards non-linear analyses, an important preliminary phase of interpretation of results of the cyclic tests carried on CLT wall systems at CNR-IVALSA within the SOFIE project, assumed as reference tests, has been undertaken. This has been made necessary to derive the effective load-displacement history of the tested shear-walls. The study carried out on non-linear component-level models showed that this numerical approach is a powerful tool that gives reliable results as long as the tests on single components used for calibration reflect their behavior in the global wall system. If it does not happen, as observed comparing global tests on shear walls and local ones on connections carried out within SOFIE project, strategies to adapt the constitutive laws of connections calibrated on local tests to their actual behavior in the global system must be adopted. For the non-linear component-level analyses carried out in this thesis it was necessary to adopt a damage variable to modify the constitutive laws of angle brackets in order to consider the reduction of their shear strength due to out-of-plane movement. Phenomenological modelling approach do not require any specific strategy to take into account for friction phenomenon or second-order effects since their constitutive laws are already calibrated to fit the global behaviour of the wall system. From a comparison between results of non-linear models obtained with the two approaches it is possible to observe that the phenomenological one fits better the cumulative energy while component-level one can predict with more accuracy the force-displacement behavior of the wall system.

In the second part of the thesis a method for the design of CLT shear walls based on axial-shear interaction domains has been proposed. Differently from other reference methods available in literature, the one developed in this work considers an elastoplastic behaviour of CLT panel in place of an elasto-brittle constitutive law and a coupled axial-shear behaviour of connections in place of an infinite shear resistance. Three criteria to describe the coupled resistance of connections have been considered: a rectangular one, an elliptic one and an innovative hybrid force-displacement. The elliptic and rectangular coupling criteria have been implemented with two different formulations. The first, simplified, assumes that the achievement of the ultimate condition of the connection coincides with the yielding point. The second formulation, more refined, considers the failure of connections happened only once they reach the ultimate displacement. Two methods for the definition of the elasto-plastic behavior of connections, labelled as #1 and #2, have been introduced. The effects of different criteria adopted for the definition of the constitutive law of timber and of the mechanical behavior of connections have been investigated through a sensitivity analysis in which the results were compared with tests on walls with the same mechanical and geometric characteristics. The sensitivity analysis showed that the adoption of an elasto-plastic constitutive law allows to obtain a much more performant result respect to the elasto-fragile behavior for timber with an increment of the shear strength of the wall system up to 40%. From a comparison between the different coupling methods it resulted that the simplified formulations of the rectangular and elliptic criteria are on the safe side respect to the refined formulations, and that the hybrid approach is anyway the most precautionary since it takes into account for the axial-shear interaction even for small working ranges. From the analysis it is possible to conclude that the set of assumptions that guarantees the best reliability of the interaction domains consists of an elasto-plastic constitutive law for timber, connections with constitutive laws according to method #2 and axial-shear coupling criterion of the connections according to force-based elliptical refined approach or to the hybrid one.

In the third and final part of the thesis, regarding the short-term structural characterization and enhancement of an innovative composite timber-based beam, a mechanics-based analytical model able to predict its internal forces and displacements has been presented. The model has been used to perform a parametric analysis to investigate the influence of the geometric properties of the composite beam on the maximum deflection, given the span, the section size of the wooden component, the loads and the constraint conditions. It resulted on one hand that the parameter that most influences the deformability of the novel composite beam is the diameter of the tensioned cable at the intrados, and that the external shear key connections are characterized by an optimum longitudinal position point along the length of the beam. Moreover, also the increment of the offset of the cable from the timber joist and the movement towards the mid-section of the internal shear keys contribute to reduce the maximum deflection. The model constitutes a reliable and manageable tool to easily design the innovative timber-steel composite member and for a better comprehension of the mechanical phenomena involved in the structural response respect to analyses carried out with numerical models. In add, it can be used to carry out multi-parametric analyses for enhancement and optimization of the structural performance of the novel composite beam.

As far as regards future developments, both component-level and phenomenological modelling approaches will be used to perform non-linear analyses on global CLT multi-storey buildings as already carried out with linear ones. This will allow an in-depth comparison of the provision potentialities on the seismic response of CLT multi-storey buildings between the different modelling approaches. The method to perform axial-shear interaction domains for CLT wall system presented in the second part of the thesis will be employed to carry out a parametric analysis to furnish interaction domains to the vary of geometrical configuration and connections arrangement. Through the analysis it will be possible to obtain parametric interaction domains that can be used by practitioners for fast and easy seismic design of CLT shear walls. With regard to the analytical model for the composite beam presented in the third part, different enhancement on its formulation can be performed, like furnishing solutions for other boundary and loading conditions, considering an elastic-gap constitutive law for the shear-key horizontal spring in order to take into account for allowance between the width steel tooth of the shear key and the timber notch, or considering creep and swelling-shrinkage phenomena. Finally, the analytical model will be used to carry out multi-parametric analyses for structural optimization investigating the mutual effect of the variation of mechanical and geometrical properties on deflections and internal forces of the composite member.

List of figures

Figure I.1-1 – CLT multi-storey timber buildings: (a) Dalston Lane building in London (United Kingdom) and (b) Forte building in Melbourne (Australia) (image credits: (a) Waugh Thistleton Architects website [15] and (b) The Possible website [16]). 12

Figure I.1-2 – High timber buildings in Norway: (a) Treet and (b) Mjøstårnet (image credits: (a) Abrahamsen & Malo [18] and (b) Moelven website [30]). 14

Figure I.1-3 – Light timber frame system: (a) wall components, (b) platform frame structure and (c) balloon frame structure (image credits: (a-b) Follesa et al. [36] and (c) Acar [37]). 15

Figure I.1-4 – Heavy timber frame system: (a) example of building [38] and (b) detail of a post-tensioned joint [7] (image credits: (a) Swedish Wood [38], (b) Buchanan et al. [7]). 15

Figure I.1-5 – CLT wall system: (a) internal crosswise layered structure, (b) structural system representation and (c) typical connection assemblies (image credits: (a) Martínez-Martínez [49], (b) Swedish Wood [38] and (c) Follesa et al. [36]). 16

Figure I.1-6 – CLT wall system sub-types: (a) platform construction and (b) balloon construction (image credits: (a) CLT Handbook [39] and (b) Structural Timber Association [55]). 17

Figure I.1-7 – Mixed CLT walls-heavy frame system: (a) 3D view of the NMIT Arts and Media Building Structure and (b) example of a 7-storey multi-storey mixed CLT walls-heavy frame system (image credits: (a) Devereux et al. [57]). 17

Figure I.1-8 – Density of structural timber used vs. number of storeys for different multi-storey timber building typologies (image credits: Ramage et al. [58]). 18

Figure I.1-9 – Efficiency of different types of connections (image credits: Ramage et al. [58]). 19

Figure I.1-10 – Connection typologies for timber structures, examples: (a) carpentry joint (skewed tenon), (b) connections with dowel-type mechanical fasteners (truss lattice joint), (c) surface connector (punched steel plate fastener) and (d) glued-in steel rods. (images credits: (a) Branco et al. [61], (b) Ballerini [62], (c) Karadelis & Brown [63], (d) Tlustochowicz et al. [64]). 19

Figure I.1-11 – Nailed mechanical connections: (a) Round smooth shank nail, (b) spiral nail, (c) ringed shank nail, (d) machine driven nails and (e) example of nailed connection (images credits: (a-d) Blaß & Sandhaas [59] and (e) Weyerhaeuser website [65]) 20

Figure I.1-12 – Stapled joints: (a) staples and (b) example of stapled connection (images credits: (a) Blaß & Sandhaas [59] and (b) Pintarič et al. [66]). 20

Figure I.1-13 – Screwed joints: (a) self-tapping screws and (b) example of screwed connection (images credits: (a) Blaß & Sandhaas [59] and (b) Fastfix website [67]). 21

Figure I.1-14 – Bolted and dowelled connections: (a) dowel connector, (b) bolt connector, (c) example of bolted connection and (d) example of dowelled connection (images credits: (a-b) Blaß & Sandhaas [59], (c-d) Setra Group webpage [69]) 22

Figure I.1-15 – Connection system for CLT assemblies: (a) example of connectors used with angle bracket and hold-down connections and (b) location of connections in multi-storey CLT buildings and their detail ID henceforth adopted. (images credits: (a) Gavric et al. [77] and (b) CLT Handbook [39]). . . 23

Figure I.1-16 – Panel-to-panel connections: (a) internal spline, (b) single surface spline, (c) double surface spline, (d) half-lapped joint, (e) butt joint and (f) example of screwing of a screwed panel-to-panel joint. (images credits: (a-d) CLT Handbook [39], (e) Loss et al. [79] and (f) Follesa et al. [80]). 24

Figure I.1-17 – Wall-to-wall connections: (a) self-tapping screws, (b) wooden profiles and (c) metal brackets (images credits: CLT Handbook [39]). 25

Figure I.1-18 – Wall-to-floor connections for platform CLT constructions: (a) self-tapping screws, (b) concealed metal plates, (c) metal brackets, (d) hold-down and (e) angle bracket (images credits: (a-c) CLT Handbook [39], (d) Progetto Energia Zero [84] and (e) Timber-Online [85]). 26

Figure I.1-19 – Wall-to-floor connections for balloon CLT constructions: (a) wooden bearing support [39] and (b-c) metal bracket (images credits: CLT Handbook [39]). 26

Figure I.1-20 – Wall-to-foundation connections: (a) visible plates, (b) concealed hardware and (c) metal shaft (images credits: CLT Handbook [39]). 27

Figure I.1-21 – Dissipative connector proposed by Schmidt & Blaß [92]: (a) representation, (b) steel plate and (c) hysteretic behavior with a gap opening t_{gap}=50 mm (images credits: Schmidt & Blaß [92]). . . 28

Figure I.1-22 – Brittle failure mechanisms of typical CLT connections: (a) tensile failure of the net cross section of the metal sheet of hold downs, (b) pull-through of the anchoring bolt of wall-to-floor angle brackets and (c) withdrawal of the nails of wall-to-foundation angle brackets (image credits: Follesa et al. [113]). 34

Figure I.1-23 – EN 14592 [164]: (a) cyclic loading protocol and (b) test setup (image credits: Izzi et al. [165]). 35

Figure I.1-24 – Evaluation of ductility of connections accordingly to Casagrande et al. [166]: (a) impairment of strength between the 1st (red) and 3rd (blue) backbone curves and (b) impairment of strength factor vs. dimensionless slip amplitude (images credits: Casagrande et al. [166]). 37

Figure I.1-25 – Minimum spacings and end-distances for self-tapping screws (image credits: Ringhofer et al. [53]). 41

Figure I.1-26 – Failure modes of steel-to-timber dowelled joints (image credits: Blaß et al. [59]). 42

Figure I.1-27 – Schematic representation of modelling techniques for a CLT wall: component-level and phenomenological approaches with linear and non-linear constitutive laws (image readapted from Pozza et al. [191]). 45

Figure I.2-1 – Multi-storey building considered as reference structure for linear analyses: (a) layout of the building with the areas of relevance for the calculation of vertical loads acting on CLT shear walls in X (blue pattern) and Y (orange pattern) directions (measurements in meters) and (b) isometric view of the 6- storey configuration. 51

Figure I.2-2 – Design spectra and spectral parameters for the three seismicity levels considered and for SLS and ULS conditions. 52

Figure I.2-3 – Component-level linear model: (a) schematic representation and (b) pictures of the finite element model for the 2-storey building configuration. 54

Figure I.2-4 – Schematic representation of the displacement contributions to inter-storey drift $d_{i\text{-}s}$. 55

Figure I.2-5 – Spectral analysis for 6-storey building configuration and PGA=0.35 g: (a) results of in terms of horizontal displacements, with underlined the opposite sliding directions of (b) lower and (c) upper springs. 56

Figure I.2-6 – Shear wall test setup and instrument position [77]. 58

Figure I.2-7 – Out-of-plane behavior of angle brackets caused by secondary moment due to eccentricity between wall and connection: (a) undeformed and deformed configurations; (b) detail of forces on connections. 59

Figure I.2-8 – Horizontal displacement components of the wall system due to: (a) rocking; (b) sliding; (c) panel elastic deformation. Sign convention: horizontal displacement positive towards right direction; vertical displacement positive upward. 60

Figure I.2-9 – Wall I.1: displacement contribution to total lateral deflection: (a) individual contributions compared with the measured displacement; (b) percentage relative to the horizontal top displacement measured in the experimental test $d_{top,meas}$. 63

Figure I.2-10 – Wall I.2: displacement contribution to total lateral deflection: (a) individual contributions compared with the measured displacement; (b) percentage relative to the horizontal top displacement measured in the experimental test $d_{top,meas}$. 63

Figure I.2-11 – Wall I.3: displacement contribution to total lateral deflection: (a) individual contributions compared with the measured displacement; (b) percentage relative to the horizontal top displacement measured in the experimental test $d_{top,meas}$. 64

Figure I.2-12 – Schematic representation of the parameters defining the hysteretic behavior of the OpenSees Pinching4 law [219], for a general connection (angle bracket or hold-down) under: (a) axial; (b) shear loading, starting from experimental data. 66

Figure I.2-13 – Results of the calibration of hysteretic law of connections: (a) hold-down loaded in the axial direction; (b) hold-down loaded in lateral direction; (c) angle bracket loaded in the axial direction; (d) angle bracket loaded in lateral direction. 67

Figure I.2-14 – Comparison between numerical simulations and test results, global behavior in terms of: (a) force-displacement curve; (b) cumulative energy. 68

Figure I.2-15 – Comparison between numerical simulations and test results, local behavior in terms of: (a) uplift displacement; (b) slip displacement 69

Figure I.2-16 – Sensitivity analyses for Wall I.1. Comparison for different levels of friction coefficient: (a) force-displacement curve; (b) cumulative energy; (c) uplift displacement; (d) slip displacement. 70

Figure I.2-17 – Sensitivity analyses for Wall I.2. Comparison for different levels of friction coefficient: (a) force-displacement curve; (b) cumulative energy; (c) uplift displacement; (d) slip displacement. 71

Figure I.2-18 – Sensitivity analyses for Wall I.3. Comparison for different levels of friction coefficient: (a) force-displacement curve; (b) cumulative energy; (c) uplift displacement; (d) slip displacement. 71

Figure I.2-19 – Sensitivity analyses for Wall I.1. Comparison between results of the numerical models "BW" and "WB": (a) force-displacement curve; (b) cumulative energy; (c) uplift displacement; (d) slip displacement. 72

Figure I.2-20 – Sensitivity analyses for Wall I.2. Comparison between results of the numerical models "BW" and "WB": (a) force-displacement curve; (b) cumulative energy; (c) uplift displacement; (d) slip displacement. 73

Figure I.2-21 – Sensitivity analyses for Wall I.3. Comparison between results of the numerical models "BW" and "WB": (a) force-displacement curve; (b) cumulative energy; (c) uplift displacement; (d) slip displacement. 73

Figure I.2-22 – Sensitivity analyses for Wall I.2. Comparison adopting different post-peak slopes of hold-downs loaded in the axial direction: (a) force-displacement; (b) cumulative energy; (c) uplift displacement; (d) slip displacement. 74

Figure I.2-23 – Sensitivity analyses for Wall I.3. Comparison adopting different post-peak slopes of hold-downs loaded in the axial direction: (a) force-displacement; (b) cumulative energy; (c) uplift displacement; (d) slip displacement. 75

Figure I.2-24– Wall I.1. Results including the damaged law for angle brackets: (a) force-displacement curve; (b) cumulative energy; (c) uplift displacement; (d) slip displacement. *76*

Figure I.2-25 – Wall I.2. Results including the damaged law for angle brackets: (a) force-displacement curve; (b) cumulative energy; (c) uplift displacement; (d) slip displacement. *77*

Figure I.2-26 – Wall I.3. Results including the damaged law for angle brackets: (a) force-displacement curve; (b) cumulative energy; (c) uplift displacement; (d) slip displacement. *77*

Figure I.3-1 – Phenomenological linear model: (a) schematic representation and (b) pictures of the finite element model for the 2-storey building configuration. *82*

Figure I.3-2 – Schematic representation of non-linear phenomenological model. *84*

Figure I.3-3 – Comparison between numerical and experimental results of phenomenological non-linear model in terms of (a) force-displacement and (b) cumulative energy curves for wall I.1 tested at CNR-IVALSA [77]. *85*

Figure I.3-4 – Comparison between numerical and experimental results of phenomenological non-linear model in terms of (a) force-displacement and (b) cumulative energy curves for wall I.2 tested at CNR-IVALSA [77]. *85*

Figure I.3-5 – Comparison between numerical and experimental results of phenomenological non-linear model in terms of (a) force-displacement and (b) cumulative energy curves for wall I.3 tested at CNR-IVALSA [77]. *85*

Figure I.4-1 – Comparison between linear modelling strategies in terms of principal elastic period T_1 (a) to the vary of building configuration for PGA=0.35 g and (b) to the vary of PGA level for 6-storey building configuration, with T_B and T_C respectively lower and upper limits of the constant spectral acceleration. *91*

Figure I.4-2 – Comparison between linear modelling strategies in terms of maximum inter-storey drift $d_{i\text{-}s,max}$ (a) to the vary of building configuration for PGA=0.35 g and (b) to the vary of PGA level for 6-storey building configuration. Red bars of histograms and underlined italic values on tables represent the sliding contribution $d_{sl,max}$. *91*

Figure I.4-3 – Comparison between linear modelling strategies in terms of base shear per unity of length v (a) to the vary of building configuration for PGA=0.35 g and (b) to the vary of PGA level for 6-storey building configuration. *92*

Figure I.4-4 – Comparison between linear modelling strategies in terms of uplift force N (a) to the vary of building configuration for PGA=0.35 g and (b) to the vary of PGA level for 6-storey building configuration. *92*

Figure I.4-5 – Comparison between linear modelling strategies in terms of uplift force N (a) to the vary of building configuration for PGA=0.35 g and (b) to the vary of PGA level for 6-storey building configuration (image credits: presentation at TSE 2017 by L. Pozza et al. [191]). *92*

Figure I.4-6 – Comparison between non-linear modelling strategies in terms of (a) force-displacement and (b) cumulative energy curves for CLT wall system configurations I.1, I.2 and I.3 tested at CNR-IVALSA [77] *94*

Figure II.1-1 – Design approaches for CLT wall systems: (a) schematic representation of a model that disregards the resistance of connections in their secondary direction (image credits: Tomasi & Smith [13]), (b) elasto-brittle (red line) and constant (black line) constitutive laws for connections and (c) rigid (black line), stress-block (blue line) and elasto-brittle (red line) constitutive laws for timber. . *116*

Figure II.1-2 – Schematic representation of models with (a) a stress block and linear constitutive law of axial forces and (b) with assumed a rigid behavior of compressed timber and a constant distribution of tensile forces on connections. *118*

Figure II.1-3 – Forces at bottom interface at rocking failure for each model: (a) Schickhofer #1, (b) Schickhofer #2, (c) Schickhofer #3, (d) Sustersic & Dujic, (e) Pei, (f) Waller-Novak, (g) Gavric & Popovski #1, (h) Gavric & Popovski #2, (i) Tomasi, (j) Casagrande, (k) Reynolds #1, (l) Reynolds #2, (m) Reynolds #3 and (n) Reynolds #4. .... *119*

Figure II.1-4 – Coupling phenomenon on connections: decay of strength and stiffness of hold-down axially-loaded connections for different levels of imposed lateral displacements (LD, values in mm) for (a) monotonic and (b) cyclic loading conditions (image credits: Pozza et al. [25]). *121*

Figure II.1-5 – Hybrid force-displacement based coupling method: (a) example of variation of the backbone envelope curve of axially-loaded hold-downs due to displacements in the secondary direction (subscripts 0 and t respectively stand for uncoupled and coupled conditions) and (b) example of linear regression analysis on experimental outcomes to derive the parameter $\delta_{V,y,1}$ *(first yielding shear displacement) of laterally-loaded angle brackets to the vary of axial displacement* δ_N *(image credits: (a) Pozza et al. [33] and (b) Pozza et al. [26]).* *122*

Figure II.2-1 – Model by Tamagnone et al. [19–21]: (a) schematic representation of the: geometrical layout and force and displacement patterns, (b) constitutive law of connections and (c) timber. *126*

Figure II.2-2 – Stress distribution coefficient k for CLT walls subjected to (a-b) horizontal force V and (c-d) bending moment M for (a-c) rigid and (b-d) CLT flexible supports (image credits: Tamagnone et al. [19]). *127*

Figure II.2-3 – Failure sub-domains: (a) sub-domains definition, (b) failure condition for sub-domains 1 and 2 for attainment of ultimate condition on furthest angle bracket and (c) furthest hold-down. *128*

Figure II.2-4 – Displacements and stresses distributions at bottom interface for sub-domain 5. .... *130*

Figure II.2-5 – Wall configurations (a) I.1 with 2 angle-brackets and configurations (b) I.2-I.3 with 4 angle-brackets tested within the SOFIE project [35] *131*

Figure II.2-6 – Interaction domains of wall configurations (a) I.1 and (b) I.2-I.3 derived with the method proposed by Tamagnone et al. [19]. Dashed vertical lines delimit the boundaries of the five sub-domains. Dotted vertical lines are indicative of the value of the vertical load N for each configuration. The markers denote the experimental tests outcomes. *131*

Figure II.3-1 – Schematic representation of the proposed model: geometrical layout and force and displacement patterns. *136*

Figure II.3-2 – Constitutive laws for: (a) compressed timber at the bottom interface; (b) connections loaded in axial direction; (c) connections loaded in lateral direction *137*

Figure II.3-3 – Bi-linearization method (solid lines) and backbone curve (dash-dot line) defined by points P1-P4 according to [26, 33]. (a) method 1 - #1; (b) method 2 - #2 .... *138*

Figure II.3-4 – Coupling force-based strength domain of connections: (a) Elliptical domain; (b) Rectangular domain. *139*

Figure II.3-5 – Coupled elasto-plastic constitutive laws (solid lines) and backbone curves (dashed lines) [26, 33] for different values of displacement in the orthogonal direction: axially-loaded hold-down connections calibrated with criterion (a) #1 and (b) #2; laterally-loaded angle bracket connections calibrated with criterion (c) #1 and (d) #2 .... *140*

Figure II.3-6 – Regression analysis for axially-loaded hold-down (blue solid line and markers) and laterally-loaded angle bracket (light blue dashed line and markers) connections. Yielding force vs. displacement in the orthogonal direction: bi-linearization method (a) #1 and (b) #2 .... *142*

Figure II.3-7 – Regression analysis for axially-loaded hold-down (blue solid line and markers) and laterally-loaded angle bracket (light blue dashed line and markers) connections. Yielding displacement vs. displacement in the orthogonal direction: bi-linearization method (a) #1 and (b) #2 .... *142*

Figure II.3-8 – Regression analysis for axially-loaded hold-down (blue solid line and markers) and laterally-loaded angle bracket (light blue dashed line and markers) connections. Ultimate displacement vs. displacement in the secondary direction for bi-linearization methods #1 and #2. .... *142*

Figure II.3-9 – Case study CLT shear wall (measures in millimeters). *143*

Figure II.3-10 – Bi-linear curves obtained with calibration criterion #1 (red) and #2 (orange): (a) hold-down in axial direction: (b) hold-down in lateral direction; (c) angle brackets in axial direction; (d) angle brackets in lateral direction. *144*

Figure II.3-11 – Comparison between the different multifailure criteria, the reference model (black line) and the uncoupled model (grey line): (a) bi-linearization method 1 - #1; (b) bi-linearization method 2 - #2. .... *145*

Figure II.3-12 – Comparison between the different criteria, the reference model (black line), the uncoupled model (grey line) and the experimental tests obtained within the SOFIE project ([35], wall I.2 and I.3) for low values of axial load N: (a) bi-linearization method 1 - #1; (b) bi-linearization method 2 - #2. .... *146*

Figure III.1-1 – Examples of different types of timber-based composite structures TBCSs: (a) Timber-Concrete TCCSs, (b) Timber-Steel TSCSs and (c) Timber-Timber composite structures TTCSs (image credits: (a) Ceccotti [2], (b) Hassanieh et al. [3] and (c) Leyder et al. [4]). *157*

Figure III.1-2 – Mechanical behavior of timber-based composite structural elements (image credits: Ceccotti [2]). *159*

Figure III.1-3 – Hybrid steel-timber structure proposed by Loss et al. [32, 33]: (a) axonometric view with indicated by the number 1 is the composite floor system and with number 2 is the wall system, (b) example of beam-to-panel connection and (c) example of panel-to-panel connection (image credits: (a) and (c) Loss et al. [33], (b) Loss et al. [32]). *161*

Figure III.1-4 – CLT-steel hybrid beam proposed by Hassanieh et al. [6] (image credits: Hassanieh et al. [6]). *162*

Figure III.1-5 – One-dimensional FEM model by Hassanieh et al. [6] (image credits: Hassanieh et al. [6]). *162*

Figure III.1-6 – Bidimensional FEM model by Hassanieh et al. [6] (image credits: Hassanieh et al. [6]). *162*

Figure III.1-7 – Beam-to-column hybrid joints tested by Keipour et al. [34] (image credits: Keipour et al. [34]). *163*

Figure III.1-8 – Static push-down displacement test setup for the experimental campaign carried out by Keipour et al. [34] (image credits: Keipour et al. [34]). *163*

Figure III.1-9 – Experimental setup of tests on CLT-steel composite structural members carried out by Chiniforush et al. [35] (image credits: Chiniforush et al. [35]) *164*

Figure III.1-10 – Connections typologies for of TBCSs: (a) notched connection, (b) dowel-type connection, (c) glued connection and (d) typical load-slip curves for the different type of connections (image credits: (a) Jiang et al. [39] (b) Lyu et al. [40] (c) Shengmin et al. [41] and Kanócz et al. [38], (d) Yeoh et al. [5]). *165*

Figure III.1-11 – Shear behaviour of dowel-type connections in TCCSs: (a) example of double-plastic hinge deformed configuration and (b) load vs. mid-span deflection of a TCC beam to the wary of the dowel-type connector (image credits: (a) Dias et al. [47] and (b) Hassanieh et al. [3]). *166*

Figure III.1-12 – Different notched types: (a) rectangular, (b) circular and (c) bird-mouth (image credits: (a-b) Deam et al. [62], (c) Khorsandnia et al. [61]). *167*

Figure III.1-13 – Shear connection proposed by Yeoh et al. [66] (image credits: Yeoh et al. [66]). *168*

Figure III.1-14 – Innovative dry shear connection systems by Crocetti et al. [14]: (a) inclined steel tubes and (b) wooden shear anchor-key (image credits: Crocetti et al. [14]). *168*

Figure III.1-15 – Modelling strategies for composite timber-based structures: (a) 1D modelling approach, (b) beam-to-solid modelling of dowel-type connectors and (c) 2D modelling approach (image credits: (a) Khorsandnia et al. [76], (b) Oudjene et al. [78], (c) Khorsandnia et al. [64]). *170*

Figure III.2-1 – View of the timber-steel composite beam in a four-point loading simply-supported configuration. *174*

Figure III.2-2 – Details of the hybrid timber-steel beam: (a) joint plates, (b) steel shear-key, (c) timber notch and (d) anchorage of shear keys on timber beam. *175*

Figure III.2-3 – Global mechanical model of the composite timber-steel structure used to define the analytical model. *175*

Figure III.2-4 – Elasto-plastic constitutive laws of (a) timber and (b) steel of the cable for the calculation of the neutral axis position on the composite mid-section.. *179*

Figure III.2-5 – Maximum elastic curvature $\chi_{el,max}$ of the composite mid-section: Case 1 (yielded timber) and Case 2 (yielded steel). *180*

Figure III.2-6 –Position of the neutral axis x in the mid-section with plastic behavior of the composite mid-section. *181*

Figure III.2-7 – Mechanical model to determine the distribution of the tensile force acting on the cable between the external and internal shear keys: (a) general and (b) detailed representation............................ *182*

Figure III.2-8 – Mechanical model of axial springs only to determine the distribution of tensile force T in the portion of cable among the internal shear keys. *183*

Figure III.2-9 – Mechanical model to derive the variation of shear force in the external shear key due to elastic displacements (a) δ_{ex} and (b) δ_{in}. *184*

Figure III.2-10 – (a) Forces acting on one of the two parts of the symmetrically loaded timber beam and (b) its statically equivalent isostatic system... *185*

Figure III.2-11 – Elastic deformation of the timber beam due to a concentrated bending moment m at distance a from the left support. *186*

Figure III.2-12 – Elastic deformation of the timber beam due to eccentric force F_c. *186*

Figure III.2-13 – Bending moment on the timber component of the timber-steel hybrid beam. *188*

Figure III.2-14 – Mechanical model for the definition of the rigid contribution of deflections (ε is an arbitrarily small little distance). *189*

Figure III.2-15 – Schematic representation of the displacement contributions to the rigid rotation of the beam derived from the mechanical model represented in Figure III.2-14. .... *190*

Figure III.2-16 – Global view of the FEM model... *192*

Figure III.2-17 – Details of the FEM model: (a) detail A, translational end-release with stiffness k_{ser} to model the notch deformability, and (b) detail B, rotational end-release to model the mid-hinge. *192*

Figure III.2-18 – Results of analytical model: (a) bending moment on timber beam M (kNm), (b) axial force on timber beam N (kN), (c) vertical deflections v of the timber beam (blue line) and of the steel cable (green line) measured respect to the timber beam axis (mm) and (d) rotations φ (deg) of timber beam. The red patch in figure (c) highlights the area where there is contact between the steel cable and the intrados of the timber beam. The asterisk marker in figure (c) reports the tests value measured during the preliminary experimental campaign [83]. *194*

Figure III.2-19 – Results of numerical model: (a) bending moment on timber beam M (kNm), (b) axial force on timber beam N (kN), (c) vertical deflections v (mm) and (d) rotations φ (deg) of timber beam. ... *195*

Figure III.2-20 – Contact between steel cable and timber beam during tests carried out in the preliminary experimental campaign presented in [83].. *196*

Figure III.2-21 – Parametric analysis on the SLS performance of the system to vary of steel hardware parameters: (a) diameter of the cable ϕ_b *vs. mid-span deflection* v_{max}*, (b) height of the plinth of the shear key* h_{sk} *vs. mid-span deflection* v_{max}*, (c) position of the external shear key* l_{ex} *vs. mid-span deflection* v_{max} *and (d) position of the internal shear key* l_{in} *vs. mid-span deflection* v_{max}.. *197*

List of tables

Table I.1-1 – Structural efficiency of timber and other traditional building materials (adapted from [3]). .. 11

Table I.1-2 – Comparison between different Codes and Standards for the seismic design of CLT buildings (table credits: Tannert et al. [149]). 32

Table I.1-3 – Low cycle ductility classes accordingly to EN 14592 [164]. 35

Table I.1-4 – Failure types and behavior for axially- and laterally-loaded dowel-type connectors. 41

Table I.1-5 – Spacings for dowel-type fasteners for laterally loading condition in CLT according to Blaß & Uibel [169]. 41

Table I.1-6 – Spacings for dowel-type fasteners for axially loading condition in CLT as a function of thread-grain angle α *according to Plüss & Brandner [175].* 41

Table I.1-7 – Values of overstrength factors γ_{Rd} *for different connection types usually employed for CLT buildings for different loading conditions by author.* 42

Table I.2-1 – Seismic mass M and vertical load W at each level for building configurations considered for linear analyses. 52

Table I.2-2 – Main mechanical parameters of connections elements. 53

Table I.2-3 – Connection pattern at each level for the considered case studies configurations. 53

Table I.2-4 – First period T_1 *for each analyzed building configuration.* 54

Table I.2-5 – Base shear forces per unit of length v and base uplift force N for each analyzed building configuration. 55

Table I.2-6 – Maximum percentage inter-storey drift $d_{i\text{-}s,max}$ *and inter-storey sliding displacement* $d_{sl,max}$ *for each analyzed building configuration.* 56

Table I.2-7 – Inter-storey sliding displacement d_{sl} *of 2-storey building with maximum values underlined.* ... 56

Table I.2-8 – Inter-storey sliding displacement d_{sl} *of 4-storey building with maximum values underlined.* ... 56

Table I.2-9 – Inter-storey sliding displacement d_{sl} *of 6-storey building with maximum values underlined.* ... 56

Table I.2-10 – Quantities measured during the tests of the walls. 58

Table I.2-11 – Positive and negative peaks of load history d_{top} *for small (violet), medium (yellow) and high (green) amplitude cycles.* 65

Table I.3-1 – Equivalent modulus of elasticity for walls of phenomenological model for each configuration and increasing level of PGA. 82

Table I.3-2 – First period T_1 *for each analyzed building configuration.* 83

Table I.3-3 – Base shear forces per unit of length v and base uplift force N for each analyzed building configuration. 83

Table I.3-4 – Maximum percentage inter-storey drift d_{max} *and inter-storey sliding displacement* $d_{sl,max}$ *for each analyzed building configuration.* 83

Table I.3-5 – Inter-storey sliding displacement d_{sl} *of 2-storey building with maximum values underlined.* ... 83

Table I.3-6 – Inter-storey sliding displacement d_{sl} *of 4-storey building with maximum values underlined.* ... 84

Table I.3-7– Inter-storey sliding displacement d_{sl} *of 6-storey building with maximum values underlined.* 84

Table I.4-1 – Comparison between component-level phenomenological and hybrid modelling approaches in terms of advantages and drawbacks. *89*

Table II.1-1 – Assumptions of different design methods for CLT shear-walls available in literature. *116*

Table II.1-2 – Lateral strength formulations of CLT shear-walls for different analytical models *117*

Table II.1-3 – Hybrid force-displacement based coupling model formulation. *122*

Table II.3-1 – List of symbols of Figure II.3-1 (alphabetical order). *136*

Table II.3-2 – Ratio ri *of the coupling equations (II.3-3) - (II.3-8) for bi-linearization methods #1 and #2 derived from linear regression analysis.* *141*

Table II.3-3 – Reference parameters of the constitutive laws of connections for bi-linearization methods #1 and #2. .... *144*

Table II.3-4 – Percentage gap between numerical and experimental tests obtained within the SOFIE project ([35]), wall I.2 and I.3 for bi-linearization methods #1 and #2 to the vary of the bi-linearization method. *147*

Table III.2-1– List of notations used in the analytical model. *177*

Table III.2-2– Geometrical characteristic of the beam configuration numerically modelled (measurement unit: mm). *194*

Table III.2-3– Geometrical characteristic of the reference beam configuration of parametric analysis (measurement unit: mm) *196*

List of publications and conferences

L. Franco, L. Pozza, A. Saetta, M. Savoia, D. Talledo, Strategies for structural modelling of CLT panels under cyclic loading conditions, Eng. Struct. 198 (2019) 109476. doi:10.1016/j.engstruct.2019.109476.

L. Franco, Analytical model to design enhancements of an innovative timber-steel composite beam, KTH Royal Institute of Technology internal report (2019).

L. Pozza, M. Savoia, L. Franco, A. Saetta, D. Talledo, Effect of different modelling approaches on the prediction of the seismic response of multi-storey CLT buildings, Int. J. Comput. Methods Exp. Meas. 5 (2017) 953–965. doi:10.2495/CMEM-V5-N6-953-965.

L. Franco, L. Pozza, A. Saetta, M. Savoia, D. Talledo, Coupled axial-shear model for analysis of CLT panels: effect of different numerical strategies, Compdyn 2017 - 6th International Conference on Computational Methods in Structural Dynamics and Earthquake Engineering, 15-17 June 2017, Rhodes, Greece.

Acknowledgments

Writing this Thesis required the help and guidance of many people that I would like to thank in the following.

Firstly, I would like to express my deepest gratitude to my supervisor Prof. Anna Saetta, for having helped me during the three years of Ph.D. and for the opportunity that she gave me to study a research topic I really care about. Her professionalism in reviewing all my works helped me in improving my scientific knowledge and taught me the critical perspective necessary to be a researcher.

I express my deep gratitude also to Ph.D. Eng. Luca Pozza, co-supervisor, for the many ideas that he gave me then developed into this thesis, for his high professionalism on timber structures that allowed me to learn a lot and that was necessary for the good result of this Thesis, and for the many reviews that improved the quality of my research activity.

I would also like to thank a lot Ph.D. Eng. Diego A. Talledo that, thanks to his strong scientific background and the many explanations, reviews and suggestions, helped me both to overcome many difficulties encountered during the Ph.D. course and taught me a working methodology.

I also express my deepest gratitude to Prof. Roberto Crocetti for the opportunity he gave me to have a study period at KTH in Stockholm, for his work as reviewer of the thesis, for his passion and deep knowledge of timber structures that he instilled in me and for the enjoyable *fikas* during my stay at KTH.

I would also like to thank a lot Prof. Roberto Tomasi whose smart review activity contributed to improve the quality of this Thesis.

My deep gratitude goes also to Prof. Magnus Wålinder for his warm welcome and his support during my staying at KTH in Stockholm.

I thank a lot Ph.D Eng. Luisa Berto for her precious hints, for always creating a pleasant working environment and for having been a wonderful teacher of Building Technology during my M. Sc. studies.

Many thanks also to Prof. Marco Savoia, who smartly gave me interesting suggestions that improved the quality of my research activity.

Thanks also to Prof. Renato Vitaliani for the original ideas and his "life lessons".

Thanks a lot my research teammates Alberto, Gianluca, Irene and Sebastiano for the suggestions and the very nice time spent together.

Thanks also to my colleagues of the Department of Civil, Environmental and Architectural Engineering of University of Padua Roberto, Lorenzo, Davide, Luca, Valentina, Giovanni and Sara.

My most sincere and deepest thanks to all my friends from my hometown for being an irreplaceable reference point in my life, particularly Soa, Ostino, Ivan, Chiara, Fenzo and especially Paolo, as well as to my university friends "calcestrussi".

I would also like to thank my mother for the support and for having always been a model of tenacity.

Finally, I would like to thank a person for having unconsciously (and probably reluctantly) taught me to be strong, therefore I take the chance to teach him something too through the words of Umberto Eco: "*ci vuole sempre qualcuno da odiare per sentirsi giustificati nella propria miseria*".